

.....

## DOCTORAL THESIS

Defended at Aix Marseille University March 31<sup>st</sup>, 2022 by:

**JONATHAN PHELIPOT**

**New fluorescent organic-  
inorganic nanohybrid materials  
for optoelectronic applications**

**Discipline**

Sciences Physique-Chimie

**Doctoral School**

ED250 - Sciences Chimiques  
de Marseille

**Laboratory/Research partners**

CINaM - Centre  
Interdisciplinaire de  
Nanosciences de Marseille

• **Composition du jury**

- Muriel HISSLER Examinatrice
- Institut Sciences Chimiques de Rennes
- Fabien DELPECH Rapporteur
- INSA Toulouse
- Johann BOUCLE Rapporteur
- Université de Limoges
- Didier GIGMES Président du jury
- Aix Marseille Université
- Jörg ACKERMANN Directeur de thèse
- Aix Marseille Université
- Olivier MARGEAT Co-directeur de
- thèse
- Aix Marseille Université
- 
-



## ▸ Affidavit

Je soussigné, Jonathan Phelipot déclare par la présente que le travail présenté dans ce manuscrit est mon propre travail, réalisé sous la direction scientifique de Dr. Jörg Ackermann & Dr. Olivier Margeat, dans le respect des principes d'honnêteté, d'intégrité et de responsabilité inhérents à la mission de recherche. Les travaux de recherche et la rédaction de ce manuscrit ont été réalisés dans le respect à la fois de la charte nationale de déontologie des métiers de la recherche et de la charte d'Aix-Marseille Université relative à la lutte contre le plagiat.

Ce travail n'a pas été précédemment soumis en France ou à l'étranger dans une version identique ou similaire à un organisme examinateur.

Fait à Marseille, le 3 janvier 2022



Cette œuvre est mise à disposition selon les termes de la [Licence Creative Commons Attribution - Pas d'Utilisation Commerciale - Pas de Modification 4.0 International](https://creativecommons.org/licenses/by-nc-nd/4.0/).

# Affidavit

I, undersigned, Jonathan Phelipot, hereby declare that the work presented in this manuscript is my own work, carried out under the scientific direction of Dr. Jörg Ackermann & Dr. Olivier Margeat in accordance with the principles of honesty, integrity and responsibility inherent to the research mission. The research work and the writing of this manuscript have been carried out in compliance with both the French national charter for Research Integrity and the Aix-Marseille University charter on the fight against plagiarism.

This work has not been submitted previously either in this country or in another country in the same or in a similar version to any other examination body.

Place Marseille..... , date 3 janvier 2022



Cette œuvre est mise à disposition selon les termes de la [Licence Creative Commons Attribution - Pas d'Utilisation Commerciale - Pas de Modification 4.0 International](https://creativecommons.org/licenses/by-nc-nd/4.0/).

# Liste de publications et participation aux conférences

## 1) Liste des publications<sup>2</sup> réalisées dans le cadre du projet de thèse :

1. Highly Emissive Layers based on Organic/Inorganic Nanohybrids Using Aggregation Induced Emission Effect.  
J. Phelipot, N. Ledos, T. Dombrey, M. P. Duffy, M. Denis, T. Wang, Y. Didane, M. Gaceur, Q. Bao, X. Liu, M. Fahlman, P. Delugas, A. Mattoni, D. Tondelier, B. Geffroy, P. Bouit, O. Margeat, J. Ackermann, M. Hissler, *Adv. Mater. Technol.* **2021**, 2100876, 2100876.
2. Nanohybrids as a tool to control the dispersion of organic emitters in solution-processed emissive layers (First author, in preparation).
3. Co-grafting of red, green and blue organic emitters on inorganic carriers toward solution-processed White Organic Light-Emitting Diodes (Second author, in preparation).

## 2) Participation aux conférences<sup>3</sup> et écoles d'été au cours de la période de thèse :

1. Oral Presentation SNAIA19 International Congress (Paris)
2. Oral Presentation NanoGe 2021 Fall (Online Meeting).
3. Poster at GDR OERA 2021 Fall Meeting (Marseille).

## Resumés (Français/Anglais):

Les matériaux émissifs jouent un rôle clé dans diverses applications telles que les LED et, pour les émetteurs organiques à l'état de l'art, le contrôle de leur morphologie au sein de la couche émissive par des techniques de dépôt en voie liquide reste un défi. Le développement de molécules organiques émissives greffables, combinées à des nanoparticules inorganiques, a ouvert de nouvelles possibilités pour contrôler la dispersion de ces émetteurs. Afin d'éviter l'effet d'extinction causé par l'agrégation lorsque de fortes concentrations d'émetteurs organiques sont présentes à la surface des nanoparticules, l'effet inverse, à savoir l'émission induite par l'agrégation, est une approche prometteuse pour générer une forte émission de lumière. En effet, dans ce cas, la forte concentration permet de geler le mouvement des molécules et de réduire les voies de désactivation non-radiatives. Cependant, même si ces nouveaux matériaux nanohybrides organiques-inorganiques présentent une forte émission, l'élaboration de couches minces par voie liquide et notamment le contrôle de la morphologie restent un défi car ces nanohybrides ont tendance à s'agréger en solution. Par conséquent, pour progresser vers l'élaboration de films minces homogènes et obtenir des dispositifs LED efficaces/reproductibles, il est nécessaire de synthétiser des solutions de nanohybrides non-agrégés. Un moyen possible de contrôler la taille des agrégats de nanohybrides en solution, de contrôler la morphologie de la couche émissive et, de manière plus surprenante, d'améliorer en même temps l'émission des fluorophores organiques, a été trouvé et consiste à utiliser le co-greffage avec de l'acide oléique à la surface des nanoparticules inorganiques. Ces nanohybrides modifiés par l'acide oléique ont ainsi été incorporés en solution dans une matrice hôte polymère, à savoir le PVK et l'oxadiazole, largement étudiés dans la littérature pour les applications OLED, pour assurer les propriétés de transport de charge dans les films minces afin d'avoir des dispositifs LED efficaces. Le contrôle de la lumière émise dans ces dispositifs électroluminescents est possible en changeant les fluorophores organiques greffés, tels que les fluorophores bleus, verts et rouges testés. En greffant simultanément ces différents émetteurs organiques à la surface des nanoparticules, nous avons également pu régler finement la couleur des dispositifs LED. Des LED à l'émission blanc chaud, blanc froid et blanc pur ont ainsi pu être obtenues par ce procédé entièrement réalisé par voie liquide, ce qui ouvre la voie à une fabrication à grande échelle.

- ▲ Light emitting materials play a key role in various applications such as LED and, for state-of-the-art organic emitting molecules, the control of their morphology within the emissive layer through solution processable deposition techniques remains challenging. The development of graftable emissive organic molecules combined with inorganic nanoparticles have opened new opportunities for controlling the emitter dispersion. In order to avoid the classical aggregation-caused quenching effect when high concentrations of organic ligands are present on nanoparticle surface, the opposite effect, namely aggregation-induced emission, is a promising approach to generate strong light emission. Indeed, in this case, the high concentration helps to freeze the motion of the molecules and to reduce the non-radiative deactivations. However, even though these new organic-inorganic nanohybrid materials show strong emission, their solution-processing for morphology control remains challenging as the nanohybrids suffer from a tendency to aggregate in solution. Therefore, to go towards the elaboration of homogeneous thin films and efficient/reproducible LED devices, aggregate-free solutions of the nanohybrids have to be synthesized. A possible way to control the size of the nanohybrid aggregates in solution, to control the morphology of the emissive layer and, more surprisingly, to enhance the emission of the organic fluorophores at the same time was found and consists in using the co-grafting with oleic acid onto the inorganic nanoparticle surfaces. These oleic acid-modified nanohybrids were thus incorporated in solution in a polymer host matrix, namely PVK and oxadiazole, widely studied in OLED literature, to ensure the charge transport properties in the thin films in order to have efficient LED devices. The control of the emitted light in these electroluminescent devices was possible by changing the grafted organic fluorophores, such as the tested blue, green and red ones. By simultaneous co-grafting of these different organic emitters on the nanoparticle surface, we could also finely tune the color of LED devices. Interestingly, warm white, cold white and pure white LED were achieved through this full solution process, which opens the way for large scale manufacturing.

# Summary

Introduction.....	1
State of the art.....	4
1) The nanosciences.....	4
a) History of the first nanomaterials.....	4
b) The origins of nanotechnologies.....	5
c) Synthesis approaches of nanocompounds.....	7
d) Toxicity of nanoparticles.....	8
e) Applications and interests of nanoparticles.....	9
2) History of LEDs.....	13
a) Fondamental functioning of light emission in light emitting diode.....	13
b) The history of light emitting diodes.....	16
c) Architecture and functioning of modern optoelectronic LED device using nanotechnologies.....	16
3) Deposition techniques and interfacial materials.....	19
a) Deposition technics of the layers.....	19
b) Materials for light emitting diode made by nanotechnologies and their processes.....	20
4) The different emissive materials in LED technologies.....	23
i) Heavy metal polymer complexes.....	24
ii) QDLEDs Quantum Dot LEDs.....	25
iii) PeLEDs Perovskite LEDs.....	27
iv) Organic LED OLED.....	31
5) Solution for future LED technology.....	36
i) TADF Polymers.....	36
ii) Aggregation Induced Emission AIE.....	37
Chapter 1: Introduction to nanohybrids using AIE phenomenon.....	56
1) The AIE nanohybrid composition.....	56
a) Inorganic core.....	57

i) ZnO.....	57
ii) ZrO <sub>2</sub> .....	60
iii) Inorganic halogenated perovskites CsPbI <sub>3</sub> .....	62
b) Organic AIE emitters (1st generation).....	65
2) Nanohybrid synthesis in solution (self-assembly).....	67
3) Analyses of the grafting.....	68
a) Density Functional Theory (DFT), Fourier Transfer Infrared (FTIR) and X-Ray photoelectron spectrometry (XPS) analyses.....	68
b) Optical analyses of the nanohybrids in solution.....	70
c) Dynamic Light Scattering DLS analyses of the nanohybrids.....	73
d) Optical analyses of the nanohybrids as thin films.....	75
e) Morphological analyses of the thin nanohybrids films by TEM and AFM	76
4) LED devices using pure AIE nanohybrids as electroluminescent layer.....	78
5) Conclusions about pure ZnO:3.....	80
6) The use of OA for reproducible and homogeneous LED device.....	80
7) Conclusions about pure ZnO:3 :OA.....	85
 Chapter 2: Nanohybrids incorporated as guests in a polymer host matrix.....	 95
1) The interest of host-guest structure using a polymer matrix.....	95
2) The choice of PVK polymer and OXD as host matrix.....	96
3) Incorporated nanohybrids in the matrix: the effect of OA.....	97
A) Morphological characterizations of M:N films with or without OA....	98
B) Optical characterizations.....	104
i) Matrix M, emissive molecule 3 and ZnO NCs in solution.....	104
ii) Luminescent materials in thin films (excited at 400 nm).....	105
iii) Emission in thin films (excited at 350 nm).....	107
iv) Photoluminescence Quantum Yield (PLQY).....	108
4) LED devices using N incorporated in the matrix M as electroluminescent layers.....	110
i) Impact of the OXD in M.....	111
ii) Effect of the electroluminescent layer thickness.....	112
iii) Effect of the PVK:OXD ratio.....	114
iv) Effect of the amount (X%) of incorporated nanohybrids N <sup>x</sup> in the matrix M.....	115

v) Effect of OA (Y) concentration in M:N <sub>10</sub> :OA <sub>Y</sub> .....	116
vi) Full solution approach to build LED.....	118
5) Conclusions of PVK:OXD used as host embedding nanohybrids as guests....	120
ANNEXES.....	122

### Chapter 3: Blue, green and red nanohybrids used as a tool to control the light

emission in LED devices.....	129
1) Presentation of the new molecules (B, G, R, Y).....	129
2) Preparation of the nanohybrids.....	132
3) Optical properties in solution.....	133
a) Emitter B.....	133
b) Emitter G.....	135
c) Emitter R.....	136
d) Emitter Y.....	138
4) Optical properties in thin films.....	139
a) Emitter B.....	139
b) Emitter G.....	141
c) Emitter R.....	142
d) Photoluminescence Quantum Yield (PLQY).....	144
5) Morphological properties of the nanohybrids.....	149
a) M:N <sub>10</sub> <sup>B</sup> .....	150
b) M:N <sub>10</sub> <sup>G</sup> .....	151
c) M:N <sub>10</sub> <sup>R</sup> .....	153
6) Hybrid RGB LED devices as proof of concept and optimization.....	154
a) Emitter B.....	156
i) Electroluminescent properties.....	156
ii) Shift in emitted color from M:B reference to M:N <sup>B</sup> :OA.....	159
b) Emitter G.....	160
i) Electroluminescent properties.....	160
ii) Shift in emitted color from M:G reference to M:N <sup>G</sup> :OA.....	163
b) Emitter R.....	164
i) Electroluminescent properties.....	164
ii) Shift in emitted color from M:R reference to M:N <sup>R</sup> :OA.....	168
7) Additional characterizations of the emissive nanohybrid layers.....	169

a) Space Charge Limited Current (SCLC) mobility.....	169
b) Post annealing of the LEDs.....	170
c) Encapsulation of LEDs based on M:(1:3)N <sub>10</sub> <sup>G</sup> :OA as electroluminescent layer.....	171
8) Conclusions & Perspectives for hybrid white LED.....	172
ANNEXES.....	174
Chapter 4: Co-grafting of several emitters on nanocrystals, towards white emission..	178
1) Elaboration of white emissive nanohybrids in solution.....	178
2) Matrix M combined with two or three emissive nanohybrids.....	179
i) White LED devices using TPBi and LiF as electron transport material..	179
ii) Optical analyzes of M:N <sup>B40/R3</sup> :OA films.....	184
iii) Morphology of M:N <sup>B40/R3</sup> films.....	185
iv) Morphology of M:N <sup>B120/G1/R5</sup> films.....	187
3) Matrix F (F8:F8BT) combined with two emissive nanohybrids.....	188
i) ZnO Co-grafting with 2 emitters in the matrix F.....	188
ii) Morphology of F:N <sup>B50/R25</sup> films.....	191
4) SCLC mobility measurements.....	192
5) Effect of the interfacial layers.....	193
i) ZnO Co-grafting with 2 emitters in the matrix M.....	193
ii) ZnO Co-grafting with 3 emitters in the matrix M.....	195
6) Conclusions.....	197
General Conclusion.....	200
Experimental section.....	202
Synthesis of nanomaterials.....	202
1) Synthesis of ZnO.....	202
2) Synthesis of ZrO <sub>2</sub> .....	203
3) Synthesis of CsPbX <sub>3</sub> .....	204
Optical characterization.....	205
1) Absorption.....	205
2) Fluorescence.....	206
3) FTIR.....	206
4) PLQY integrative sphere (Palaiseau LPICM).....	207
Morphological characterizations.....	211

1) Dynamic Light Scattering (DLS).....	211
2) Transmission Electron Microscopy (TEM).....	212
3) Scanning Electron Microscopy (SEM).....	213
4) Atomic Force Microscopy (AFM).....	213
5) Profilometry.....	214
6) X-Ray Photoelectron Spectroscopy (XPS) (collaboration with Mats Fahlman –University of Linköping).....	214
7) X-Ray Diffraction (XRD).....	215
<b>Devices elaboration.....</b>	<b>216</b>
1) Cleaning of ITO substrate ultrasonic baths and UV ozone.....	216
2) Glovebox.....	217
3) Centrifuge machine.....	217
4) Spin coater.....	218
5) Preparation of a regular architecture LED.....	219
6) Preparation of hybrid active layers.....	220
7) Preparation of SCLC devices.....	220
<b>Bibliography.....</b>	<b>222</b>

# Introduction:

Nowadays, LED technology is a booming field with a key role in the sustainable development. The famous and classic Thomas Edison's bulbs were progressively replaced by the LED technology, which is more economic, more efficient and more sustainable for our society. As illustrated in the state of the art chapter, several LED technologies are existing and are under development. These last present lots of advantages and drawbacks, that require deeper investigations to face the future challenges, such as:

- The large scale production of LEDs, which is possible using both liquid and evaporation methods (organic light emitting diode for instance).
- The low cost manufacturing of the LEDs thanks to the liquid deposition approach instead of the evaporation one. Indeed, the liquid approach is more economic, as it does not require high vacuum level, like in evaporation method.
- The quality of the emitted light, such as the quantum dot LEDs, that present higher spectral purity compared to the OLED, but they mainly used as photoluminescent compounds in LED devices and not as electroluminescent ones.
- The nature of the emitter, as it can be fluorescent with 25% of the charges converted to light emission, or phosphorescent with 75% of conversion or more recently thermally active delayed fluorescence that is able to transform 100% of the charges into light emission.
- The green / non-toxic property of the used emissive materials, with potential problems for instance using the perovskites materials that are very efficient but toxic.
- The abundance of materials (iridium complexes are very efficient nowadays but are rare materials).
- The stability of the LED devices, such as perovskites or OLED devices, that are known to be quite unstable under air, moisture and UV, therefore requiring an encapsulation of the device.

To face these challenges, original approaches are needed for both the material side and the device elaboration, combining the advantages of several LED technologies, for instance the combination of polymer host matrix including emissive guests. Indeed, guest-host structures are known in the OLED field but still suffer from severe drawbacks such as emitter phase segregation for both solution and evaporation processes. The morphology control of organic emitters within a matrix by solution process is of peculiar interest in the field.

The present work lies in this context. It was possible thanks to the ANR project “Fluohyb”, that started in 2017 and finished in 2022. The ANR project was led by Pr. Muriel Hissler from Institut des Sciences Chimiques de Rennes, with her PhD student, Nicolas Ledos, who was in charge to synthesize the graftable organic emitters. The collaborators Dr. Bernard Geffroy, Dr. Denis Tondelier and the post-doc Dr. Payal Manzhi from Laboratoire de Physique des Interfaces et Couches Minces (LPICM) were in charge of the characterizations of the optimized LED devices that were routinely elaborated in Centre Interdisciplinaire de Nanosciences de Marseille (CINaM). My work was done under the supervision of Dr. Olivier Margeat and Dr. Jörg Ackermann. It was firstly about synthesizing inorganic nanoparticles that could be grafted with various organic emitters from Pr. Muriel Hissler group to create organic-inorganic nanohybrids. The study was done first at the liquid state, and then, once the nanohybrid structures were well-dispersed, they were used as electroluminescent layer to build LED devices. My first goal was to do a proof of concept of LED using these nanohybrids, and the second was to optimize these systems to demonstrate that the color is easily tunable thanks to the nanohybrid composition, by presenting blue, green and red emitting LEDs. The final goal was to achieve white emission LEDs using these nanohybrids as electroluminescent layer. Therefore, the presented work explores an original alternative to some drawbacks of OLED which are mostly done via evaporation process. This work is divided in five chapters, with a first one discussing the state of the art in the field of materials used in LED, and then four experimental chapters:

- Chapter 1 focuses on the building of inorganic-organic nanohybrid structures, that are done with ZnO nanocrystals of 5 nm in diameter grafted with emissive organic fluorophores via self-assembly at the liquid state. Once the nanohybrids were synthesized and controlled in solution, they were used as electroluminescent layer in a regular architecture of LED devices, as a proof of concept. Charge transport limitations forced us to envisage the use of an embedding matrix for such a role.

- Chapter 2 studies therefore the incorporation of emissive nanohybrids as guests inside a solution of polymer host matrix. The new emissive materials were characterized and then used as electroluminescent layer in a regular architecture of LED devices, and showed an improvement compared to the pure nanohybrids employed in the chapter 1. The new LED devices were afterward optimized thanks to morphology control of the materials composing the electroluminescent layer.

- Chapter 3 highlights the use of new nanohybrids of different colors, assumed to be more efficient than the 1<sup>st</sup> emitter used in the chapters 1 and 2. These new nanohybrids are characterized and used in LED devices, allowing for blue, green, red and yellow emitting LEDs, as proof of concept, and follow the same optimization process as in chapter 2.

- Chapter 4 is finally dedicated to the design of different white LEDs using white emissive nanohybrids, namely cold white, warm white and pure white. That was done by the co-grafting of the different organic emitters from chapter 3 on same ZnO nanocrystal surface, and then incorporated to the polymer host matrix. The adjustments to obtain a white display were done by changing the composition of the luminescent nanohybrids before adding them to the matrix.

Finally, a general conclusion gives a summary of the most important points raised by this work, together with some outlooks for future related work.

# State of the Art

## 1) The nanosciences

### a) History of the first nanomaterials

During the 4<sup>th</sup> century after the death of Jesus Christ, the glassmakers of the Roman Empire created the first known nanomaterial in history, without knowing it, which is one of the most interesting examples of nanotechnology and still observable at the British Museum. The Lycurgus Cup was done by working glass in presence of metal salts of gold, silver, and copper, which then formed nanoparticle alloys. [1–6]. As shown by the following figure bellow, depending on the lighting conditions, the Lycurgus Cup changes color, as it appears red when light is transmitted through the glass and opaque green in direct incidence by the reflected light. In the end of 20<sup>th</sup> century, investigations were done by Transmission Electron Microscopy and X-Ray Diffraction to know more about the secret behind the colors of the Lycurgus Cup [6]. The analyses revealed that the colors were due to the presence of Ag-Au-Cu nanoalloys, with different diameters from 50 to 100 nm incorporated in a glass matrix [3, 6]. The opaque green color is related to the light scattering of the Ag nanoparticles while the gold ones, which absorb at 520 nm, induce the red color of the cup.



*Figure 1 : Lycurgus Cup, Left : Opaque green, reflected light due to Ag nanoparticles, Right : Red transmitted light due to Au nanoparticles.*

Over the centuries other nanotechnology skills were found. Not only nanoparticle alloys were used in medieval church windows to add vibrant colors [2, 7], but also with shiny ceramic lusters in Islamic World between the 9<sup>th</sup> and 17<sup>th</sup> centuries. [2, 7, 8] Italian Renaissance ceramics were also examples of a nanotechnology use in the 15<sup>th</sup>-16<sup>th</sup> centuries, by coloured glazes, which were thin films used for ceramics as lusters, potteries [2, 9, 10]. Even if nanotechnology was first used for decorative aspect, the Ottoman Damascus Empire used it

to perform weapons from the 13<sup>th</sup> to 18<sup>th</sup> centuries. They were using carbon nanotubes and cementite nanowires to increase the strength, toughness, and sharpness of their sabers over the time. [2, 11] These ancient artists, scientists, forgers were using nanotechnology with intention, but they could not explain why these objects exhibited these properties. The first explanations came out in 1857, thanks to Michael Faraday who did voluntarily the synthesis of « red » gold nanoparticles, by reducing the gold salts with the white phosphorous [2, 12–14]. Depending on the light conditions Michael Faraday explored the optical and electronic properties of the Au nanoparticle, which is one of the most interesting. Moreover, these stable solutions are still observable at the Faraday Museum in London. Subsequently, many new characterization techniques emerged to deeper investigate the secrets of nanosciences. For instance, X-Ray Diffraction in 1895 for crystalline structures investigations ; RAMAN spectrometry for molecular and external compositions of a material in 1928 ; Scanning Electron or Transmission Electron Microscopies that allow « direct » observation of physical and chemical characterizations of many materials since 1937-1938; XPS (X-Ray Photoelectron Spectrometry) for studying the energy levels and their transitions at the atomic scale since 1969 ; STM Scanning Tunneling Microscopy in 1981 and AFM (Atomic Force Microscopy) for surface characterizations in 1982. [2]

### b) The origins of nanotechnologies

In 1959, the famous physicist Richard Feynman, during the American Society Conference, introduced the concept of nanoscience by a talk « There is Plenty of Room at the Bottom », where he meant the storage of many informations in a very small area and that science could achieve machine construction at the molecular level. He described the interests of the nanotechnologies and how scientists could control it, namely atoms or molecules. [2, 7, 15]. Richard Feynman is considered as a pioneer of nanosciences as far as he brought significant improvements in the field, describing mainly two approaches to synthesize nano compounds, « bottom up » and « top down ». However, the definition of this new field first appeared in a 1974's article during a conference from British Society in London, written by Norio Tanigushi [16]. Nanotechnology was created from the Greek word Nannos which means very small. Nano is the unit of length in metric system which correspond to 1 billion times smaller than a meter. [7] To put in perspective, a tennis ball is around 100,000,000 nm while the diameter of carbon nanotubes used by Ottoman Damascus Empire for their sabers was around 1 nm [17]. The development of nanoscience can be traced to the time of the Greeks and Democritus in the 5<sup>th</sup> century before christ, when scientists considered the question of whether matter is continuous, and thus infinitely divisible into smaller pieces, or composed of small, indivisible,

and indestructible particles, which scientists now call atoms. Nowadays, the official scientist convention says that one object is considered “nano” if at least one of the dimensions is below 100 nm. Moreover, the nanoscience is defined as the investigation of structures at the nanoscale, while the nanotechnologies are the applications using these structures. [1]

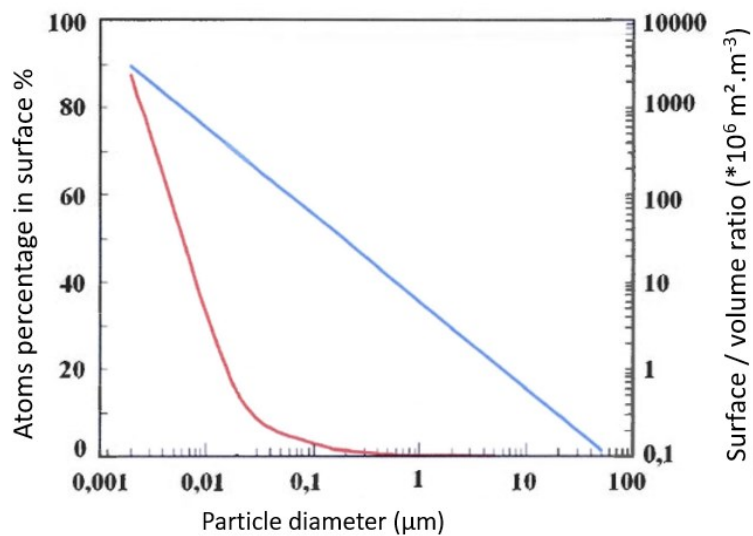
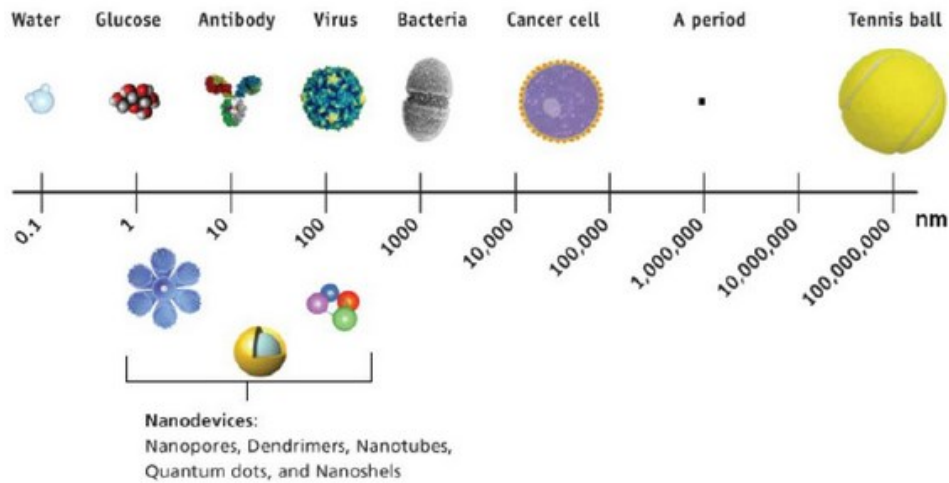


Figure 2 : Top : different objects, different sizes (nm unit) [7] Bottom : surface/volume ratio of nanoparticles and % of atoms in surface according to their diameter [18]

Nanomaterials take their special properties due to quantum effects, or to the surface / volume ratio, which is higher than for microscale objects (figure 2), there are many different possible shapes, and even some exotic combinations such as micelle for instance, [1, 19–21] depending on the synthesis conditions.

### c) Synthesis approaches of nanocompounds

The nanocompounds used in these technologies are made via two methods and are presented in the following figure 3.

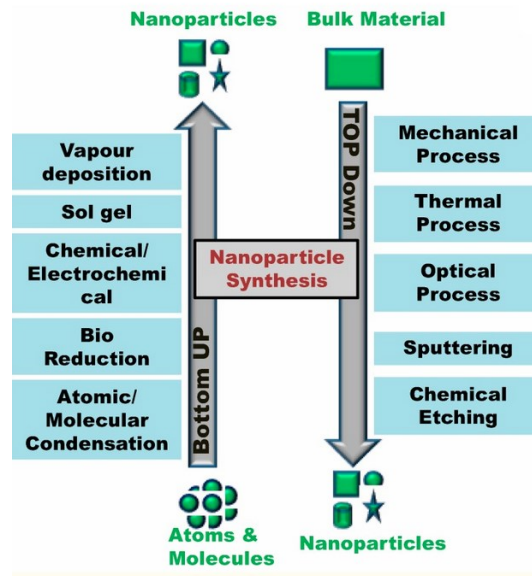


Figure 3 : Bottom Up vs Top Down nanoparticles synthesis approaches [2]

The most conventional method is the Top down approach. It is easy to process, as the synthesis starts from a bulk material and end with nanoparticles. For instance, the first nanomaterials in history were made by mechanical and thermal processes, when ancient scientists took bulk sands and mixed it with metallic salts in order to create gold-silver-copper nanoparticles over 50 nm. [2] However, the Sputtering and Chemical Etching are quite recent, and can be very accurate for nanodesign engineering, for example in microelectronic using Electronic Lithography to write many informations in a very small area, thanks to ion or electron beam. The case of memory cards in smart phones refers to it, by developing the technology to enhance their performances while decreasing their sizes. In another hand, the bottom-up approach is more recent, and it has been used to build nanoparticles from 1 to 100 nm, aggregate by aggregate, molecules by molecules or atoms by atoms via physical or chemical way and controlled by self-assembly of atoms or molecules. This creates highly pure nanomaterials in solid (Electrochemical), or in solution (Sol-Gel). [2, 19–21] Indeed, through bottom up electrochemical synthesis, it is possible to grow  $\text{TiO}_2$  nanotubes on a titanium surface by anodization process, for instance in the medical field, to improve the performances -lifetime, mechanical stress, fixation to the body, anticorrosion property- of the actual prosthesis. [22, 23] The Sol-Gel synthesis may begin with a metal precursor, a solvent and a

reactant to generate highly pure crystalline metal oxide nanoparticles such as ZnO, ZrO<sub>2</sub>, TiO<sub>2</sub>, SiO<sub>2</sub>, with homogeneous shape and size. The reaction is driven by self-assembly. [24, 25] Moreover, during the synthesis or in the end, the use of surface ligand is sometimes used, [26] in order to stabilize the nanocompounds synthesized via self-assembly and to take advantages from the different entities. Other bottom-up approaches to synthesize nanoparticle exist such as co precipitation method. [27, 28]

#### d) Toxicity of nanoparticles

Nanoparticles are widely used as benefits for our society improvements, and health technology. For instance, the most efficient process to unpolluate water is based on the use of aluminum and iron nanoparticles from 2 to 2.5 nm of diameter obtained by precipitation of aluminum (Al<sup>13</sup>) and iron (Fe<sup>24</sup>) salts incorporated in polymers. These technics predate the « nano » fashion from the 2000's [29–31]. In the biomedical applications, the size and the physicochemical properties of the nano iron oxides are significant because they can strongly affect the residing time of nanoparticles in the blood and their bioavailability [32]. For example, nanoparticles of size between 10 and 100 nm have an optimal residence time in the blood circulation, while particles of 200 nm, or smaller than 10 nm are retained by the spleen or renal system respectively (drug delivery systems). Indeed, the case of silver nanoparticles is sometimes compared to trojans capable of crossing biological barriers and certain cell walls, thus accumulating in different organs. [33] The development of nanotechnology was initially launched without a full analysis of the risks that nanomaterials can represent on human health and the environment. This lack of risk assessment was initially based on toxicological knowledge of macroscopic sized materials of the same nature, as the example of solar creams with TiO<sub>2</sub>. The investigations of the risks are becoming important with the developing field of nanotechnologies and the increasing number of products containing nanomaterials in their composition. The emission of manufactured nanomaterials into the environment, during production or degradation of products containing nanomaterials is a recognized fact [34]. Concentrations were measured of 8 µg/L of TiO<sub>2</sub> particles between 20 and 300 nm sizes in urban surface water, due to the deterioration of the paintings of the buildings and various objects. It was shown that the toxicity depends on the size, on the morphology but also on the stability of the nanoparticles, capable for example to transform into metallic ions by degradation (oxidation) processes [33, 35].

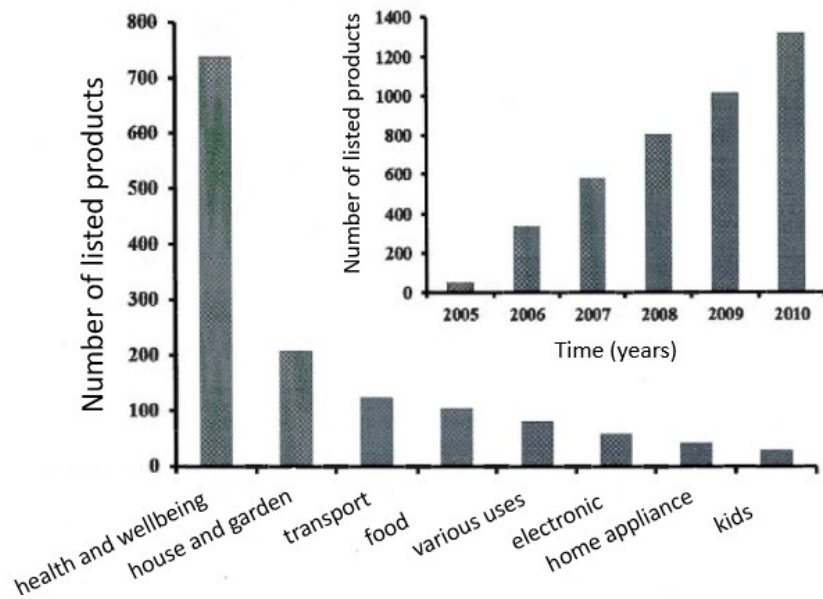


Figure 4 : number of listed products over the year and by categories (in 2010) [18]

In the same way, antimicrobial textiles containing silver nanoparticles can release up to 45 % of their total content in silver, in the form of metal ions, nanoparticles and macroparticles of silver, during the washing or sweat exposure. Effectively, different types of nanomaterials are used and are on rise of production in the market today. The most used nanomaterials are metallic nanoparticles such as silver, metal oxides, gold, quantum dots and carbon-based nanomaterials like nanotubes of carbon and fullerenes and known to be toxic [36]. Due to their reactivity, nanomaterials interact quickly with the environmental matrix. Generally, nanomaterials are poorly mobile as they are quickly agglomerated with the components of the environment. Nevertheless, the interaction between nanomaterials and the environment is influenced by various factors that can modify the reactivity and stability of nanomaterials. For example in the literature, nanoparticles of ZnO or TiO<sub>2</sub> incorporated in a polymer are more mobile in soils and can contaminate them due to their higher stability [37, 38]. However, it is still difficult to assess the level of contamination by nanomaterials in the environment because of the complexity of analytical methods at the nano scale, and the difficulty to distinguish artificial nanoparticles from natural colloids present in ecosystems and the great diversity of existing nanomaterials [39]. Therefore, each nanomaterial has its own toxicological profile. Knowledges about their effects on human health are not precise enough, but studies suggest the possible occurrence of inflammatory, respiratory, cardiovascular, or neurological effects. [40]

## e) Applications and interests of nanoparticles

Even if the nanotechnology may represent nonvisible objects and therefore a possible unknown danger, the nanotechnology is the most growing and promising field of the 21<sup>st</sup> century, it is involved in various applications which are presented briefly in the following scheme.

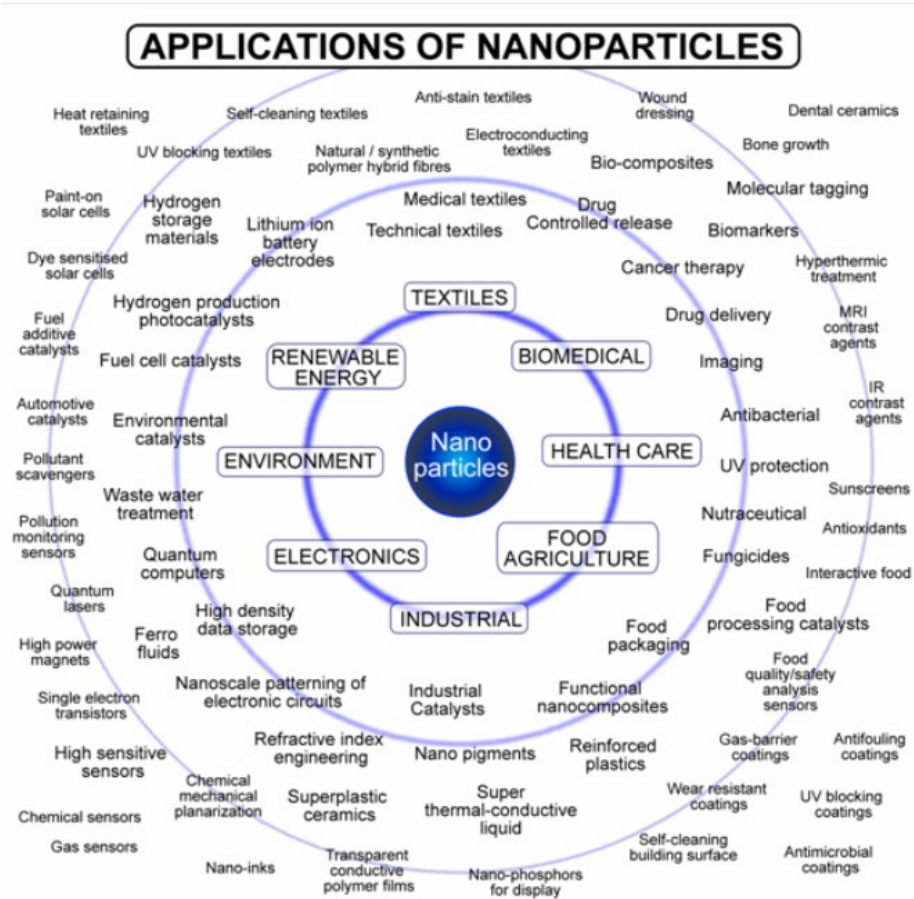


Figure 5 : Fields and applications of the nanoparticles [19]

In the 2000's, nanotechnology faced controversy and public mistrust. Twenty years after, the modern nanotechnology progresses in every field of the science but also in the society. [2] In the common use, the field of the textile is taking advantage from the nanotechnology. Nowadays, clothes can be connected, and are even more suitable for certain sports than the regular clothes with aerodynamic or anti sweat properties, such as swimming, athleticism or hiking. Moreover, the nanotechnologies are very often more economic because less materials are required compared to the traditional macro methods. [41] Agriculture and food are a major question of the 21<sup>st</sup> century, as far as the Earth population is increasing year after year, and nanotechnology is a promising solution against the lack of food thanks to the smart food

packaging [42]. Recently, nanotechnologies are applied in the medical health domain and show remarkable progress for the treatment of cancer by the creation of « nanomachines ». Such examples include the improvements of prosthesis, drug delivery systems, imaging, and antibacterial property. [2, 19, 22, 23]

The biggest challenge of our era is probably related to the global warming effect, which is due to the destructive human activity on Earth. The nanotechnologies bring encouraging solutions to slow down this natural phenomenon. The first alternative consists of reducing the emission of the toxic gases which trap the sun rays into the atmosphere and produces the global warming effect. These gases are mainly emitted via extracting, producing, transforming, and consuming resources. The renewable energies are a part of the solution, as the idea is to transit from fossil fuel energies to the renewable ones which sometimes use nanotechnologies, such as hydraulic, biomass, wind and photovoltaic. This solution is sustainable and shows huge progress over the last years, but still it is consuming precious materials which are not unlimited on Earth, therefore improvements need to be done. The increase of the global warming effect is also related to the consumption of energy which grows year after year simultaneously with the technology. A part of the problem is related to the waste of energies and thus resources. Therefore, at the beginning of the 2000's, the concern of our society about the environment and particularly the reduction of power consumption has led to a very strong growth in the field of energy. It is important to improve the way of consuming, for instance the optoelectronic devices such as TV, smartphones, boards, and public space lighting in cities can be improved with nanotechnologies. The different areas addressed by light emitting diodes (LEDs) are the energy saving via the public lighting –one company has developed electricity free glowing plants for public park and garden- [43], the medical field, the automotive market, the information and communication technologies and many others. Currently the LEDs covers the emission wavelength from ultraviolet 350 nm to infrared 2,000 nm. [44, 45] In the 21<sup>st</sup> century, different technologies are competing for the public lighting market (Figure 6).

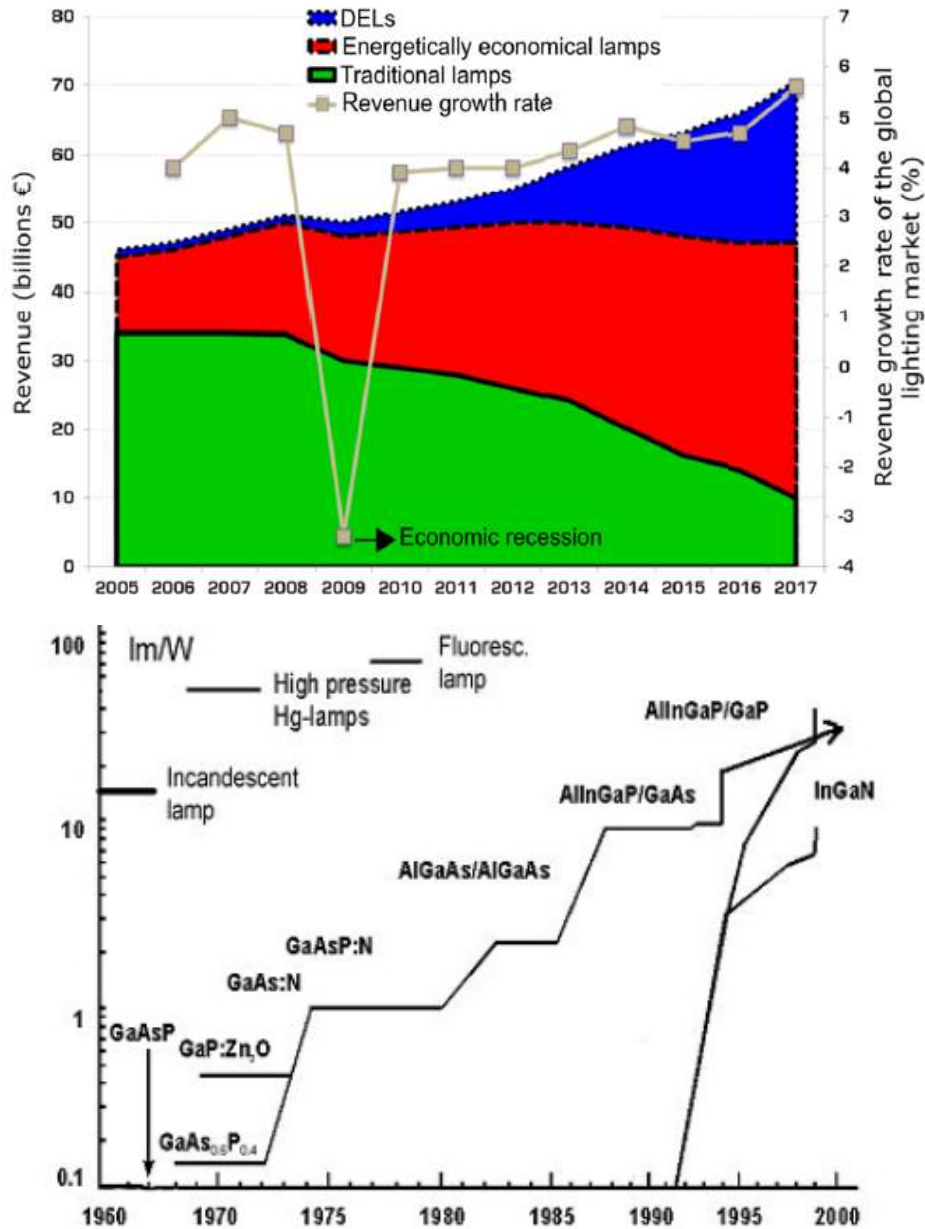


Figure 6 : Bottom :Public lighting revenues ( $10^9\text{€}$ ) and growth rate of the global lighting market (%) of the different technologies : blue : LED ; red : energetically economical lamp ; green : traditionnal lamps [44] ; Top : Different luminous intensities ( $\text{lm/W}$ ) of lighting devices and their evolution in the end of 20th century [45]

Additionally, the competition of the lighting market also takes place inside LED technologies because of the numerous existing technologies under development. For instance, organic light emitting diode OLED is a very promising nanotechnology, bringing new properties such as flexible substrate, low cost and large manufacturing with organic –renewable- materials. Some other LED technologies are very efficient, but they use rare or toxic materials, and will be discussed in the following parts.

## 2) History of LEDs

### a) Fondamental functioning of light emission in light emitting diode

The radiation emitted by LEDs is no longer produced by temperature such as the traditional incandescent lamp but by a completely different phenomenon, which does not involve temperature rising like for a tungsten filament. Therefore, this is a huge benefit concerning the efficiency of the LED devices which is widely better. The lighting phenomenon is related to the quantum physics of semi-conductors. The semi-conductors like silicon carbide, GaAs or metal oxides (ZnO TiO<sub>2</sub>...) are materials having an energy bandgap, unlike metals and insulators.

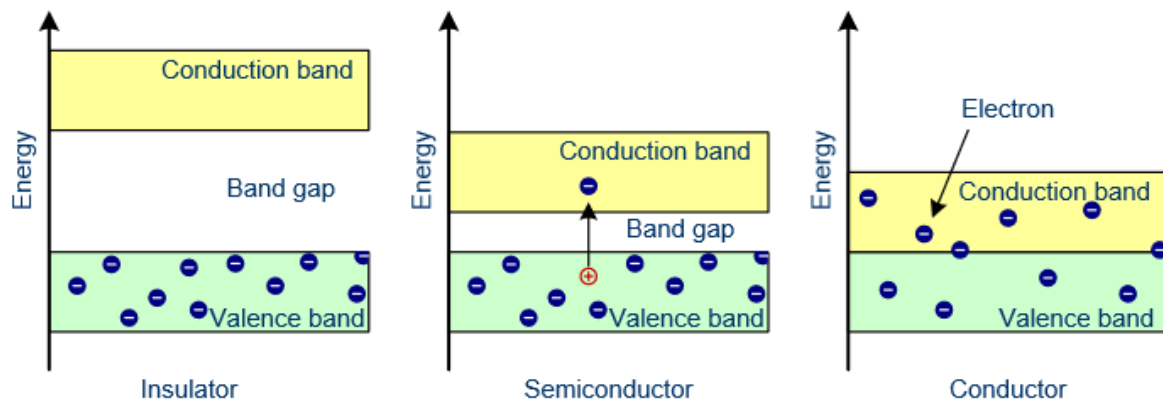


Figure 7 : Schematic representation of band diagram of Insulator (plastic), Semiconductor (ZnO, GaAs, GaN...), Conductor (metals) [46]

All kinds of atoms have electron(s) around the nucleus. There are mainly two bands, which are responsible for atomic bonds in molecules, these last are called valence bands. The external band contains free electrons, which can conduct electric current. This band is the conduction band. For a metal (conductor) the conduction band is not empty and contains electrons which is enough for certain electrons to be conductors. In an insulator such as glass, there are no free electrons that can access to the conduction band. In order to make a material conductor, it is possible to force the electron to go from valence to conduction band, by giving enough energy to the electron « travel ». This is done for instance by applying electrical voltage to the material, or thermal energy or light. In a semi-conductor, the application of a low voltage is enough to move electrons from the valence to the conduction band, and therefore to make it conductive. In an insulator, a very high voltage is required, well above the usual limits. For example, 220V is not enough for the rubber to be conductive, that is why it is a very practical insulator.

In a light emitting diode, the light is obtained at the junction, at the precise moment when an electron fills a hole, known as the hole electron recombination. It corresponds to an electron which passes from the conduction to the valence band, in other words it goes from an excited state (high energy level) to the ground state (lower energy level). Therefore, during the hole electron recombination, the excited electron loses a certain amount of energy to go back to the ground state. The energy loss can be then transformed in a photon. If this photon is in the visible range, the diode emits coloured light. In the case of LED, the light comes from the injection of the charges followed by the stabilization of the semiconductor by the electron hole recombination.

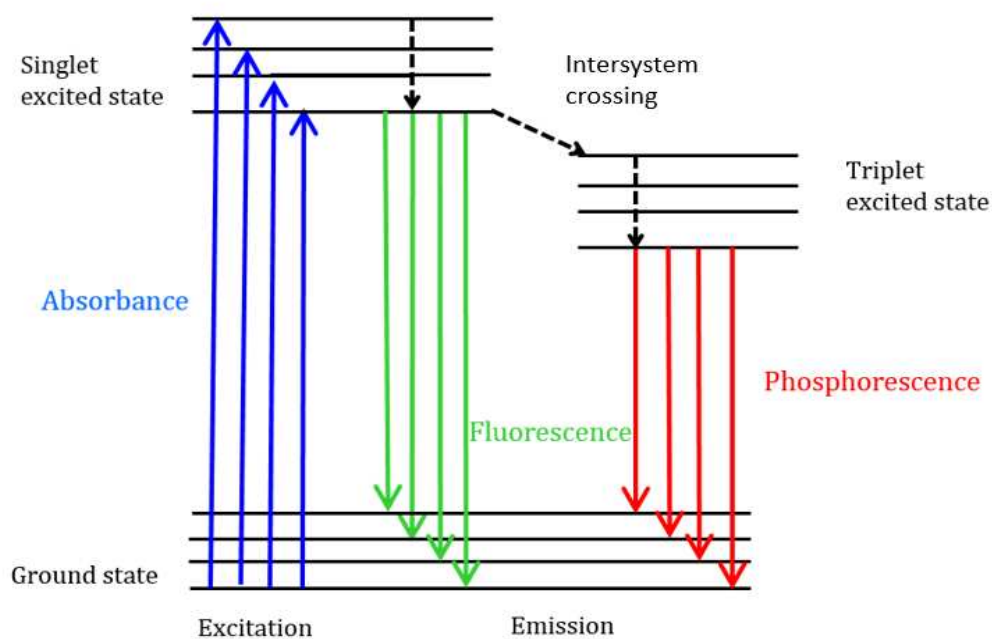


Figure 8 : Jablonski diagram illustrating absorbance (blue), fluorescence (green) and phosphorescence (red) according to the energy level transitions

There are four kinds of phenomena presented in the Jablonski diagram, which concern the emission of light. First, there is a passage on a higher energy level when an atom or a molecule absorbs energy which corresponds to an excited state. It can be electronic for atoms, electronic and/or vibrational for molecules. The excited state is thermodynamically unstable, atoms and molecules will very quickly restore the energy received and return to the stable ground state. The time interval between the absorbance and the release of energy is called the lifetime of the excited state. Usually, these are very short times,  $10^{-12}$ s for the vibration state,  $10^{-8}$  to  $10^{-9}$ s for the electronic state. The energy restitution takes place with two different processes: by photon emission via radiative processes which concern the luminescence phenomenon; or by heat emission via non-radiative processes (internal conversion or

vibrational relaxation). The radiative processes depend on the physical process which caused the excitation of the atom or molecule:

- Chemiluminescence : energy is created by an exothermic chemical reaction.
- Thermoluminescence : energy is created by heating.
- Bioluminescence : energy is created by reactions in living organisms (bacterias, plants and animals).
- Electroluminescence : energy is created by an electric discharge.
- Photoluminescence : energy is created by the absorbance of photons (fluorescence, phosphorescence, thermally activated delayed fluorescence).

The photoluminescence referred as "fluorescence" appears when the excited atom or molecule is in an excited singlet state energy level, and returns to the ground state via photon emission. In this case there is a big loss of energy due to the intersystem crossing from the excited singlet to the triplet state (~75% for organic fluorescent emitter), resulting that only 25% of the charges can potentially be transformed in photon from the excited singlet to the ground state. The phosphorescence phenomenon is close to the fluorescence one, but the excited singlet state is not the final state before emission. Indeed, by intersystem crossing, the charges pass from singlet to triplet excited state before producing the light emission. The phosphorescent materials are visible for longer time than fluorescent compounds after interruption of the excitation source, because phosphorescent lifetime are longer than fluorescent one [47]. An internal quantum efficiency of 100% can ideally be achieved from phosphorescent emitting materials, whereas it is much less for fluorescent emitters because of the loss of the charges. [48–51] The last radiative process discovered and understood respectively in 1961 and 1986 is the Thermally Activated Delayed Fluorescence (TADF). It presents much higher lifetime than phosphorescent and fluorescent processes. [52–55] Indeed, the process involves an emission of light due to the electron transition from excited singlet to the ground state. The difference with fluorescence is that TADF phenomenon uses intermediate transitions between excited singlet and excited triplet states which are called intersystem crossing (singlet to triplet) and reverse intersystem crossing (triplet to singlet). This way of light emitting avoids the loss of charges from singlet to triplet excited states, and then it increases the theoretical external and internal quantum efficiencies of the materials.

## b) The history of light emitting diodes

The first concept of electroluminescence was discovered in 1907 by Henry Joseph Round, when he applied 10 volts on SiC crystal which produced a yellow light and showed that semi-conductors (used for radio) emit light under electrical current. In 1921, Oleg Lossev confirmed the observations of Henry Joseph Round, as he created the first diode with SiC and ZnO crystals and wrote the first LED patent in 1927. Georges Destriau investigated the emission of ZnS by applying electrical current in 1936 and gave the meaning of the word electroluminescence. From 1955 to 1961, Rubin Braunstein discovered infrared emission from GaAs and other semi-conductors, and the infrared LED was created in 1961 by Bob Biard and Gary Pittman from Texas Instruments. Today, infrared LEDs are still used for remote control. Then in 1962, Nick Holonyak, considered as a father of LED technology, invented the first usable visible spectrum LED which was red, predicting that the light emitting diode will replace one day the classic incandescent bulbs of Thomas Edison. Additionally, Nick Holonyak communicated on the major breakthrough and interests of the LED, which are more sustainable, more efficient, and almost 80% more economic than the other technologies. Ten years after, George Craford made the first yellow LED by the development of nitrogen doped GaAsP [56], which was 10 times brighter than the red one. The green LED were also invented thanks to the GaP semi-conductor [57, 58]. In the 1990's, Shuji Nakamura invented the first efficient blue LED by replacing the classic SiC with GaN semi-conductor which opened the way for white LEDs used in common lighting. White LEDs have transformed illumination technology, including architectural lighting, indoor and outdoor lighting, traffic, and railway signaling. In another hand, Shuji Nakamura was also the inventor of the UV LED, which was used to purify water. [59, 60] At the same time, several new electroluminescent displays have emerged and are still under development nowadays, for instance: the organic LED (invented in 1987 by Ching W. Tang and Steven V. Slyke) [61], the iridium complex LED, the quantum dot LED, the perovskite LED and others, with their own benefits and drawbacks.

## c) Architecture and functioning of modern optoelectronic LED device using nanotechnologies

A common and regular optoelectronic architecture made in nanotechnology is illustrated by the upper figure. It is composed of different thin layers which all play important roles in the well functioning of the device. The whole device thickness is generally from 100 to 5000 nm,

depending on the way the materials were build, and on the final application. For instance, in LED, a voltage is applied at the electrodes to inject charges in the device. The charges travel separately from each electrode (blue) and are transported via the interfacial transport layers (orange), until they arrive in the emissive layer (green), where the recombination process operates and thus creates light emission. The light is emitted through the glass substrate, which means that the electrode on this side has to be a transparent electrode. In order to respect the efficient recombination of the holes and electrons in the emissive layer, it is important to have coherent thicknesses regarding the different materials which compose the device. The quality of the coated films must be as perfect as possible, namely smooth (pin-hole free together with low roughness). If the morphology of the layers is rough, meaning composed by aggregates, holes or defects, this leads to major electrical issues in the device, such as electrical shortages, electrical breakdowns, intense Joule effect and premature degradation of the materials. [61]

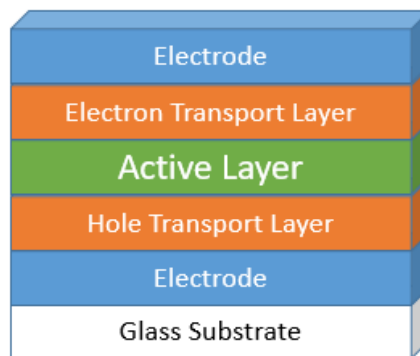


*Figure 9 : Regular optoelectronic device architecture, blue : electrodes ; orange : interfacial charge transport layers ; green : active layer*

Also, the architecture can be inverted, as the polarity can be reversed by switching the hole by the eletron transport layer. This kind of structure is used to improve some parameters of the device, such as stability which remains a challenge for development of many new LED technologies. [61] Such optoelectronic devices are characterized according to electrical values describing the behavior of the diode. For instance, the threshold voltage or working tension (volt) gives a value for which the LED lights up, and  $v$  is often reported as the beginning of the exponential intensity-voltage curve. The luminous efficacy (lumen/W) is the amount of light produced for each watt of electricity consumed. Another important value is the current efficiency given in candela/A. In the literature, luminance is characterized by value in candela/m<sup>2</sup>, and it is important to note that candela unit takes in consideration the human eye sensitivity, therefore, green light has higher candela luminance values than red or blue emitting devices, at constant efficacy. Thus, electroluminescence spectra or photopic coefficient must be evaluated in order to compare precisely two different LED perfomances. The external

quantum efficiency EQE is the most represented performance indicator to compare different LED. It gives the ratio of the emitted photons over injected charges. [62] The EQE(%) can be expressed as the product of four main influencing parameters:

$$\text{EQE}(\%) = \gamma \cdot \eta_{\text{rad,eff}} \cdot \eta_{\text{S/T}} \cdot \eta_{\text{out,eff}} = \text{IQE}(\%) \cdot \eta_{\text{out,eff}}$$

The first factor,  $\gamma$ , represents the electrical efficiency. It is linked to the injected charges that do not contribute to the recombination process for the light emission. Generally,  $\gamma$  is considered as the charge balance, and it depends on the transport charge properties of the different layers which compose the device. Furthermore,  $\eta_{\text{rad,eff}}$  the second factor is the effective radiative efficiency representing the competition between the nonradiative and radiative rates of the emitter. This can be either a singlet (fluorescence/TADF) or a triplet state (phosphorescence). The third factor,  $\eta_{\text{S/T}}$  relates the exciton rate that can unexcite radiatively due to the quantum mechanics spin selection rule. The factor  $\eta_{\text{out,eff}}$  is the outcoupling efficiency. It depends on the optical environment and on the orientation of the transition dipole moment of the emitters. [62] Internal quantum efficiency IQE is the ratio of electronic charges collected to the incident and absorbed photons. Other efficiency appellations are found in the literature such as the photoluminescence quantum yield  $\Phi_{\text{PL}}$ , which is translated as the ratio of the number of emitted photons to the number of absorbed photons per unit time.

Furthermore, the color of the emitted light is evaluated using the CIE (Commission Internationale de l'Eclairage) diagram, as presented by the following figure 10. The window to achieve white (warm or cold) light display is very narrow and the proportion of blue, green and red emitters must be accurate.

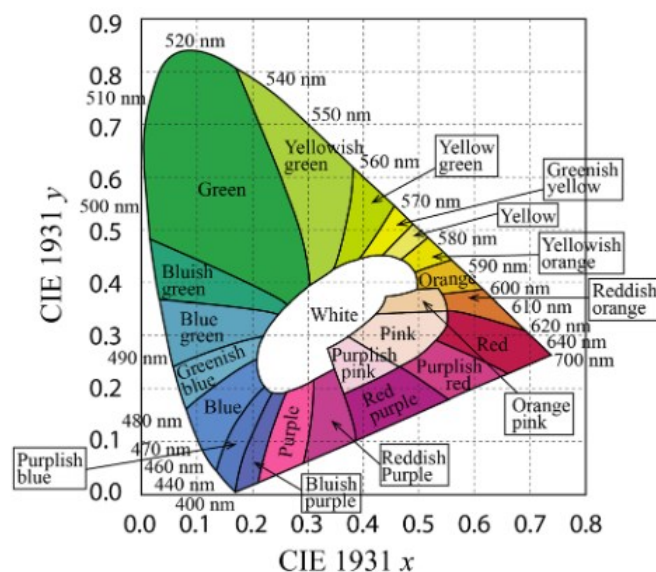


Figure 10 : Commission Internationale de l'Eclairage CIE diagram [63]

### 3) Deposition techniques and interfacial materials

#### a) Deposition technics of the layers

In perspective of building an optoelectronic device, the nanosciences and nanotechnologies are very useful thanks to their special properties. The as-synthesized molecules or nanoparticles can be used as emissive layer material, as interfacial layer, or even as electrode (transparent conductive oxides, metal, graphene oxide). [64, 65] The nanotechnology skills allow a very precise and controlled elaboration. In research field, one of the most used technics is the (thermal) evaporation, which allows the construction of smooth and homogeneous layer with an extreme accuracy regarding the thickness. The solid source is heated until the material turns into a gas phase and then condenses on the surface of the substrate. Even if evaporation process is very advantageous by the quality aspects, it remains highly energy consuming, because a high vacuum ( $\sim 10^{-6}$  mbar) is required to avoid any contamination. The evaporation process can operate at a large scale, but it demands huge amount of energy, which is contrary to the ideas about reducing energy consumption and global warming effect [66, 67]. To reduce the manufacturing costs, solution processing of materials is widely considered. There are mainly four techniques among others (figure 11) to deposit nanomaterials by solution process : spin-coating for small area, doctor blade coating, screen-printing and ink-jet printing for larger surfaces. These elaboration techniques are represented by the following figure.

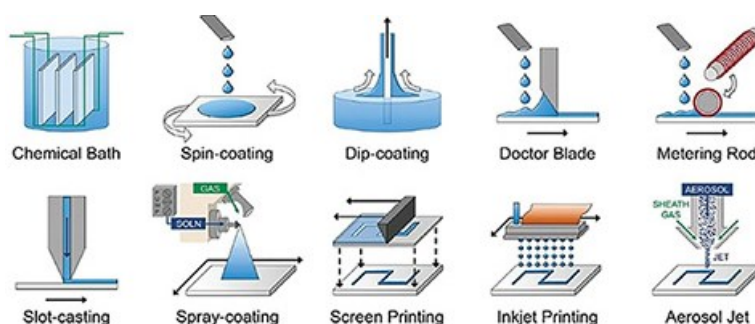


Figure 11 : Deposition techniques by solution process, for elaboration of optoelectronic devices, (a) spin-coating ; (b) doctor blade coating ; (c) screen-printing ; (d) ink-jet printing copyright 2011, Royal Society of Chemistry.

Concerning the morphology of the thin film, these liquid methods highly depend on the deposition speed and the time of the process, also on the viscosity and the concentration of the coated solutions, and finally on the drying speed. The solution process has the advantage

to be more economic because it consumes less energy, but still the morphology of the film remains smoother for the evaporation method. [68–70] All the processes can be operated in air, or for better stability and performances in a controlled inert atmosphere (glovebox).

#### b) Materials for light emitting diode made by nanotechnologies and their processes

In LED device, interfacial transport layers are not mandatory, but they help to enhance the performances, such as the brightness, the threshold voltage and the other parameters. The thickness of the transport layers is generally thin, typically below 40 nm. These materials must be as transparent as possible, to avoid photon absorption / emission, and also be highly conductive to provide efficient charge transport. For instance, metal oxide nanoparticle solutions are widely used in optoelectronic devices as electron or hole transport layers because of their transparency and conductivity properties: ZnO, NiO<sub>x</sub>, ZrO<sub>2</sub>, TiO<sub>2</sub>, HfO<sub>2</sub>, SnO<sub>2</sub>, WO<sub>x</sub> nanoparticles are mainly reported. [71–76] For examples ZnO, TiO<sub>2</sub> and SnO<sub>2</sub> are low work-function and n-type oxides, which offer electron transporting and hole blocking properties and thereby can be applied as electron transport layers. Nevertheless, WO<sub>x</sub>, V<sub>2</sub>O<sub>5</sub>, and MoO<sub>x</sub> are n-type oxides but with high workfunction, these oxides do not have the electron block property, and are commonly used as hole transport layer. In opposite, the NiO<sub>x</sub> is a p-type semiconductor with a wide bandgap and work function, it has the properties of hole transporting and electron blocking and thus is used as hole transport layer. [77–79] However, very often, to be well-processed, these metal oxide nanoparticles need to be stabilized in solution by surface ligand in order to have homogeneous sized nanoparticles and make smooth thin films. Few strategies have been developed and are presented in the following figure 12 to avoid aggregation of the nanoparticles in solution.

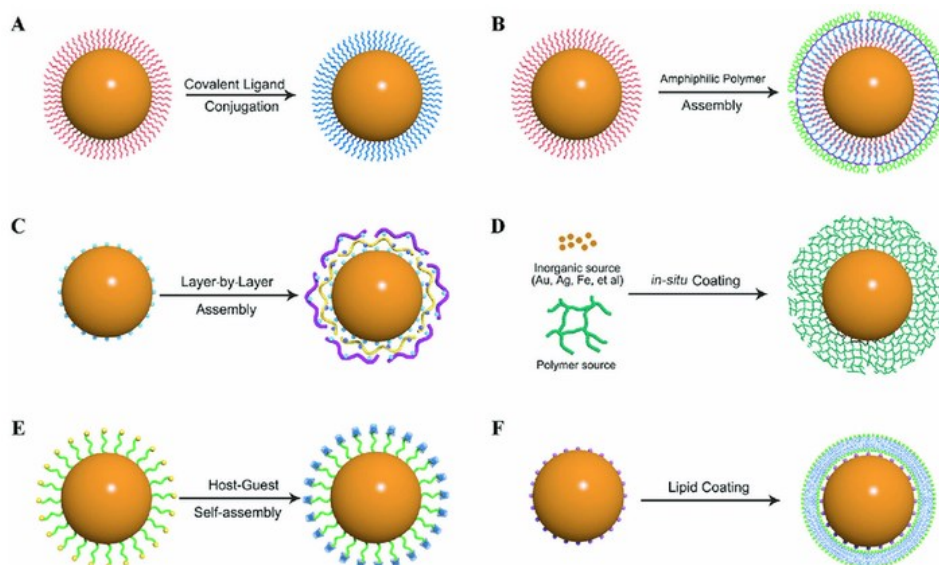


Figure 12 : Different strategies to graft ligand on surface of nanoparticle, A : Covalent ligand bond ; B : Amphiphilic polymer assembly ; C : Electrostatic layer-by-layer assembly ; D : In situ ligand coating during synthesis ; E : Host-guest supramolecular ligand self-assembly ; F : Lipid shell coating. [80]

Effectively, the previously presented metal oxides such as ZnO nanoparticles can be functionalized by covalent ligand bond. In another hand, it is common to add surface ligand during synthesis process for instance in the case of inorganic quantum dots perovskites. The grafting unit of the ligand is often a hydroxy group from a carboxylic or a phosphonic acid. Moreover, in literature, efficient ligand are often composed of long alkyl chain [81, 82]. The Layer-by-Layer Assembly process is more often used for the medical field, to build dendrimers to treat cancers and strong diseases [2, 26].

Depending on the process, the metal oxide nanoparticles require surface stabilization thanks to a ligand. Most often, for solution process metal oxides, a stabilization needs to be done to have homogeneous objects in solution and to obtain further smooth layer. However, for evaporated metal oxides it does not need surface stabilization, it is the case of  $\text{MoO}_x$ .

#### Hole transport materials:

Suitable polymers are also widely used as transport layers, for instance the poly(3,4-ethylenedioxythiophene) polystyrene sulfonate (PEDOT :PSS) or N,N'-Di(1-naphthyl)-N,N'-diphenyl-(1,1'-biphenyl)-4,4'-diamine (NPB) for hole transport. Metal oxides (nanoparticles) such as  $\text{NiO}_x$ ,  $\text{WO}_x$ ,  $\text{MoO}_x$  and else are also employed as hole transport materials.

### Electron transport materials:

Some polymers are used as electron transport / injection materials in LED device, such as the 2,2',2''-(1,3,5-Benzinetriyl)-tris(1-phenyl-1-H-benzimidazole) (TPBi), Poly(9,9-bis(3'-(N,N-dimethyl)-N-ethylammonium-propyl-2,7-fluorene)-alt-2,7-(9,9-dioctylfluorene)) (PFN) and N,N'-Bis(N,N-dimethylpropan-1-amine oxide)perylene-3,4,9,10-tetracarboxylic diimide (PDINO). [83]

Metals or metallic complexes can also play the role of transport layer such as calcium, cesium, tris(8-hydroxyquinoléine) aluminium (III) ( $\text{Alq}_3$ ), Copper(II) phthalocyanine (CuPc). Furthermore, buffer layers are sometimes employed as additional films to enhance the performances and allow a better electrical behavior in the device, avoiding recombination charges in an undesired place, for instance in the interfacial layers. The main used ones for LED are bathocuproine (BCP), lithium fluoride (LiF), cesium fluoride (CsF), and some metal oxides nanoparticles [77–79, 84, 85] Metal oxides nanoparticles such as  $\text{ZrO}_2$ , ZnO,  $\text{SnO}_2$ ,  $\text{TiO}_2$  and else are also employed as hole transport materials.

### Electrode materials:

According to the literature, the silver and aluminium are the most used materials as top electrode in LED device. The ITO Indium Tin Oxide is widely employed as transparent electrode in optoelectronic devices (solar cells, photodetectors, LEDs...). ITO is a rare material which cannot be used in the future as the quantities are limited. However, it is the most suitable material nowadays because of its easy manufacturing, transparency and conductivity properties. [86] Consequently, investigations have been done to replace ITO, and the best candidates are graphene oxide, silver nanowires, Fluorinated Tin Oxide FTO and carbon nanotubes [64, 65, 86–89].

The energy levels of these materials are shown by the energy diagram of the figure 13.

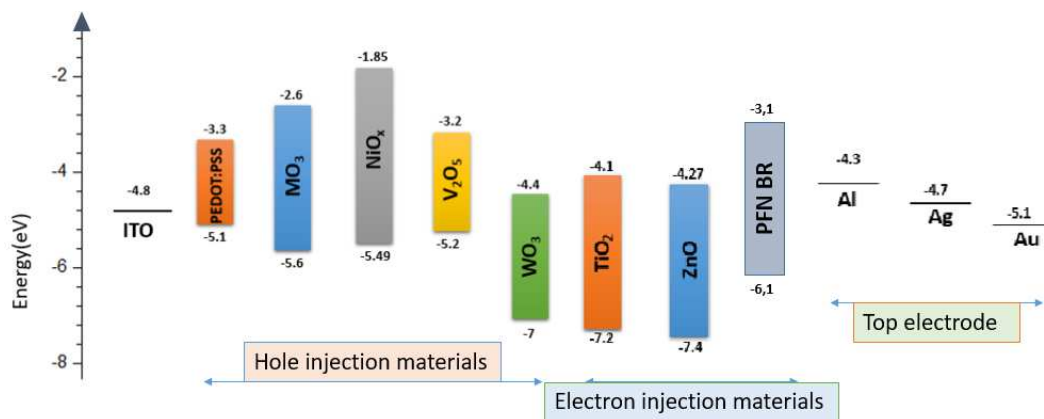


Figure 13: energy diagram (eV) of the hole and electron injection materials, and the different used top electrodes.

The different materials used for the electroluminescent active layer in LED are presented in the following part which highlights the different LED technologies with their advantages and drawbacks.

#### 4) The different emissive materials in LED technologies

Silicium carbide and gallium doped semiconductors were the first inorganic electroluminescent materials discovered. Since then, strong improvements of the performances and properties in LED technology have been done. In recent years, new solution processed semiconductors such as TiO<sub>2</sub>, ZnO and others have achieved rapid progresses due to their high performances and low cost compared to the commercially available semiconductors such as gallium derivatives.

Different LED technologies are presented in this part with their advantages and drawbacks, as well as the methods to build white LED. They can be classified in three families of emissive layer, namely the inorganic LED, the organic ones and finally the hybrid organic-inorganic devices. Some differences exist between inorganic LEDs and organic LEDs. The first one is the architecture of the device. According to the literature, inorganic LEDs are fabricated by growing inorganic layers on substrates of sapphire, silicon, or GaAs wafers [90], while OLEDs are built by the stacking of organic carbon-based electroluminescent materials on a glass or plastic substrate. Moreover, OLEDs can be processed on larger area, they are surface lights, and thanks to the properties of organic material, they can be made very thin (below 500 nm device thickness) and flexible. The flexibility of the devices is an additional problem as far as the substrate is unstable, and it degrades by time and under ambient conditions. [91] Additionally, in the case of OLED, the influence of the temperature is less significant than in inorganic LEDs, a reason for this being their large surface area, which improves the thermal convection and provides a low voltage application. Therefore, the OLEDs are intended to replace large scale light sources for indoor lighting but also for decorative and mood lighting applications. Regarding the manufacturing, OLEDs are recyclable and cheap because of the abundance of the materials. On another hand, inorganic LEDs present higher performance and better spectral purity than OLED. Their manufacturing costs remain also higher with higher energy consumption than OLED. Also, inorganic LEDs are used very often as point light sources ( $\mu$ LED) [92], and are mainly applied in residential, commercial, and street lighting. [93]

The following sub-sections will now introduce the different LED technologies, with their advantages, drawbacks and also their performances.

### i) Heavy metal polymer complexes

Iridium based electroluminescent materials are known to be very efficient and therefore used as fluorescent, phosphorescent or TADF emitter in LED. Usually, the heavy metal is incorporated as a host in a polymer matrix (guest). Thanks to the energy transfer from the matrix to the iridium complex, the light is emitted. Ir(III) emitters can harvest both singlet and triplet excitons for light emission with theoretical internal quantum efficiency IQE of 100%, the characteristic of TADF effect. [94] The iridium materials present many advantages in terms of electrical performances, such as a long lifetime, a spectral purity with narrow emission band, a high brightness thanks to the property of the heavy metal, a high efficiency and a good stability requiring minimal encapsulation compared to classic organic LEDs. For instance, in the literature, it is often found EQE value around 30 %, with luminance values about 50.000 cd/m<sup>2</sup> [95] for turn-on voltage of 3,0 volts and high stability above 50.000 hours [96]. The wide interest for heavy metals such as iridium [96], ruthenium [97], copper [98], europium, platinum [99] integrated inside a polymer to form an emissive complex lead toward a fast development of the technology. Therefore, there is a large panel of synthesized and used iridium complexes which covers the full visible light spectrum, with some examples illustrated in the following figure 14 : iridium complexes blue [100, 101], green [102] and red [95].



Figure 14 : structure of iridium complexes with spectral emission in the region of a) blue, b) green c) red [95, 100, 102]

As previously explained, one of the main goals for LED development is to achieve a white LED. As the literature shows, the color is tunable according to the structure of the complex, and there are mainly three approaches to build white inorganic iridium-based LED. The first is

the combination of one phosphorescent iridium complex (most often yellow, orange or red) on a blue emissive GaN chip. Then, double or triple colored phosphorescent organometallic complexes can be associated with blue GaN chips. The building of the device is processed by mixing the organometallic complexes with an epoxy resin and then coated on the surface of blue GaN chips. Also, it can be vacuum deposited or spincoated as emissive material on PEDOT:PSS hole transport layer (see below organic LED part). [99, 103–109] However, even if this lighting technology is very attractive and efficient, it remains very challenging for future because of important drawbacks. Indeed, this LED technology faces moisture sensitivity, thermal degradation, and quenching sometimes even at low temperatures, depending on the structure of the organometallic complex. Another significant disadvantage is linked to the combined thicknesses of many emissive layers in the device which causes an increase in operating voltage. [104, 110]. The major issue is related to the heavy metals themselves. The purchasing price is high because these materials are very rare and not abundant on Earth. Also, it is very polluting to harvest and transform these heavy metals from raw to usable materials for LED. Consequently, the large-scale manufacturing process for white LED is not easy to implement and is hard to operate even at a small scale, especially with the limited quantities of GaN chips and other rare compounds (heavy metals, electrodes, semiconductors...). On another hand, some other metal ions such as  $\text{Cu}^+$ ,  $\text{Eu}^{3+}$ , or  $\text{Pr}^{3+}$  are used to face the lack of iridium and show encouraging results [111, 112].

## ii) QDLEDs Quantum Dot LEDs

Quantum Dot (QD) nanocrystals are a class of nanomaterials with in general a size between 1 nm and few tens of nm. The combination of several inorganic materials, for instance Zn, Cd, Pb with S, Se or others leads to an emissive semiconductor nanocrystal. There are various existing QD materials such as ZnS, ZnSe, CdS, CdSe PbS, CdSe, InP and many others, briefly illustrated by the transmission electron microscopy images below [113]:

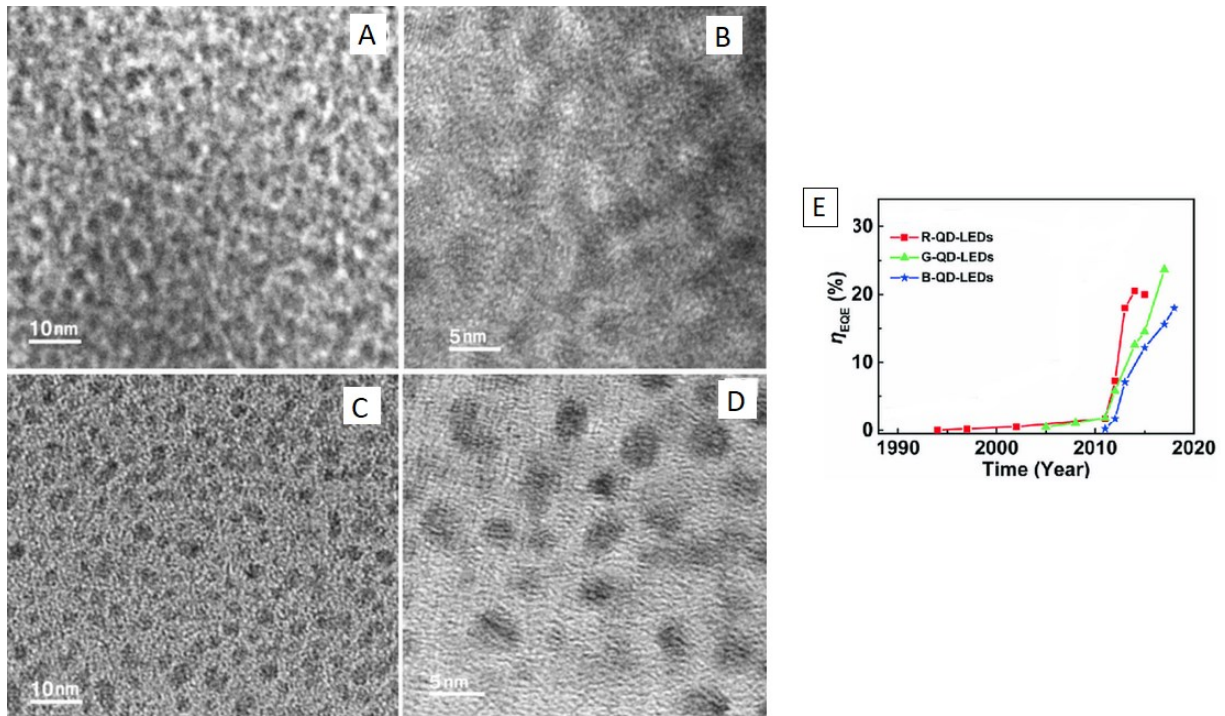


Figure 15 : transmission electron microscopy images : (a,b) : CdSe QDs (c,d) CdSe/ZnS core shell QDs [113], (e) external quantum efficiency evolution of QDLED red, green, blue over the years [114]

QD technology is very promising approach for future LED applications as it uses the benefits of the nanoscale and more precisely the increasing surface/volume ratio compared to micro materials, in order to gain electrical and optical properties. Also, the color is easily tunable from ultraviolet to near infrared wavelengths, opening the way to a wide panel of applications. These QDs are characterized by narrow emission peaks with a width of 50 nm for some materials which is difficult to achieve by other technologies (organic or conventional phosphorescent emitters). According to the structural and composition parameters of the QD, the color can be tuned, for instance CdSe nanocrystals cover the full visible light spectrum by variation of the nanoparticle size : 1 nm diameter gives blue emission while 5 nm gives red. [96, 115] Additionally, the association of two inorganic materials in certain cases can be named a core-shell nanoparticle. The QD LEDs using core shell structures extends photoluminescence lifetime and minimizes drastically non radiative Auger recombination of the charges by separation of hole electron pairs in the core (CdSe) from surface defects on the shell (CdS, ZnS, PbS). [116–118] With optimized surface chemistry, core shell QDs show near 100% photoluminescence yield and represent the best choice as emissive materials for QDLEDs, especially for commercialized products such as quantum dot TV or flexible smartphone from Samsung [95, 118]. Indeed, due to their quantum properties, the QDs are known in the literature to be highly emissive materials with excellent colour tunability and

saturation, high photoluminescence quantum yield with electrical and thermal stabilities [119–122]. The commercial QDs are known to be very efficient in photoluminescence, but it is not the case about their electroluminescence properties which are still under development. During the last ten years, the QDLED is among the best lighting technologies with low operating voltage and EQE above 20% for red, green and blue emitters (figure 15E) with more than 10,000 cd/m<sup>2</sup> for each. It is important to take in consideration, in order to build white QDLED, that most often, blue QDs offer lower performances than red and green QDs when used in device, namely EQE and luminance values [123]. In 2019, huge luminance peak values were achieved in the literature [123], for instance 350,000 ; 650,000 and 60,000 cd/m<sup>2</sup> respectively for red, green and blue QDLEDs [124–129]. More importantly, the total thickness of QDLEDs is generally below 300 nm and QDs are solution processable, promising low cost and large-scale manufacturing into solid state devices, for instance via printing. [130] However, the large-scale process remains challenging for this technology even if the materials are abundant, due to the toxicity of some materials such as Pb, Cd and the employed solvents. Also, the inkjet printing, which is used to deposit the electroluminescent layers has many problems such as low resolution, poor uniformity, and is far from mature for mass-producing QDLEDs. [131, 132]

Additionally, according to their optical properties and sizes, a same QD material presents different degradation speeds. Indeed, the blue QD represents generally smaller size and lower stability due to the increasing surface quantum effect compared to the red and green ones, leading to premature degradations of the nanocompounds. Consequently, blue QDLEDs are complicated to process as the blue QDs are unstable. The stability depends also on the used QDs, for instance ZnS nanocrystals are known to be very stable, but some other QDs can degrade by time, UV exposure and oxygen contamination [133]. To face this stability problem, some techniques have emerged such as the employment of better covalent grafted ligand, most often carboxylic or phosphonic acid on the surface of the QDs. [132, 134–137]

The white QDLED is often manufactured by the stacking of RGB layers [119], by RGB « pixels » for micro QDLED [138], or by the combination of different QDs in a same photoluminescent solution. [139] Today, the QDs are mainly efficient in photoluminescence, but it is not the case regarding the electroluminescence, which induces an important research mobilization.

### iii) PeLEDs Perovskite LEDs

Perovskite nanocrystals are a class of QD materials with a size between 1 and 15 nm, that can be fully inorganic, or organic-inorganic hybrid with ABX<sub>3</sub> structure, where A is an organic

or inorganic cation, B is usually Pb, and X is a halide (Cl, Br or I<sup>-</sup>). The full inorganic perovskite structure adopts the cubic or orthorhombic crystalline phase. Their cubic crystalline structures are competitive and used in a wide range of applications such as optoelectronic devices: lasers, solar cells, photodetectors, and LEDs. The orthorhombic phase is more stable thermodynamically below  $T < 320^{\circ}\text{C}$  and thus, under ambient conditions, the cubic phase transforms via oxygen contamination, UV exposure and time. [133] The following figure 16 illustrates the different existing materials for perovskite structures and shows transmission electron microscopy image from red cubic CsPbI<sub>3</sub> and their emission properties.

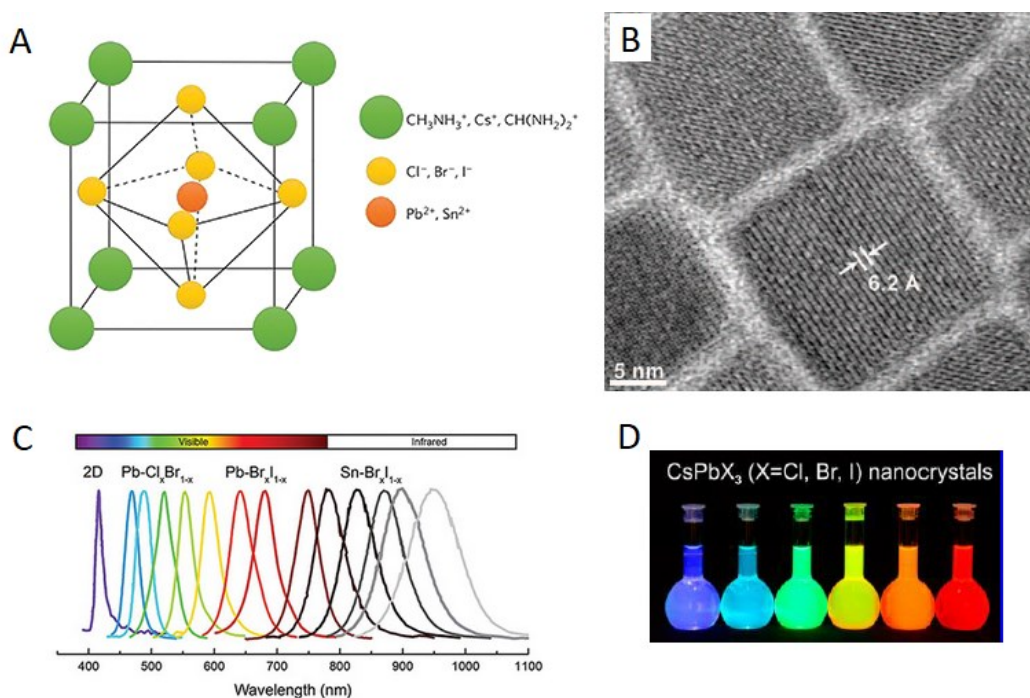


Figure 16 : A : perovskite structure with the different existing materials [140] ; B : transmission electron microscopy image from red cubic CsPbI<sub>3</sub> [133] ; C : [140] ; D : [141] perovskite QD emission according to their structures.

### Advantages:

Syntheses of perovskite QDs, nanowires, or quantum wells are possible via simple colloidal methods. [133] Metal halide perovskites are emerging nanomaterials with potential for low cost manufacturing from abundant raw materials compared to the commercially available semiconductors and with a high energy efficiency. Metal halide perovskites are direct band gap semiconductors, and thanks to their defect tolerant properties, these materials are highly efficient in electroluminescence with large charge carrier diffusion length, long carrier lifetime and high quantum yield efficiency. The emission of the perovskites is very pure and narrow with 10 to 100 nm spectral width depending on the size dispersion and on the chosen

compounds. The emitted colour is controlled from violet to near infrared by changing the size of the QDs, their dimensions (3D, 2D) and the halide composition, thus allowing an « easy » white PeLED manufacturing [133, 140, 141]. Moreover, these nanomaterials are solution processable with low device thickness (below 300 nm), meaning low building prices which open an easy large-scale production. Additionally, the quantum properties of the perovskites and the thin film thickness allow the construction of flexible devices [128]. These characteristics make perovskites competitive with currently existing light-emitting optoelectronic devices such as OLED and QLED, and some of them are presented in the following figure 17. [133]

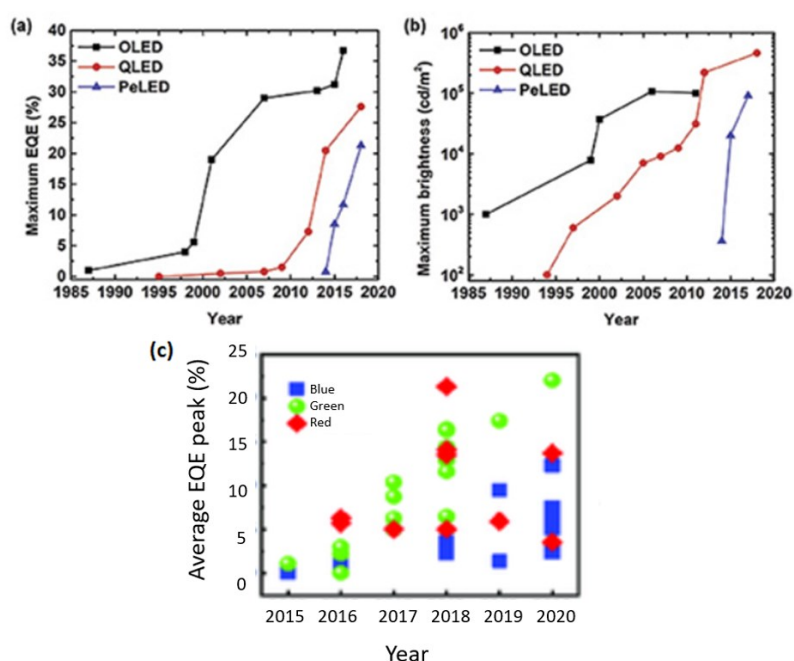


Figure 17 : Performance comparisons over the years of organic OLED, quantum dots QLED and perovskites PeLED (a) maximum EQE % (b) maximum brightness cd/m<sup>2</sup>. [140–144] (c) average peak EQE % depending on the color of PeLED in the last 5 years [145]

### Drawbacks:

In another hand, this technology suffers from several disadvantages such as stability: perovskites materials are highly sensitive from moisture and UV exposure and are redox active [146]. The premature degradation of the nanocrystals occurs by the transformation of the cubic crystalline structure, to the orthorhombic phase for the cesium lead halide perovskites. Some strategies have appeared to use surface ligand in order to stabilize the cubic phase, to increase the charge carrier confinement and to limit the formation of defects and the ions

migration. The surface ligand directly influences the aggregation growth and the optical properties of the perovskites. [147] Additionally, it was shown that mixed halide or cation perovskite structures demonstrate higher ambient stability. [148, 149] The stability of PeLED can be improved by recent new approach as the reduction of the dimension of the material. Indeed, morphology engineering has been developed such as 2D PeLED to limit the density of the defects and also for their better stability under moisture condition due to their higher formation energy. In details, the 2D structure leads to an increase of the quantum and dielectric confinements thanks to the large molecules (it mainly uses long-chain ammonium inserted between perovskites such as phenylethylammonium, naphthylmethylammonium, butylammonium) which allow to separate the structure into 2D sheets/arrays, which are insulating materials and with a dielectric constant strongly different from the perovskite crystal. Therefore, this makes possible to confine the charge carriers in the sheets. [147, 150–152] Also, the higher exciton binding energy of 2D perovskites leads to the improvement of the electroluminescence efficiency of PeLED [153]. In addition, the large-scale manufacturing is not only affected by the stability of the PeLED but also by the toxicity of the elements such as Pb which is highly soluble in water.

#### Performances:

In terms of device performances, all inorganic cesium lead halide QDs attracted much attention due to their improved thermal stability. [154] The scientists have achieved EQE values above 20% for red and green QDs, and below 20 % concerning blue perovskite QD. Low operating voltages about 2,0 to 3,0 V and maximum brightness over 100,000 cd/m<sup>2</sup> have been reported for the PeLED [140–144]. Moreover, the blue QDs presents lower performances than the red and green emitters, that can be explained by the smaller size of the QDs and the higher defect density. It is known that the phase stability of these nanocrystals is directly associated to the composition of the perovskite material. [155] Approaches have been carried out in the literature to develop Pb free perovskites as Cs<sub>3</sub>Cu<sub>2</sub>I<sub>5</sub>, Rb<sub>2</sub>CuX<sub>3</sub>, K<sub>2</sub>CuX<sub>3</sub>, X = Br, Cl, CsSnX<sub>3</sub> X = I, Br with photoluminescence quantum yield comparable with lead halide perovskites even if their PeLED performances remain lower [145, 156–159].

#### White PeLED:

The white PeLED can be built with three methods: the first is to use perovskite QDs as individual pixels RGB, the second is to mix the emitters together in a same solution and to coat them, or the third is to build RGB multilayers. [160–162]

#### iv) Organic LED OLED

In 1960, Martin Pope from New York University first developed an injecting ohmic electrode in contact with an organic crystal of anthracene, and three years later he observed the electroluminescence under vacuum from this kind of organic crystal, using silver electrode and small area device [163, 164]. This first achieved OLED had poor performances and ultra high operational voltage, noneoftheless this was a proof of concept. Later, in 1987, the first double layer OLED with separate hole and electron transporting layers was reported [165]. In this device, by applying an electric field in an OLED, holes are injected through the highest occupied molecular orbit (HOMO) while electrons through the lowest unoccupied molecular orbit (LUMO). In the end, the charges recombine in the organic emissive molecules (in the emissive layer).

##### Material characteristics:

The emission band is usually determined by the type and the structure of organic molecule in the active layer, but also by the energy difference of the HOMO and LUMO levels of the organic material. Namely, high energy represents the blue color, while low energy a red emission [166]

The OLEDs are classified in three families: the first generation are the fluorescent compounds, such as anthracene which are the less efficient [163, 164], the second is related to the phosphorescent emission process, and more recently the performant thermally activated delayed fluorescence (TADF) materials. The OLED families are classified depending on the emission phenomenon, but also on the values of internal efficiency. For instance, fluorescent emitters are generally less emissive than phosphorescent or TADF ones, even if there are fluorescent emitters with almost 100% photoluminescence quantum yield treated in the results part. Independently of their efficiency limitation (due to 25% singlet against 75% triplet loss), the fluorescent materials take advantage of long lifetimes for stable blue emitters [167]. Some examples of phosphorescent or TADF emitters are organo metallic complexes presented before, but also, it exists TADF [168–170] or phosphorescent efficient molecules without any heavy metals [171, 172].

Moreover, the organic emitters can be arranged in three kinds of materials: conjugated dendrimers, conjugated polymers, and small molecules. Small molecules are usually evaporated materials with low molecular weight, for instance the Biphen, AlQ<sub>3</sub>, or CuPC. Conjugated polymers are semi crystalline and widely used in the literature, such as the solution processable poly(n-vinylcarbazole) PVK, or Poly(9,9-dioctylfluorene-alt-

benzothiadiazole) F8BT, that can be employed as pure active layer, or as emissive host matrix for the incorporation of additional emissive compounds (guests), such as dyes or QDs. [173, 174] Dendrimers are amorphous branched molecules consisting of light emitting cores to which one or more branches (dendrons) are attached. The dendrimer composition allows accurate modifications of the core for the management of the emitted light. The branching groups are there to control the charge transport, and the processing / solubilization properties can be modified by the utilisation of surface groups. [166] Dendrimer nanocompounds are often used in the medical or biological field to treat strong diseases. [175]

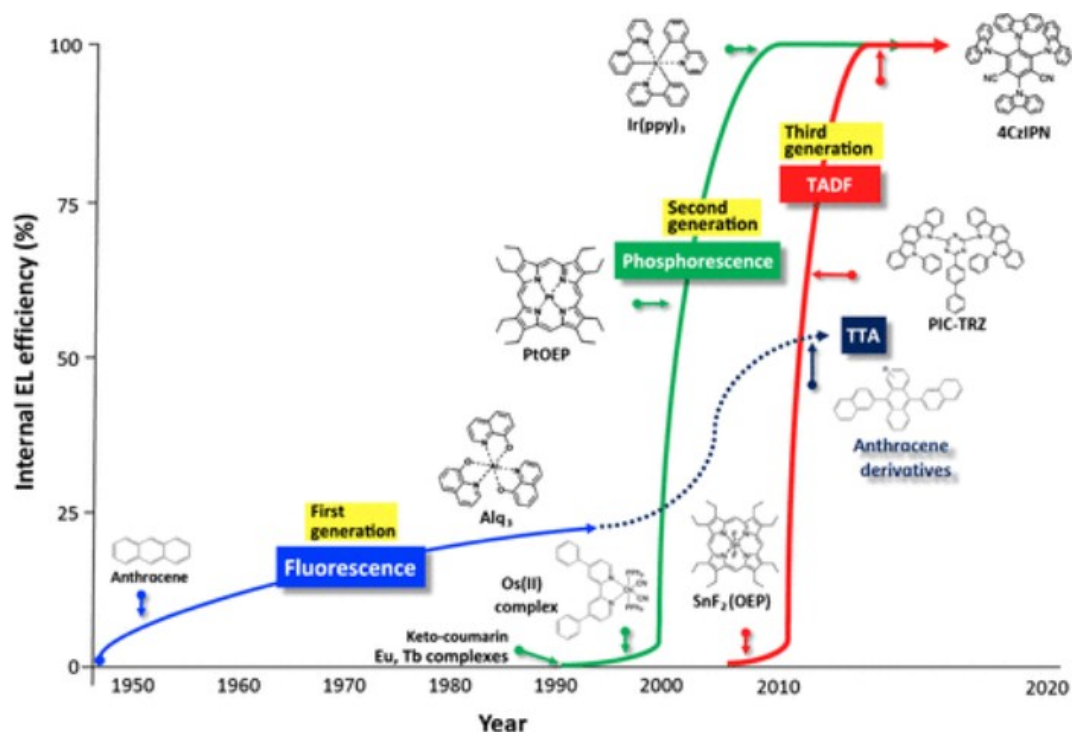


Figure 18 : different generations of OLED over the years, classified by internal efficiency %, blue fluorescence, green phosphorescence, red TADF [176]

Over the past 25 years (figure 18), the research and development of OLEDs became very important for industry and academia. OLED is one of the most efficient and sustainable LED technology for the future challenges of our society, such as global warming. OLED displays offer some features that grant them superior properties against approved technologies such as liquid crystal displays (LCD), because OLEDs do not require a backlight system in comparison to LCDs. [177, 178] Also, some organic emitters are very cheap and often eco friendly materials, in addition to be easily recyclable in comparison to all other LED technologies.

### Performances of the OLEDs:

The manufactured OLEDs are usually very thin, below 500 nm, with wide viewing angles, high contrast colors, and fast response time. The most performant emissive materials are still processed via evaporation method, but some emissive materials are solution processable, which makes this technology very attractive for large scale production, with the different printing skills.. Additionally, organic light emitting technology opens the possibility to realize transparent and flexible devices. For instance, nowadays commercial high-end smartphone, smartwatches, or smart OLED TV show that OLEDs are already present in our life. Even if this technology has been developed until commercial applications, it suffers from several drawbacks, and need to be improved to continue the competition. Indeed, the luminescence emission of organic compounds is wide and less pure than QDs meaning that the white OLEDs have worst quality than the other technologies such as QDLEDs or PeLEDs, as illustrated in the following figure 19.

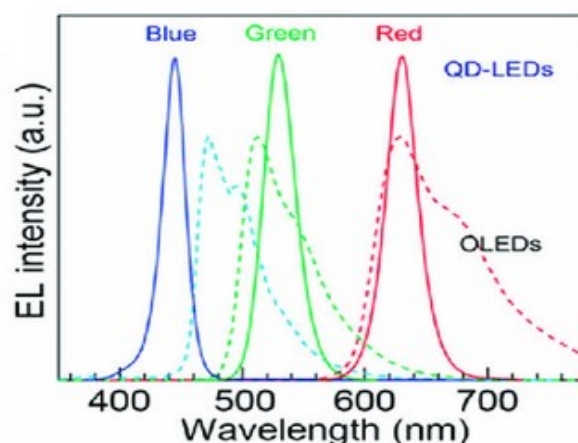


Figure 19: QDLEDs (continuous) vs OLEDs (dashes) emission field comparison [114]

The major disadvantage is related to the organic compounds which are highly UV and moisture sensitive, unstable chemically and thermally, requiring encapsulation of each device. Additionally, the blue organic emitters offer worse stability than green and red ones. In the literature [179, 180], some investigations have been found about the stability of different coloured fluorescent and phosphorescent emitters used in OLEDs.

Table 1 : half lifetime  $T_{50}$  (hours) of organic emitters red green blue (phosphorescent/fluorescent) and their CIE coordinates [179, 180]

Color \ OLED	PhOLEDs		Fluorescent OLED	
	1931 CIE coordinates	$T_{50}$ [h]	1931 CIE coordinates	$T_{50}$ [h]
	Red	(0.64, 0.36)	900 000	(0.67, 0.33)
Green	(0.31, 0.63)	400 000	(0.31, 0.63)	200 000
Blue	–	<100	(0.14, 0.12)	11 000

As expected by theory, phosphorescent emitters are globally more stable than fluorescent ones and the blue emitters are less stable than the two other colors. This can be explained by the homo lomo energy difference, which is higher for the blue emitters [181]. This high energy leads to problems regarding the operation lifetime because of the too fast degradation of the material. Also, blue emitters face more electrical issue and performance losses under a high voltage [182]. Therefore, the reduction of the operational voltage is crucial to improve power conversion efficiency and to avoid early degradation phenomenons. The stability of OLEDs is worse than the QDLEDs, because of the organic nature of the compounds, but it can be improved by the engineering of the device architecture, by encapsulation of the OLED, or by the chosen materials.

In 2021, most of the OLEDs are still limited between 20 to 35% EQE [178, 183] due to the outcoupling efficiency factor, the different refractive indexes and the absorption of the layers composing the device. However, in the literature, some OLEDs were achieved with very high EQE, sometimes above 50% with low operating voltage around 3V thanks to the use of oriented emitters [184]. Some examples of organic emitters used as electroluminescent material in OLED, from the 1<sup>st</sup> to the 3<sup>rd</sup> generation are presented with their EQE in the following figure 20.

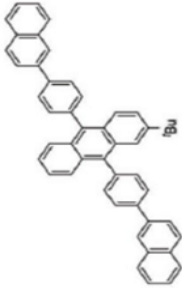
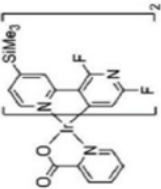
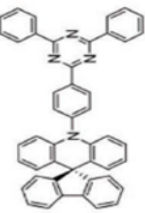
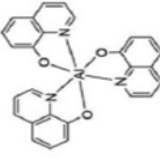
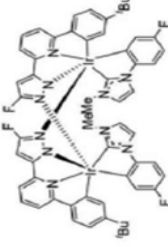
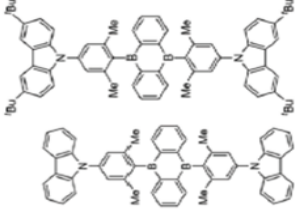
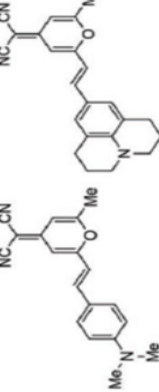
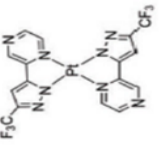
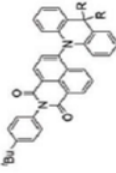
OLED emissive materials	1 <sup>st</sup> generation based on fluorescent emitters	2 <sup>nd</sup> generation based on phosphorescent emitters	3 <sup>rd</sup> generation based on TADF emitters
Blue	 <p><b>Bu2NapAn</b>  <math>\lambda_{em} = 444</math> nm            EQE = 5.17%  <i>J. Mater. Chem.</i> 2010, 20, 1560–1566.</p>	 <p><b>Ir-2</b>  <math>\lambda_{em} = 450</math> nm            EQE = 31.9%  <i>Adv. Mater.</i> 2019, 31, 1908102.</p>	 <p><b>spiroAC-TRZ</b>  <math>\lambda_{em} = 480</math> nm            EQE = 36.7%  <i>Adv. Mater.</i> 2016, 28, 6976–6983.</p>
Green	 <p><b>Alq3</b>  <math>\lambda_{em} = 550</math> nm            EQE = 1%  <i>Appl. Phys. Lett.</i> 1987, 51, 913–915.</p>	 <p><b>[Ir-21]</b>  <math>\lambda_{em} = 480</math> nm            EQE = 27.6%  <i>Adv. Optical Mater.</i> 2018, 6, 1900083.</p>	 <p><b>CzDBA</b>  <math>\lambda_{em} = 528</math> nm            EQE = 37.8%</p> <p><b>BuCzDBA</b>  <math>\lambda_{em} = 542</math> nm            EQE = 32.4%  <i>Nat. Photonics</i> 2018, 12, 235–240.</p>
Red	 <p><b>DCM1</b>  <math>\lambda_{em} = 570</math>-620 nm            EQE = 2.3%</p> <p><b>DCM2</b>  <math>\lambda_{em} = 610</math>-650 nm            EQE = 2.3%  <i>J. Appl. Phys.</i> 1989, 65, 3610.</p>	 <p><b>Pt(ppz)<sub>3</sub></b>  <math>\lambda_{em} = 740</math> nm            EQE = 24%  <i>Nat. Photonics</i> 2016, 11, 63–68.</p>	 <p><b>NALDPPAC</b>  <math>\lambda_{em} = 594</math> nm            EQE = 28.2%</p> <p><b>NALOMAC</b>  <math>\lambda_{em} = 597</math> nm            EQE = 23.4%  <i>Adv. Mater.</i> 2018, 30, 5, 1704981.</p>

Figure 20 : OLED emissive molecules, from 1<sup>st</sup> to 3<sup>rd</sup> generation with their associated EQE.

### White OLED:

The color of the emitted light strongly depends on the chemical composition of the polymer and the nature of the side groups which can be emissive dyes, thus the emitted color is easily tunable leading to “simple” white OLED manufacturing. The combination and the engineering of the organic polymers allow an easy color tunability with high brightness devices over 100,000 cd/m<sup>2</sup> (Figure 20), thus opening the way to easy process white OLEDs, and to a wide panel of applications. White OLED can be processed via two approaches, the first is the co evaporation of small molecules at the same time, which gives high quality of layers, but which requires high energy and technology for a deep vacuum level. The second is the solution approach, which is much easier and processable, but with a drop of quality compared to the first one. The white emissive layer can be built by mixing polymers together, or by the consecutive stacking of RGB emissive layers. [185–188]

## **5) Solution for future LED technology**

A part of the solution for future LED technology is a sustainable development of the LED. For that, the solution process materials are the best candidates to reduce the manufacturing costs and to open the way to easier large-scale production compared to the most used evaporated ones. Moreover, in the case of OLED, the new TADF emitters from the 3<sup>rd</sup> generation emitters show higher performances compared to phosphorescent and fluorescent emitters, as far as it can harvest 100 % of the injected charges for luminescence phenomenon. In addition, it was previously studied that the combination of different materials / technologies of LED can lead to very efficient optoelectronic devices. For instance, the combination of the organic materials (for instance polymers used in OLEDs) with inorganic QDs to take benefit from both entities. [189–191]

### **i) TADF Polymers**

TADF polymers are very promising emissive materials as they are able to convert 100% of the charges in light emission, in contrast with fluorescent (25% conversion) or phosphorescent (75% conversion) materials. Although most of the TADF materials are usually small organic molecules due to a direct design for their electronic structures, the processing

is expensive (evaporation method) and cannot be used for large manufacturing. Compared with small molecules, polymers are widely suitable for solution processing, showing a great potential in low cost processing and large scale production. [192–194] However, unlike small molecule, TADF polymers have different molecular weights, and present defects in the structure. Nowadays, TADF polymers still face many issues, such as complex synthesis, limited variety, and relatively low efficiency of devices using TADF compounds. In addition, due to the charge transfer effect of the conjugated structure, the emission wavelength of TADF polymer shows a large red shift, leading to the majority of TADF polymer emission concentrated in orange and green light emission, which is unfavorable for achieving blue light emission of TADF polymer neither white light emission. [194, 195]

ii) Aggregation Induced Emission AIE:

The Aggregation Induced Emission (AIE) phenomenon is very promising and original for the light emission. Indeed, the molecules which are nonemissive or weakly emissive in the solution state are found to emit strongly in the aggregate form or in solid state. The phenomenon is explained by the restriction of intramolecular rotation, for instance the phenyl groups of the emissive molecule (such as HPS). Thus, blocking non-radiative desexcitation pathways benefit to the radiative ones [196, 197] . The opposite phenomenon is called Aggregation Caused Quenching (ACQ), met when  $\pi$  -  $\pi$  stacking occurs between the emissive molecules (such as Perylene), and is represented by the following figure 21.

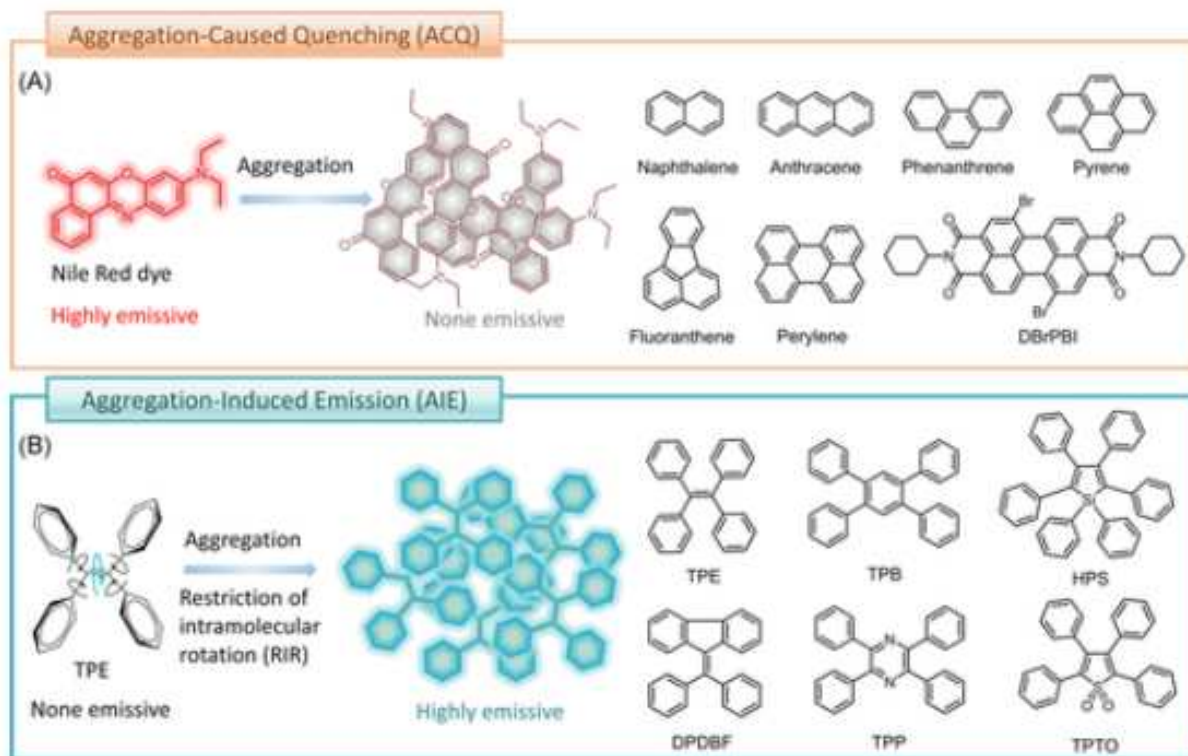


Figure 21 : A) Aggregation Caused Quenching vs B) Aggregation Induced Emission phenomena from liquid to solid state [197–199]

The construction of highly emissive emitters is hampered by the energy gap law and the ACQ effect. Aggregation induced emission (AIE) molecules could avoid the undesirable ACQ effect and emit intense light in the aggregated state, which is one of the most promising class of materials to fabricate high performance OLED with a high external quantum efficiency and low turn on voltage. As presented in the literature [198, 199], the first AIE molecules were processed by evaporation method, and could not be combined with quantum dots for instance. The AIE technology is very promising because by changing the electronic structure of the molecule, the emitted color is controlled. However, the development of red and near infrared (NIR) AIE molecules remains challenging due to the intrinsic narrow bandgap [200, 201].

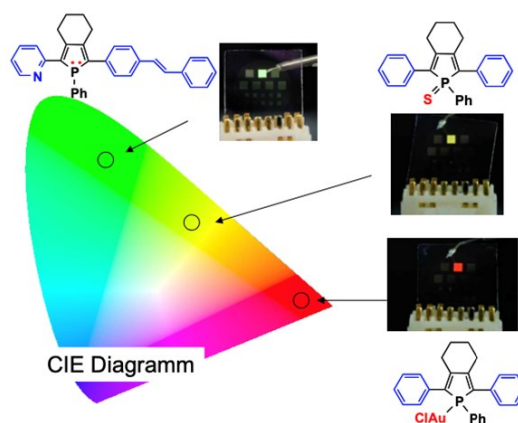


Figure 22: Different AIE molecules for different color in CIE diagram [202]

The AIE emitters are difficult to process via liquid approach, because of the agglomeration of the molecules. This problem can be avoided by the modification of the AIE structure itself, or thanks to the grafting of the AIE molecules with for instance, nanocrystals. For this purpose, the AIE molecule should have a grafting unit, such as the presented examples in figure 22, where a modification of the phosphorous group for a POOH group could be such a grafting unit. Indeed, the POOH attach groupment is known to be better, more robust, and stable than the classic carboxylate COOH on nanocrystal surface. [81, 136, 203] The solution process of AIE molecule, or hybrid nanocrystal-AIE will open a cheaper and more economic large scale manufacturing. Additionally, the method to build a white LED is easier with the liquid approach through colloidal self assembly and should help to avoid phase segregation of the different emitters, which is difficult with regular OLED emitters by evaporation. The interest of doing hybrid nanocrystal AIE structures is to use the properties of the AIE molecule, usually transporting holes and responsible for the emitted color, with the inorganic nanocrystals, possibly providing electron transport. Also, the inorganic core can be involved in the emission, for instance by using emissive metal halide perovskites. The combination of both entities can possibly create a hybrid ambipolar structure, which could be used as pure, or even incorporated in a host matrix as it is widely done by recent approaches in LED technologies.

Such a strategy using grafted emitters on nanocrystal is the main purpose of this thesis. The following chapters will explore the possibilities:

- Chapter 1: Introduction to nanohybrids using AIE phenomenon
- Chapter 2: Controlling the morphology of nanohybrids within a matrix
- Chapter 3: Blue, green and red nanohybrids used as a tool to control the light emission in LED devices
- Chapter 4: Co-grafting of several emitters on nanocrystal towards white emission

## Bibliography:

- [1] Nanotechnology — An Introduction for the Standards Community. [accessed 2021 Dec 20]. <https://www.astm.org/jai13110.html>
- [2] Bayda S, Adeel M, Tuccinardi T, Cordani M, Rizzolio F. The History of Nanoscience and Nanotechnology: From Chemical–Physical Applications to Nanomedicine. *Molecules*. 2019;25(1):112. doi:10.3390/molecules25010112
- [3] Freestone I, Meeks N, Sax M, Higgitt C. The Lycurgus Cup — A Roman nanotechnology. *Gold Bulletin*. 2007;40(4):270–277. doi:10.1007/BF03215599
- [4] British Museum. [accessed 2021 Dec 20]. <https://www.britishmuseum.org/>
- [5] Wagner FE, Haslbeck S, Stievano L, Calogero S, Pankhurst QA, Martinek KP. Before striking gold in gold-ruby glass. *Nature*. 2000;407(6805):691–692. doi:10.1038/35037661
- [6] Barber D, Freestone I. An investigation of the origin of the colour of the Lycurgus Cup by analytical TEM. *Archaeometry*. 2007;32:33–45. doi:10.1111/j.1475-4754.1990.tb01079.x
- [7] Nanotechnology W, Awan I, Hussain S, ul Haq A, Khan A. Wondrous Nanotechnology. *Journal-Chemical Society of Pakistan*. 2016;38(No. 06, 2016 1026).
- [8] Pradell T, Climent-Font A, Molera J, Zucchiatti A, Ynsa M, Roura P, Crespo D. Metallic and Nonmetallic Shine in Luster: An Elastic ion Backscattering Study. *Journal of Applied Physics*. 2007;101:103518–103518. doi:10.1063/1.2734944
- [9] Charles P. Poole Jr., Frank J. Owens. *Introduction to Nanotechnology* ISBN: 978-0-471-07935-4. 2003 May [accessed 2021 Dec 20]. <https://www.wiley.com/en-us/Introduction+to+Nanotechnology-p-9780471079354>
- [10] Ball P. Renaissance potters were nanotechnologists | *Nature* <https://doi.org/10.1038/news030623-17>. 2003 <https://doi.org/10.1038/news030623-17> [accessed 2021 Dec 20]. <https://www.nature.com/articles/news030623-17>
- [11] Reibold M, Paufler P, Levin AA, Kochmann W, Pätzke N, Meyer DC. Carbon nanotubes in an ancient Damascus sabre. *Nature*. 2006;444(7117):286–286. doi:10.1038/444286a
- [12] Pinna N, Niederberger M. Surfactant-free nonaqueous synthesis of metal oxide nanostructures. *Angewandte Chemie (International Ed. in English)*. 2008;47(29):5292–5304. doi:10.1002/anie.200704541
- [13] Lekeufack DED. Synthèse et fonctionnalisation des nanoparticules d'or pour des applications en optique: perspective en photocatalyse HAL Id: tel-00838627. :239 pages.
- [14] X. The Bakerian Lecture. —Experimental relations of gold (and other metals) to light | *Philosophical Transactions of the Royal Society of London*. [accessed 2021 Dec 20]. <https://royalsocietypublishing.org/doi/10.1098/rstl.1857.0011>
- [15] Feynman RP. There's Plenty of Room at the Bottom: An Invitation to Enter a New Field of Physics. In: Goddard WA, Brenner D, Lyshewski SE, Iafate GJ, editors. Boca Raton, FL: CRC Press; 2012. p. 3–12. <https://resolver.caltech.edu/CaltechAUTHORS:20141219-151712733>

- [16] Ling CF, Koo SGM. On Value Premium, Part II: The Explanations. *Journal of Mathematical Finance*. 2012;02(01):66–74. doi:10.4236/jmf.2012.21008
- [17] Qin C, Peng L-M. Measurement accuracy of the diameter of a carbon nanotube from TEM images. *Physical Review B*. 2002;65(15):155431. doi:10.1103/PhysRevB.65.155431
- [18] FRANÇOIS PERREAULT. UNIVERSITÉ DU QUÉBEC À MONTRÉAL TOXICITÉ DES NANOPARTICULES MÉTALLIQUES CHEZ DIFFÉRENTS MODÈLES BIOLOGIQUES THÈSE PRÉSENTÉE COMME EXIGENCE PARTIELLE. 2012 [accessed 2021 Dec 20]. <https://docplayer.fr/68887839-Universite-du-quebec-a-montreal-toxicite-des-nanoparticules-metalliques-chez-differents-modeles-biologiques-these-presentee-comme-exigence-partielle.html>
- [19] Vincent P, Lyon UCB. Polytech-Lyon Cours : La Nanotechnologie (la nanoscience), les différents aspects liés à cette révolution technologique. 2013 2014:59 pages.
- [20] BAJJOU O. Memoire Online - Méthodes de synthèse des nanomatériaux. [https://www.memoireonline.com/11/12/6461/m\\_Methodes-de-synthese-des-nanomateriaux0.html](https://www.memoireonline.com/11/12/6461/m_Methodes-de-synthese-des-nanomateriaux0.html)
- [21] Iqbal P, Preece JA, Mendes PM. Nanotechnology: The “Top-Down” and “Bottom-Up” Approaches. In: *Supramolecular Chemistry*. John Wiley & Sons, Ltd; 2012. <https://onlinelibrary.wiley.com/doi/abs/10.1002/9780470661345.smc195>. doi:10.1002/9780470661345.smc195
- [22] Khudhair D, Bhatti A, Li Y, Hamedani HA, Garmestani H, Hodgson P, Nahavandi S. Anodization parameters influencing the morphology and electrical properties of TiO<sub>2</sub> nanotubes for living cell interfacing and investigations. *Materials Science & Engineering. C, Materials for Biological Applications*. 2016;59:1125–1142. doi:10.1016/j.msec.2015.10.042
- [23] Kulkarni M, Mazare A, Gongadze E, Perutkova Š, Kralj-Iglič V, Milošev I, Schmuki P, A Iglič null, Mozetič M. Titanium nanostructures for biomedical applications. *Nanotechnology*. 2015;26(6):062002. doi:10.1088/0957-4484/26/6/062002
- [24] De Keukeleere K, De Roo J, Lommens P, Martins JC, Van Der Voort P, Van Driessche I. Fast and Tunable Synthesis of ZrO<sub>2</sub> Nanocrystals: Mechanistic Insights into Precursor Dependence. *Inorganic Chemistry*. 2015;54(7):3469–3476. doi:10.1021/acs.inorgchem.5b00046
- [25] Becheri A, Dürr M, Lo Nostro P, Baglioni P. Synthesis and characterization of zinc oxide nanoparticles: application to textiles as UV-absorbers. *Journal of Nanoparticle Research*. 2008;10:679–689. doi:10.1007/s11051-007-9318-3
- [26] Anderson SD, Gwenin VV, Gwenin CD. Magnetic Functionalized Nanoparticles for Biomedical, Drug Delivery and Imaging Applications. *Nanoscale Research Letters*. 2019;14(1):188. doi:10.1186/s11671-019-3019-6
- [27] Petcharoen K, Sirivat A. Synthesis and characterization of magnetite nanoparticles via the chemical co-precipitation method. *Materials Science and Engineering: B*. 2012;177(5):421–427. doi:10.1016/j.mseb.2012.01.003
- [28] Kandpal ND, Sah N, Loshali R, Joshi R, Prasad J. Co-precipitation method of synthesis and characterization of iron oxide nanoparticles. *Journal of scientific & industrial research vol 73 pp 87-90*. 2014;73:4.

- [29] Bottero JY, Cases JM, Fiessinger F, Poirier JE. Studies of hydrolyzed aluminum chloride solutions. 1. Nature of aluminum species and composition of aqueous solutions. *The Journal of Physical Chemistry*. 1980;84(22):2933–2939. doi:10.1021/j100459a021
- [30] Bottero J-Y, Lartiges B. Séparation liquide/solide par coagulation-floculation : les coagulants-floculants, mécanismes d'agrégation, structure et densité des floes. / Liquid/solid separation by coagulation-floculation, coagulants-floculants, floes structure and density. *Sciences Géologiques, bulletins et mémoires*. 1993;46(1):163–174. doi:10.3406/sgeol.1993.1902
- [31] Bottero JY, Manceau A, Villieras F, Tchoubar D. Structure and mechanisms of formation of iron oxide hydroxide (chloride) polymers. *Langmuir*. 1994;10(1):316–319. doi:10.1021/la00013a046
- [32] Günter Oberdörster, , Eva Oberdörster, , and Jan Oberdörster. Nanotoxicology: An Emerging Discipline Evolving from Studies of Ultrafine Particles | *Environmental Health Perspectives* | Vol. 113, No. 7 <https://doi.org/10.1289/ehp.7339>. 2005 [accessed 2021 Dec 20]. <https://ehp.niehs.nih.gov/doi/full/10.1289/ehp.7339>
- [33] Wen H, Dan M, Yang Y, Lyu J, Anliang S, Cheng X, Chen L, Xu L. Acute toxicity and genotoxicity of silver nanoparticle in rats. *PLOS ONE*. 2017;12:e0185554. doi:10.1371/journal.pone.0185554
- [34] Gottschalk F, Nowack B. The release of engineered nanomaterials to the environment. *Journal of Environmental Monitoring*. 2011;13(5):1145–1155. doi:10.1039/C0EM00547A
- [35] Abramenko NB, Demidova TB, Abkhalimov EV, Ershov BG, Krysanov EY, Kustov LM. Ecotoxicity of different-shaped silver nanoparticles: Case of zebrafish embryos. *Journal of Hazardous Materials*. 2018;347:89–94. doi:10.1016/j.jhazmat.2017.12.060
- [36] Ken Donaldson, Robert Aitken, Lang Tran, Vicki Stone, Rodger Duffin, Gavin Forrest, Andrew Alexander. Carbon Nanotubes: A Review of Their Properties in Relation to Pulmonary Toxicology and Workplace Safety | *Oxford Academic Toxicological Sciences*, Volume 92, Issue 1, July 2006, Pages 5–22. [accessed 2021 Dec 20]. <https://doi.org/10.1093/toxsci/kfj130>
- [37] Petosa AR, Brennan SJ, Rajput F, Tufenkji N. Transport of two metal oxide nanoparticles in saturated granular porous media: Role of water chemistry and particle coating. *Water Research*. 2012;46(4):1273–1285. doi:10.1016/j.watres.2011.12.033
- [38] Auffan M. NANOPARTICULES D'OXYDES MÉTALLIQUES : RELATIONS ENTRE LA RÉACTIVITÉ DE SURFACE ET DES RÉPONSES BIOLOGIQUES [phdthesis]. Université Paul Cézanne - Aix-Marseille III; 2007. <https://tel.archives-ouvertes.fr/tel-00308503>
- [39] Simonet BM, Valcárcel M. Monitoring nanoparticles in the environment. *Analytical and Bioanalytical Chemistry*. 2009;393(1):17–21. doi:10.1007/s00216-008-2484-z
- [40] Nanomatériaux, nanoparticules. Effets sur la santé - Risques - INRS. [accessed 2021 Dec 20]. <https://www.inrs.fr/risques/nanomateriaux/effets-sante.html>
- [41] Application of nanotechnology in sports clothing and flooring for enhanced sport activities, performance, efficiency and comfort: a review - Tina Harifi, Majid Montazer, 2017 *Journal of Industrial Textiles* Vol 46. Issue 5. [accessed 2021 Dec 20]. <https://journals.sagepub.com/doi/abs/10.1177/1528083715601512>

- [42] Thiruvengadam M, Rajakumar G, Chung I-M. Nanotechnology: current uses and future applications in the food industry. Springer-Verlag GmbH Germany, part of Springer Nature 2018. 3 Biotech. 2018;8(1):74. doi:10.1007/s13205-018-1104-7
- [43] Engineers create plants that glow. MIT News | Massachusetts Institute of Technology. [accessed 2021 Dec 20]. <https://news.mit.edu/2017/engineers-create-nanobionic-plants-that-glow-1213>
- [44] Baillot R, Deshayes Y. Light-emitting Diodes: State-of-the-Art GaN Technologies .Reliability Investigation of LED Devices for Public Light Applications. 2017. doi:10.1016/B978-1-78548-149-9.50001-8
- [45] Craford MG. LEDs challenge the incandescents. IEEE Circuits and Devices Magazine. 1992;8(5):24–29. doi:10.1109/101.158509
- [46] Conductors – Insulators – Semiconductors - Fundamentals - Semiconductor Technology from A to Z - Halbleiter.org. [accessed 2021 Dec 20]. <https://www.halbleiter.org/en/fundamentals/conductors-insulators-semiconductors/>
- [47] Valeur B. L'énigme de la photoluminescence. Pourscience.fr. [accessed 2021 Dec 20]. <https://www.pourscience.fr/sd/histoire-techniques/https://www.pourscience.fr/sd/histoire-techniques/l-enigme-de-la-photoluminescence-6560.php>
- [48] Wu C, Chen H-F, Wong K-T, Thompson ME. Study of Ion-Paired Iridium Complexes (Soft Salts) and Their Application in Organic Light Emitting Diodes. Journal of the American Chemical Society. 2010;132(9):3133–3139. doi:10.1021/ja9097725
- [49] Tong B, Mei Q, Wang S, Fang Y, Meng Y, Wang B. Nearly 100% internal phosphorescence efficiency in a polymer light-emitting diode using a new iridium complex phosphor. Journal of Materials Chemistry. 2008;18(14):1636–1639. doi:10.1039/B800977E
- [50] Adachi C, Baldo MA, Thompson ME, Forrest SR. Nearly 100% internal phosphorescence efficiency in an organic light-emitting device. Journal of Applied Physics. 2001;90(10):5048–5051. doi:10.1063/1.1409582
- [51] Efficient Nondoped Blue Fluorescent Organic Light-Emitting Diodes (OLEDs) with a High External Quantum Efficiency of 9.4% @ 1000 cd m<sup>-2</sup> Based on Phenanthroimidazole–Anthracene Derivative - Tang - 2018 - Advanced Functional Materials - Wiley Online Library. [accessed 2021 Dec 20]. <https://onlinelibrary.wiley.com/doi/abs/10.1002/adfm.201705813>
- [52] Mammedov D. Thermally activated delayed fluorescence. 2021 Dec 18 [accessed 2021 Dec 20]. <https://www.wiki.en-us.nina.az/TADF.html>
- [53] Huang T, Jiang W, Duan L. Recent progress in solution processable TADF materials for organic light-emitting diodes. Journal of Materials Chemistry C. 2018;6(21):5577–5596. doi:10.1039/C8TC01139G
- [54] Zhao F, Ma D. Approaches to high performance white organic light-emitting diodes for general lighting. Materials Chemistry Frontiers. 2017;1(10):1933–1950. doi:10.1039/C6QM00365F
- [55] Kim K-H, Kim J-J. Origin and Control of Orientation of Phosphorescent and TADF Dyes for High-Efficiency OLEDs. Advanced Materials. 2018;30(42):1705600. doi:10.1002/adma.201705600
- [56] Perry TS. M. George Craford [biography]. IEEE Spectrum. 1995;32(2):52–55. doi:10.1109/6.343989

- [57] Development of High-bright and Pure-white LED Lamps. [accessed 2021 Dec 20].  
[https://www.jstage.jst.go.jp/article/jlve/22/1/22\\_1\\_1\\_2/\\_article](https://www.jstage.jst.go.jp/article/jlve/22/1/22_1_1_2/_article)
- [58] Bright Pure Green Emission from N-free GaP LED's | Nishizawa, Jun-ichi; Okuno, Yasuo; Koike, Masayoshi; Sakurai, Fumitoshi | download. [accessed 2021 Dec 20].  
<https://ur.booksc.eu/book/63703136/36b1b4>
- [59] Schubert EF. Light-Emitting Diodes. 2nd ed. Cambridge: Cambridge University Press; 2006.  
<http://ebooks.cambridge.org/ref/id/CBO9780511790546>. doi:10.1017/CBO9780511790546
- [60] Amin F. Light Emitting Diodes (LEDs) ELE 432 Assignment # 3 Vijay Kumar Peddinti. [accessed 2021 Dec 20].  
[https://www.academia.edu/37095634/Light\\_Emitting\\_Diodes\\_LEDs\\_ELE\\_432\\_Assignment\\_3\\_Vijay\\_Kumar\\_Peddinti](https://www.academia.edu/37095634/Light_Emitting_Diodes_LEDs_ELE_432_Assignment_3_Vijay_Kumar_Peddinti)
- [61] Approaches for Long Lifetime Organic Light Emitting Diodes - Sudheendran Swayamprabha - Advanced Science - Volume8, Issue1 January 6, 2021 2002254. [accessed 2021 Dec 20].  
<https://onlinelibrary.wiley.com/doi/full/10.1002/advs.202002254>
- [62] Ashcroft CM, Bodart-Le Guen C, Campana F, Cicoira F, Cole JM, Dailey J, Deibel C, Ehrenfreund E, Frohna K, Fusella MA, et al. List of contributors. In: Ostroverkhova O, editor. Handbook of Organic Materials for Electronic and Photonic Devices (Second Edition). Woodhead Publishing; 2019. p. xiii–xvii. (Woodhead Publishing Series in Electronic and Optical Materials).  
<https://www.sciencedirect.com/science/article/pii/B9780081022849099927>. doi:10.1016/B978-0-08-102284-9.09992-7
- [63] Lin Y-C, Karlsson M, Bettinelli M. Inorganic Phosphor Materials for Lighting. Springer International Publishing Switzerland 2016. Topics in Current Chemistry (Cham). 2016;374(2):21.  
 doi:10.1007/s41061-016-0023-5
- [64] Ng F-L, Jaafar MM, Phang S-M, Chan Z, Salleh NA, Azmi SZ, Yunus K, Fisher AC, Periasamy V. Reduced Graphene Oxide Anodes for Potential Application in Algae Biophotovoltaic Platforms. Scientific Reports. 2014;4(1):7562. doi:10.1038/srep07562
- [65] Cheng X, Long J, Wu R, Huang L, Tan L, Chen L, Chen Y. Fluorinated Reduced Graphene Oxide as an Efficient Hole-Transport Layer for Efficient and Stable Polymer Solar Cells. ACS Omega. 2017;2(5):2010–2016. doi:10.1021/acsomega.7b00408
- [66] Eccher J, Zajaczkowski W, Faria GC, Bock H, von Seggern H, Pisula W, Bechtold IH. Thermal Evaporation versus Spin-Coating: Electrical Performance in Columnar Liquid Crystal OLEDs. ACS Applied Materials & Interfaces. 2015;7(30):16374–16381. doi:10.1021/acsomega.5b03496
- [67] Kim S-K, Seok H-J, Kim D-H, Choi D-H, Nam S-J, Kim S-C, Kim H-K. Comparison of NiO x thin film deposited by spin-coating or thermal evaporation for application as a hole transport layer of perovskite solar cells. RSC Advances. 2020;10(71):43847–43852. doi:10.1039/D0RA08776A
- [68] Hu L, Song J, Yin X, Su Z, Li Z. Research Progress on Polymer Solar Cells Based on PEDOT:PSS Electrodes. Polymers 2020, 12, 145; doi:10.3390/polym12010145. Polymers. 2020;12(1):145. doi:10.3390/polym12010145
- [69] Kumar S, Kim H, Kim D, Iyer S. Spin and doctor-blade coated PEDOT:PSS back electrodes in inverted organic solar cells Solar Energy Volume 204, 1 July 2020, Pages 64-70. 2020. doi:10.1016/j.solener.2020.04.071

- [70] Cho N, Kim J. Doctor Blade-Coated Polymer Solar Cells. *Polymer Korea*. 2016;40:818. doi:10.7317/pk.2016.40.5.818
- [71] Enhancing the electroluminescence of OLEDs by using ZnO nanoparticle electron transport layers that exhibit the Auger electron effect. *Molecular Crystals and Liquid Crystals: Vol 663, No 1*. [accessed 2021 Dec 20]. doi.org/10.1080/15421406.2018.1468099
- [72] Nanomaterials for Solution-Processed OLEDs. Avantama AG. 2020 May 1 [accessed 2021 Dec 20]. <https://avantama.com/nanomaterials-solution-processed-oleds/>
- [73] Al-Asbahi BA, Haji Jumali MH, Yap CC, Mat Salleh M. Influence of TiO<sub>2</sub> Nanoparticles on Enhancement of Optoelectronic Properties of PFO-Based Light Emitting Diode Volume 2013, ID 561534, 7 pages. *Journal of Nanomaterials*. 2013 [accessed 2021 Dec 20];2013. <https://www.hindawi.com/journals/jnm/2013/561534/>. doi:10.1155/2013/561534
- [74] Solution Processed Metal Oxide. *Thin Films for Electronic Applications - 1st Edition*. 2020 Jun [accessed 2021 Dec 20]. <https://www.elsevier.com/books/solution-processed-metal-oxide-thin-films-for-electronic-applications/cui/978-0-12-814930-0>
- [75] Post-treatment-Free Solution-Processed Non-stoichiometric NiO<sub>x</sub> Nanoparticles for Efficient Hole-Transport Layers of Organic Optoelectronic Devices - Jiang - 2015 - *Advanced Materials Volume 27, Issue 18 May 13, 2015 Pages 2930-2937*. [accessed 2021 Dec 20]. <https://onlinelibrary.wiley.com/doi/abs/10.1002/adma.201405391>
- [76] Haixia X, Yin X, Liu J, Guo Y, Chen P, Que W or WX, Wang G, Gao B. Low temperature solution-derived TiO<sub>2</sub>-SnO<sub>2</sub> bilayered electron transport layer for high performance perovskite solar cells. *Applied Surface Science*. 2018;464. doi:10.1016/j.apsusc.2018.09.146
- [77] Xiaoyong Liang† a, Sai Bai† b, Xin Wang a, Xingliang Dai a, Feng Gao b, Baoquan Sun c, Zhijun Ning d, Zhizhen Ye \*a and Yizheng Jin. Colloidal metal oxide nanocrystals as charge transporting layers for solution-processed light-emitting diodes and solar cells - *Chemical Society Reviews* DOI:10.1039/C6CS00122J ,2017, 46, 1730-1759. [accessed 2021 Dec 20].
- [78] Ayllon JA, Lira-Cantu M. Application of MEH-PPV/SnO<sub>2</sub> bilayer as hybrid solar cell. *Applied Physics A*. 2009;95(1):249–255. doi:10.1007/s00339-008-5023-z
- [79] Meyer J, Hamwi S, Kröger M, Kowalsky W, Riedl T, Kahn A. Transition metal oxides for organic electronics: energetics, device physics and applications. *Advanced Materials (Deerfield Beach, Fla.)*. 2012;24(40):5408–5427. doi:10.1002/adma.201201630
- [80] Shen J, Zhang W, Qi R, Mao Z-W, Shen H. Engineering functional inorganic-organic hybrid systems: Advances in siRNA therapeutics. *Chemical Society Reviews*. 2018;47. doi:10.1039/C7CS00479F
- [81] Wang A, Yan X, Zhang M, Sun S, Yang M, Shen W, Pan X, Wang P, Deng Z. Controlled Synthesis of Lead-Free and Stable Perovskite Derivative Cs<sub>2</sub>SnI<sub>6</sub> Nanocrystals via a Facile Hot-Injection Process. *Chemistry of Materials*. 2016;28(22):8132–8140. doi:10.1021/acs.chemmater.6b01329
- [82] An Efficient Method for the Surface Functionalization of Luminescent Quantum Dots with Lipoic Acid Based Ligands - La Rosa - 2017 - *European Journal of Inorganic Chemistry - Wiley Online Library*. [accessed 2021 Dec 20]. <https://chemistry-europe.onlinelibrary.wiley.com/doi/full/10.1002/ejic.201700781>

- [83] Yadav RAK, Dubey DK, Chen S-Z, Liang T-W, Jou J-H. Role of Molecular Orbital Energy Levels in OLED Performance. *Scientific Reports*. 2020;10(1):9915. doi:10.1038/s41598-020-66946-2
- [84] Wang Y-M, Teng F, Zhou Q-C, Wang Y-S. Multiple roles of bathocuproine employed as a buffer-layer in organic light-emitting diodes. *Applied Surface Science*. 2006;252(6):2355–2359. doi:10.1016/j.apsusc.2005.04.006
- [85] Liu J. Deep-blue efficient OLED based on NPB with little efficiency roll-off under high current density. *Applied Physics A* volume 123, Article number: 191 (2017). 2017. doi:10.1007/S00339-017-0840-6
- [86] Christopher J.M. Emmotta Antonio Urbinaab Jenny Nelsona. Environmental and economic assessment of ITO-free electrodes for organic solar cells. *Solar Energy Materials and Solar Cells* Volume 97, February 2012, Pages 14-21. [accessed 2021 Dec 20]. doi.org/10.1007/s00339-017-0840-6
- [87] Fluorine Tin Oxide as an Alternative to Indium Tin Oxide in Polymer LEDs - Andersson - 1998 - *Advanced Materials* - Volume10, Issue11 August, 1998 Pages 859-863. [accessed 2021 Dec 20]. [https://doi.org/10.1002/\(SICI\)1521-4095\(199808\)10:11<859::AID-ADMA859>3.0.CO;2-1](https://doi.org/10.1002/(SICI)1521-4095(199808)10:11<859::AID-ADMA859>3.0.CO;2-1)
- [88] Chien Y-M, Lefevre F, Shih I, Izquierdo R. A solution processed top emission OLED with transparent carbon nanotube electrodes. *Nanotechnology*. 2010;21:134020. doi:10.1088/0957-4484/21/13/134020
- [89] Benefits, Problems, and Solutions of Silver Nanowire Transparent Conductive Electrodes in Indium Tin Oxide (ITO)-Free Flexible Solar Cells - Azani - 2020 - *Advanced Energy Materials* - Wiley Online Library. [accessed 2021 Dec 20]. <https://onlinelibrary.wiley.com/doi/abs/10.1002/aenm.202002536>
- [90] Krames MR, Shchekin OB, Mueller-Mach R, Mueller GO, Zhou L, Harbers G, Craford MG. Status and Future of High-Power Light-Emitting Diodes for Solid-State Lighting. *Journal of Display Technology*. 2007;3(2):160–175.
- [91] Aleksandrova M. Specifics and Challenges to Flexible Organic Light-Emitting Devices. *Advances in Materials Science and Engineering*. 2016;2016:e4081697. doi:10.1155/2016/4081697
- [92] Minwoo Choi, Bongkyun Jang, Wonho Lee, Seonwoo Lee, Tae Woong Kim, Hak-Joo Lee, Jae-Hyun Kim, Jong-Hyun Ahn. Stretchable Active Matrix Inorganic Light-Emitting Diode Display Enabled by Overlay-Aligned Roll-Transfer Printing - *Advanced Functional Materials* - Volume27, Issue11 March 17, 2017 1606005. [accessed 2021 Dec 20]. <https://doi.org/10.1002/adfm.201606005>
- [93] Bender VC, Marchesan T, Alonso J. Solid-State Lighting: A Concise Review of the State of the Art on LED and OLED Modeling. *Industrial Electronics Magazine, IEEE*. 2015;9:6–16. doi:10.1109/MIE.2014.2360324
- [94] Holder E, Langeveld-Voss BMW, Schubert US. New trends in the use of transition metal-ligand complexes for applications in electroluminescent devices. *Advanced Materials*. 2005;17(9):1109–1121. doi:10.1002/adma.200400284
- [95] Lu G-Z, Li X, Liu L, Zhou L, Zheng Y-X, Zhang W-W, Zuo J-L, Zhang H. Efficient phosphorescent red iridium(III) complexes containing a four-membered Ir–S–C–S ring backbone and large hindered spacers for high-performance OLEDs. *Journal of Materials Chemistry C*. 2019;7(13):3862–3868. doi:10.1039/C9TC00440H

- [96] Zhang H, Rogers JA. Recent Advances in Flexible Inorganic Light Emitting Diodes: From Materials Design to Integrated Optoelectronic Platforms. *Advanced Optical Materials*. 2019;7(2):1800936. doi:10.1002/adom.201800936
- [97] Lalevée J, Blanchard N, Tehfe M-A, Peter M, Morlet-Savary F, Fouassier J. Household LED irradiation under air: Cationic polymerization using iridium or ruthenium complex photocatalysts. *Polymer Bulletin - POLYM BULL*. 2012;68. doi:10.1007/s00289-011-0541-9
- [98] Ange Stoianov†, Christophe Gourlaouen†, Sergi Vela†, and Chantal Daniel†. Luminescent Dinuclear Copper(I) Complexes as Potential Thermally Activated Delayed Fluorescence (TADF) Emitters: A Theoretical Study | *The Journal of Physical Chemistry A*. [accessed 2021 Dec 20]. <https://pubs.acs.org/doi/10.1021/acs.jpca.7b11793>
- [99] Tang H, Meng G, Chen Z, Wang K, Zhou Q, Wang Z. Warm White Light-Emitting Diodes Based on a Novel Orange Cationic Iridium(III) Complex. *Materials (Basel, Switzerland)*. 2017;10(6):E657. doi:10.3390/ma10060657
- [100] Bai R, Meng X, Wang X, He L. Blue-Emitting Iridium(III) Complexes for Light-Emitting Electrochemical Cells: Advances, Challenges, and Future Prospects. *Advanced Functional Materials*. 2020;30(33):1907169. doi:10.1002/adfm.201907169
- [101] Park SW, Kim YS. Theoretical study of new blue iridium complexes comprising a bipyridine derivative and various ancillary ligands. *Journal of Nanoscience and Nanotechnology*. 2014;14(7):5313–5316. doi:10.1166/jnn.2014.8418
- [102] Lu G-Z, Liu L, Tu Z-L, Zhou Y-H, Zheng Y-X. Two green iridium(III) complexes containing the electron-transporting group of 4-phenyl-4H-1,2,4-triazole for highly efficient OLEDs. *Journal of Materials Chemistry C*. 2019;7(7):2022–2028. doi:10.1039/C8TC06010J
- [103] Ye Y, Sun R, Chen M, Tang H, Dong X, Wang K, Wang Z. Application of an orange–yellow emitting cationic iridium(III) complex in GaN-based warm white light-emitting diodes. *Journal of Materials Science: Materials in Electronics*. 2018;29(2):1554–1561. doi:10.1007/s10854-017-8065-1
- [104] Meng G, Chen Z, Tang H, Liu Y, Wei L, Wang Z. Application of a novel cationic iridium(III) complex as a red phosphor in warm white light-emitting diodes. *New Journal of Chemistry*. 2015;39(12):9535–9542. doi:10.1039/C5NJ02032H
- [105] Schubert EF, Kim JK. Solid-state light sources getting smart. *Science (New York, N.Y.)*. 2005;308(5726):1274–1278. doi:10.1126/science.1108712
- [106] Chen L, Lin C-C, Yeh C-W, Liu R-S. Light Converting Inorganic Phosphors for White Light-Emitting Diodes. *Materials*. 2010;3(3):2172–2195. doi:10.3390/ma3032172
- [107] Dwivedi J, Kumar P, Kedawat G, Gupta BK. New emerging rare-earth free yellow emitting 2D BCNO nanophosphor for white light emitting diodes. *New Journal of Chemistry*. 2015;39(7):5161–5170. doi:10.1039/C5NJ00602C
- [108] Hass G, Jacobus GF, Hunter WR. Optical Properties of Evaporated Iridium in the Vacuum Ultraviolet from 500 Å to 2000 Å \* *Journal of the Optical Society of America* Vol. 57, Issue 6, pp. 758-762 (1967). 1967;57(6):758–762. doi:10.1364/JOSA.57.000758

- [109] Sessolo M, Tordera D, Bolink HJ. Ionic Iridium Complex and Conjugated Polymer Used To Solution-Process a Bilayer White Light-Emitting Diode. *ACS Applied Materials & Interfaces*. 2013;5(3):630–634. doi:10.1021/am302033k
- [110] Zhang G, Chou H-H, Jiang X, Sun P, Cheng C-H. Highly efficient white organic light-emitting diodes based on broad excimer emission of iridium complex. *Organic Electronics*. 2010;11. doi:10.1016/j.orgel.2010.04.016
- [111] Photoluminescence Characteristic of Ce<sup>3+</sup>-Eu<sup>3+</sup> Co-doped Y<sub>3</sub>Al<sub>5</sub>O<sub>12</sub> Phosphor Prepared by Combustion Method: *Molecular Crystals and Liquid Crystals: Vol 513, No 1*. [accessed 2021 Dec 20]. <https://www.tandfonline.com/doi/abs/10.1080/15421400903195908>
- [112] Enhancement of red spectral emission intensity of Y<sub>3</sub>Al<sub>5</sub>O<sub>12</sub>:Ce<sup>3+</sup> phosphor via Pr co-doping and Tb substitution for the application to white LEDs. *Journal of Luminescence Volume 126, Issue 2, October 2007, Pages 371-377*. [accessed 2021 Dec 20]. <https://doi.org/10.1016/j.jlumin.2006.08.093>
- [113] a R B, Anjalin M. Comparative investigation of structural and morphological properties of CdSe/ZnS and CdSe/ZnSe core/shell nanoparticles. *Der Pharma Chemica*. 2015;7:67–72.
- [114] Chen F, Guan Z, Tang A. Nanostructure and Device Architecture Engineering for High-Performance Quantum-Dot Light-Emitting Diodes. *Journal of Materials Chemistry C*. 2018;6. doi:10.1039/C8TC04028A
- [115] Molaei M, Marandi M, Saievar-Iranizad E, Taghavinia N, Liu B, Sun HD, Sun XW. Near-white emitting QD-LED based on hydrophilic CdS nanocrystals. *Journal of Luminescence*. 2012;132(2):467–473. doi:10.1016/j.jlumin.2011.08.038
- [116] Lim J, Park Y-S, Klimov VI. Optical gain in colloidal quantum dots achieved with direct-current electrical pumping. *Nature Materials*. 2018;17(1):42–49. doi:10.1038/nmat5011
- [117] Hines MA, Guyot-Sionnest P. Synthesis and Characterization of Strongly Luminescing ZnS-Capped CdSe Nanocrystals. *The Journal of Physical Chemistry*. 1996;100(2):468–471. doi:10.1021/jp9530562
- [118] Pal BN, Ghosh Y, Brovelli S, Laocharoensuk R, Klimov VI, Hollingsworth JA, Htoon H. ‘Giant’ CdSe/CdS Core/Shell Nanocrystal Quantum Dots As Efficient Electroluminescent Materials: Strong Influence of Shell Thickness on Light-Emitting Diode Performance. *Nano Letters*. 2012;12(1):331–336. doi:10.1021/nl203620f
- [119] Jung S-M, Lee TH, Bang SY, Han SD, Shin D-W, Lee S, Choi HW, Suh Y-H, Fan X-B, Jo J-W, et al. Modelling charge transport and electro-optical characteristics of quantum dot light-emitting diodes. *npj Computational Materials*. 2021;7(1):1–11. doi:10.1038/s41524-021-00591-9
- [120] Ekimov AI, Onushchenko AA. Quantum size effect in three-dimensional microscopic semiconductor crystals. *Bibcode: 1981JETPL..34..345E. Soviet Journal of Experimental and Theoretical Physics Letters*. 1981;34:345.
- [121] Taesoo Lee, Donghyo Hahm, Kyunghwan Kim, Wan Ki Bae, Changhee Lee, Jeonghun Kwak. Highly Efficient and Bright Inverted Top-Emitting InP Quantum Dot Light-Emitting Diodes Introducing a Hole-Suppressing Interlayer - Lee - 2019 - Small - Volume15, Issue50 December 13, 2019 1905162. [accessed 2021 Dec 20]. <https://doi.org/10.1002/smll.201905162>

- [122] Dai X, Zhang Z, Jin Y, Niu Y, Cao H, Liang X, Chen L, Wang J, Peng X. Solution-processed, high-performance light-emitting diodes based on quantum dots. *Nature*. 2014;515(7525):96–99. doi:10.1038/nature13829
- [123] Shen H, Gao Q, Zhang Y, Lin Y, Lin Q, Li Z, Chen L, Zeng Z, Li X, Jia Y, et al. Visible quantum dot light-emitting diodes with simultaneous high brightness and efficiency. *Nature Photonics*. 2019;13(3):192–197. doi:10.1038/s41566-019-0364-z
- [124] Kim T-H, Chung D-Y, Ku J, Song I, Sul S, Kim D-H, Cho K-S, Choi BL, Min Kim J, Hwang S, et al. Heterogeneous stacking of nanodot monolayers by dry pick-and-place transfer and its applications in quantum dot light-emitting diodes. *Nature Communications*. 2013;4(1):2637. doi:10.1038/ncomms3637
- [125] All inorganic quantum dot light emitting devices with solution processed metal oxide transport layers | MRS Advances | Cambridge Core. [accessed 2021 Dec 20]. <https://www.cambridge.org/core/journals/mrs-advances/article/abs/all-inorganic-quantum-dot-light-emitting-devices-with-solution-processed-metal-oxide-transport-layers/8322C9D9B31581CD62D4B01E3D2101E8>
- [126] Jesuraj J, Hafeez H, Rhee S, Kim DH, Song M, Kim C, Ryu S. Effects of Doping Concentration and Emission Layer Thickness on Recombination Zone and Exciton Density Control in Blue Phosphorescent Organic Light-Emitting Diodes. *ECS Journal of Solid State Science and Technology*. 2017;6:R170–R174. doi:10.1149/2.0321712jss
- [127] Won Y-H, Cho O, Kim T, Chung D-Y, Kim T, Chung H, Jang H, Lee J, Kim D, Jang E. Highly efficient and stable InP/ZnSe/ZnS quantum dot light-emitting diodes. *Nature*. 2019;575(7784):634–638. doi:10.1038/s41586-019-1771-5
- [128] Choi MK, Yang J, Hyeon T, Kim D-H. Flexible quantum dot light-emitting diodes for next-generation displays. *npj Flexible Electronics*. 2018;2(1):1–14. doi:10.1038/s41528-018-0023-3
- [129] Bang SY, Suh Y-H, Fan X-B, Shin D-W, Lee S, Choi HW, Lee TH, Yang J, Zhan S, Harden-Chaters W, et al. Technology progress on quantum dot light-emitting diodes for next-generation displays. *Nanoscale Horizons*. 2021;6(2):68–77. doi:10.1039/D0NH00556H
- [130] Kim T-H, Cho K-S, Lee EK, Lee SJ, Chae J, Kim JW, Kim DH, Kwon J-Y, Amaratunga G, Lee SY, et al. Full-colour quantum dot displays fabricated by transfer printing. *Nature Photonics*. 2011;5(3):176–182. doi:10.1038/nphoton.2011.12
- [131] Peihua Yang, Long Zhang, Dong Jin Kang, Robert Strahl, Tobias Kraus. High-Resolution Inkjet Printing of Quantum Dot Light-Emitting Microdiode Arrays - *Advanced Optical Materials* - Volume8, Issue1 January 3, 2020 1901429. [accessed 2021 Dec 20]. <https://doi.org/10.1002/adom.201901429>
- [132] Zhang H, Su Q, Chen S. Quantum-dot and organic hybrid tandem light-emitting diodes with multi-functionality of full-color-tunability and white-light-emission. *Nature Communications*. 2020;11(1):2826. doi:10.1038/s41467-020-16659-x
- [133] Abhishek Swarnkar Ashley R. Marshall Erin M. Sanehira Boris D. Chernomordik David T. Moore Jeffrey A. Christians Tamoghna Chakrabarti and Joseph M. Luther. Quantum dot–induced phase stabilization of  $\alpha$ -CsPbI<sub>3</sub> perovskite for high-efficiency photovoltaics *Science* • 7 Oct 2016 • Vol 354, Issue 6308 • pp. 92–95 • DOI: 10.1126/science.aag2700. [accessed 2021 Dec 20].

- [134] Garcia-Cortes M, Sotelo González E, Fernández-Argüelles MT, Encinar JR, Costa-Fernández JM, Sanz-Medel A. Capping of Mn-Doped ZnS Quantum Dots with DHLA for Their Stabilization in Aqueous Media: Determination of the Nanoparticle Number Concentration and Surface Ligand Density. *Langmuir*. 2017;33(25):6333–6341. doi:10.1021/acs.langmuir.7b00409
- [135] Zhang Y, Clapp A. Overview of Stabilizing Ligands for Biocompatible Quantum Dot Nanocrystals. *Sensors*. 2011;11(12):11036–11055. doi:10.3390/s111211036
- [136] La Rosa M, Avellini T, Lincheneau C, Silvi S, Wright IA, Constable EC, Credi A. An Efficient Method for the Surface Functionalization of Luminescent Quantum Dots with Lipoic Acid Based Ligands. *European Journal of Inorganic Chemistry*. 2017;2017(44):5143–5151. doi:10.1002/ejic.201700781
- [137] Koh W, Park S, Ham Y. Phosphonic Acid Stabilized Colloidal CsPbX<sub>3</sub> (X=Br, I) Perovskite Nanocrystals and Their Surface Chemistry. *ChemistrySelect*. 2016;1:3479–3482. doi:10.1002/slct.201600809
- [138] Chieh-Yu Kang, Chun-Ho Lin, Chih-Hao Lin, Ting-You Li, Sung-Wen Huang Chen & al. Highly Efficient and Stable White Light-Emitting Diodes Using Perovskite Quantum Dot Paper - *Advanced Science* - Volume6, Issue24 December 18, 2019 1902230. [accessed 2021 Dec 20]. <https://doi.org/10.1002/advs.201902230>
- [139] Svenja Wepfer<sup>†‡</sup>, Julia Frohleiks<sup>†‡</sup>, A-Ra Hong<sup>§</sup>, Ho Seong Jang<sup>§</sup>, Gerd Bacher<sup>‡</sup>, and Ekaterina Nannen. Solution-Processed CuInS<sub>2</sub>-Based White QD-LEDs with Mixed Active Layer Architecture | *ACS Applied Materials & Interfaces* 2017, 9, 12, 11224–11230. [accessed 2021 Dec 20]. <https://doi.org/10.1021/acsami.6b15660>
- [140] Lianfeng Zhao, Barry P. Rand. Metal-halide perovskites: Emerging light-emitting materials — Princeton University. [accessed 2021 Dec 20]. <https://collaborate.princeton.edu/en/publications/metal-halide-perovskites-emerging-light-emitting-materials>
- [141] Loredana Protesescu<sup>†‡</sup>, Sergii Yakunin<sup>†‡</sup>, Maryna I. Bodnarchuk<sup>†‡</sup>, Franziska Krieg<sup>†‡</sup>, Riccarda Caputo<sup>†</sup>, Christopher H. Hendon<sup>§</sup>, Ruo Xi Yang<sup>§</sup>, Aron Walsh<sup>§</sup>, and Maksym V. Kovalenko\*. Nanocrystals of Cesium Lead Halide Perovskites (CsPbX<sub>3</sub>, X = Cl, Br, and I): Novel Optoelectronic Materials Showing Bright Emission with Wide Color Gamut | *Nano Letters* 2015, 15, 6, 3692–3696. [accessed 2021 Dec 20]. <https://doi.org/10.1021/nl5048779>
- [142] Yasuhiro Shirasaki, Geoffrey J. Supran, Mounqi G. Bawendi & Vladimir Bulović. Emergence of colloidal quantum-dot light-emitting technologies | *Nature Photonics* 7, 13-23 (2013). [accessed 2021 Dec 20]. <https://doi.org/10.1038/nphoton.2012.328>
- [143] Sutherland BR, Sargent EH. Perovskite photonic sources. *Nature Photonics*. 2016;10(5):295–302. doi:10.1038/nphoton.2016.62
- [144] Li X, Zhao Y-B, Fan F, Levina L, Liu M, Quintero-Bermudez R, Gong X, Quan LN, Fan J, Yang Z, et al. Bright colloidal quantum dot light-emitting diodes enabled by efficient chlorination. *Nature Photonics*. 2018;12(3):159–164. doi:10.1038/s41566-018-0105-8
- [145] Liu M, Grandhi GK, Matta S, Mokurala K, Litvin A, Russo S, Vivo P. Halide Perovskite Nanocrystal Emitters. *Advanced Photonics Research*. 2021;2(3):2000118. doi:10.1002/adpr.202000118
- [146] Zhao L, Kerner RA, Xiao Z, Lin YL, Lee KM, Schwartz J, Rand BP. Redox Chemistry Dominates the Degradation and Decomposition of Metal Halide Perovskite Optoelectronic Devices. *ACS Energy Letters*. 2016;1(3):595–602. doi:10.1021/acscenergylett.6b00320

- [147] Guohui Li, Keqiang Chen, Yanxia Cui, Yupeng Zhang, Yue Tian, Bining Tian, Yuying Hao, Yucheng Wu, Han Zhang. Stability of Perovskite Light Sources: Status and Challenges - *Advanced Optical Materials* Volume8, Issue6 March 19, 2020 1902012. [accessed 2021 Dec 20]. <https://onlinelibrary.wiley.com/doi/abs/10.1002/adom.201902012>
- [148] Sutton RJ, Eperon GE, Miranda L, Parrott ES, Kamino BA, Patel JB, Hörantner MT, Johnston MB, Haghighirad AA, Moore DT, et al. Bandgap-Tunable Cesium Lead Halide Perovskites with High Thermal Stability for Efficient Solar Cells. *Advanced Energy Materials*. 2016;6(8):1502458. doi:10.1002/aenm.201502458
- [149] Chen D, Chen X, Wan Z, Fang G. Full-Spectral Fine-Tuning Visible Emissions from Cation Hybrid Cs<sub>1-m</sub>FAPbX<sub>3</sub> (X = Cl, Br, and I, 0 ≤ m ≤ 1) Quantum Dots. *ACS Applied Materials & Interfaces*. 2017;9(24):20671–20678. doi:10.1021/acsami.7b05429
- [150] Tsai H, Nie W, Blancon J-C, Stoumpos CC, Asadpour R, Harutyunyan B, Neukirch AJ, Verduzco R, Crochet JJ, Tretiak S, et al. High-efficiency two-dimensional Ruddlesden–Popper perovskite solar cells. *Nature*. 2016;536(7616):312–316. doi:10.1038/nature18306
- [151] Fu Y, Zhu H, Chen J, Hautzinger MP, Zhu X-Y, Jin S. Metal halide perovskite nanostructures for optoelectronic applications and the study of physical properties. *Nature Reviews Materials*. 2019;4(3):169–188. doi:10.1038/s41578-019-0080-9
- [152] Tianqi Niu, Jing Lu, & al. High performance ambient-air-stable FAPbI<sub>3</sub> perovskite solar cells with molecule-passivated Ruddlesden–Popper/3D heterostructured film - *Energy & Environmental Science* (RSC Publishing) 2018,11, 3358-3366. [accessed 2021 Dec 20]. <https://pubs.rsc.org/en/content/articlelanding/2019/ee/c8ee02542h/unauth>
- [153] Cohen B-E, Wierzbowska M, Etgar L. High Efficiency and High Open Circuit Voltage in Quasi 2D Perovskite Based Solar Cells. *Advanced Functional Materials*. 2017;27(5):1604733. doi:10.1002/adfm.201604733
- [154] Liu M, Zhang H, Gedamu D, Fourmont P, Rekola H, Hiltunen A, Cloutier SG, Nechache R, Priimagi A, Vivo P. Halide Perovskite Nanocrystals for Next-Generation Optoelectronics. *Small*. 2019;15(28):1900801. doi:10.1002/sml.201900801
- [155] Huang H, Bodnarchuk MI, Kershaw SV, Kovalenko MV, Rogach AL. Lead Halide Perovskite Nanocrystals in the Research Spotlight: Stability and Defect Tolerance. *ACS Energy Letters*. 2017;2(9):2071–2083. doi:10.1021/acsenenergylett.7b00547
- [156] Wang L, Shi Z, Ma Z, Yang D, Zhang F, Ji X, Wang M, Chen X, Na G, Chen S, et al. Colloidal Synthesis of Ternary Copper Halide Nanocrystals for High-Efficiency Deep-Blue Light-Emitting Diodes with a Half-Lifetime above 100 h. *Nano Letters*. 2020;20(5):3568–3576. doi:10.1021/acs.nanolett.0c00513
- [157] Luo J, Wang X, Li S, Liu J, Guo Y, Niu G, Yao L, Fu Y, Gao L, Dong Q, et al. Efficient and stable emission of warm-white light from lead-free halide double perovskites. *Nature*. 2018;563(7732):541–545. doi:10.1038/s41586-018-0691-0
- [158] Zhifang Tan, Yanmeng Chu & al. Lead-Free Perovskite Variant Solid Solutions Cs<sub>2</sub>Sn<sub>1-x</sub>TexCl<sub>6</sub>: Bright Luminescence and High Anti-Water Stability - *Advanced Materials* -Volume32, Issue32 August 13, 2020 2002443. [accessed 2021 Dec 20]. doi.org/10.1002/adma.202002443

- [159] Zhang R, Mao X, Zheng D, Yang Y, Yang S, Han K. A Lead-Free All-Inorganic Metal Halide with Near-Unity Green Luminescence Volume14, Issue5 May 2020 2000027. *Laser & Photonics Reviews*. 2020;14(5):2000027. doi:10.1002/lpor.202000027
- [160] Shaocong Hou & al. Efficient Blue and White Perovskite Light-Emitting Diodes via Manganese Doping - *JOULE* Volume 2, Issue 11, 21 November 2018, Pages 2421-2433. [accessed 2021 Dec 20]. doi.org/10.1016/j.joule.2018.08.005
- [161] Zhang M, Wang M, Yang Z, Li J, Qiu H. Preparation of all-inorganic perovskite quantum dots-polymer composite for white LEDs application. *Journal of Alloys and Compounds*. 2018;748:537–545. doi:10.1016/j.jallcom.2018.03.179
- [162] Yoon HC, Kang H, Lee S, Oh JH, Yang H, Do YR. Study of Perovskite QD Down-Converted LEDs and Six-Color White LEDs for Future Displays with Excellent Color Performance. *ACS Applied Materials & Interfaces*. 2016;8(28):18189–18200. doi:10.1021/acsami.6b05468
- [163] Bulk Conductivity in Organic Crystals | H. KALLMANN & M. POPE *Nature* volume 186, pages 31–33 (1960). [accessed 2021 Dec 20]. doi.org/10.1038/186031a0
- [164] Pope M, Kallmann HP, Magnante P. Electroluminescence in Organic Crystals. *The Journal of Chemical Physics*. 1963;38(8):2042–2043. doi:10.1063/1.1733929
- [165] Tang CW, VanSlyke SA. Organic electroluminescent diodes. *Applied Physics Letters*. 1987;51(12):913–915. doi:10.1063/1.98799
- [166] Principles and Applications of Organic Light Emitting Diodes (OLEDs) - Kalyani, N. Thejo, Swart, Hendrik C., Dhoble, Sanjay J. - Livres. [accessed 2021 Dec 20].
- [167] Zou S-J, Shen Y, Xie F-M, Chen J-D, Li Y-Q, Tang J-X. Recent advances in organic light-emitting diodes: toward smart lighting and displays. *Materials Chemistry Frontiers*. 2020;4(3):788–820. doi:10.1039/C9QM00716D
- [168] Lundberg P, Lindh EM, Tang S, Edman L. Toward Efficient and Metal-Free Emissive Devices: A Solution-Processed Host–Guest Light-Emitting Electrochemical Cell Featuring Thermally Activated Delayed Fluorescence. *ACS Applied Materials & Interfaces*. 2017;9(34):28810–28816. doi:10.1021/acsami.7b07826
- [169] Zhang J, Chen W, Chen R, Liu X-K, Xiong Y, Kershaw SV, Rogach AL, Adachi C, Zhang X, Lee C-S. Organic nanostructures of thermally activated delayed fluorescent emitters with enhanced intersystem crossing as novel metal-free photosensitizers. *Chemical Communications*. 2016;52(79):11744–11747. doi:10.1039/C6CC05130H
- [170] The contributions of molecular vibrations and higher triplet levels to the intersystem crossing mechanism in metal-free organic emitters - *Journal of Materials Chemistry C* (RSC Publishing) DOI:10.1039/C7TC01958K. [accessed 2021 Dec 20]. <https://pubs.rsc.org/en/content/articlehtml/2017/tc/c7tc01958k>
- [171] Lee DR, Lee KH, Shao W, Kim CL, Kim J, Lee JY. Heavy Atom Effect of Selenium for Metal-Free Phosphorescent Light-Emitting Diodes. *Chemistry of Materials*. 2020;32(6):2583–2592. doi:10.1021/acs.chemmater.0c00078

- [172] Nan Gan, Huifang Shi, Zhongfu An & al. Recent Advances in Polymer-Based Metal-Free Room-Temperature Phosphorescent Materials - 2018 - Advanced Functional Materials - Volume28, Issue51 December 19, 2018 1802657. [accessed 2021 Dec 20]. <https://doi.org/10.1002/adfm.201802657>
- [173] Park JY, Advincula RC. Tunable electroluminescence properties in CdSe/PVK guest–host based light-emitting devices. *Physical Chemistry Chemical Physics*. 2014;16(18):8589–8593. doi:10.1039/C4CP00066H
- [174] Annalisa Bruno & al. Insights on photophysical proprieties of DCM dye in PVK host matrix - Bruno - 2013 - Polymer Composites Volume34, Issue9 September 2013 Pages 1500-1505. [accessed 2021 Dec 20]. <https://doi.org/10.1002/pc.22441>
- [175] Patel P. Dendrimer Applications : A review [https://www.researchgate.net/publication/264290119\\_Dendrimer\\_Applications\\_A\\_review](https://www.researchgate.net/publication/264290119_Dendrimer_Applications_A_review). *International Journal Of Pharma and Bioscience*. 2013;4:454.
- [176] Adachi C, Sandanayaka ASD. The Leap from Organic Light-Emitting Diodes to Organic Semiconductor Laser Diodes. *CCS Chemistry*. 2020 Aug 1 [accessed 2021 Dec 20]. <https://www.chinesechemsoc.org/doi/abs/10.31635/ccschem.020.202000327>. doi:10.31635/ccschem.020.202000327
- [177] Hartmut Yersin (Editor). *Highly Efficient OLEDs: Materials Based on Thermally Activated Delayed Fluorescence* ISBN: 978-3-527-33900-6 January 2019 608 Pages. Wiley.com. [accessed 2021 Dec 20]. <https://www.wiley.com/en-us/Highly+Efficient+OLEDs%3A+Materials+Based+on+Thermally+Activated+Delayed+Fluorescence-p-9783527339006>
- [178] Hong G, Gan X, Leonhardt C, Zhang Z, Seibert J, Busch JM, Bräse S. A Brief History of OLEDs—Emitter Development and Industry Milestones. *Advanced Materials*. 2021;33(9):2005630. doi:10.1002/adma.202005630
- [179] Sudheendran Swayamprabha S, Dubey DK, Shahnawaz, Yadav RAK, Nagar MR, Sharma A, Tung F-C, Jou J-H. Approaches for Long Lifetime Organic Light Emitting Diodes - Sudheendran Swayamprabha - *Advanced Science* - Volume8, Issue1 January 6, 2021 2002254. *Advanced Science*. 2021;8(1):2002254. doi:10.1002/advs.202002254
- [180] APS -APS March Meeting 2018 - Event - How Organic Light Emitting Diodes Revolutionized Displays (and maybe lighting). In: *Bulletin of the American Physical Society*. Vol. Volume 63, Number 1. American Physical Society. <https://meetings.aps.org/Meeting/MAR18/Session/L32.3>
- [181] Lee J-H, Chen C-H, Lee P-H, Lin H-Y, Leung M, Chiu T-L, Lin C-F. Blue organic light-emitting diodes: current status, challenges, and future outlook. *Journal of Materials Chemistry C*. 2019;7(20):5874–5888. doi:10.1039/C9TC00204A
- [182] Murawski C, Leo K, Gather MC. Efficiency Roll-Off in Organic Light-Emitting Diodes. *Advanced Materials*. 2013;25(47):6801–6827. doi:10.1002/adma.201301603
- [183] Chatterjee T, Wong K-T. Perspective on Host Materials for Thermally Activated Delayed Fluorescence Organic Light Emitting Diodes. *Advanced Optical Materials*. 2019;7(1):1800565. doi:10.1002/adom.201800565

- [184] Song J, Kim K-H, Kim E, Moon C-K, Kim Y-H, Kim J-J, Yoo S. Lensfree OLEDs with over 50% external quantum efficiency via external scattering and horizontally oriented emitters. *Nature Communications*. 2018;9(1):3207. doi:10.1038/s41467-018-05671-x
- [185] Chu C, Ha J, Choi J, Lee S, Rhee J, Lee D, Chung J, Kim H, Chung K. 25.4: Advances and Issues in White OLED and Color Filter Architecture. *Sid Symposium Digest of Technical Papers*. 2007;38. doi:10.1889/1.2785504
- [186] Dubey D, Sahoo S, Wang C-W, Jou J-H. Solution process feasible highly efficient white organic light emitting diode. *Organic Electronics*. 2019;69. doi:10.1016/j.orgel.2019.03.001
- [187] Duarte LGTA, Germino JC, Berbigier JF, Barboza CA, Faleiros MM, Simoni D de A, Galante MT, Holanda MS de, Rodembusch FS, Atvars TDZ. White-light generation from all-solution-processed OLEDs using a benzothiazole–salophen derivative reactive to the ES IPT process. *Physical Chemistry Chemical Physics*. 2019;21(3):1172–1182. doi:10.1039/C8CP06485G
- [188] Deepak KumarDubey & al. Simple-structured efficient white organic light emitting diode via solution process - *Microelectronics Reliability* Volume 83, April 2018, Pages 293-296. [accessed 2021 Dec 20]. doi.org/10.1016/j.microrel.2017.07.076
- [189] Cai Z, Chen H, Guo J, Zhao Z, Tang BZ. Efficient Aggregation-Induced Delayed Fluorescence Luminogens for Solution-Processed OLEDs With Small Efficiency Roll-Off. *Frontiers in Chemistry*. 2020;8:193. doi:10.3389/fchem.2020.00193
- [190] Yin X, He Y, Wang X, Wu Z, Pang E, Xu J and Wang J. Recent Advances in Thermally Activated Delayed Fluorescent Polymer—Molecular Designing Strategies | *Front. Chem.* 8:725. [accessed 2021 Dec 20]. doi: 10.3389/fchem.2020.00725
- [191] Zou S-J, Shen Y, Xie F-M, Chen J-D, Li Y-Q, Tang J-X. Recent advances in organic light-emitting diodes: toward smart lighting and displays. *Materials Chemistry Frontiers*. 2020;4(3):788–820. doi:10.1039/C9QM00716D
- [192] Volume21, Issue41, November 6, 2009, Hongbin Wu & al. Efficient Polymer White-Light-Emitting Devices for Solid-State Lighting - *Advanced Materials* -Volume21, Issue41 november 6, 2009 Pages 4181-4184. [accessed 2022 Jan 5]. <https://doi.org/10.1002/adma.200900638>
- [193] Gustafsson G, Cao Y, Treacy GM, Klavetter F, Colaneri N, Heeger AJ. Flexible light-emitting diodes made from soluble conducting polymers. *Nature*. 1992;357(6378):477–479. doi:10.1038/357477a0
- [194] Yin X, He Y, Wang X, Wu Z, Pang E, Xu J, Wang J. Recent Advances in Thermally Activated Delayed Fluorescent Polymer—Molecular Designing Strategies. *Frontiers in Chemistry*. 2020;8:725. doi:10.3389/fchem.2020.00725
- [195] Yuchao Liu & al. All-organic thermally activated delayed fluorescence materials for organic light-emitting diodes | *Nature Reviews Materials* volume 3, Article number: 18020 (2018). [accessed 2022 Jan 5]. doi.org/10.1038/natrevmats.2018.20
- [196] Hong Y, Lam JWY, Tang BZ. Aggregation-induced emission: phenomenon, mechanism and applications. *Chemical Communications*. 2009;(29):4332–4353. doi:10.1039/B904665H
- [197] Ackermann J, Margeat O, Hissler M, Bouit PA. Nanomatériaux Hybrides Luminescents À Émission Induite Par Agrégation. 2015 Aug 27 [accessed 2021 Dec 20]. <https://patentscope.wipo.int/search/fr/detail.jsf?docId=WO2015124802>

- [198] Hong Y, Lam JWY, Tang BZ. Aggregation-induced emission. *Chemical Society Reviews*. 2011;40(11):5361–5388. doi:10.1039/C1CS15113D
- [199] Tu L, Xie Y, Li Z, Tang B. Aggregation-induced emission: Red and near-infrared organic light-emitting diodes. *SmartMat*. 2021;2(3):326–346. doi:10.1002/smm2.1060
- [200] Zhao Q, Sun JZ. Red and near infrared emission materials with AIE characteristics. *Journal of Materials Chemistry C*. 2016;4(45):10588–10609. doi:10.1039/C6TC03359H
- [201] Shipan Wang & al. Highly Efficient Near-Infrared Delayed Fluorescence Organic Light Emitting Diodes Using a Phenanthrene-Based Charge-Transfer Compound - *Angewandte Chemie International Edition - Volume54, Issue44 October 26, 2015 Pages 13068-13072*. [accessed 2021 Dec 20]. <https://onlinelibrary.wiley.com/doi/abs/10.1002/anie.201506687>
- [202] Joly D, Tondelier D, Deborde V, Geffroy B, Hissler M, Réau R. Phosphole-based  $\pi$ -conjugated electroluminescent materials for OLEDs. *New Journal of Chemistry*. 2010;34(8):1603–1611. doi:10.1039/CONJ00122H
- [203] Koh W, Park S, Ham Y. Phosphonic Acid Stabilized Colloidal CsPbX<sub>3</sub> (X=Br, I) Perovskite Nanocrystals and Their Surface Chemistry. *ChemistrySelect*. 2016;1:3479–3482. doi:10.1002/slct.201600809

# Chapter 1: Introduction to nanohybrids using AIE phenomenon

In this chapter, we will explore the possibilities to associate an organic emitter displaying Aggregation Induced Emission (AIE) properties and to bond it with a nanocrystal (NC) structure. The optical and morphological properties of this new nanohybrid material will be investigated, in order to achieve a LED using pure nanohybrids as emissive layer.

## 1) The AIE nanohybrid composition

Firstly, we describe the strategy to design AIE nanohybrids. A nanohybrid is composed of an inorganic core with an organic shell which emits light according to the AIE phenomenon. For instance, inorganic cores can be based on nanocrystals of various sizes and shapes, such as spherical metal oxide nanoparticles, cubic perovskites or even metallic nanowires. The core may play the role of electron transporter in thin films, and also, depending on the materials, it may participate in light emission. The organic part is based on an emitting compound, in this chapter using AIE phenomenon, playing the role of surface ligand for the inorganic nanocrystal. The AIE effect is expected to be even more efficient when the AIE organic molecule is grafted to the surface of the inorganic nanocrystals, therefore this molecule needs both a grafting group and AIE generation groups (such as phenyl groups that may have their rotation frozen upon grafting). Moreover, the organic shell should be designed as a hole transporter in thin film, meaning that the inorganic organic nanohybrid could display ambipolar transport, and thus being theoretically usable as electroluminescent active layer in optoelectronic devices. The combination of organic and inorganic parts is very promising because the properties from both entities can be unified in a single compound. This liquid colloidal approach may solve some technical issues related to other LED technologies such as the conception of white LED, lifetime issues and manufacturing costs. The different tested materials and their properties are presented in the following part.

### a) Inorganic core

In this part, two metal oxide nanoparticles widely studied in literature were selected –ZnO and ZrO<sub>2</sub>- in order to be easily fonctionnalisable on their surface by COOH or POOH groupment.

#### i) ZnO

The ZnO nanoparticles were synthesized via hydrothermal synthesis: alcoholysis of acetate zinc precursor in a basic solution (methanol and KOH). The ZnO nanoparticles are synthesized voluntarily without adding any surface ligand stabilizer. However, on the surface of ZnO some OH and residual acetate groupments remain.

#### Morphological aspects:

Pure synthesized ZnO nanocrystals are first characterized in morphology via TEM images presented in figure 1.

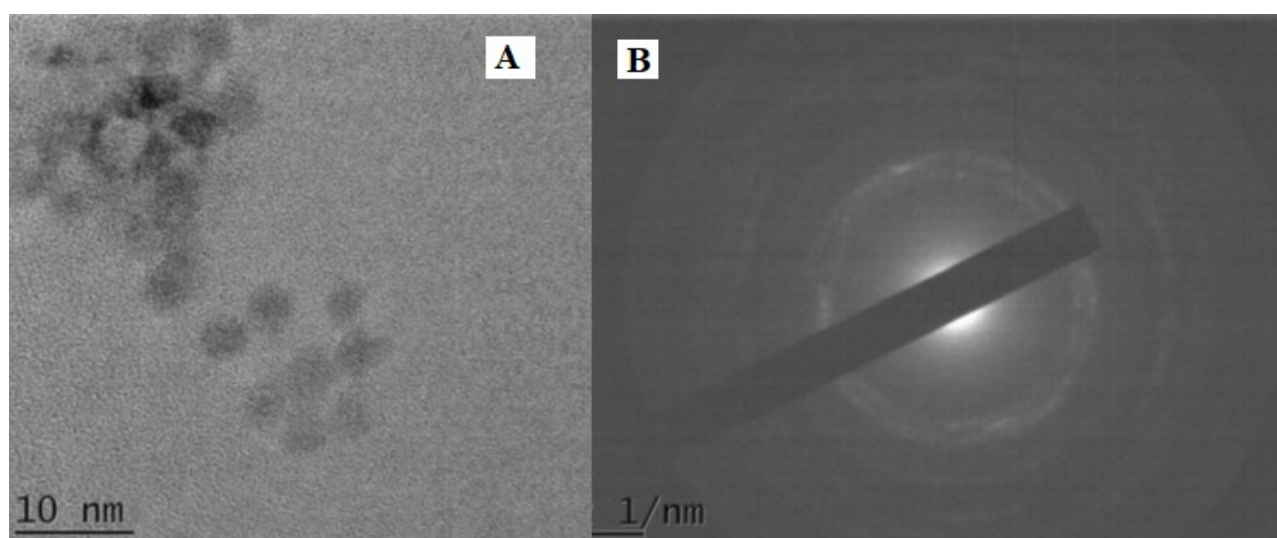


Figure 1 : A) TEM image of ZnO B) Diffraction pattern of ZnO

The TEM measurements show that the synthesized ZnO nanoparticles are homogeneous in size and shape, these last take a spherical form with an average diameter of 5 nm. In another hand, the TEM image reveals that the nanocrystals present a relatively low size distribution.

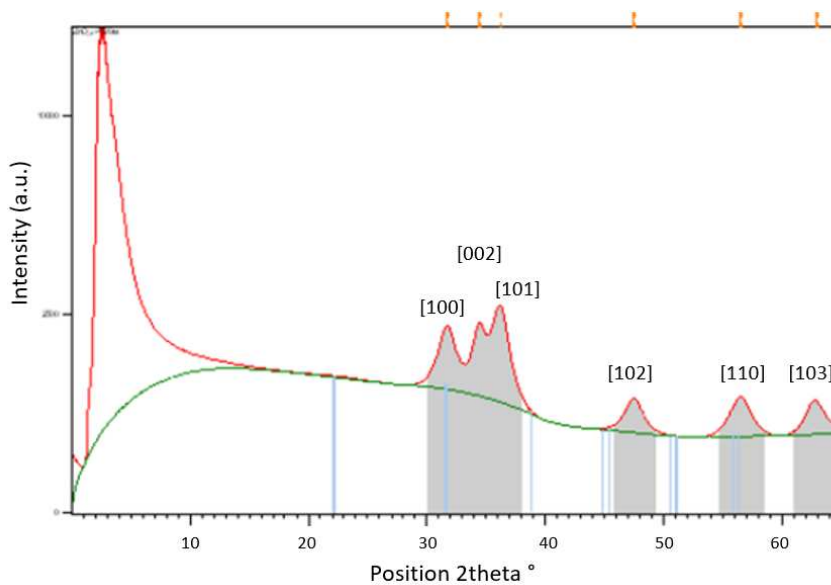
The crystalline structure of the ZnO nanoparticle were investigated further using XRD measurements and the observations show that the nanocrystals adopt the classic hexagonal wurtzite structure according to JCPDS files (annexe 1). The ZnO nanocrystal has different orientations / plans. However, the calculous of the crystal sizes was done thanks to Scherrer

equation and show that the ZnO is crystalline with crystal sizes from 5.1 to 8.3 nm. The favorite growth crystal plan is then [002]. These results confirm the first observations done in TEM.

Scherrer Equation for the crystal size

$$\frac{K\lambda}{FWHM * \cos(\theta)}$$

with K=0.89 shape factor,  $\lambda=1.5418\text{\AA}$  from  $K\alpha_{1/2}$  of Copper ;  $\theta$  et FWHM in radian.



Plan	d spacing (Å)	2theta (°)	FWMH (°)	Larg Instr (°)	Crystal Sizes Scherrer (nm)
100	2,822	31,712	1,75	0,28	5,6
002	2,605	34,424	1,27	0,28	8,3
101	2,482	36,195	1,69	0,27	5,8
102	1,915	47,485	1,75	0,27	5,8
110	1,629	56,508	2,04	0,28	5,1
103	1,480	62,777	1,67	0,29	6,7

Figure 2 : XRD powder of ZnO NCs and its crystalline parameters

The hexagonal wurtzite structure, according to the bibliography [1] is the most stable form of ZnO. It would provide piezo/pyroelectric properties because it does not have central symmetry. Moreover, this metal oxide nanoparticle is known to be an n-type semi-conductor, thus can be beneficial for the envisaged LED system or for other applications.

### Optical properties:

The optical behavior of the ZnO nanocrystals (NCs) is investigated by UV-visible absorbance and correlated fluorescence spectroscopies, as presented in figure 3:

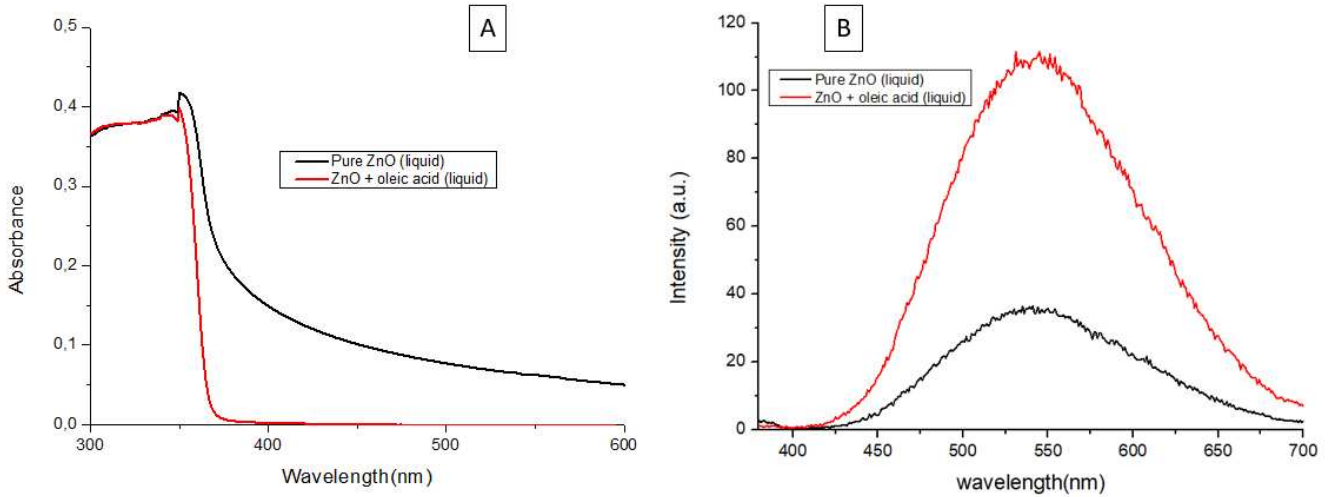


Figure 3 : A)absorbance B)fluorescence ( $\lambda_{exc} = 350 \text{ nm}$ ) spectra of pure ZnO (black) and ZnO stabilized with oleic acid (red) in solutions

The UV Vis absorbance spectra show that the absorption threshold are close to 350 nm, thus evaluating an optical bandgap of  $E = 3.31 \text{ eV}$ , which correspond to the ZnO wurtzite nanoparticle (5 nm diameter) found in literature [1] with :

$$E = \frac{hc}{\lambda}$$

$h = \text{Planck constant } 6,63 \cdot 10^{-34} \text{ (J/s)}; c = \text{speed of light } 3.00 \cdot 10^8 \left(\frac{m}{s}\right); \lambda = \text{wavelength (m)}$

The absorbance curves show that the solution of pure ZnO (black curve) has light scattering signal over 400 nm, due to high aggregation of the nanocrystals in solution. On the contrary, the monodisperse and stabilized ZnO NCs with oleic acid (red curve) present no light scattering signal related to aggregation. Interestingly, the objects inside the pure ZnO NCs which are aggregated show a lower emission in fluorescence intensity than the smallest monodisperse ZnO oleic acid, in the same ZnO concentration. According to these results, the oleic acid allows a stabilization of the ZnO nanoparticle but also an increase in the photoluminescence properties of the ZnO, which emits in the green region when excited at 350 nm. As the ZnO NCs were synthesized under basic conditions due to KOH reactant, the surface of the metal oxide has many hydroxy groups (OH), which will allow the grafting with an organic surface emitter. Therefore, the choice of ZnO to compose an electroluminescent layer is relevant because it is a transparent material, in addition to have interesting electrical properties for optoelectronic applications [2]

ii) ZrO<sub>2</sub>

The ZrO<sub>2</sub> nanoparticles were synthesized via alcoholysis of a zirconia precursor (zirconium isopropoxide) in a basic solution of benzyl alcohol. The ZrO<sub>2</sub> nanoparticles are synthesized voluntarily without surface ligand stabilizer, even if on surface of zirconia nanoparticles, some hydroxy groups and residual zirconium isopropoxide groups remain. [3]

Morphological aspects :

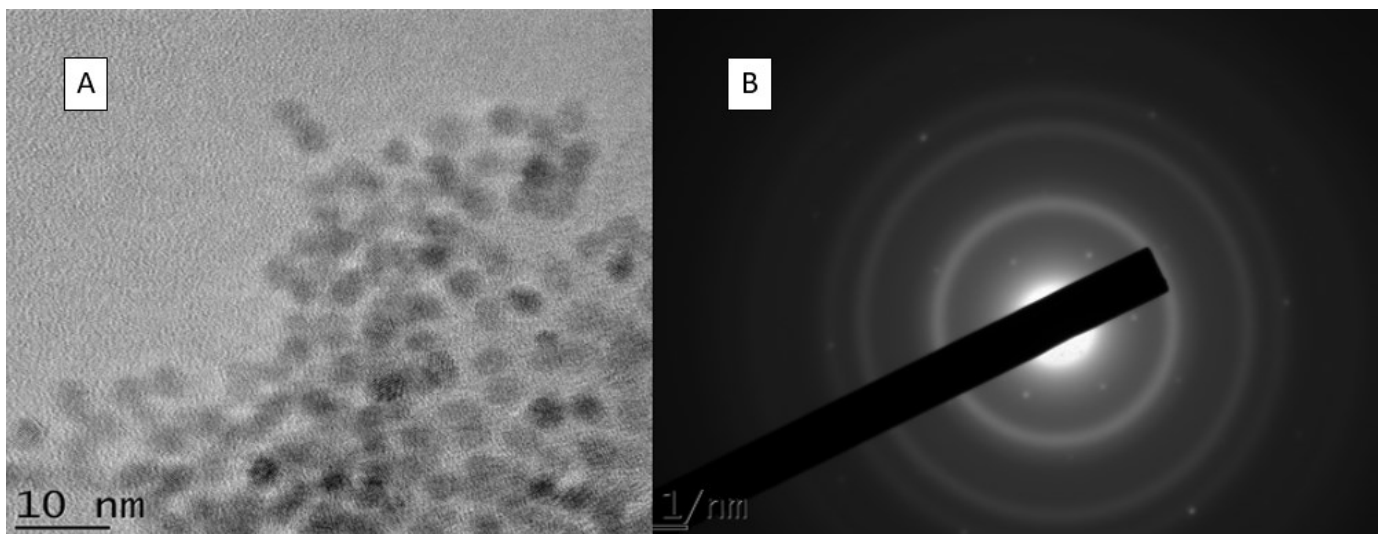
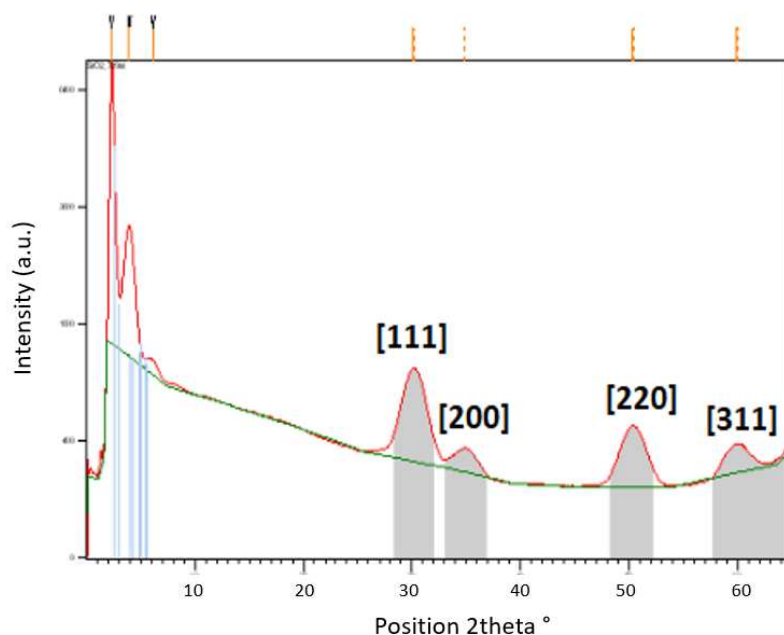


Figure 4 : A) TEM image B) diffraction image of ZrO<sub>2</sub> nanocrystals

The morphological characterizations of the synthesized ZrO<sub>2</sub> were done with TEM and XRD. The TEM pictures reveal, as for ZnO NCs, a spherical nanoparticle shape with an average diameter of 4 nm. The size and shape distributions of the NCs are very homogeneous. Moreover, the diffraction TEM picture shows that the ZrO<sub>2</sub> is composed of diffraction rings, thus crystalline ZrO<sub>2</sub> with different orientations/plans. The crystallinity of the particles is investigated further by XRD.



Orientation cristalline	d-spacing (Å)	Position ° (2θ)	FWHM ° (2θ)	Largeur instrumentale ° (2θ)	Taille des cristallites Scherrer (nm)
111	2,960	30,14	2,41	0,32	3,9
200	2,580	34,75	2,23	0,29	4,3
220	1,810	50,33	2,43	0,29	4,1
311	1,540	59,94	2,47	0,26	4,1

Figure 5 : XRD powder of  $ZrO_2$  NCs and its crystalline parameters

It is deduced that we have monocrystals of  $ZrO_2$  taking the cubic crystalline structure (cf. JCPDS annexe 2). The diffraction peaks are roughly of the same width, indicating that there is no preferential plan of crystal growth, thus, according to Scherrer equation, cubic  $ZrO_2$  NCs sizes are about 3.9 to 4.3 nm. Therefore, correlated to TEM images, this may suggest a complete crystallization of the  $ZrO_2$  nanoparticle.

#### Optical properties:

The cubic  $ZrO_2$  material is known to be a non-emissive semi-conductor because of its high bandgap, compared to ZnO, for instance. However, cubic  $ZrO_2$  is used in literature for optoelectronic devices, as interfacial layer in photovoltaic [4] or for sensor [5] applications. At first, absorbance investigations were done in order to check if it was possible to obtain well-dispersed  $ZrO_2$  NCs in solution. Indeed, many carboxylic surface ligands were tried, with different length of alkyl chain, namely, oleic acid (18C), stearic acid (18C), dodecanoic acid (12C) and citric acid (6C), and the related solutions measured by absorbance spectroscopy in figure 6.

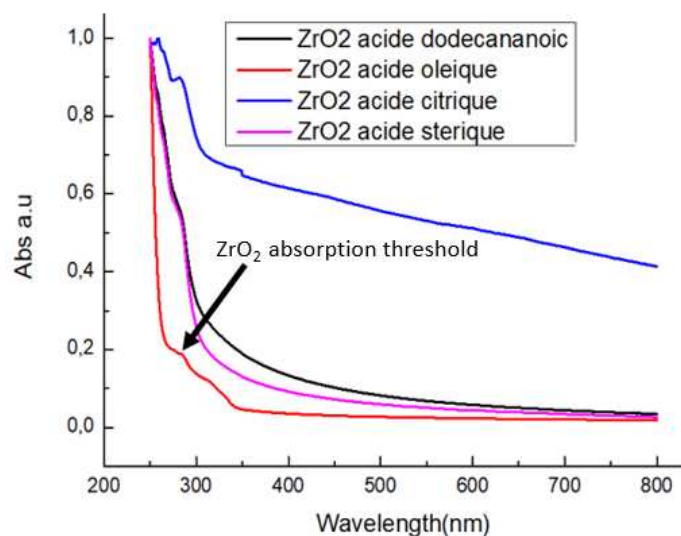


Figure 6 : absorbance spectra of  $ZrO_2$  NCs grafted with different carboxylic acids with various length of alkyl chain

The same behavior as ZnO NCs has been observed, as the oleic acid represents an efficient surface ligand to stabilize the nanoparticle of zirconia: there is no light scattering signal in the visible region, in comparison with the other ligands. Moreover, the absorption threshold of the cubic  $ZrO_2$  NCs is reported at 280 nm, equivalent to an optical bandgap of 4.31 eV, thus, explaining why the material is non emissive. In contrast, the ZnO NCs also absorb in UV area, but it emits light in the visible range because of his structural defects, that is different for  $ZrO_2$  NCs.

### iii) Inorganic halogenated perovskites $CsPbI_3$

#### Optical properties:

The choice of red emissive  $CsPbI_3$  perovskites is interesting because of the complicated synthesis of efficient red organic emitters. Indeed, the more the material is characterized by red or infrared emission, the lower the bandgap of the emitters. Therefore, it is easier to pass this energy barrier by non-radiative relaxation (loss of energy by vibration of the molecule). The inorganic  $CsPbI_3$  are then ideal candidates to build a hybrid electroluminescent material. They are known as highly emissive materials, and the use of iodide provides a red emission. In addition, the stabilization of these NCs is insured by the stabilization with organic surface ligands. Thus, it is essential to clean the surface in order to synthesize the nanohybrids, namely to graft emitters on the  $CsPbI_3$  surface. On the other hand, the perovskite materials have a low stability under atmospheric conditions and UV exposure. The synthesized  $CsPbI_3$  were first stored outside the glovebox, to avoid any contamination. Many sizes of quantum dots

containing iodide were synthesized and optically analyzed, ranging from 3.5 to 12.5 nm, according to the temperature of the synthesis (from 60 to 185°C), cf. Table 1 [6, 7].

Table 1 : synthesis temperature of CsPbI<sub>3</sub> related to the size of the quantum dots

Temperature	Quantum dots size (nm)
60°C	3,4
100°C	4,5
130°C	5
150°C	6,8
170°C	8
180°C	9
185°C	12,5

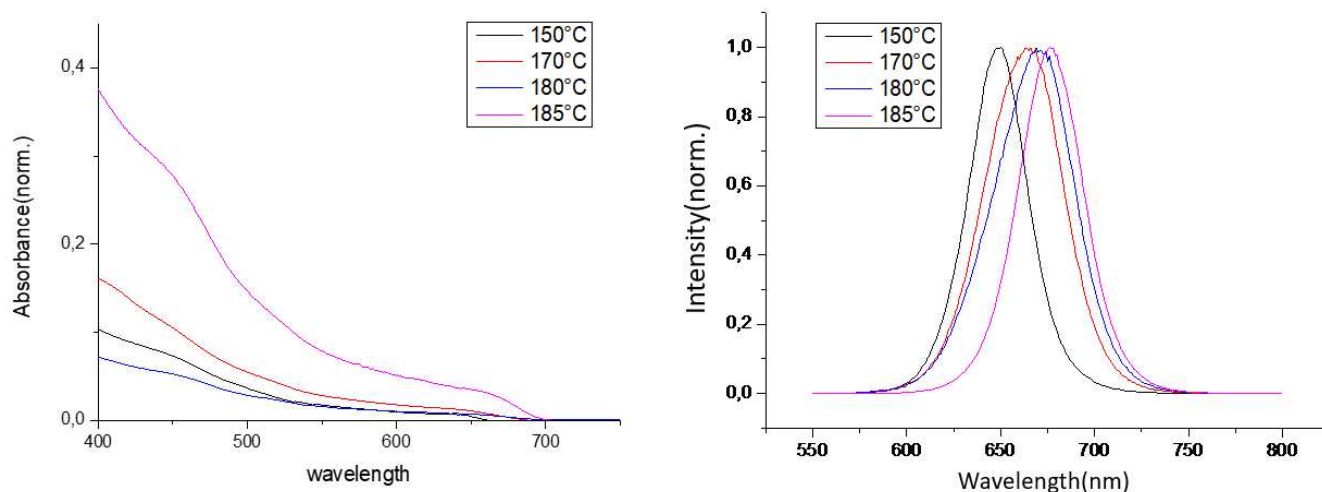


Figure 7 : absorbance and fluorescence  $\lambda_{exc} = 450$  nm spectra of CsPbI<sub>3</sub> NCs, comparing optical properties of different sizes of the quantum dots.

According to the literature [8], and to the optical measurements, the main absorption band related to CsPbI<sub>3</sub> NCs is found at 450 nm. According to the size of the perovskites NCs, the color shifts from orange for the smallest sizes to dark red for the bigger ones. Therefore, this material is really relevant as emitter, as far as the emitted color is controlled via the temperature in the synthesis process. Then, the NCs were analyzed in morphology with TEM, and optically, at different times after the end of the synthesis in order to investigate their stability. The synthesized CsPbI<sub>3</sub> of 12.5 nm were divided in two solutions, one stored in the dark, one stored under fume hood (indoor light), their emission spectra are presented by the figure 8.

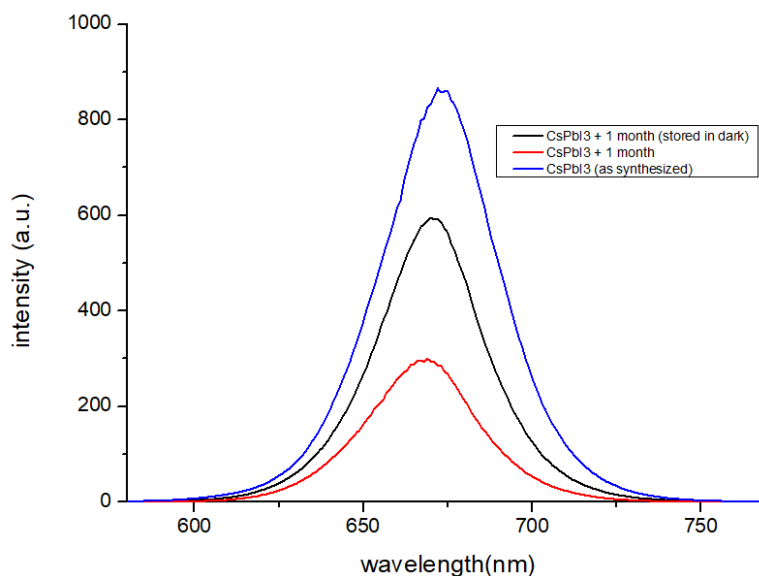


Figure 8 : emission spectra  $\lambda_{exc} = 450$  nm of as synthesized 12.5 nm diameter CsPbI<sub>3</sub> NCs (blue curve) and evolving after 1 month (dark (black curve) vs indoor light storage (red curve))

The quantum dots were excited at 450 nm, the main absorbance peak of CsPbI<sub>3</sub>. After one month, the fluorescence intensity of the CsPbI<sub>3</sub> had decreased, this may be due to oxygen penetration inside the storage vial. However, this is also explained in the literature by ions migration [6, 7]. Contrastingly, the influence of the light is important on the degradation mechanism. Indeed, the CsPbI<sub>3</sub> NCs stored in the dark display more intense fluorescence and are thus more stable after 1 month than the other solution. The other NCs sizes follow the same degradation trend as the bigger NCs, in addition, the smaller sizes degrade faster.

### Morphological aspects :

According to the literature [8], the highly emissive form of CsPbI<sub>3</sub> is cubic, while the most stable under ambient conditions is the orthorhombic crystalline structure. Therefore, TEM pictures were realized in order to check the evolving shape and crystalline phase of the quantum dots, cf. figure 9.

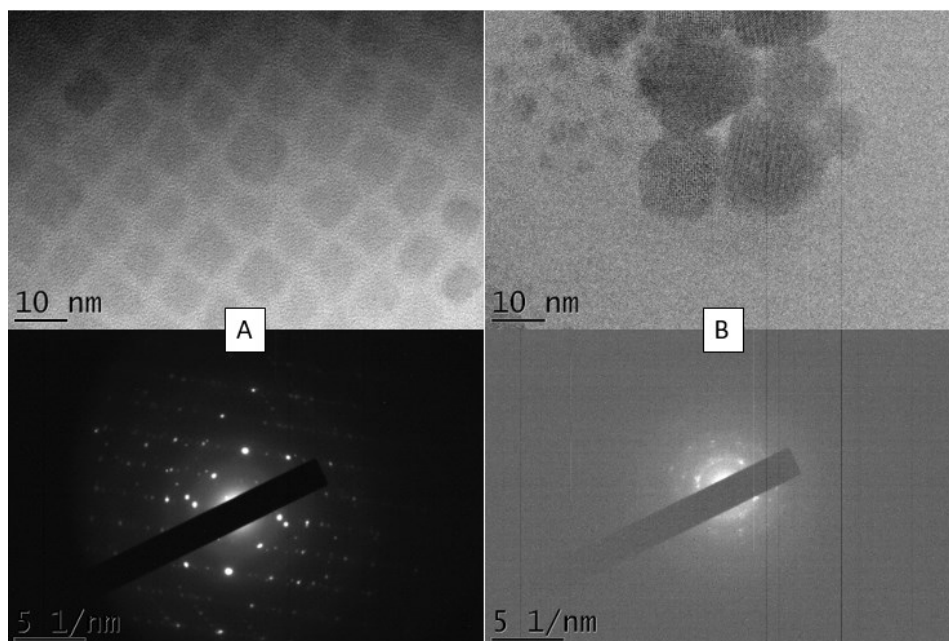


Figure 9 : TEM image + diffraction image of A) As synthesized CsPbI<sub>3</sub> at 180°C B) CsPbI<sub>3</sub> + 1 month

The TEM and diffraction images confirm the observations done in the previous fluorescence spectra. Indeed, the synthesized CsPbI<sub>3</sub> are quite homogeneous in size and shape with cubic shape about 10 nm, and the diffraction image reveals a very pure and mono crystalline order. However, as predicted, after 1 month, the crystalline phase evolves from cubic to probably orthorhombic structure. [6, 7] In addition, the size and shape distributions are very broad: some CsPbI<sub>3</sub> are cubic and about 15 nm, some others are smaller around 5 nm and non-cubic. Finally, due to the poor stability of the perovskites, we decided to not include them to create the hybrid structure. However, this material has a huge potential for future efficient and stable hybrid LED.

### b) Organic AIE emitters (1<sup>st</sup> generation)

The first generation of organic emitters using AIE effect (made by the group of Pr. Muriel Hissler at Institut des Sciences Chimiques de Rennes) are organic molecules with POOH grafting unit (or POPh (Ph=Phenyl) and thus non graftable unit, as reference). The presented molecules in this part are bluish-green emitters, and their optical properties will be shown in the next parts.

Table 2: Photophysical datas of the AIE molecules 1 to 4 with [a] measured in DCM solution ( $c = 10^{-5}$  M). [b] Measured relative to quinine sulfate ( $H_2SO_4$ , 0.1 M),  $\phi_{ref} = 0.54$ . [c] Measured relative to anthracene in ethanol,  $\phi_{ref} = 0.27$  [d] Measured in powder. [e] absolute quantum yield measured in Hamamatsu integration sphere

Compound	$\lambda_{abs}^{liq[a]}$ [nm]	$\lambda_{em}^{liq[a]}$ [nm]	$\phi_{liq}^{[a,b]}$ [%]	$\lambda_{em}^{solid[d]}$ [nm]	$\phi_{powder}^{[d,e]}$ [%]
<b>1</b>	323	363	26 <sup>[c]</sup>	394	-
<b>2</b>	378	513	0.1	534	14
<b>3</b>	380	545	0.2	542	15
<b>4</b>	400	524	0.5	532	46

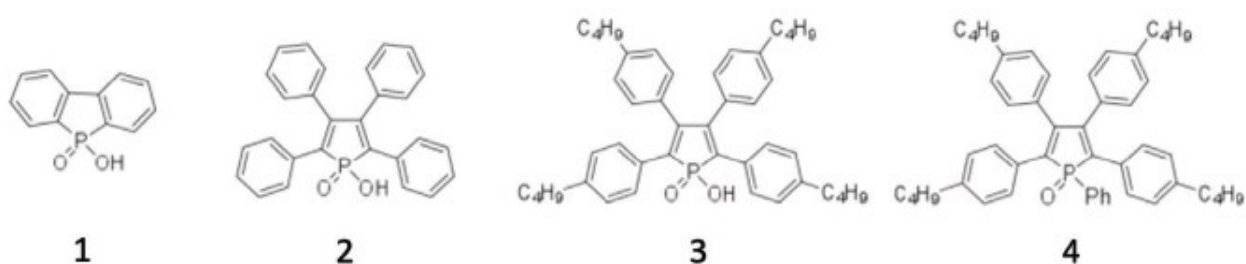


Figure 10: AIE molecules, green emitters with different structures and graftable/non graftable unit

The first conclusion of these 4 organic emitters is that the photoluminescence quantum yield is not so high at the solid state. The second conclusion is found comparing the molecule 3 and 4, knowing that these molecules are similar but the molecule 4 is non graftable onto metal oxide surface. We observe that the hydroxy grafting unit is known to be non-radiative pathway as expected [9], and this is why 3 has only 15 % photoluminescence yield while 4 has 46%. In theory, with an ideal grafting by combining 3 with ZnO NCs, it should be possible to reach the photoluminescence yield of the non graftable 4. The advantage of using nanohybrids ZnO:3 is very important, because it unlocks the solution process, while 4 can be only processed by evaporation method (to obtain homogeneous and smooth surface), and cannot be linked with NCs.

In addition, some other 1<sup>st</sup> generation AIE emitters were done previously by the group of Pr. Muriel Hissler and have different structures than 1, 2, 3 and 4. The color of 5 is bluish-green but 6 is in the yellow orange area, and their excitation / emission fluorescence spectra are shown in figure 11.

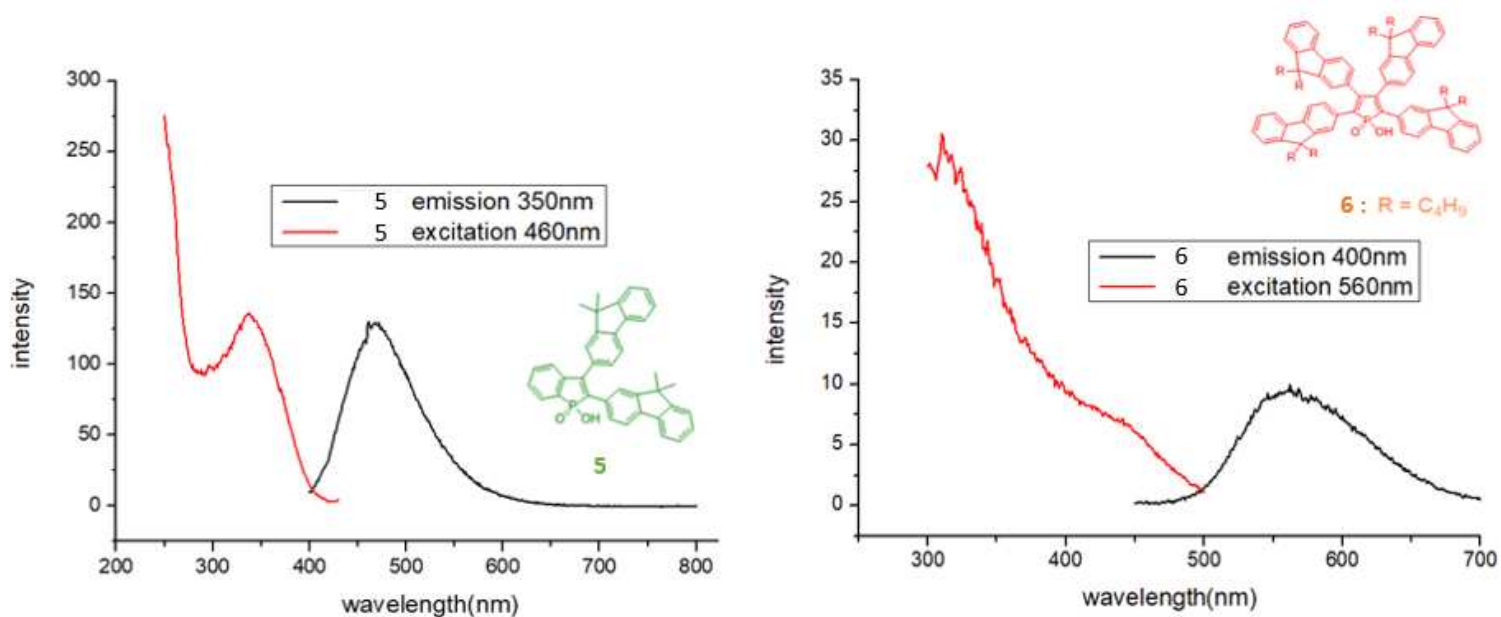


Figure 11 : emission / excitation spectra of the different AIE emitters, 5 (left) ; 6 (right).

## 2) Nanohybrid synthesis in solution (self-assembly)

The nanohybrids are built via self-assembly by mixing the organic emitter and the inorganic NCs solutions in chlorobenzene and chloroform solvents. The process is described by the following figure 12. The grafting rate/speed can also be increased by stirring and temperature.

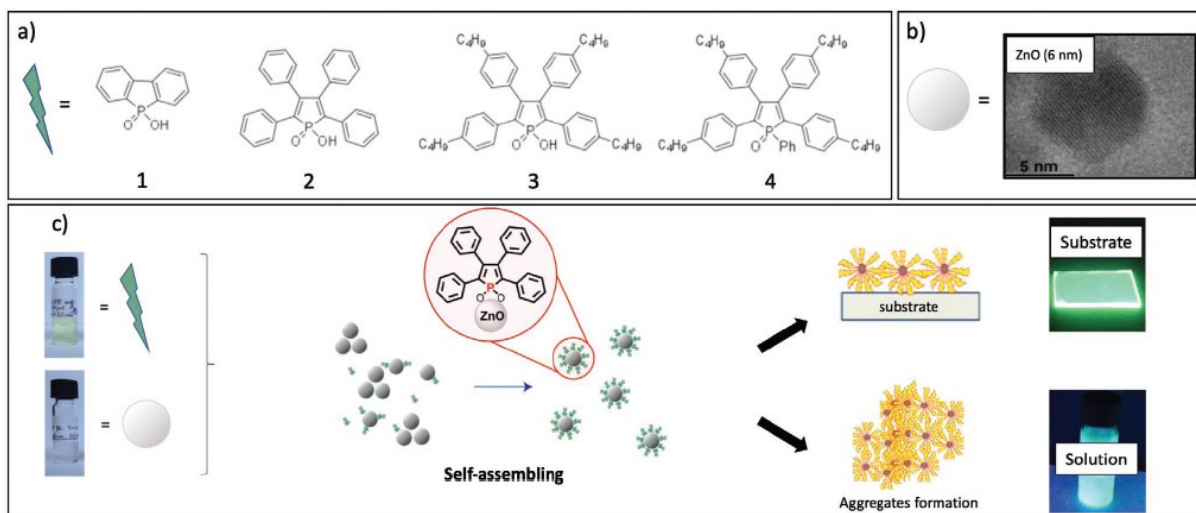


Figure 12 : a) Molecular structures of the AIE fluorescent molecules (1, 2, 3) bearing phosphole unit to bind to ZnO surface; molecule 4 is a reference phosphole without grafting unit. b) Zinc oxide nanoparticles used for the study. c) Scheme of the aggregation-induced emission (AIE) effect when molecules are grafted onto ZnO nanoparticles forming highly emissive materials, used as layer on a substrate or aggregates in solution.

The building of the nanohybrids occurs in solution, which is a major advantage of this approach, thus allowing a large scale production of thin films by solution processes. However, the self-assembly of both entities can lead to nanohybrid aggregate formation, which is highly undesirable to prepare homogeneous thin films and to move toward efficient solution processable LED device. The solution becomes processable as electroluminescent active layer only once we have theoretically well-dispersed nanohybrids, otherwise the opposite case leads to electrical issues such as short cut or fast degradation under voltage application.

### 3) Analyses of the grafting

#### a) Density Functional Theory (DFT), Fourier Transfer Infrared (FTIR) and X-Ray photoelectron spectrometry (XPS) analyses

The DFT calculations and the XPS analyses of the nanohybrids were investigated in order to know if the grafting between the organic and inorganic part was efficient, but also to analyze if the AIE effect really occurs as expected. The study was done with ZnO NCs. The grafting mode of the AIE molecule onto metal oxide surface of a nanoparticle was studied by DFT calculations thanks to a collaboration with Dr. Alessandro Mattoni (Cagliari University) below and correlated FTIR analyses, cf. figure 13.

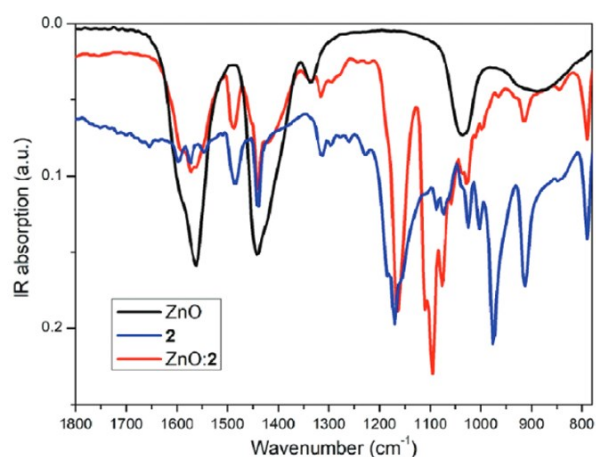
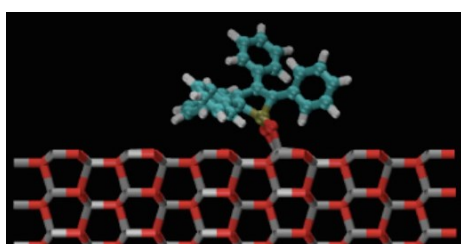


Figure 13 : Left scheme : DFT calculations AIE molecule 2 (cyan) + metal oxide surface (red), Right scheme: FTIR absorption spectra of ZnO (black) ; AIE molecule 2 (blue) ; nanohybrid (red)

Theoretical calculations were realized by density functional theory (DFT) to study the different possible binding modes of **2** onto ZnO surfaces. The band alignment in the case of **2** bonded on the non-polar (01-10) crystalline ZnO surface has been calculated (annexe 3). The DFT calculations suggest a bidentate grafting mode of the AIE molecule on the metal oxide surface, by covalent bond with the proton spontaneously moving from the POOH group to the surface, reacting with the surface hydroxy groups. Also, it shows that the rotations of the phenyl groupments of the emissive molecule are stopped once attached on the metal oxide surface, as expected by AIE phenomenon. In addition, the FTIR spectra of the different species reveal that the POOH grafting unit (stretching mode P-OH at  $950\text{ cm}^{-1}$ ) of the AIE molecule (blue) disappeared when the emitter is combined with the inorganic NC. The bidentate grafting mode is also predicted by the PO- stretching mode appearing peak at  $1100\text{ cm}^{-1}$ . Therefore, thanks to DFT model and FTIR spectra it is found that we created colloidal solution of nanohybrid, inducing a stabilization of the ZnO NC by the organic AIE emitter **2**.

The grafting between the two parts was investigated from the energy level by XPS measurements, looking for carbon and oxygen 1s levels, thanks to a collaboration with Pr. Mats Fahlman (Linköping University), cf. figure 14.

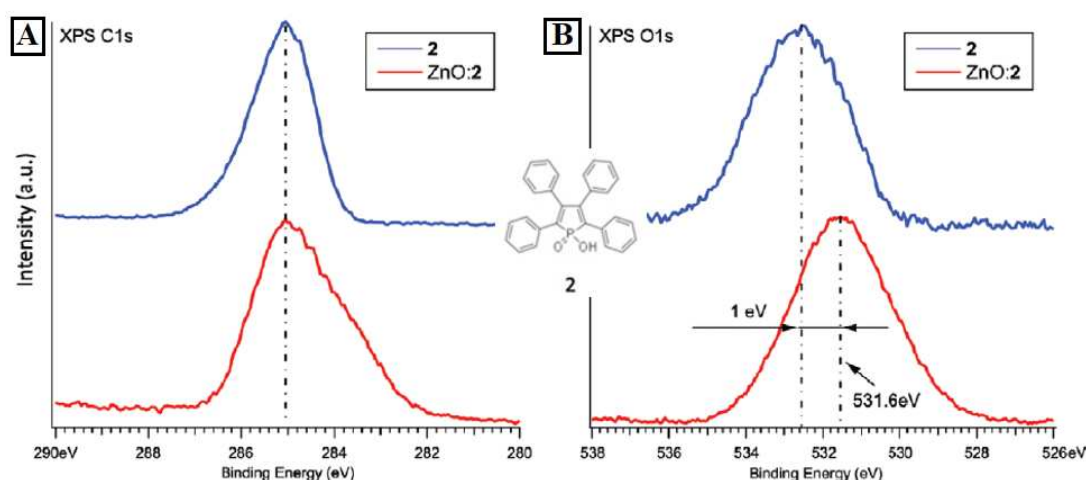


Figure 14 : XPS spectra of compounds **2** and ZnO:2, A) C1s level B) O1s level.

A downshift of the molecular levels is found with a weak charge displacement only visible at the O-Zn bond. The XPS analyses suggest the occurrence of charge transfer from the ZnO to the ligand **2** during grafting as a more electron rich environment in the molecule produces a shift toward lower binding energy in the XPS core level spectra. Also, the XPS analysis of nanohybrids ZnO:2 compared to the non-grafted ligand **2** show a new shoulder for C1s peak

at lower binding energy after grafting (annexe 4). This shift is most likely due to charge transfer from the ZnO nanoparticle surface to carbon atoms. [10]

### b) Optical analyses of the nanohybrids in solution

The impact of the combination of organic and inorganic part is studied via UV-visible absorption measurements. The absorption and emission spectra of the AIE molecules 1 to 4, before and after adding ZnO in the chloroform solution were studied in figure 15 / 16 / 17. The table 2 of photophysical datas summarizes the optical parameters of the ligands.

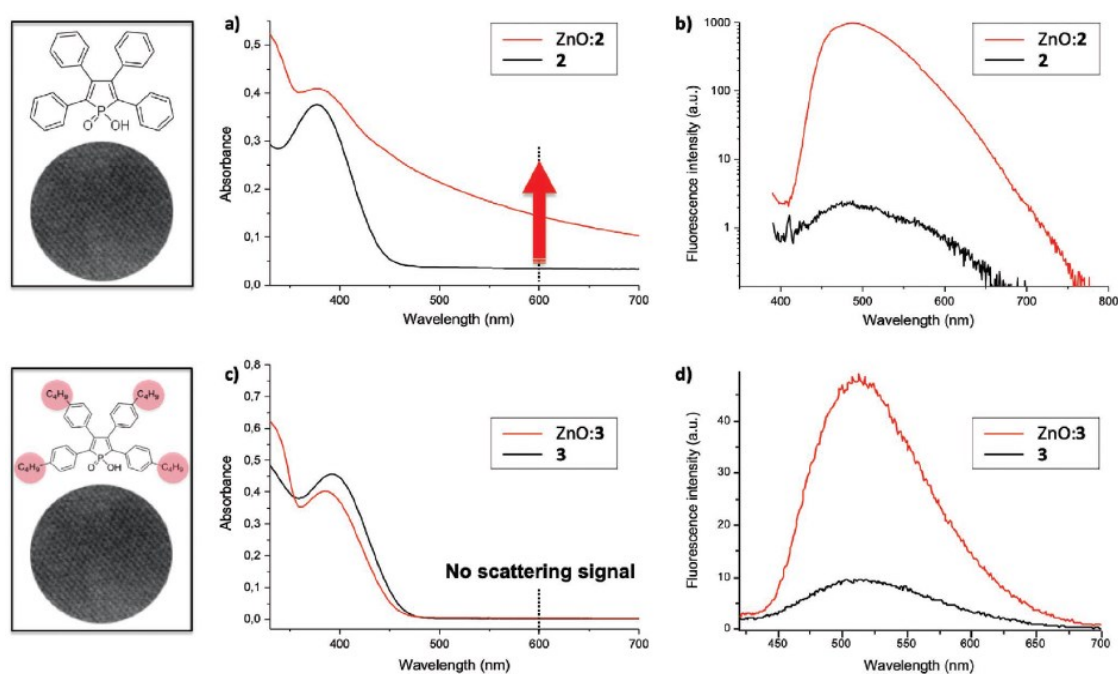


Figure 15 : Top: absorption spectra (a) and emission spectra at  $\lambda_{ex} = 380$  nm (b) of 2 and ZnO:2 in chloroform solution. Bottom: absorption spectra (c) and emission spectra at  $\lambda_{ex} = 380$  nm (d) of 3 and ZnO:3 in chloroform solution.

The AIE ligands 2 to 4 exhibit  $\pi-\pi^*$  absorption band centered around 380 to 410 nm in the UV-visible region (Figure 15; Figure 16), which is blue-shifted down to 280 nm for ligand 1 (Figure 17a). As anticipated, compounds 2–4 present a very weak emission in solution centered around 500–530 nm while compound 1, as expected from its planar structure, displays in solution a higher emission at 360 nm (Table photophysical data).

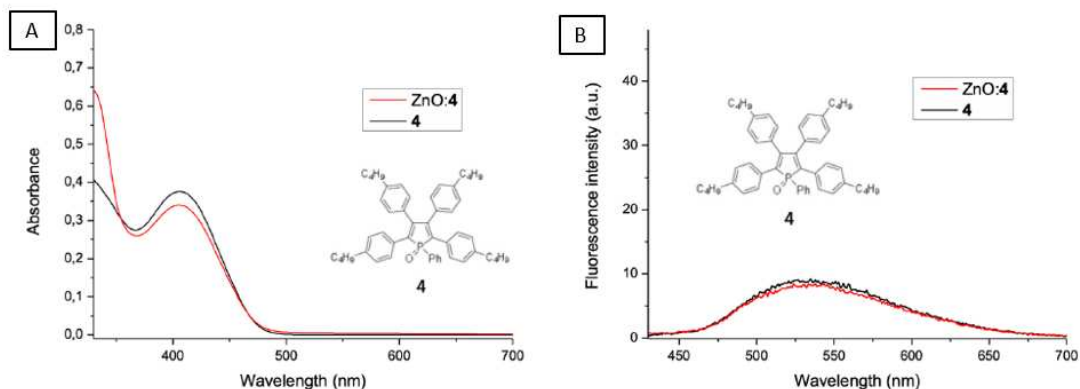


Figure 16 : a) absorption and b) fluorescence spectra at  $\lambda_{ex}=400$  nm of the non graftable molecule 4 (black curves) and the ZnO mixed with 4 (red curves).

Then, the effects of their grafting on ZnO nanoparticles on the optical properties have been investigated. When the concentration of ZnO nanoparticles was increased (monitored by UV absorption – Figure 17b) in a chloroform solution of 1, a severe quenching of the characteristic emission of the ligand was observed (Figure 17c). The grafting of 1 onto ZnO nanoparticles leads to strong aggregation caused quenching (ACQ) effect due to the  $\pi$ - $\pi$  stacking at the ZnO surface. [11] Then finally, by continuing the addition of ZnO, the classical ZnO defect emission at 550 nm gradually appeared. [12]

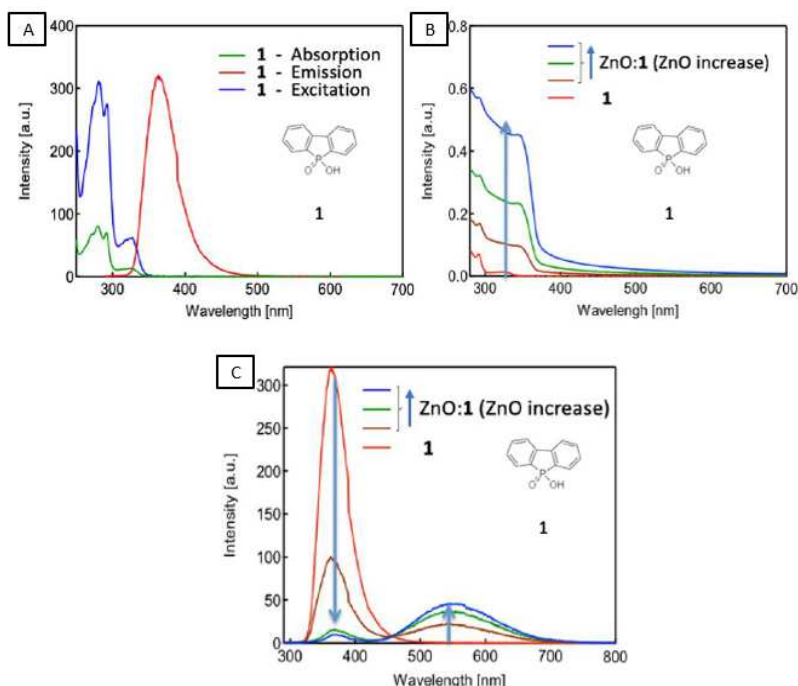


Figure 17 : a) Absorption spectrum (in green), emission spectrum at  $\lambda_{ex}=280$  nm (in red) and excitation spectrum measured at  $\lambda_m=360$  nm (in blue) for molecule 1 in solution. b) Absorption spectra of nanohybrids ZnO:1 when increasing the ZnO concentration. c) Fluorescence spectra at  $\lambda_{ex}=280$  nm of the molecule 1 and the nanohybrids ZnO:1 when increasing the ZnO concentration. Increase of ZnO in the solution increases the amount of grafted 1 but the emission of 1 is quenched due to the intermolecular interaction (ACQ effect).

Interestingly, the grafting of ligands 2 and 3 showed a completely different behavior. Indeed, in these cases, an emission enhancement was observed. The mass ratio between ZnO nanoparticles and the organic compounds was optimized to generate the highest emission and was found equal to ZnO:emissive molecule = 2:1.

The emission of ligand 2 is enhanced by a factor up to 500 by the injection of ZnO into the solution. Additionally, there is a strong light scattering signal appearing in the absorption spectrum of ZnO:2 indicating the formation of large nanohybrids aggregates while grafting (Figure 15a). Morphological analyses confirmed the presence of these tens to hundreds of nanometers large aggregates in solution, and will be shown in the following part.

In contrast, grafting of 3 leads to nanohybrids ZnO:3 which are highly soluble in chloroform, as validated by DLS / TEM analyses and the absence of any noticeable scattering signal (Figure 15b). It can be explained by the presence of alkyl chains on the four phenyl groupments. Ligand 3 only shows an emission enhancement in the range of 6 to 10 (Figures 15b,d). In the case of compound 4, the reference molecule without grafting unit, there is no change in absorption and emission introduced by the presence of ZnO nanoparticles (Figure 16).

This indicates clearly that the optical changes observed for ligands 2 and 3 are directly related to their grafting onto ZnO nanoparticle surfaces. Due to the fact that both ligands 2 and 3 are composed of the same hydroxyoxophosphole grafting unit and only differ by the presence of long alkyl chains in the case of 3, it may be supposed that the much higher emission enhancement in solution in the case of ZnO:2 compared to ZnO:3 is related to the restriction of phenyl ring rotation through the interactions between nanohybrids inside the large aggregates. Moreover, the nanohybrid structures (ZnO:2 and ZnO:3) have a shift in emission towards smaller wavelengths compare to the AIE molecules alone, about 30 nm, which indicates a modification of the electronical and structural properties and thus an efficient bond between organic and inorganic parts. Same shifts were observed for molecules 5 and 6 (annexe 5).

In order to understand the grafting process and the cause of strong AIE effect in depth, the time evolution of the luminescence spectra was studied for the nanohybrids ZnO:2 and ZnO:3, right after injection of the ZnO nanoparticles in solution. Simultaneously, the time evolution of their absorption spectra was recorded at 600 nm, namely, at a wavelength without ligand absorption but well located to measure the optical signal related to light scattering upon aggregates formation (Figure 18).

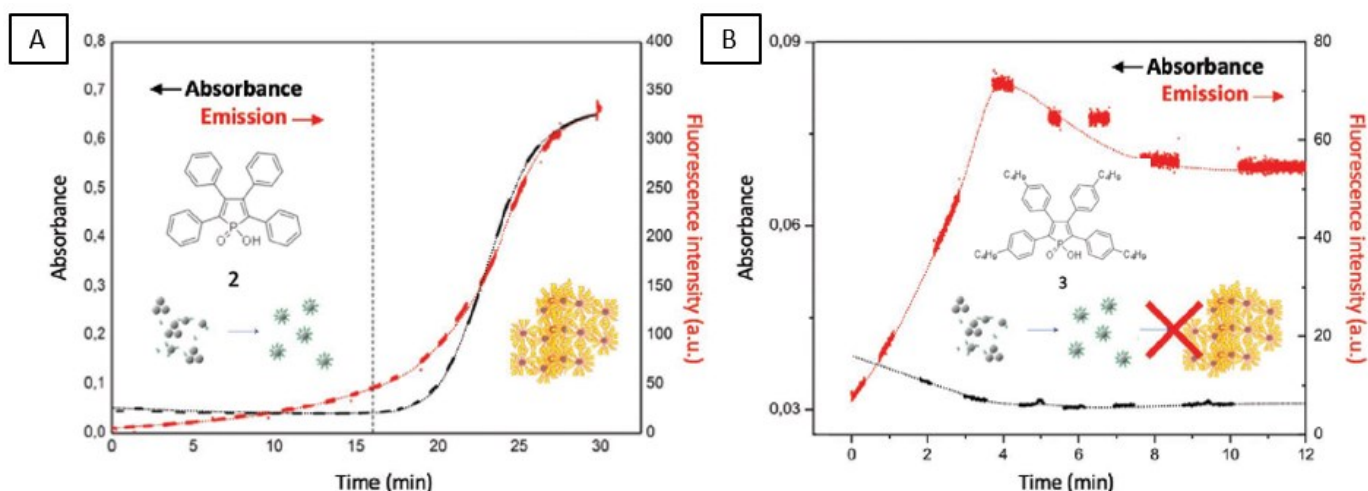


Figure 18 : Time resolved absorbance measured at 600 nm (black lines) and fluorescence intensity  $\lambda_{ex}=400$  nm (red lines) of ZnO:2 (a) and ZnO:3 (b) nanohybrids. Zero minute corresponds to the time when ZnO was injected into molecules solution in chloroform.

After injection of ZnO nanoparticles, both nanohybrids ZnO:2 and ZnO:3 showed, first, a weak decrease in light scattering during the first minutes (black curves), indicating that the grafting of the molecules weakly reduced the cluster size of ZnO nanoparticles. In the case of nanohybrids ZnO:3, the light scattering signal remained then stable thanks to the solubility of these nanohybrids in solution, whereas the fluorescence intensity increased to reach the stable emission enhancement in a factor of 6 to 10. This moderate increase can be rationalized on the basis of the chemical modification of the fluorophore upon grafting (loss of the O-H vibrator). Interestingly, in the case of nanohybrids ZnO:2, a different behavior with two phases was observed. During the first 15 min (see vertical dotted line as eye guide in Figure 18a), the first phase was similar for both nanohybrids as the fluorescence intensity of ZnO:2 increased by the same typical factor of 8 to 12. After these 15 min, during the second phase, the scattering signal started to increase strongly and saturated in intensity after 30 min, indicating the formation of ZnO:2 nanohybrids large aggregates. The corresponding fluorescence intensity increased quickly and simultaneously by another factor of 10 with the large aggregates formation. The later emission enhancement during this second phase can be directly addressed to the restriction of phenyl ring rotation during the large aggregates formation, namely, the AIE effect.

### c) Dynamic Light Scattering DLS analyses of the nanohybrids

DLS analyses helped to characterize the initial ZnO solution, especially to determine whether ZnO nanoparticle clusters about 100 nm large were present in the starting solution. Considering that the size of the ZnO nanoparticles is 5 nm ( $\pm 1$  nm), there are small clusters

already present in solution before grafting. Even though the nanohybrids ZnO:3 were observed in absorbance without scattering signal, the solution of the hybrid structures is analyzed and presented in the following figure.

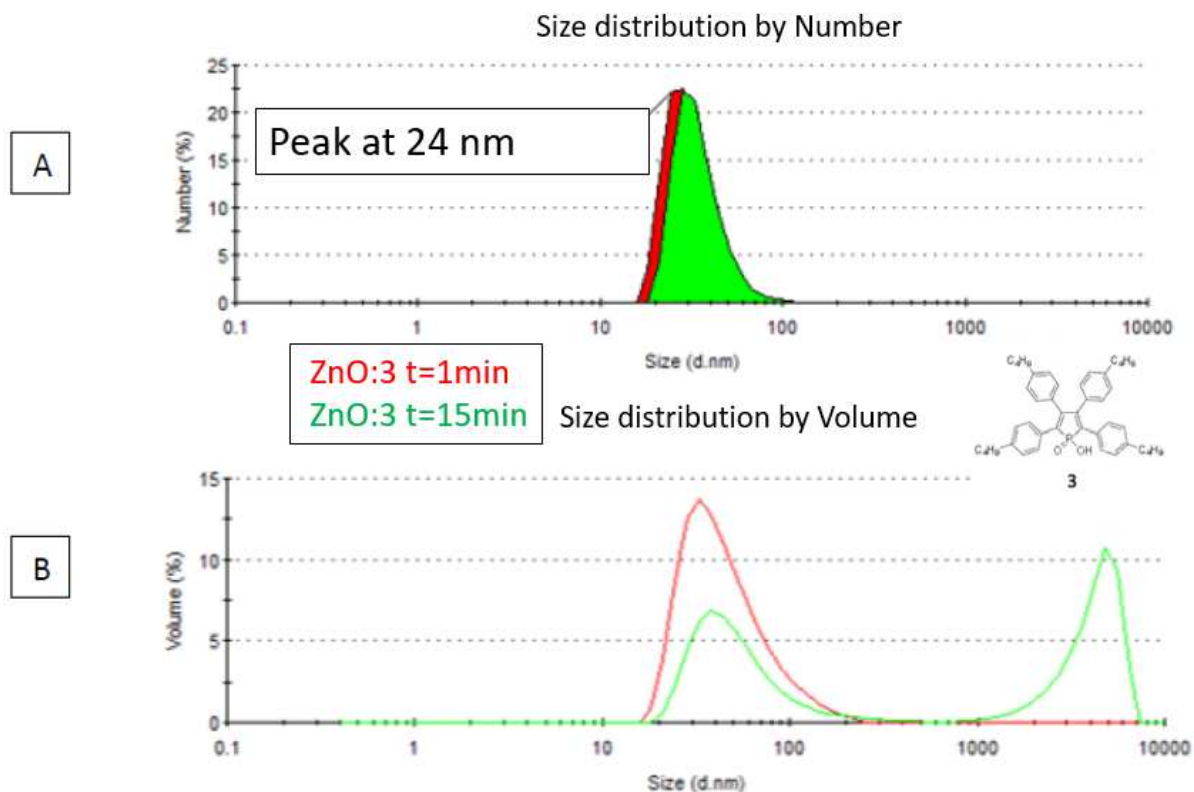


Figure 19 : DLS in time after grafting, red : ZnO:3 + 1min ; green : ZnO:3+ 15min, A) Size distribution by Number B) Size distribution by Volume.

The observations in DLS show that the nanohybrids ZnO:3 are not well-dispersed. Considering that the DLS radius is higher than the real one (Stokes-Einstein equation), the DLS size of ZnO:3 cannot be higher than 10 to 15 nm. The datas show that the biggest nanohybrid population measures from 20 to 40 nm 1 minute after grafting. In addition, there is no aggregate formation over 100 nm, and the solution does not evolve much in number after 15 minutes (Figure 19A). However, in volume, after 15 minutes, very large nanohybrid clusters are merging over microns, which are highly undesirable for thin film elaboration and efficient LED device and large-scale production because of electrical issues, as short cut and performances losses. Furthermore, emitters 5 or 6 associated with ZnO were also analyzed, and the results were similar than the nanohybrid ZnO:3 but the aggregate formation evolved faster upon 15 minutes (annexes 6). It is assumed that the ZnO:3 solution is processable for few minutes (<15 minutes) to obtain smooth and, in theory, homogeneous surface before the formation of large nanohybrid clusters.

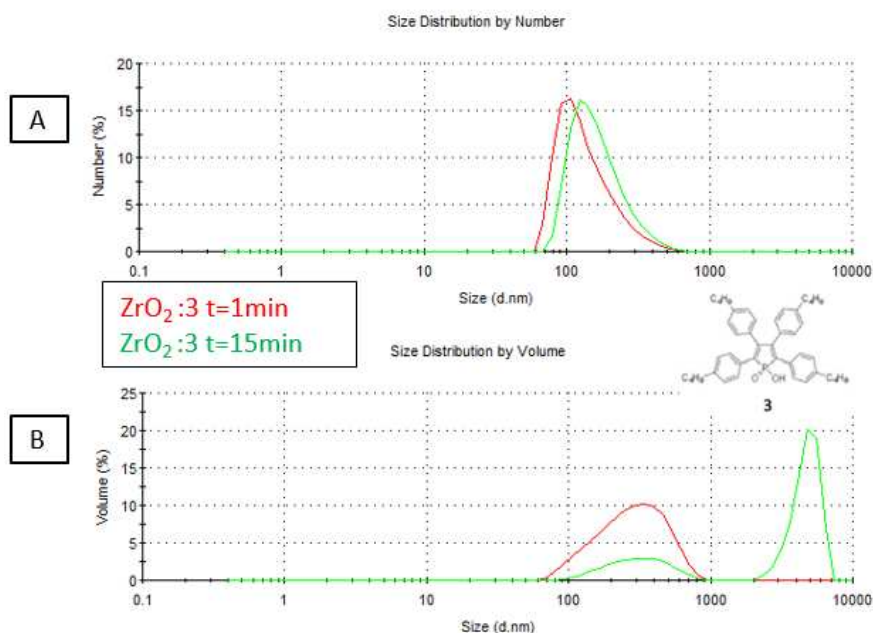


Figure 20 : DLS in time after grafting, red :  $ZrO_2:3$  + 1 min ; green :  $ZrO_2:3$  + 15 min, A) Size distribution by Number B) Size distribution by Volume.

In contrast, the inorganic core  $ZrO_2$  combined with 3 gave very high amount of aggregates in number (Figure 20) after 1 minute (red). After 15 minutes, in volume it is more than 20% of large clusters above 2 microns. Therefore, it is assumed that it is linked directly to the surface of  $ZrO_2$  which is less accessible than the  $ZnO$  one. Indeed, the pH of the solution during the synthesis is more basic for  $ZnO$ , meaning more hydroxyl (OH) groups are present on the surface. Despite the  $ZrO_2:3$  induces an increase in fluorescence intensity, as  $ZnO:3$  and as expected by the AIE phenomenon (annexe 7), it was decided for morphology and stability reasons that the  $ZnO$  is the best of the three candidates ( $ZnO$ ,  $ZrO_2$ ,  $CsPbI_3$ ) as inorganic core to build efficient emissive nanohybrid structure.

#### d) Optical analyses of the nanohybrids as thin films

Thin nanohybrid films can be processed once the solution is transparent and without any aggregate. Related to the previous observations, it is only the case of  $ZnO:3$  within the first minutes. The electroluminescent solution of  $ZnO:3$  was spin coated on a glass substrate and analyzed by fluorescence spectroscopy (Figure 21). The enhancement of the fluorescence intensity shows clearly that ligand 3, even grafted onto  $ZnO$  nanoparticles, still owns intramolecular rotation of phenyl rings in solution, but processing into thin films definitely freezes phenyl rotations via intermolecular interactions and thus generates a stronger AIE effect.

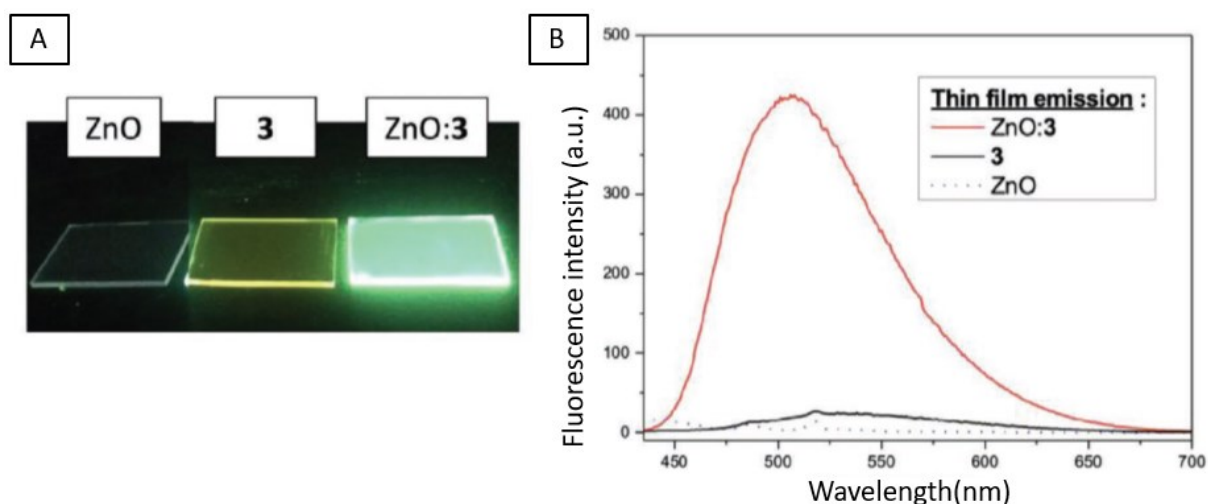


Figure 21 : A) emissive layers under source light (400 nm excitation) B) thin film emission  $\lambda_{ex}=400$  nm of ZnO:3 ; ZnO (dotted) ; 3.

In order to deduce if the AIE effect is efficient, the photoluminescence quantum yield (PLQY) was investigated in the Table 3 on ZnO or ZrO<sub>2</sub> combined with 3. The PLQY increases by a factor 3 for the hybrid ZnO:3 compared to 3, which is a witness of the AIE phenomenon. The maximum PLQY of the molecule 4, which is the non graftable version of 3, has 45%, meaning in theory that the grafting between both entities is not perfect. In opposite, the PLQY of ZrO<sub>2</sub>:3 remains comparable to the free molecule 3, showing that the grafting of 3 on ZrO<sub>2</sub> NCs may be not as efficient as on ZnO NCs. Moreover, all the electroluminescent layers were stored in dark under atmospheric conditions, but still their PLQY did not decrease after 20 weeks, proving a good stability in air.

Table 3 : Photoluminescence quantum yield for thin films : 3 ; ZnO:3 ; ZrO<sub>2</sub>:3

PLQY +/- 10%	Measurement 1 week after	Measurement 20 weeks after
3	11+/-1	12+/-1
ZnO:3	34+/-3	31+/-3
ZrO <sub>2</sub> :3	14+/-1	16+/-2

### e) Morphological analyses of the thin nanohybrids films by TEM and AFM

#### Transmission Electron Microscopy (TEM):

TEM images confirm the aforementioned ZrO<sub>2</sub>:3 gave large aggregates in solution, ranging from 100 to 600 nm. Moreover, the ZnO:3 film has a nice average morphology but still it

remains some smaller and less concentrated nanohybrid aggregates about 100 nm. The luminescent solution of ZnO:3 will then be studied in classic LED device.

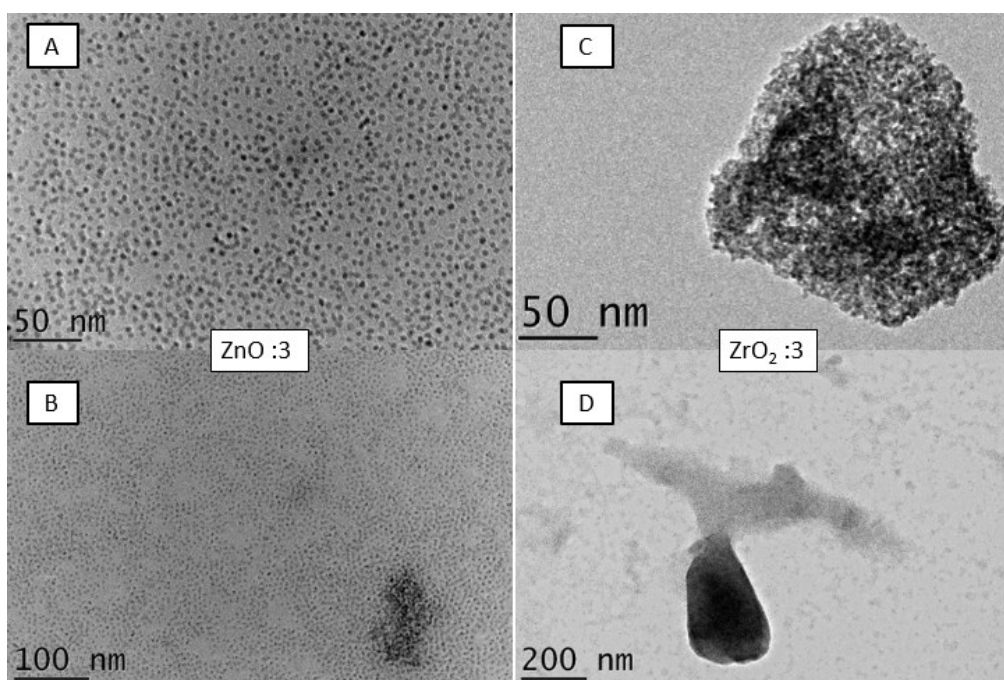


Figure 22 : TEM images from solutions of A,B) ZnO:3 ; C,D) ZrO<sub>2</sub>:3

### Atomic Force Microscopy AFM:

The morphology of the luminescent films was investigated thanks to AFM measurements, the morphology of the nanohybrids ZnO:3, ZnO:2 ; ZrO<sub>2</sub>:3 ; ZrO<sub>2</sub>:2 was investigated. The layers were spin-coated from solutions about 12 mg/mL in order to have a relevant thickness (table 4).

Table 4 : thickness of thin films coated from nanohybrids solutions at 12 mg/mL (determined by profilometry).

Layers	ZnO:5	ZnO:6	ZnO:3	ZrO <sub>2</sub> :3
Thickness (nm)	47+/-4	32+/-4	65+/-4	35+/-4

As predicted by the previous optical observations (figure 15a), the ZnO:2 gives an aggregated morphology with a quite high roughness (RMS > 7.0 nm). The ZnO:3, which previously showed a better quality of dispersion in solution (no light scattering signal in absorbance visible, narrow peak in DLS), has a RMS roughness of 2.5 nm, which is suitable to be used in LED device. However, the ZrO<sub>2</sub>:2 and ZrO<sub>2</sub>:3 nanohybrids follow the same trend as ZnO nanohybrids, but with a poorer surface quality and higher RMS roughness (17.3 and 5.1 nm respectively). Indeed, the ZnO nanohybrid layers are quite homogeneous on 5 x 5 μm surface range, whereas it is not the case of the ZrO<sub>2</sub> nanohybrids. The surface homogeneity is very important in order to avoid electrical issues in the working optoelectronic device. Therefore, this shows

that ZnO is the best candidate among the three presented NCs, for suitable and reproducible LEDs. Some other nanohybrids were investigated, such as ZnO:5 ; ZnO:6, and gave high roughness (RMS > 6,0 nm) but are quite homogeneous. (annexe 8) As luminescent solution for LED elaboration, the ZnO :3 is the most suitable to build an efficient LED device

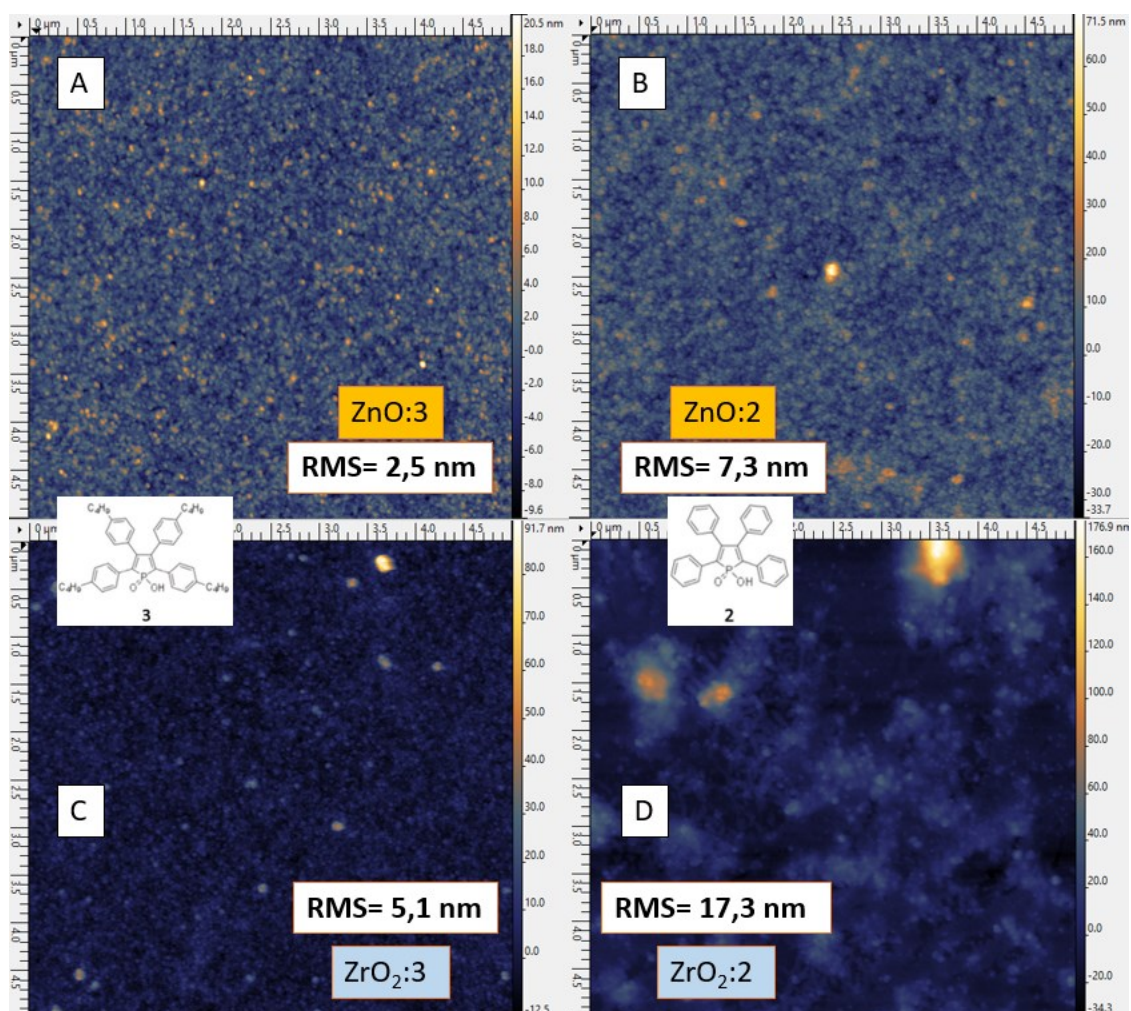


Figure 23 : AFM images (5 x 5 μm range) of A) ZnO:3 B) ZnO:2 C) ZrO<sub>2</sub>:3 D) ZrO<sub>2</sub>:2

#### 4) LED devices using pure AIE nanohybrids as electroluminescent layer

While ZnO:2 films were not suitable for device application due to their poor quality, thanks to the acceptable optical quality of nanohybrids ZnO:3 thin films, the electroluminescent properties of this material were studied as light emitting layer in simple LED structures. The device structure (Figure 24c) is ITO / CuPc / HTL / ZnO:3 / mCP / Alq<sub>3</sub> / LiF / Al with CuPc as the hole injection layer and mCP as the hole blocking layer, to avoid emission from Alq<sub>3</sub>. The

hole transport layer (HTL) is a 20 nm thick film of polyvinylcarbazole used to reduce the leakage current within the device, potentially caused by nanohybrid aggregates. The emitting layer ZnO:3 is solution processed on the stack from concentrated nanohybrids solution, and gave medium surface homogeneity (1 layer out 4 without nanohybrids clusters).

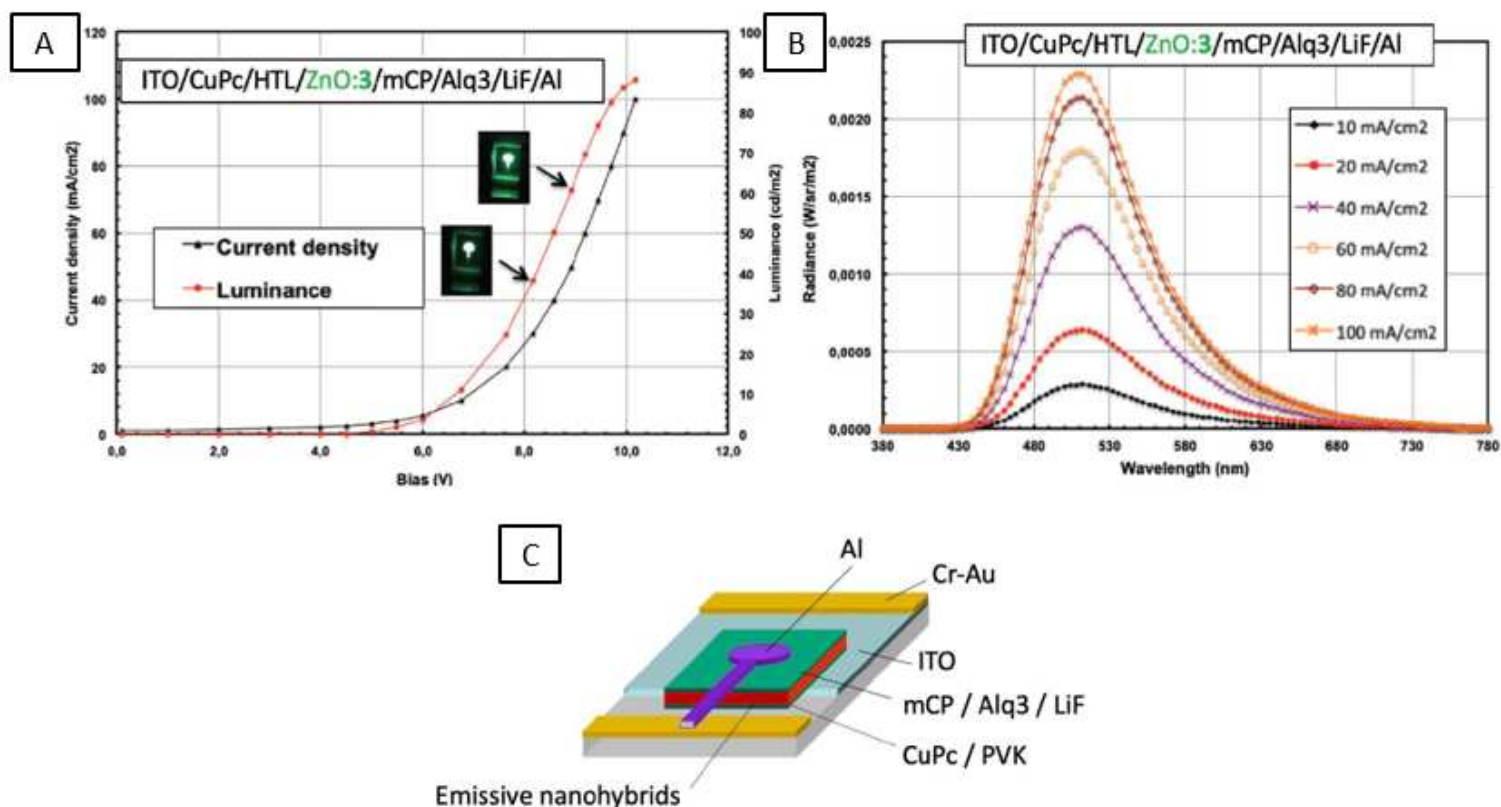


Figure 24 : a) Electroluminescent  $J$ - $V$ - $L$  curves of the light emitting diodes (LEDs) devices. b) Radiance spectra of the LED devices as a function of current density c) Scheme of the structure of the LED devices.

The current density–voltage–luminance ( $J$ - $V$ - $L$ ) curves of the diode (Figure 24a) show a threshold voltage near 4V with a maximum emission at 90 cd m<sup>-2</sup> for a current density of 100 mA cm<sup>-2</sup>. Inset shows two photograph images of the diode working at 30 and 50 mA cm<sup>-2</sup>, respectively, having homogeneous emission over the whole emitting surface (0.28 cm<sup>2</sup>). The electroluminescence spectrum is very similar to the photoluminescence spectrum of nanohybrid ZnO:3 (maximum at 514 nm) proving that the emission comes from the nanohybrid layer (Figure 24b). The reproducibility of this LED device is medium, because of the presence of ZnO:3 aggregates about 100 nm, that appear quickly in solution and cause short-cuts. These results show that this new class of nanohybrid material is able to act as emissive layer in solution-processed LED devices, even though the low luminance and its saturation at high current densities deserve optimizations in the following chapter.

## 5) Conclusions about pure ZnO:3

To summarize, novel fluorescent nanohybrids, based on  $\pi$ -extended hydroxyoxophosphole ligands grafted onto ZnO surface, were designed and studied. The restriction of the intramolecular motions of the organic fluorophore, through either aggregates formation in solution or processing into thin films, is found to form highly emissive materials due to a strong AIE effect. Theoretical calculations and XPS analysis show that electronic coupling between the AIE ligands and the ZnO nanoparticles occurs leading to partial charge transfer to the ligand from the ZnO core. Preliminary results on the use of these nanohybrids as solution processed emissive layers for lighting applications indicate high quantum efficiencies in the thin films allowing electroluminescence, but also medium LED reproducibility/homogeneity because of nanohybrid clusters appearing in solution. This allowed us to publish these results in *Advanced Materials Technologies* [13]. The next chapters will explore the potential of these nanohybrids by stabilizing them with a surface co-ligand. The best candidate is the OA which is known to stabilize ZnO NCs and to increase the fluorescence intensity of the nanoparticles. Indeed, we expected that the OA could increase the homogeneity of the hybrids ZnO:3 to go towards lower surface roughness and thus reproducible LED devices. Also, in order to increase the LED performances, more efficient charge transport layers should be used together with multicolor highly emissive graftable AIE molecules, possibly leading to major advances compared to pure organic materials or inorganic nanoparticles for lighting devices.

## 6) The use of OA for reproducible and homogeneous LED device

The oleic acid is a monounsaturated fatty acid with 18 carbon atoms, its name comes from the Latin *oleum* which means "oil". It is the most abundant fatty acid in nature.

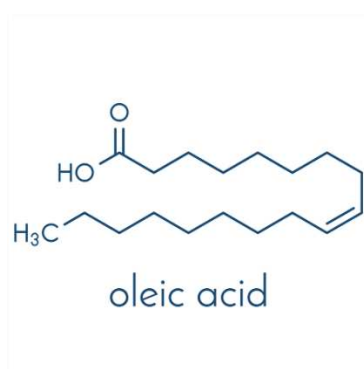


Figure 25: oleic acid structure  $C_{18}H_{34}O_2$

The oleic acid is very often used as surface ligand during synthesis, or post synthesis, in order to stabilize nanoparticles and to avoid aggregation and degradation of the particles, as shown

on figure 3a, the use of OA with ZnO NCs induces a drastic decrease of the light scattering signal in the visible area. The OA shows a very nice grafting of the metal oxides presented, and in this part is combined with ZnO:3 or ZrO<sub>2</sub>:3 in order to increase the solubility of the nanohybrids, and to have reproducible LED devices. In the beginning, we started from previous studies [14] and decided that 5 mg/mL of pure ZnO solution may be stabilized with 1 μL of pure OA to have well-dispersed nanoparticles. The same amount of OA was therefore initially tried with ZnO:3, and the impact of the OA concentration will be investigated in the following part, with a new structure named ZnO:3:OA.

The oleic acid (OA) is compared (for morphology reasons) to the molecule 3 because it is an efficient surface ligand to stabilize the ZnO, or ZrO<sub>2</sub> nanoparticles, according to the previous absorbance results (figures 3a / 6).

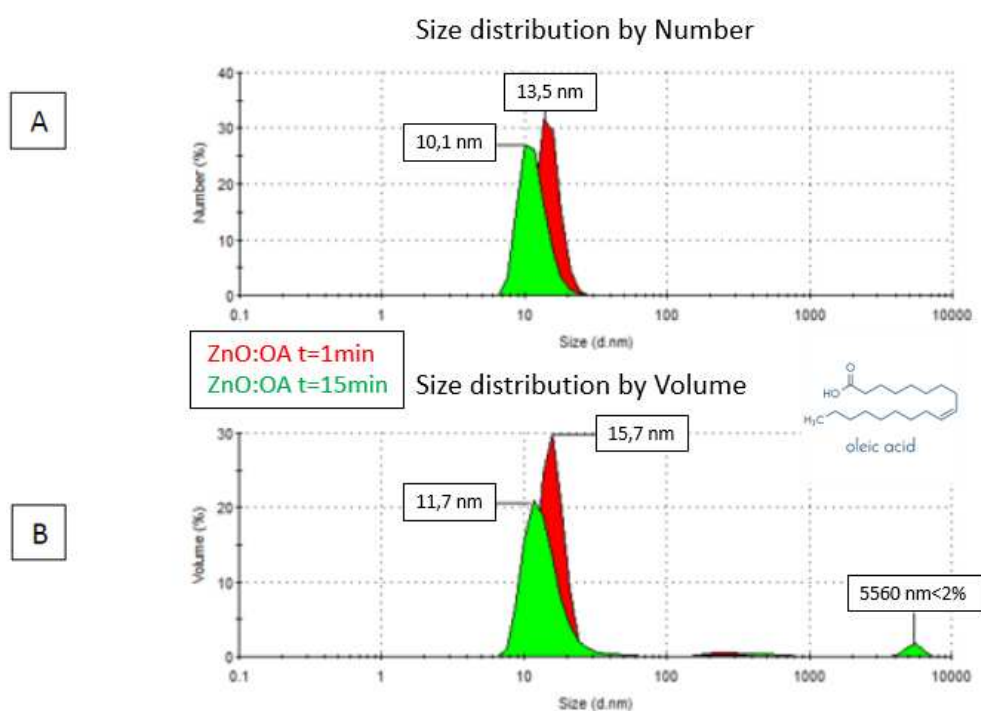


Figure 26 : DLS in time after grafting, red : ZnO:OA + 1min ; green : ZnO:OA + 15min, A) Size distribution by Number B) Size distribution by Volume.

As expected, the OA induces a nice quality of grafting with the ZnO surface. Moreover, even after 15 minutes in contact with the air, the solution remains quite stable. Indeed, the main peaks by volume and number are relatively low and narrow 10 to 15 nm, thus about single to double nanohybrids with a low rate of aggregate formation, namely less than 5% above 1000 nm after 15 minutes.

It is important to have in mind that the grafting kinetic of 3 with ZnO varies a lot from one (ZnO or 3) batch to another. The reproducibility was considered as medium. Thus, it explains the difficulty to have a total control of the objects in solution and thus to control the surface roughness of the thin films. Therefore, the OA as co surface ligand was used and investigated with the hybrid NCs also as a tool to gain in reproducibility.

### ZnO:3 OA

The optical properties of ZnO:3:OA were analyzed thanks to fluorescence measurements, and the related Table 5 of PLQY in thin films.

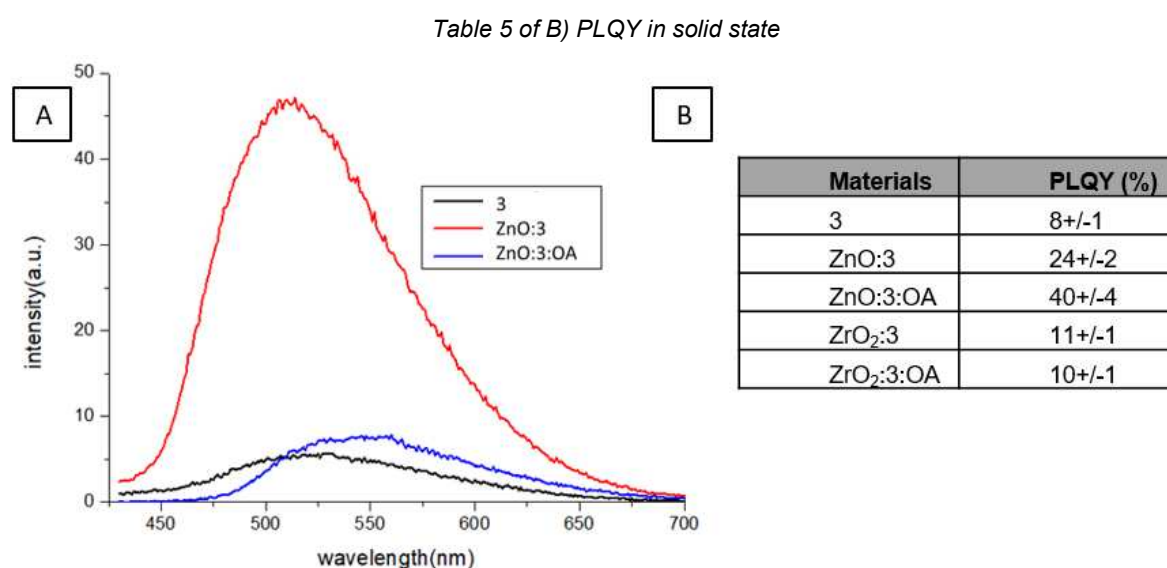


*Figure 27 : A) Fluorescence spectra in solution of molecule 3 ; ZnO:3 ; ZnO:3:OA excited at 400 nm and related to the B) Table 5 of PLQY in solid state*

According to the figure 27, the important AIE effect of ZnO:3 is related to large aggregate formation as far as the solution was turbid and a partial grafting between organic and inorganic parts. Indeed, a factor 10 in fluorescence intensity is noted between 3 and nanohybrid ZnO:3. Furthermore, adding OA with the ZnO:3 did not change much the emission spectrum. There is a slight shift, this time towards the higher wavelengths compare to 3. The ZnO does not emit light when excited at 400 nm, namely on the main absorbance peak of 3, meaning that the emission of ZnO:3:OA and ZnO:3 is due to the hybrid structures. The quantification of the photoluminescence is illustrated by the table 5, and it is observed that the ZnO:3 is poorly grafted with 3 as far as the PLQY increases only from 8 to 24% (+/- 2%). Thus, it means that ZnO:3 at this time is still composed of potentially non-grafted emitters. However, by adding OA to the nanohybrids, the PLQY increases up to 40% (+/- 4%), which is the value of the non graftable version of 3 (4). Therefore, it means that adding OA involves a better dispersion of the NCs, allowing for a more efficient grafting of emitters.

The nanohybrids ZnO:3:OA were investigated with TEM and AFM images as shown in figure 28.

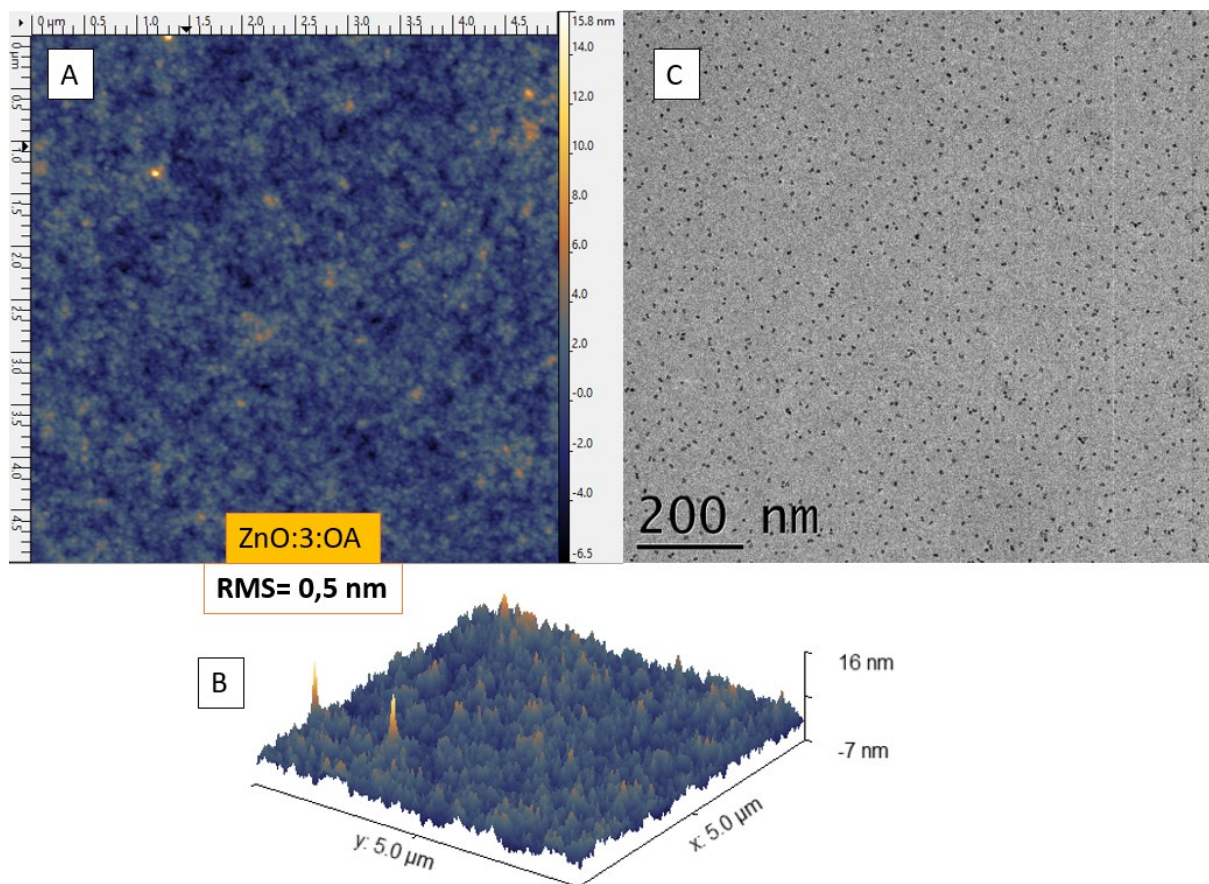


Figure 28 : A) AFM image 5x5  $\mu\text{m}$  range B) 3D AFM image C) TEM image of ZnO:3:OA

Compared with the previous AFM and TEM observations, for ZnO:3 sample, the addition of OA to these nanohybrids lead to very smooth surface. Indeed, the AFM measurement gives a RMS roughness about only 0.5 nm, with a very high homogeneity over the whole surface, without any noticeable clusters (Figure 28). The same observation was done with the TEM image. The analyzed surface is still very small, 5 x 5  $\mu\text{m}$  range in AFM and nearly 1 x 1  $\mu\text{m}$  in TEM, but many areas were observed and give the same results, proving the absence of aggregates. It was concluded that adding OA with ZnO:3 leads to reproducible and very smooth layers, meaning near well-dispersed nanohybrids. Moreover, the adding of OA does not change significantly the emission spectrum, and it increases the PLQY (compared with the molecule 3). Therefore, this new electroluminescent material is tested in a serie of LED devices.

This time, a more classic and simple device architecture was used, namely, ITO with coated PEDOT:PSS (40 nm) as hole transport layer, the electroluminescent material based on pure ZnO:3:OA (80 nm), and followed by lithium fluoride (1 nm) barrier layer with aluminium electrode (100nm).

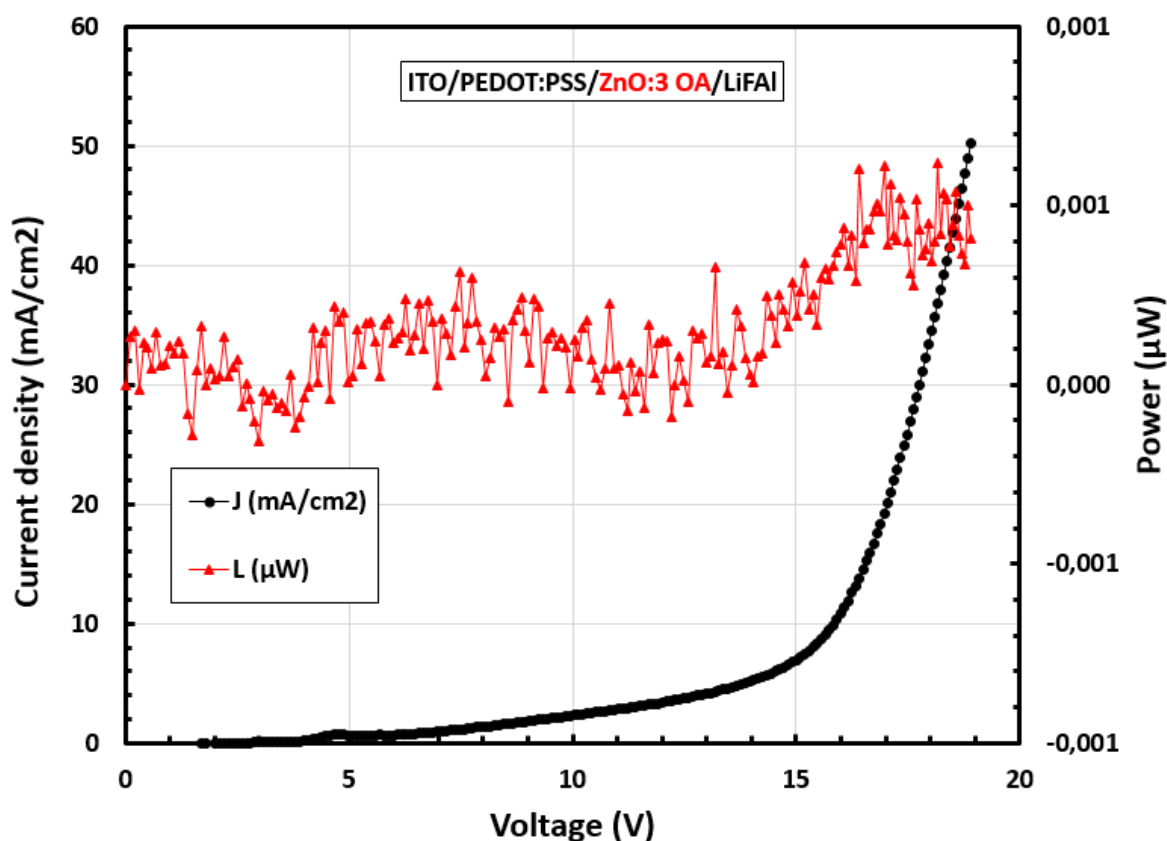


Figure 29 : JVL measurement of LED device containing ZnO:3:OA active layer.

The optoelectronic devices show an honorable working tension approximately around 6V (Figure 29). However, the light was generated only close to 15V, which is a very high voltage compared to the literature [15–19]. Furthermore, the power is very low, below 0.001 µW, which means that the generated light is very weak. At least, the devices were reproducible, and all the devices of the serie were functioning, showing that the combination of OA with the nanohybrids ZnO:3 leads to convenient surface morphology. The maximum emission peak of these LEDs was reported at 530 nm, thus corresponding to the emission of the nanohybrids ZnO:3:OA (bluish green color). However, only 5 % of the active areas were shining, indicating the presence of few aggregates and an insulating behavior. The insulating behavior is attributed to the OA which is a fatty compound that may reduce the transport properties of the initial nanohybrids.

## ZrO<sub>2</sub>:3:OA

The ZrO<sub>2</sub>:3 is a turbid solution attributed to the presence of big aggregates in solution as seen before. In another hand, adding OA to these nanohybrid lead to transparent solution, and no light scattering signal was found. Thus, in theory, the solution is not composed of large aggregates, but the PLQY of ZrO<sub>2</sub>:3:OA is still very low and close to the value of molecule 3 (Table 5). Consequently, it is assumed that the OA is mostly grafted with ZrO<sub>2</sub> NCs, which is not the case of 3. We may again think that molecule 3 grafting does not occur on ZrO<sub>2</sub> NCs. The morphology of ZrO<sub>2</sub>:3:OA film was very smooth and almost without aggregates, but the previous results showed that the ZrO<sub>2</sub> is grafted with OA, thus molecule 3 should be in periphery around ZrO<sub>2</sub>:OA.

The ZrO<sub>2</sub>:3:OA was also tried in LED device as emissive layer, and the surface morphology was reproducible, being as good as the ZnO:3:OA layers. However, the behavior of such LEDs using these nanohybrids was totally insulating, even worse than the LEDs using ZnO:3:OA. Indeed, no light emission, neither diode behavior (non exponential intensity voltage curve) were measured (annexe 9). Working with the ZrO<sub>2</sub> was definitely cancelled in the following chapters.

## **7) Conclusions about pure ZnO:3 :OA**

According to the previous results, it is evident that to have reproducible devices with smooth and homogeneous layers, the OA is required as additional ligand to the nanohybrids. Indeed, the OA breaks the nanohybrid clusters in order to have ideal well-dispersed nanohybrids in solution. Interestingly, the OA increases the PLQY of the nanohybrids, thanks to a better ability of grafting for the AIE emitter within these well-dispersed solutions. On another hand, LED devices with OA were tried, and even if the devices are reproducible, it suffers from insulating behavior from the fatty acid. Therefore, new investigations were done in the following chapters, by including the nanohybrids in a polymer host matrix, in order to increase the transport properties, and also to improve the solubility of the electroluminescent nanohybrid materials. In addition, the performances of the devices can be improved by using more efficient AIE molecule, or by using more convenient NCs. The transport charge layers in the device can also be optimized to have better efficiencies.

## Annexes :

### 1) JCPDS ZnO

#### Peaklist(1.5418)

No.	h	k	l	d [Å]	2Theta[deg]	I [%]
1	1	0	0	2,81430	31,796	57,0
2	0	0	2	2,60332	34,450	44,0
3	1	0	1	2,47592	36,282	100,0
4	1	0	2	1,91114	47,578	23,0
5	1	1	0	1,62472	56,651	32,0
6	1	0	3	1,47712	62,919	29,0
7	2	0	0	1,40715	66,439	4,0
8	1	1	2	1,37818	68,023	23,0
9	2	0	1	1,35825	69,162	11,0
10	0	0	4	1,30174	72,628	2,0
11	2	0	2	1,23801	77,026	4,0
12	1	0	4	1,18162	81,447	1,0
13	2	0	3	1,09312	89,696	7,0
14	2	1	0	1,06384	92,878	3,0
15	2	1	1	1,04226	95,402	6,0
16	1	1	4	1,01595	98,717	4,0
17	2	1	2	0,98464	103,058	2,0
18	1	0	5	0,97663	104,249	5,0
19	2	0	4	0,95561	107,552	1,0
20	3	0	0	0,93812	110,521	3,0
21	2	1	3	0,90694	116,423	8,0
22	3	0	2	0,88256	121,732	4,0
23	0	0	6	0,86768	125,361	1,0
24	2	0	5	0,83703	134,143	3,0
25	1	0	6	0,82928	136,745	1,0
26	2	1	4	0,82370	138,750	2,0
27	2	2	0	0,81247	143,186	3,0

#### Crystallographic parameters

Crystal system: Hexagonal  
Space group: P63mc  
Space group number: 186

a (Å): 3,2498  
b (Å): 3,2498  
c (Å): 5,2066  
Alpha (°): 90,0000  
Beta (°): 90,0000  
Gamma (°): 120,0000

## 2) JCPDS ZrO<sub>2</sub>

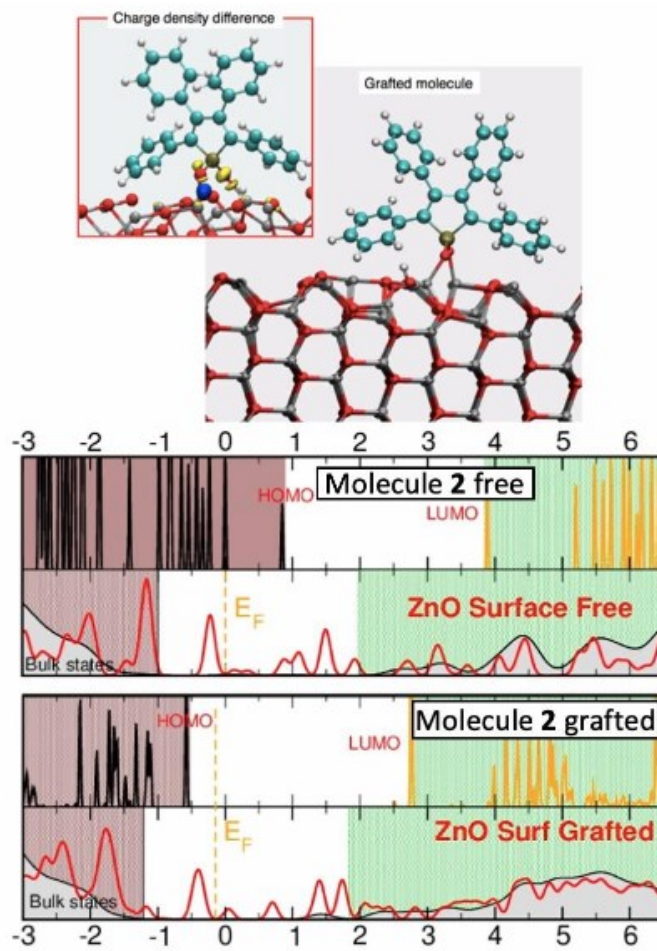
### Peak list (1.5418)

No.	h	k	l	d [Å]	2Theta[deg]	I [%]
1	1	1	1	2,96463	30,144	100,0
2	2	0	0	2,56448	34,988	17,0
3	2	2	0	1,81521	50,262	32,0
4	3	1	1	1,54668	59,791	16,0
5	2	2	2	1,48102	62,734	2,0
6	4	0	0	1,28085	74,007	1,0
7	3	3	1	1,17697	81,837	2,0
8	4	2	0	1,14676	84,481	3,0
9	4	2	2	1,04697	94,837	1,0
10	3	3	3	0,98647	102,792	1,0
11	5	3	1	0,86685	125,573	1,0
12	6	0	0	0,85472	128,826	1,0

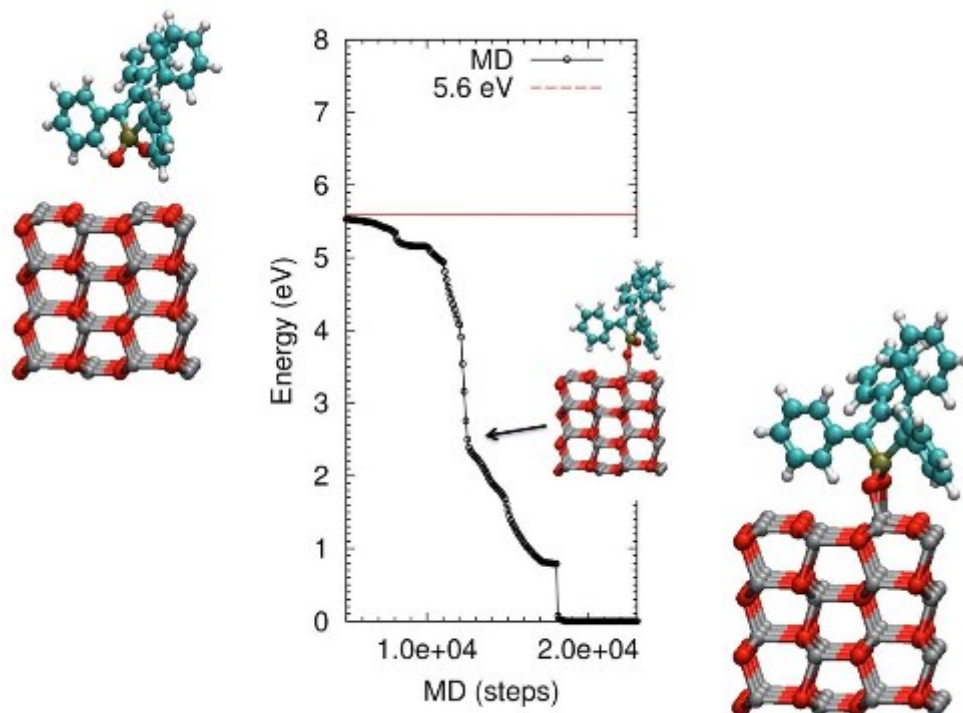
### Crystallographic parameters

Crystal system:	Cubic
Space group:	Fm-3m
Space group number:	225
a (Å):	5,1280
b (Å):	5,1280
c (Å):	5,1280
Alpha (°):	90,0000
Beta (°):	90,0000
Gamma (°):	90,0000
Volume of cell (10 <sup>6</sup> pm <sup>3</sup> ):	134,85
Z:	4,00

### 3) XPS

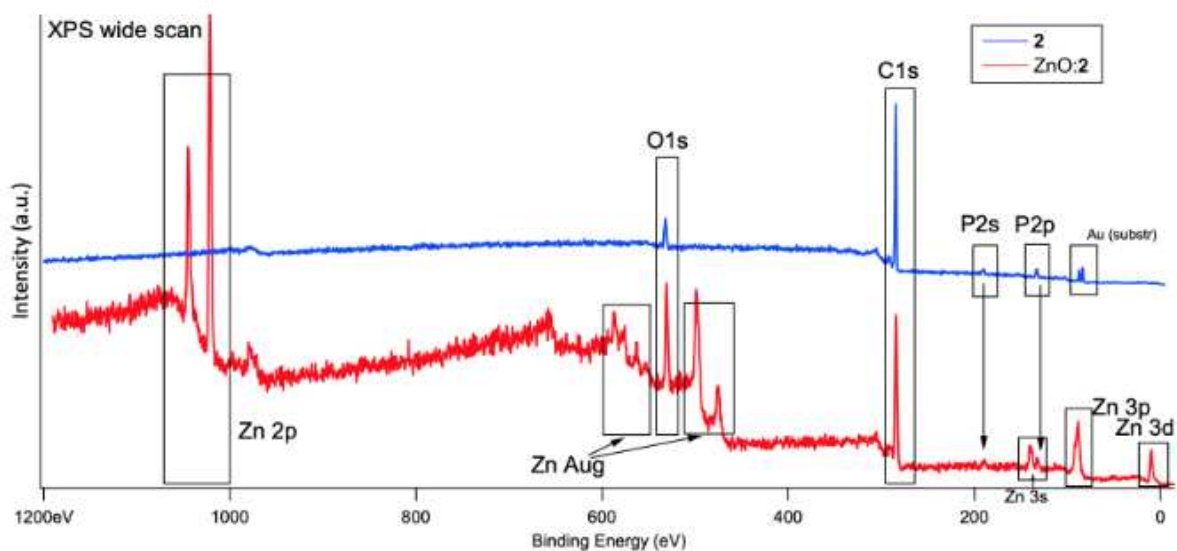


DFT calculation of the interactions of 2 and the ZnO surface to form ZnO:2 nanohybrids. Top: Grafted molecule on the surface (right) and charge energy difference upon grafting (inset). Bottom: Band alignment of the molecular levels with respect to the surface for the case of separated components (upper panels) and after grafting (lower panels). Green (brown) shadowed regions indicate the empty (full) electronic levels of the molecule and the surface. Using the marker atom method, the electronic levels have been aligned. It is found a downshift of the molecular levels upon grafting



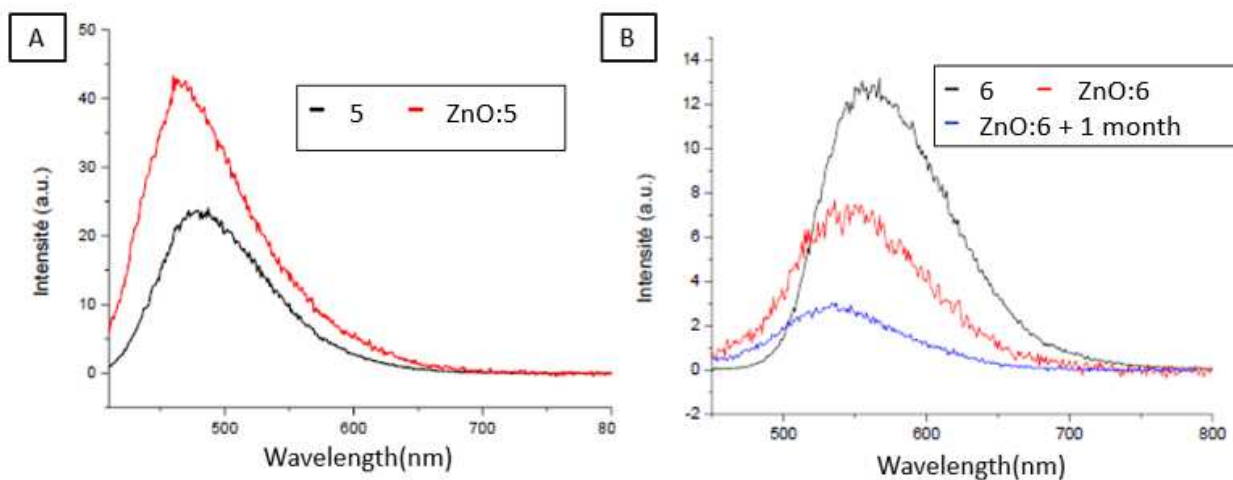
Energy profile calculated by MD during the anchoring of the de-protonated tetraphenylhydroxyoxoposphole in the bi-dentate configuration on top of the (10-10) ZnO surface. The bidentate bound state occurs through the subsequent formation of two O(mol)-Zn(surface) links each providing a binding energy of about 2.5-2.8 eV (according to the classical force field).

#### 4) XPS



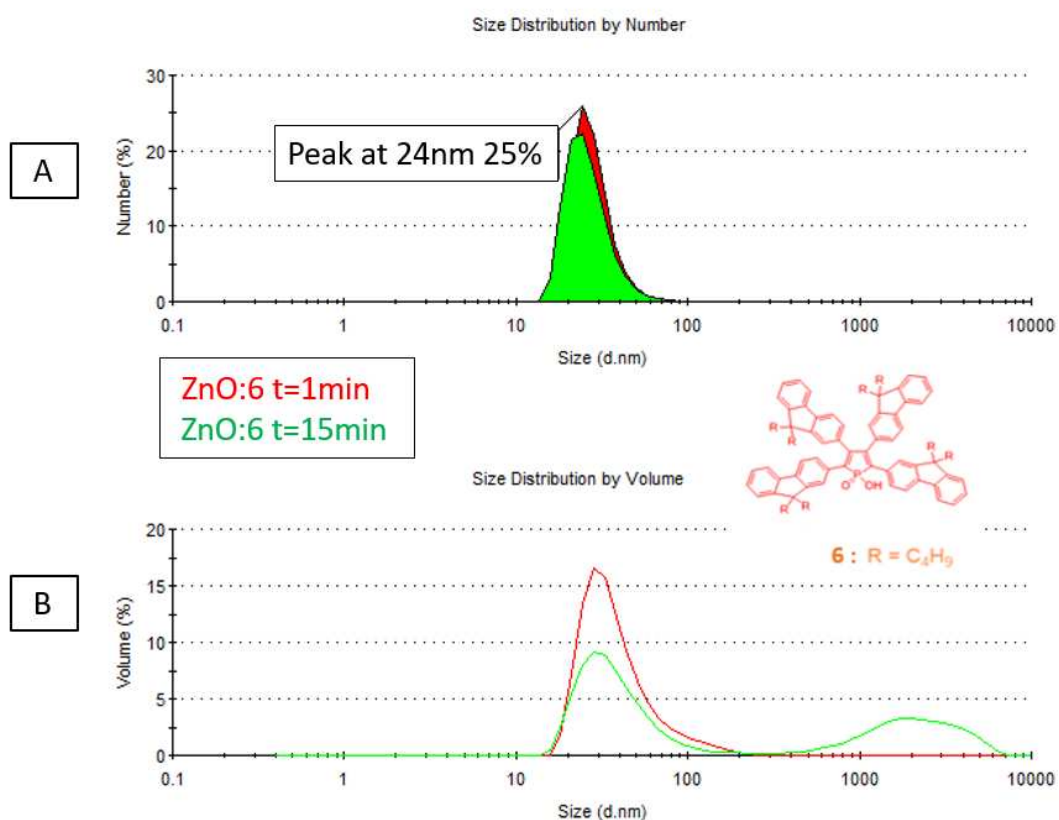
XPS wide scan of compounds 2 and ZnO:2

5) Fluorescence spectras of A) ZnO:5 and 5 ( $\lambda_{ex} = 350 \text{ nm}$ ) B) ZnO:6 and 6 ( $\lambda_{ex} = 400 \text{ nm}$ ) bonded with ZnO NCs

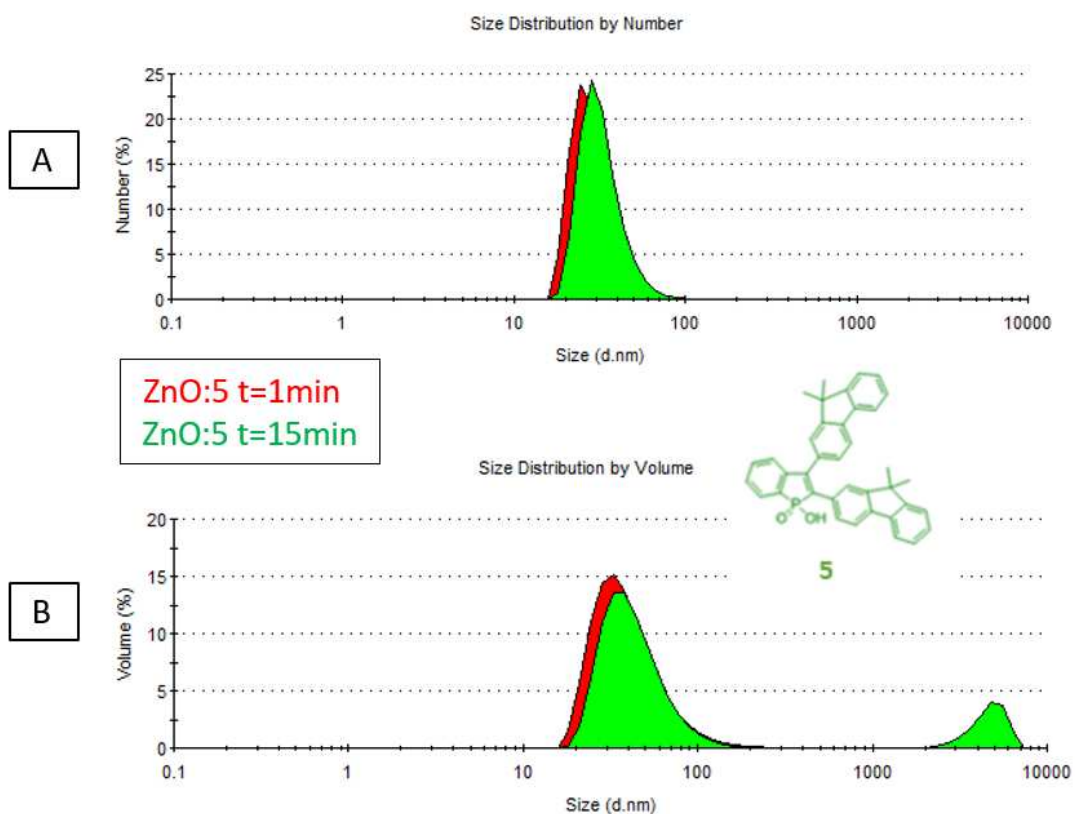


Note: Molecule 6 presents higher intense emission than the ZnO:6, but this is due to the very low solubility of 6 in solution

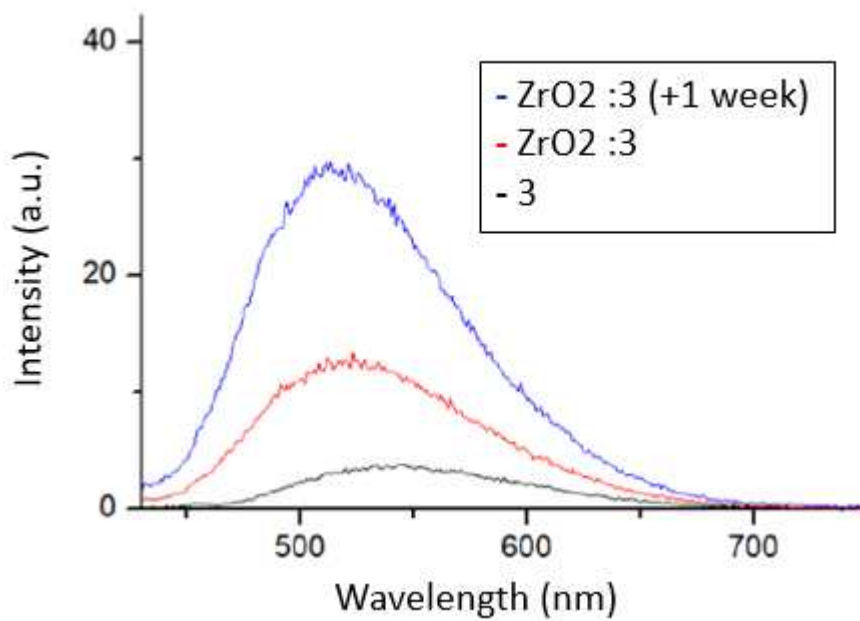
6) DLS size distribution of ZnO:6 A) by number B) by volume



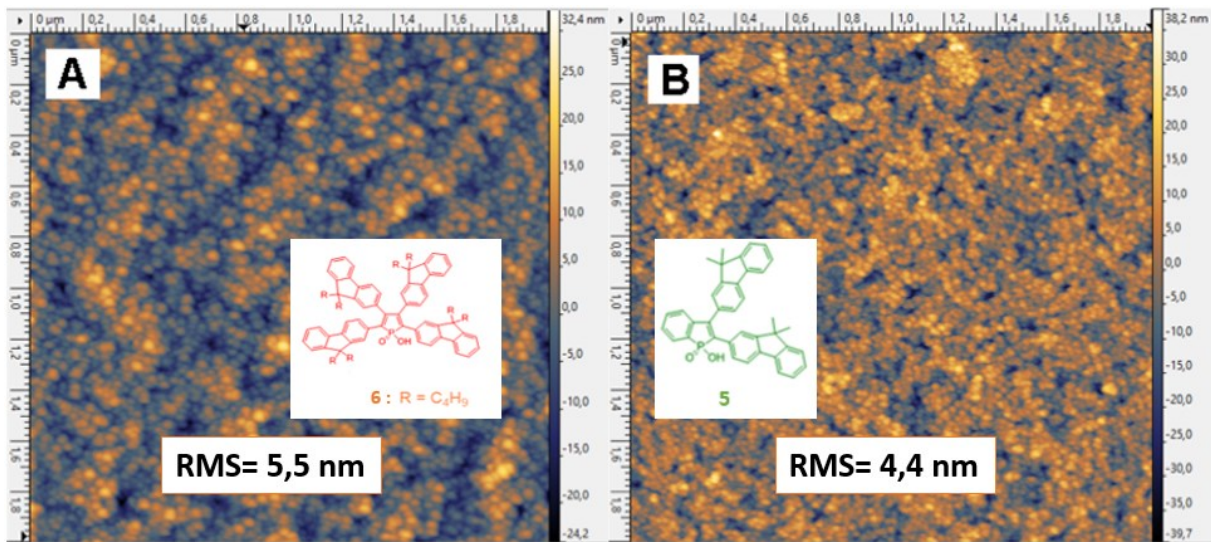
DLS size distribution of ZnO:5 A) by number B) by volume



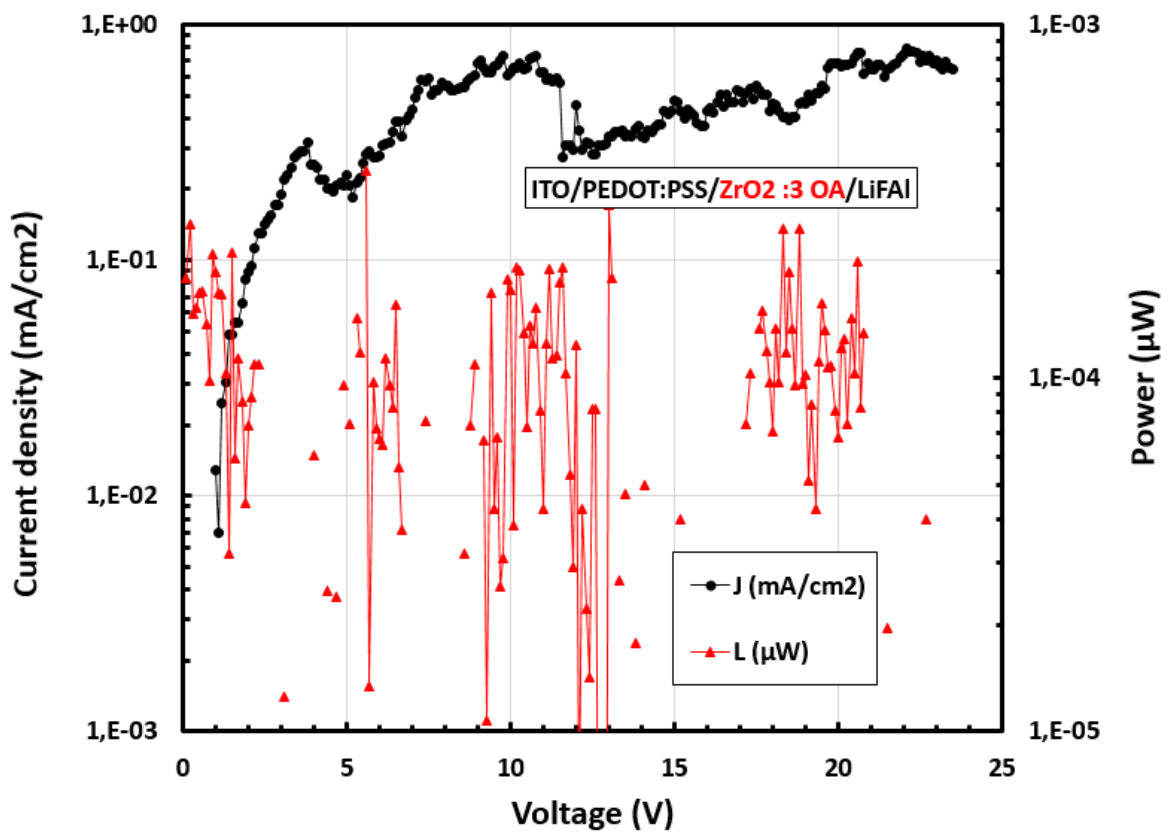
7) ZrO<sub>2</sub>:3, 3 fluorescence spectra at  $\lambda_{ex} = 400$  nm



8) AFM on thin films of B) ZnO:5 A) ZnO:6 at 2x2  $\mu\text{m}$  range



9) JVL curve of LED device using ZrO<sub>2</sub>:3:OA as emissive layer



## Bibliography:

- [1] Varughese G, Jithin PW, Usha KT. Determination of Optical Band Gap Energy of Wurtzite ZnO: Ce Nanocrystallites. *Physical Science International Journal*. 2015;146–154. doi:10.9734/PSIJ/2015/14151
- [2] Sofiani Z. Thèse, Contributions à l'étude des propriétés optiques nonlinéaires de nanoparticules en couches minces à base de ZnO, 2007. <https://tel.archives-ouvertes.fr/tel-00152894>
- [3] Katrien De Keukeleere†, Jonathan De Roo†‡∇, Petra Lommen†, José C. Martins∇, Pascal Van Der Voort§, and Isabel Van Driessche\*†. Fast and Tunable Synthesis of ZrO<sub>2</sub> Nanocrystals: Mechanistic Insights into Precursor Dependence | *Inorganic Chemistry* 2015 , 54, 7, 3469–3476. [accessed 2022 Jan 21]. doi.org/10.1021/acs.inorgchem.5b00046
- [4] Ramachari D, Esparza D, López-Luke T, Romero VH, Perez-Mayen L, De la Rosa E, Jayasankar CK. Synthesis of co-doped Yb<sup>3+</sup>-Er<sup>3+</sup>:ZrO<sub>2</sub> upconversion nanoparticles and their applications in enhanced photovoltaic properties of quantum dot sensitized solar cells. *Journal of Alloys and Compounds*. 2017;698:433–441. doi:10.1016/j.jallcom.2016.12.026
- [5] Sun Z, Zhang X, Na, Liu Z, Han B, An G. Synthesis of ZrO<sub>2</sub>-Carbon Nanotube Composites and Their Application as Chemiluminescent Sensor Material for Ethanol. *The Journal of Physical Chemistry B*. 2006;110(27):13410–13414. doi:10.1021/jp0616359
- [6] Zhao L, Rand BP. Metal-halide perovskites: Emerging light-emitting materials Pages (from-to) 18-22 Number of pages 5 Journal Information Display Volume 36 Issue number 4 State Published - 2018. *Information Display*. 2018;36(4):18–22. doi:10.1002/j.2637-496X.2018.tb01134.x
- [7] Protesescu L, Yakunin S, Bodnarchuk MI, Krieg F, Caputo R, Hendon CH, Yang RX, Walsh A, Kovalenko MV. Nanocrystals of Cesium Lead Halide Perovskites (CsPbX<sub>3</sub>, X = Cl, Br, and I): Novel Optoelectronic Materials Showing Bright Emission with Wide Color Gamut. *Nano Letters*. 2015;15(6):3692–3696. doi:10.1021/nl5048779
- [8] Abhishek SwarnkarAshley R. MarshallErin M. SanehiraBoris D. ChernomordikDavid T. MooreJeffrey A. ChristiansTamoghna Chakrabartiand Joseph M. Luther. Quantum dot-induced phase stabilization of α-CsPbI<sub>3</sub> perovskite for high-efficiency photovoltaics *Science* • 7 Oct 2016 • Vol 354, Issue 6308 • pp. 92-95 • DOI: 10.1126/science.aag2700. [accessed 2021 Dec 28].
- [9] Nayak MK, Dogra SK. Photophysics of 1-hydroxy- and 1-methoxy-9-fluorenone: II. Non-radiative deactivation. *Journal of Photochemistry and Photobiology A: Chemistry*. 2005;169(3):299–307. doi:10.1016/j.jphotochem.2004.07.011
- [10] Bao Q, Liu X, Xia Y, Gao F, Kauffmann L-D, Margeat O, Ackermann J, Fahlman M. Effects of ultraviolet soaking on surface electronic structures of solution processed ZnO nanoparticle films in polymer solar cells. *Journal of Materials Chemistry A*. 2014;2(41):17676–17682. doi:10.1039/C4TA02695K
- [11] Martini C, Poize G, Ferry D, Kanehira D, Yoshimoto N, Ackermann J, Fages F. Oligothiophene Self-Assembly on the Surface of ZnO Nanorods: Toward Coaxial p-n Hybrid Heterojunctions. *ChemPhysChem*. 2009;10(14):2465–2470. doi:10.1002/cphc.200900552
- [12] Gong Y, Andelman T, Neumark GF, O'Brien S, Kuskovsky IL. Origin of defect-related green emission from ZnO nanoparticles: effect of surface modification. *Nanoscale Research Letters*. 2007;2(6):297. doi:10.1007/s11671-007-9064-6

- [13] J.Phelipot & al. Highly Emissive Layers based on Organic/Inorganic Nanohybrids Using Aggregation Induced Emission Effect - *Advanced Materials Technologies* - 2022. [accessed 2021 Dec 28].  
<https://onlinelibrary.wiley.com/doi/abs/10.1002/admt.202100876>
- [14] Ben Dkhil S, Duché D, Gaceur M, Thakur A, Bencheikh F, Escoubas L, Simon J, Guerrero A, Bisquert J, Garcia-Belmonte G, et al. Interplay of Optical, Morphological, and Electronic Effects of ZnO Optical Spacers in Highly Efficient Polymer Solar Cells. *Advanced Energy Materials*. 2014;4.  
doi:10.1002/aenm.201400805
- [15] Sudheendran Swayamprabha. Approaches for Long Lifetime Organic Light Emitting Diodes - *Advanced Science* - Volume8, Issue1 January 6, 2021 2002254. [accessed 2021 Dec 20].  
<https://onlinelibrary.wiley.com/doi/full/10.1002/advs.202002254>
- [16] Ange Stoïanov†, Christophe Gourlaouen†, Sergi Vela†, and Chantal Daniel†. Luminescent Dinuclear Copper(I) Complexes as Potential Thermally Activated Delayed Fluorescence (TADF) Emitters: A Theoretical Study | *The Journal of Physical Chemistry A*. [accessed 2021 Dec 20].  
<https://pubs.acs.org/doi/10.1021/acs.jpca.7b11793>
- [17] Tang H, Meng G, Chen Z, Wang K, Zhou Q, Wang Z. Warm White Light-Emitting Diodes Based on a Novel Orange Cationic Iridium(III) Complex. *Materials (Basel, Switzerland)*. 2017;10(6):E657.  
doi:10.3390/ma10060657
- [18] Lu G-Z, Li X, Liu L, Zhou L, Zheng Y-X, Zhang W-W, Zuo J-L, Zhang H. Efficient phosphorescent red iridium(III) complexes containing a four-membered Ir–S–C–S ring backbone and large hindered spacers for high-performance OLEDs. *Journal of Materials Chemistry C*. 2019;7(13):3862–3868.  
doi:10.1039/C9TC00440H
- [19] Bender VC, Marchesan T, Alonso J. Solid-State Lighting: A Concise Review of the State of the Art on LED and OLED Modeling. *Industrial Electronics Magazine, IEEE*. 2015;9:6–16.  
doi:10.1109/MIE.2014.2360324

## Chapter 2: Nanohybrids incorporated as guests in a polymer host matrix

### 1) The interest of host-guest structure using a polymer matrix

Currently, luminescent polymers are the major choice to fabricate economical optoelectronic devices. Narrow bandgap polymers with robust, high film-forming properties have emerged, which is extremely beneficial for simple solution processing. [1–3] However, these polymers still suffer from dispersion in the structure and reproducibility issues, in addition to metal catalyst residues that, in many cases, result in low purity including defects, which limit their electroluminescent performances. [4] In contrast, small molecules have the advantages of clearly defined structures, easy purification and better photoluminescence performance. In the past few years, tremendous progresses have been made in the design of solution processable TADF molecular emitters and the corresponding solution processed TADF OLEDs have achieved state of the art EQEs over 20% for several color ranges. [5–7] As the TADF molecules involve the triplet excited state in their emission channel and as the triplet state has a significantly longer lifetime than the singlet excited state, the former is easily perturbed by external factors such as concentration quenching, exciton migration or triplet–triplet annihilation. [8] Consequently, the devices made from neat film of molecular emitters often exhibit poor performances due to these detrimental effects. To overcome this issue, the emitters are generally dispersed as guests into host materials in suitable concentrations. [9]

The appropriate guest / host combination selection plays a key role in determining the emissive characteristics in the film state. However, the solution processing of guest / host doped OLEDs faces well known phase separation problems, inducing serious aggregation of the molecules and resulting in emission quenching effects. [10, 11] Although some specific approaches have shown how to avoid this problem, [12, 13] controlling the dispersion of organic emitters in a host matrix by solution method remains a key challenge in the field. Indeed, a tool to control the arrangement of various types of emitters in the host material would allow for the unrestricted use of all promising types of emitters (thermally-activated delayed fluorescence, [3, 5] multi resonance TADF, [14] aggregation induced delayed fluorescence [15, 16]). In the previous chapter, we showed that nanohybrids made from the grafting of organic emitters (hydroxyoxophospholes) onto zinc oxide (ZnO) nanocrystals were presenting aggregation induced emission effect allowing for highly photoluminescent thin films. [17] The LED devices

made from neat films of these nanohybrids as emissive layer led to limited performances, mainly attributed to charge transport properties limitations in the layer. However, in this chapter, it is shown that this grafting technique can be used to control the spatial arrangement of the organic emitters in a polymer host material, when using dispersion of these nanohybrids as guests into such host. The dispersion of the organic emitters within the host material is indeed directly connected in this case to the dispersion of the emitter carriers (i.e. the nanohybrids) within the host material. To sum up, the advantages of the incorporation of the nanohybrids in a host matrix are numerous:

- Better control of the morphology, including surface morphology, to avoid the cluster formation
- Increase the transport properties in comparison with the use of pristine nanohybrids ZnO:3 OA
- Possible energy transfer from the matrix to the hybrid NCs
- If the matrix is a luminescent material, it can also play a role regarding the emitted color.

## 2) The choice of PVK polymer and OXD as host matrix

Upon polymerization, N-vinylcarbazole monomer gives polyvinylcarbazole (PVK) which is thermally and chemically stable and has photoconductive properties as well as low dielectric loss. Polyvinylcarbazole is a temperature resistant thermoplastic polymer. It is photoconductive and therefore forms the basis of photorefractive polymers and light emitting diodes. [18] The PVK is reported in literature as a hole transporting material. [19, 20] Oxadiazoles (OXD) are a class of heterocyclic aromatic chemical compound of the azole family with the molecular formula  $C_2H_2N_2O$ , OXD is able to transport the electrons. [21, 22] PVK material has energy levels from -2.2 to -5.8 eV, while OXD from -3.0 to -6.3 eV. [23, 24] Therefore, the combination of PVK and OXD leads to an ambipolar material, which can be used as electroluminescent material, and as a host matrix for various organic emitters [25–28] (and for the nanohybrids in our case). As established in literature, the PVK, or the PVK:OXD blends are blue electroluminescent compound used as 1<sup>st</sup> generation material for OLED, with moderate-to-low performances. [23] The choice of PVK:OXD as polymer host matrix is relevant in our case, because this material is well-known and has been widely studied in literature. Moreover, the luminous performances displayed by the matrix PVK:OXD are in the range of the ones given by the molecules developed by our collaborators from Sciences Chimiques Rennes.

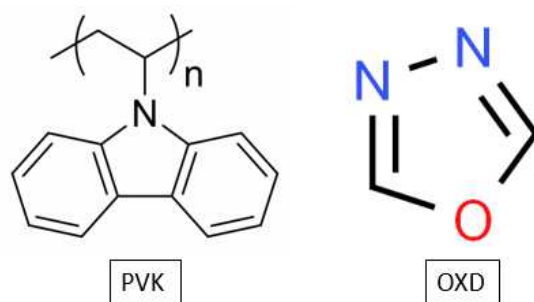


Figure 1 : Chemical structure of Polyvinylcarbazole (PVK) and oxadiazole (OXD)

### 3) Incorporated nanohybrids in the matrix: the effect of OA

The preparation of the electroluminescent layer is illustrated by the figure 2. The host matrix PVK:OXD (referred as M) is prepared one day in advance in solution of chlorobenzene and chloroform (volume ratio 4:1), with concentrations of 20:10 mg/mL (PVK:OXD). The next day, once the M solution is clear, the nanohybrids N are prepared as shown before in colloidal solution via self-assembly. The nanohybrids are added into the M solution, in a specific concentration referred as X% of the PVK mass. After 5 minutes of stirring and hybrid structure assembly, the OA may be added in solution.

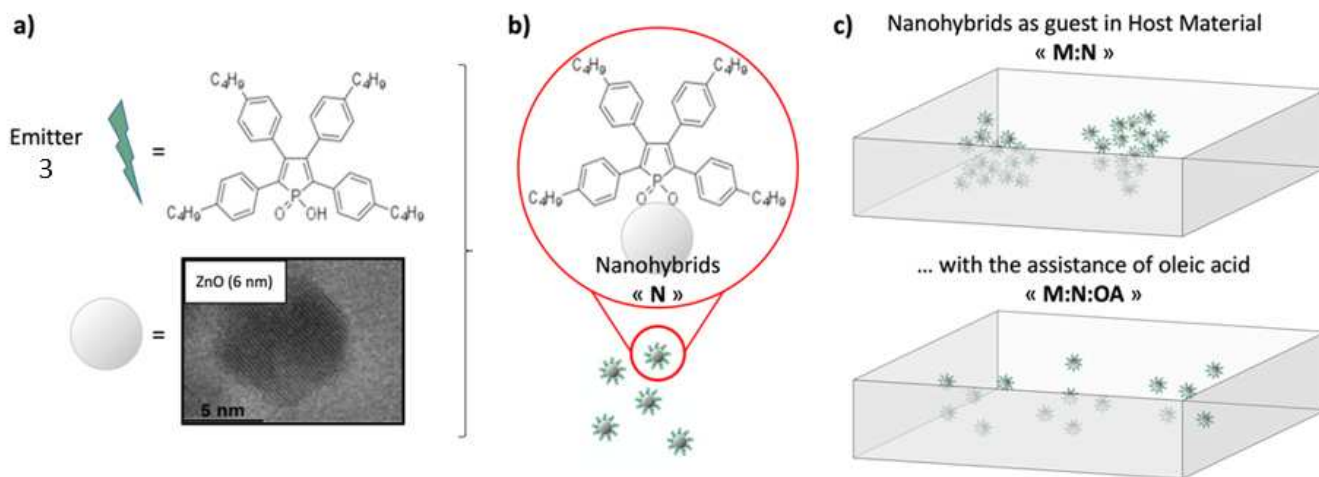


Figure 2 : Schemes of a) the individual organic emitter 3 and ZnO NCs, b) the nanohybrids N, and c) the emissive layers using dispersed nanohybrids within the host material with (M:N:OA) or w/o (M:N) the use of oleic acid.

To investigate the properties of this new electroluminescent material, different parameters were tried, namely:

- The thickness of the active layer by controlling the amount of PVK. Indeed, it is often found in literature that electroluminescent OLED layer should be about 40 nm thick, as thicker active layer leads to bigger threshold voltage
- The ratio of PVK:OXD, which is correlated to the ambipolar property of the matrix M
- The amount of nanohybrids N (ZnO:3) added in M, namely X = 5% ; 10% ; 15% (and the resulting sample will be referred as M:N<sub>x</sub>)
- The amount of OA, which may induce insulative behavior in the device. An additional question is also whether OA is still required to obtain reproducible smooth surface morphology. The presence of OA in the sample will be identified in the sample name (i.e. M:N<sub>x</sub>:OA)

### A) Morphological characterizations of M:N films with or without OA

In order to investigate the morphology of the layer and to directly visualize the spatial arrangement of the nanohybrids N within the host layer M, Transmission Electron Microscopy (TEM) was employed. For sample preparation, a modification of the floating-layer technique was applied. [29] Firstly, a sacrificial PEDOT:PSS material was spin-coated on a substrate before the M:N emissive layer was spin-coated on top of it. After a brief annealing to dry the layers, the PEDOT:PSS film was dissolved in deionized water. Floating thin films of the emissive layer M:N (OA) were then recovered and deposited on a holey carbon coated TEM grid as shown in Figure 3a.

The emissive layer presented in the following part is referred as M:N<sub>10</sub> sample, as a solution containing 10% w/w of nanohybrids with respect to the host matrix was prepared and spin-coated. The resulting TEM images are represented in Figures 3b/c at two different magnifications. From the large area in Figure 3b, the layer M:N<sub>10</sub> reveals nanohybrid aggregates over a micron scale, highlighted on the picture by the white dotted circles. The presence of high amounts of aggregated nanohybrid structures is confirmed in Figure 3c, proving the poor ability of the nanohybrids to be homogeneously dispersed within the host matrix. These undesirable aggregates may cause recurring electrical short circuits in corresponding LED devices and therefore need to be removed to obtain functional and reproducible LED devices. For this purpose, to avoid the agglomerate formation and improve the homogeneous dispersion of the nanohybrids within the host layer, a low amount of an additional surfactant was used as additive to the M:N<sub>10</sub> solution. In this respect, as discussed in chapter 1, oleic acid was chosen as it is known as a classical surfactant used during

nanocrystal synthesis and also very efficient to ensure the dispersion and stability of nanocrystals in solution. [30]

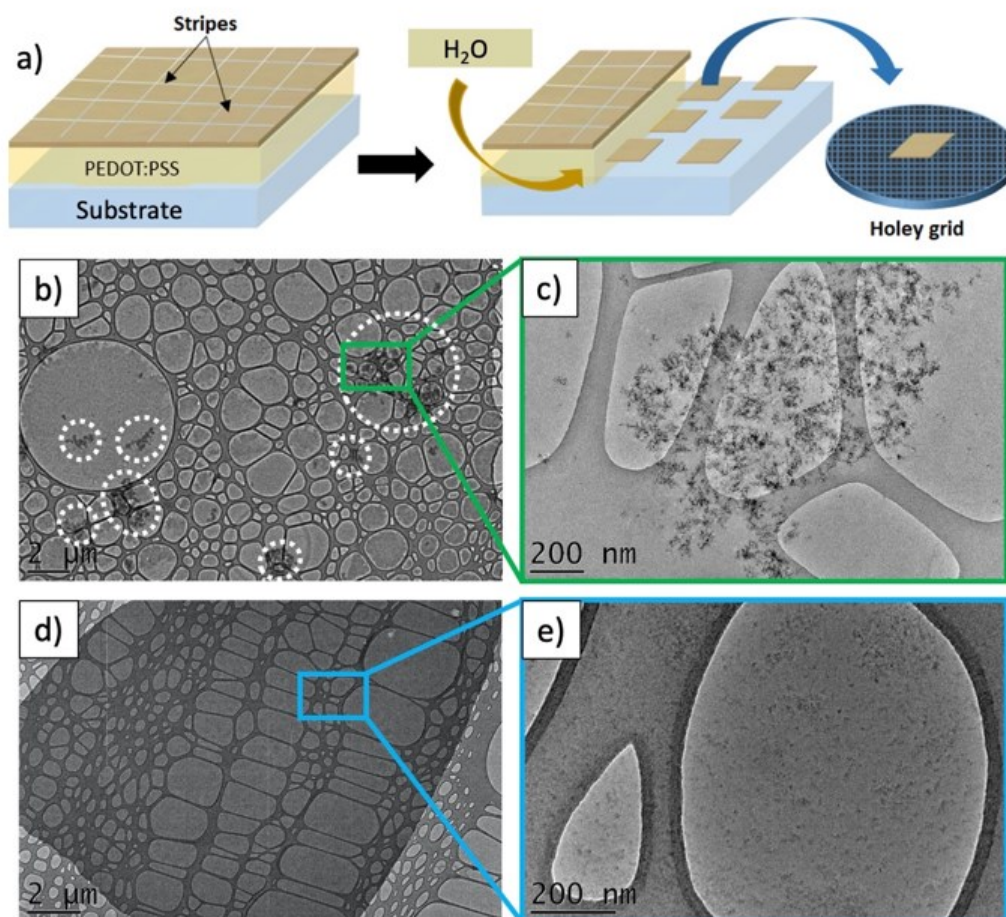


Figure 3: a) Scheme of the floating-layer technique used for depositing film on the holey carbon coated TEM grid. b-c) TEM images of the layer  $M:N_{10}$  at two magnifications. d-e) TEM images of the layer  $M:N_{10}:OA$  at two magnifications.

The layer referred as  $M:N_{10}:OA$  corresponds to the blend including the oleic acid treatment in solution (addition of 0.2% v/v). The resulting TEM images are represented in Figures 3d/e again at two different magnifications. Interestingly, the  $M:N_{10}:OA$  layer morphology is completely different from the one obtained with  $M:N_{10}$ . Even if slightly denser areas composed of nanohybrids are noticeable, no aggregate can be found over the whole layer. The oleic acid treatment appears to be an efficient method to avoid the formation of aggregates and to ensure the homogeneous dispersion of the nanohybrids within the entire layer. Moreover, the same trends were observed when using other quantities of nanohybrids, as in the case of solutions containing 5 or 15% w/w of nanohybrids with respect to the host matrix, layers referred as  $M:N_5$  and  $M:N_{15}$ , that present the same morphology improvement using OA, i.e.  $M:N_5:OA$  and  $M:N_{15}:OA$ , respectively, as shown in Figure 4.

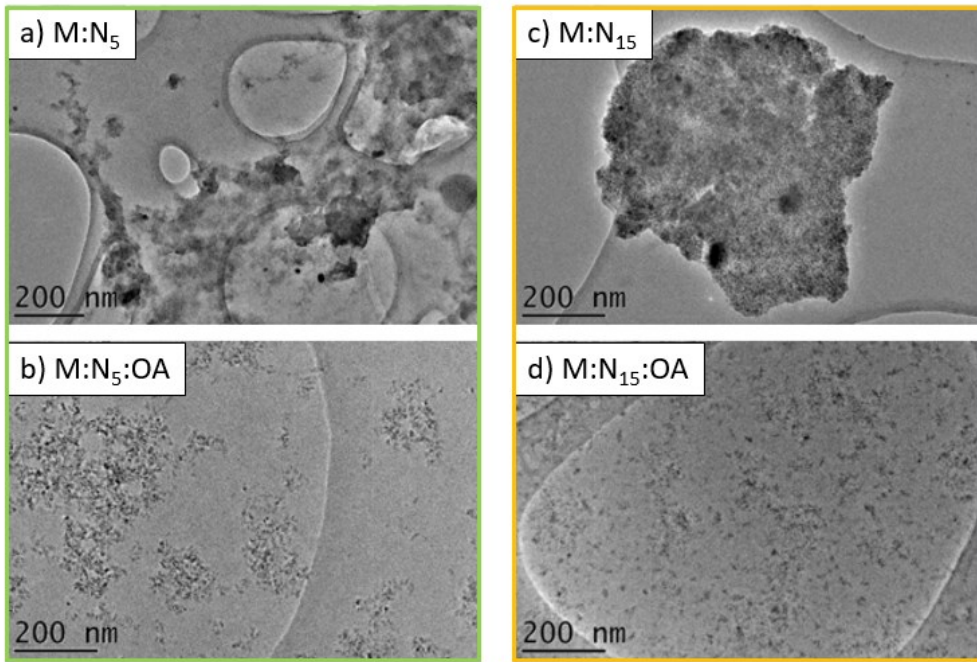


Figure 4 : a-b) TEM images of the layer M:N<sub>5</sub>:OA. c-d) TEM images of the layer M:N<sub>15</sub>:OA.

The spatial distribution of the nanohybrids within the layer was also studied using Secondary-Electron Microscopy (SEM) on a cross-section of the sample (Figure 5) to determine whether the nanohybrids were simply homogeneously spread at the top or bottom interface or vertically well dispersed. Even if the contrast is very light, the nanohybrids N appear as bright spots, present over the whole 50 nm thick layer, with slightly denser areas at the top of the layer, however ruling out any clear vertical segregation.

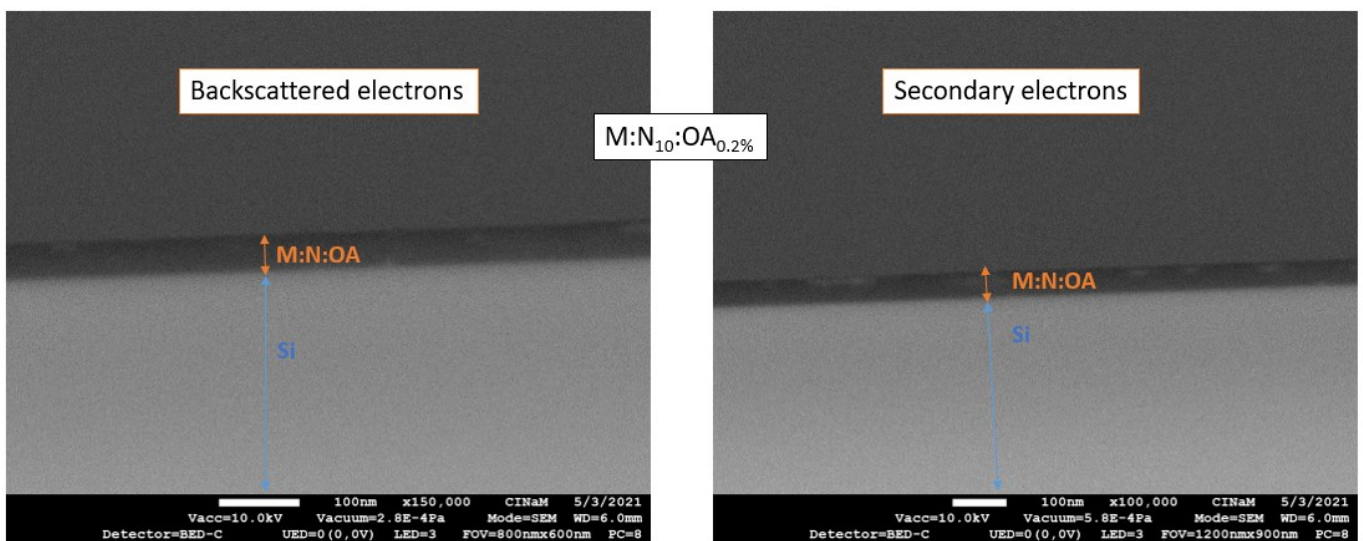


Figure 5 : Spatial distribution of the nanohybrids N:OA<sub>0.2%</sub> in M using Secondary or Backscattered Electron Microscopy (SEM) on a cross-section of the sample

The surface morphology was further studied by Atomic Force Microscopy. AFM images from the layer containing 10% of nanohybrids N are presented in Figure 6, with or without the use of OA in the spin-coated solution, while the related roughness values of the layers are given in Table 1. In the absence of OA in the solution, M:N<sub>10</sub> layer surface shows the presence of irregular nanohybrid aggregates within the host matrix, large on a micron scale and as height as 80 nm (Figures 6a/b). This inhomogeneous surface is characterized by a very high roughness, measured at 11.1 nm from the 10 x 10 μm image. On the opposite, the M:N<sub>10</sub>:OA emissive layer presents a very smooth surface morphology, without any noticeable aggregate over the whole surface (Figures 6c/d), as already pointed out by the TEM and SEM cross-section image. The surface roughness is, as expected, much lower and measured at 1.1 nm from the same 10 x 10 μm scale.

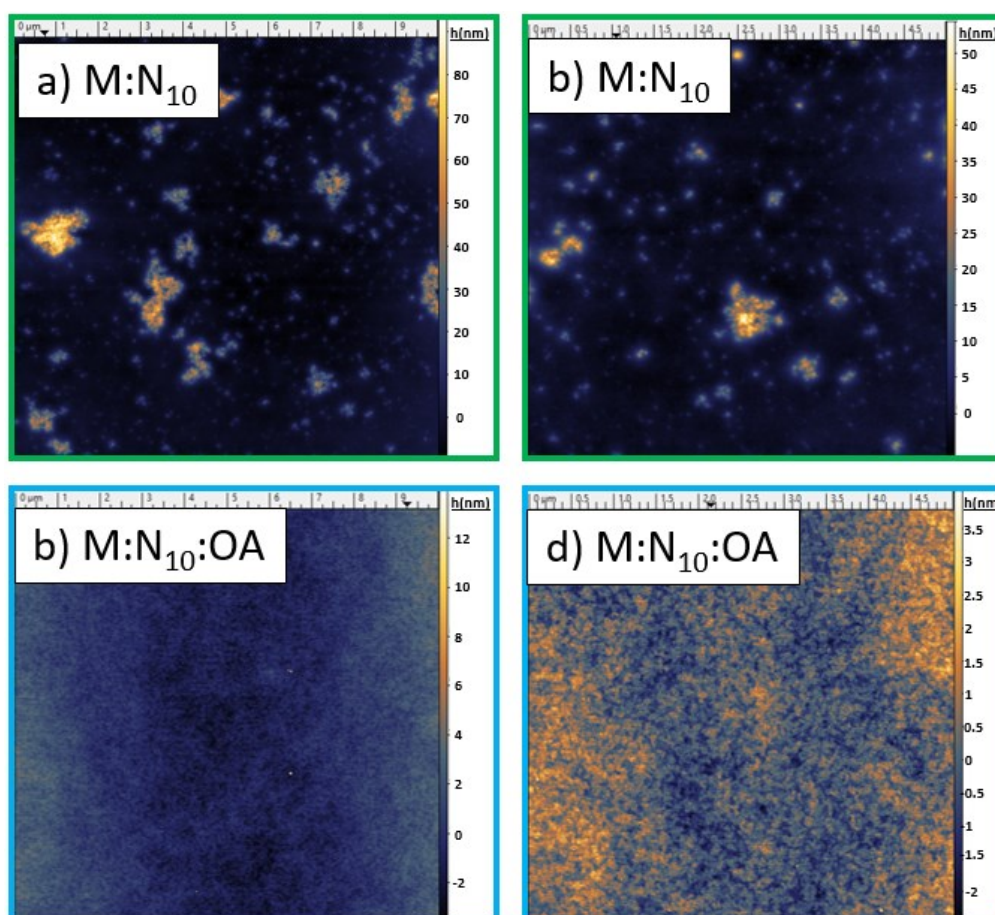


Figure 6 : AFM images of the layer M:N<sub>10</sub> at 10 x 10 μm scale (a) and 5 x 5 μm scale (b). AFM images of the layer M:N<sub>10</sub>:OA at 10 x 10 μm scale (c) and 5 x 5 μm scale (d).

The same trends were observed with the other amounts of incorporated nanohybrids in the matrix M, cf. Figure 7 and Table 1. The M:N<sub>5</sub> and M:N<sub>15</sub> thin films, based on the neat host/guest materials, present high roughness values of 6.0 and 4.8 nm, respectively, caused by the

presence of underlying aggregates. After OA addition in the solution, the roughness of the resulting thin films decreases significantly to reach RMS = 1.4 nm (M:N<sub>5</sub>:OA) and 1.6 nm (M:N<sub>15</sub>:OA). These low roughness values are in the range of those obtained in other spin-coated guest-host films used in electroluminescent OLED devices. [31, 32]

Table 1. Root mean square roughness obtained from 10 x 10 μm AFM measurements of layers containing 5, 10 and 15% of nanohybrids N, with or w/o using OA in the spin-coated solution.

	M:N <sub>5</sub>	M:N <sub>5</sub> :OA	M:N <sub>10</sub>	M:N <sub>10</sub> :OA	M:N <sub>15</sub>	M:N <sub>15</sub> :OA
<b>RMS roughness (nm)</b>	6.0 +/- 0.6	1.4 +/- 0.1	11.1 +/- 1.0	1.1 +/- 0.1	4.8 +/- 0.5	1.6 +/- 0.1

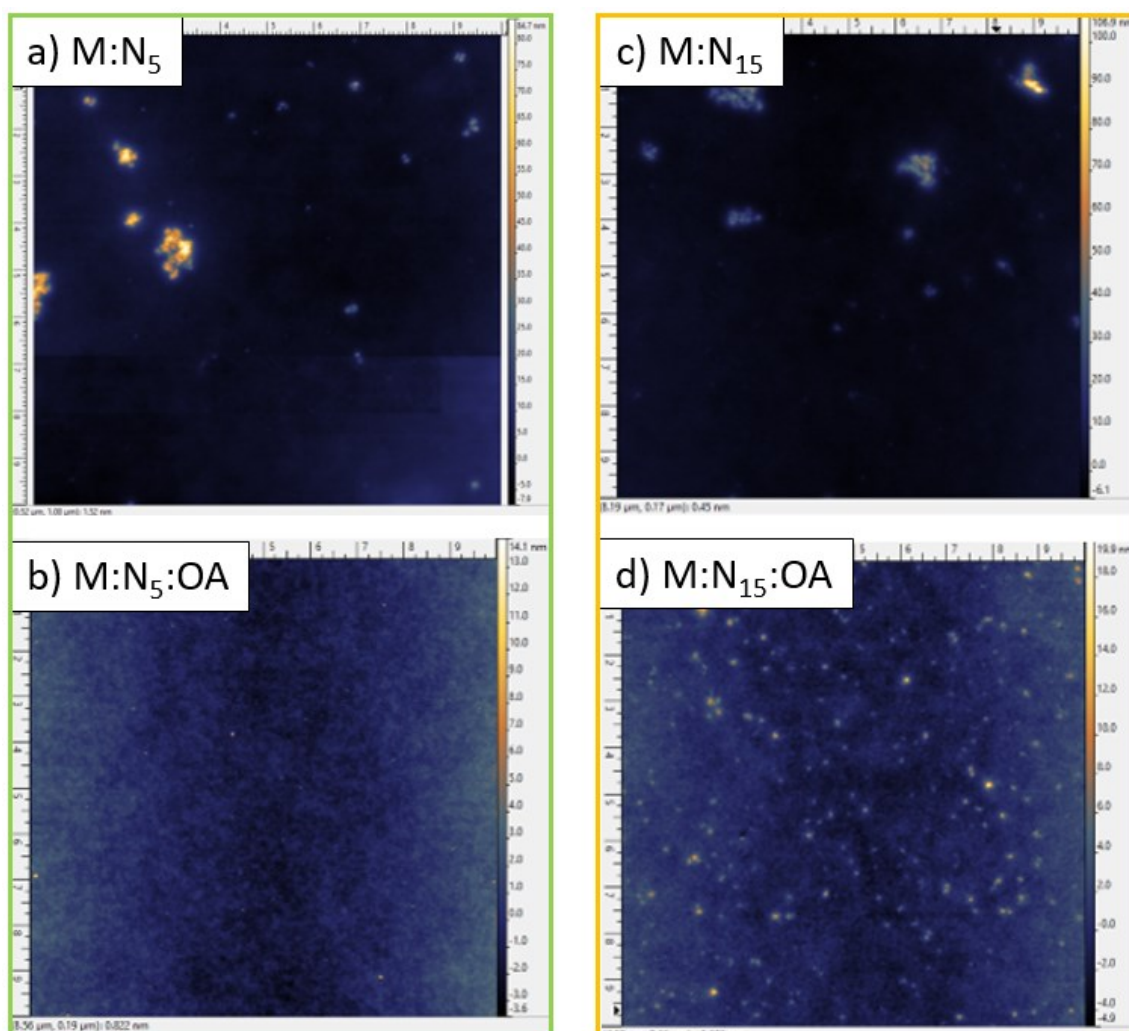


Figure 7 : AFM images of the layer M:N<sub>5</sub> at 10 x 10 μm scale (a) M:N<sub>5</sub>:OA (b). AFM images of the layer M:N<sub>15</sub> at 10 x 10 μm scale (c) M:N<sub>15</sub>:OA (d).

It was observed that increasing the amount of OA in the solution does not further improve the morphology of the layer, as shown in Figure 8. However, employing lower amounts of OA in solution gave rise to the formation of aggregates of various sizes.

To conclude, the use of a low amount of OA as additional surfactant appears as a mandatory treatment of the host/guest solution, in order to avoid nanohybrids aggregates and ensure the homogeneous dispersion of the nanohybrids within the matrix in thin films. Thus, this treatment is perfectly adapted to obtain smooth film with low roughness, as required to elaborate reproducible and functional LED devices. The following part will focus on analyzing the optical properties of these layers, to evaluate the effects of both the matrix M and the OA treatment on these nanohybrids.

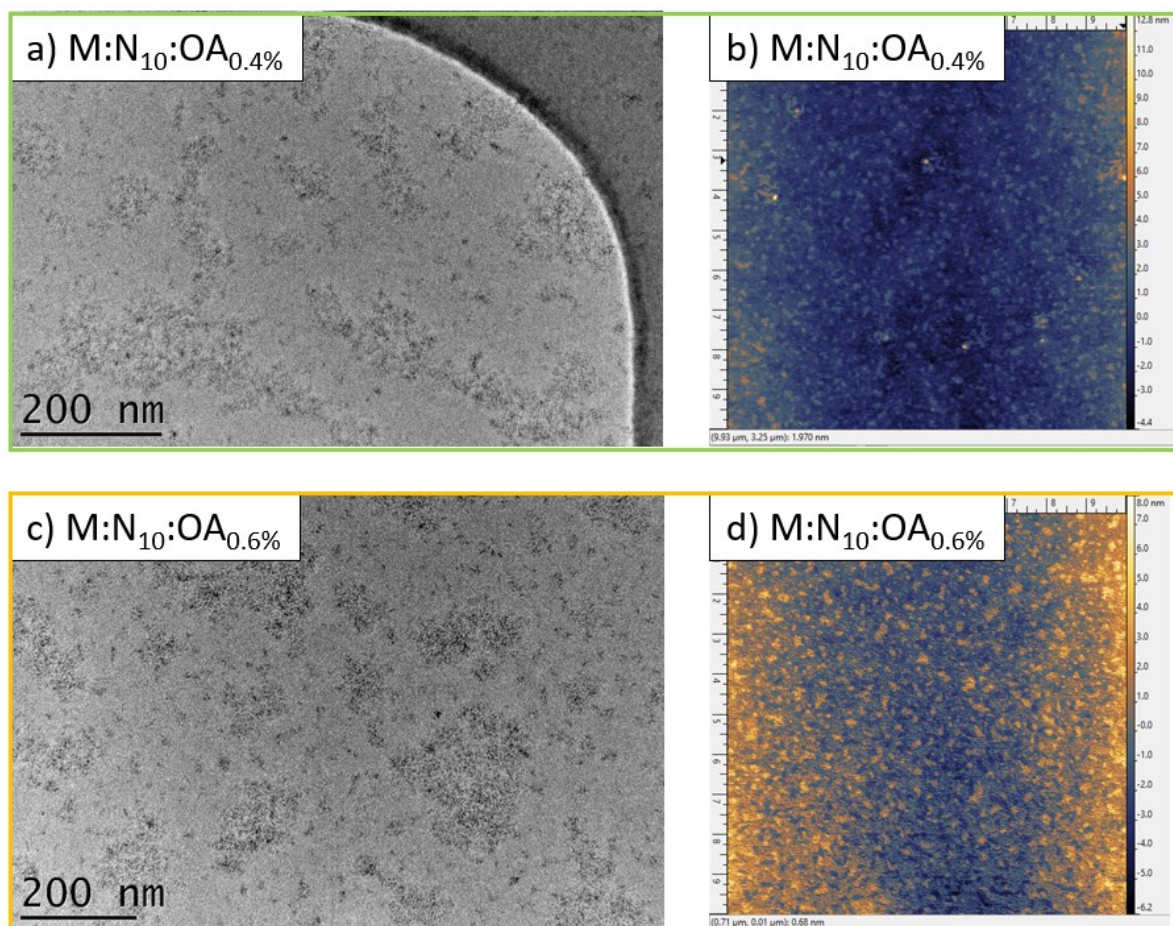


Figure 8 : a-c) TEM and AFM 10 x 10 μm images of M:N<sub>10</sub>:OA<sub>0.4%</sub> b-d) TEM and AFM 10x10 μm images of M:N<sub>10</sub>:OA<sub>0.6%</sub>

## B) Optical characterizations

### i) Matrix M, emissive molecule 3 and ZnO NCs in solution:

It is important to know what are the optical properties of the different materials which compose the electroluminescent layer. Preliminary tests were done on the pure nanohybrid structure N, studied at the liquid state. As shown in the chapter 1, the emitter 3 has a maximum absorbance peak at 400 nm, and the same spectral shape was observed for nanohybrids N with a blue shift about 20 nm. The ZnO würtzite nanocrystal absorption threshold is reported close to 350 nm, and the ZnO as a green [33] or blue luminescent material [34], depending on the used surface ligand. The host matrix M is also referenced with an absorption at 350 and 250 nm and known as blue emitter (Figure 9a).

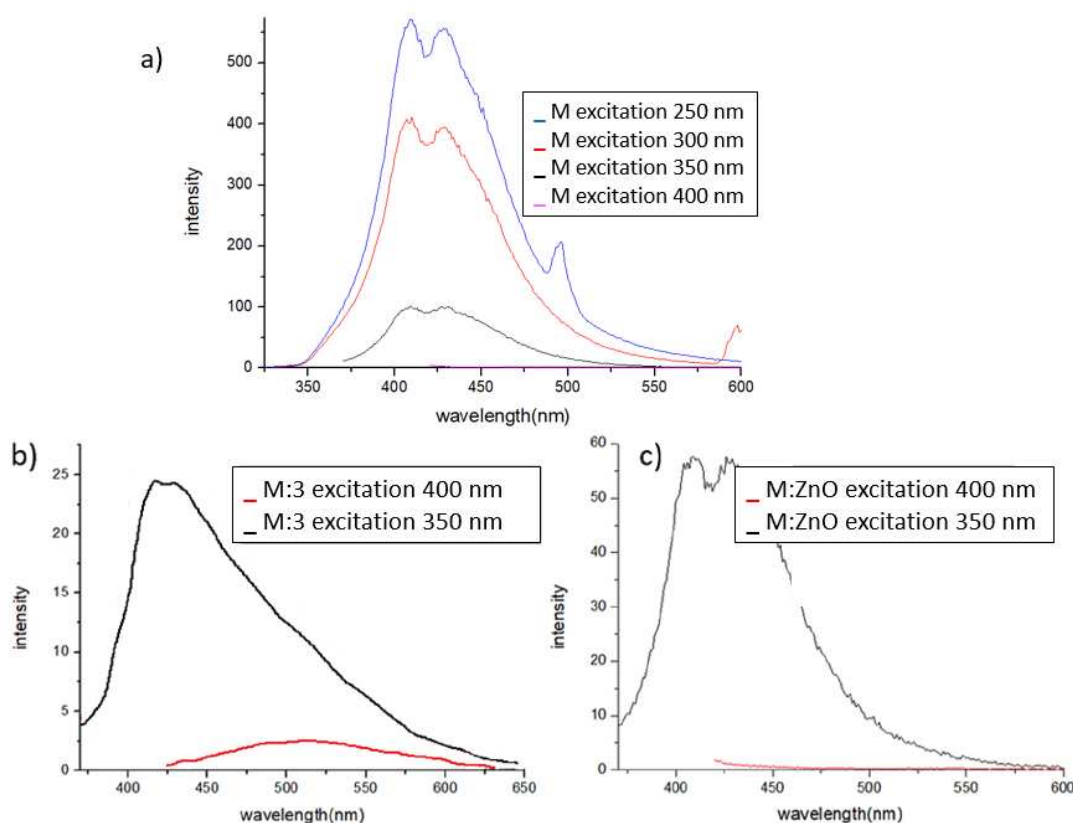


Figure 9 : Fluorescence spectra in liquid state of a) PVK:OXD (M) at different excitation wavelengths b) M:3 c) M:ZnO excited at 350 and 400 nm

Firstly, in figure 9a, the emission peaks of the matrix M observed at 500 and 600 nm are considered as artefacts. The matrix M emits light when excited at 350 nm or less, and M does not emit light when excited at 400 nm, and the same behavior is observed for ZnO and M:ZnO

(Figure 9c). Therefore, in figure 9b, the contrast of the M:3 emission is notable between excitation wavelengths at 350 and 400 nm. The excitation at 400 nm reveals the emission of the single molecule 3 with a maximum peak around 510 nm – as expected. When excited at 350 nm, thus on the matrix M, an emission band from 350 to 600 nm is observed, corresponding to a bluish-green color. It was assumed that a partial energy transfer occurs from the matrix M to the emissive molecule 3, explaining the broader emission of M:3 compared to M.

ii) Luminescent materials in thin films (excited at 400 nm):

The M:N<sub>10</sub> samples absorbance spectra are illustrated by the Figure 10. The spectra are normalized from 0 to 1 in the range of 330 to 430 nm. All the samples had the same thickness, namely 100 +/- 5 nm according to profilometry measurements.

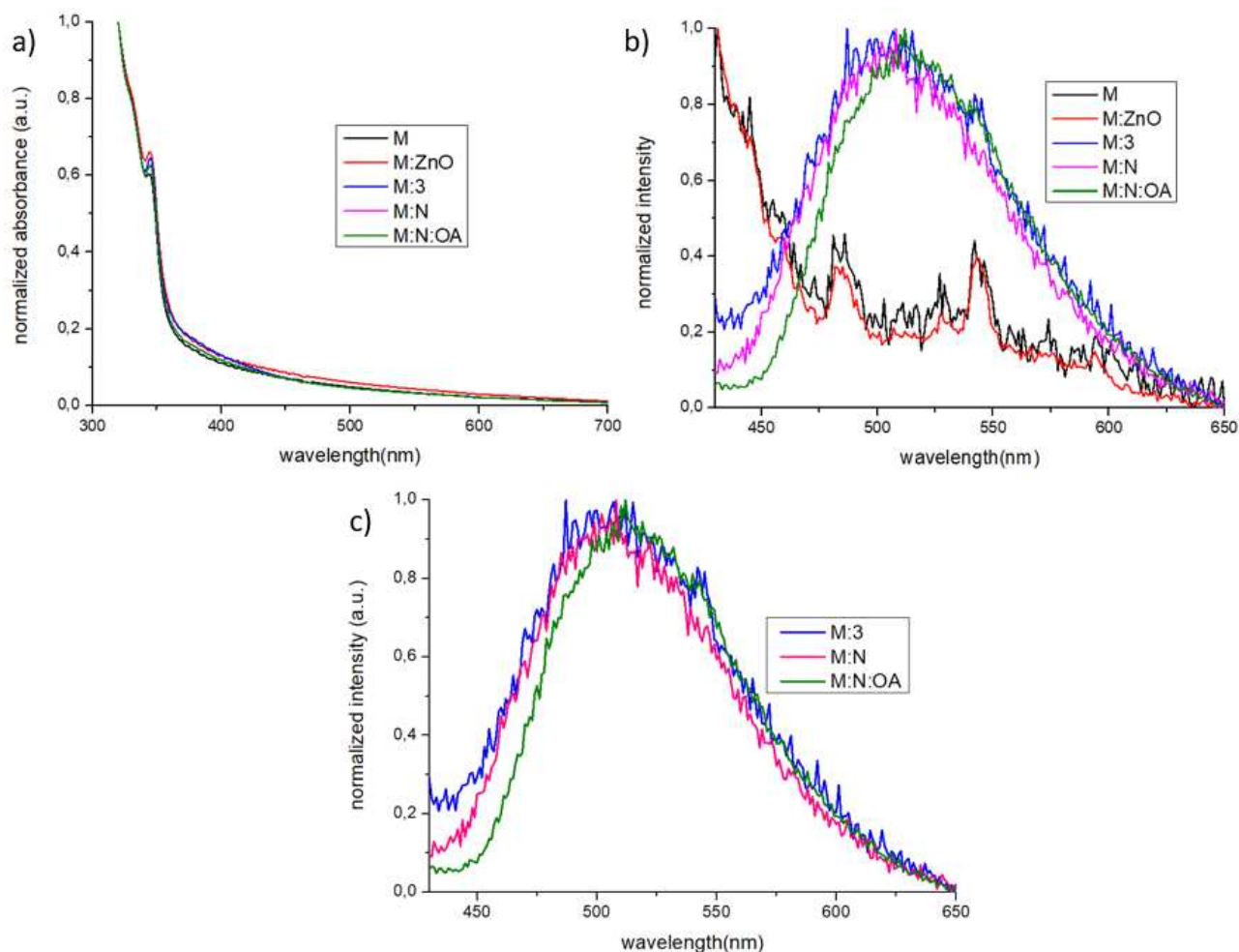


Figure 10 : Thin films A) Normalized absorbance B) Normalized intensity fluorescence spectra excited at 400 nm C) normalized intensity fluorescence spectra excited at 400 nm of M(black); M:ZnO(red); M:3(blue); M:N(pink); M:N:OA(green).

As shown by Figure 10a, all the curves present similar absorption spectral shape, it is related to the host matrix M largely predominant in front of the amount of guest, respectively 10% of N, ZnO and emissive molecule 3. The first information is the absence of light scattering signal of the luminescent layers in the visible area, which is characteristic of an aggregate-free layer and appreciated to go toward efficient LED devices. Even though the absorbance tends to 0 at 400 nm and further, the black curve representing M is the lowest one, which is coherent because it represents the host matrix without any guest. Therefore, the M:N, M:ZnO and M:3 curves have higher absorbance at 400 nm. Also, the M:N absorbance value at 400 nm is lower than M:ZnO and M:3, and it may be due to the presence of aggregates, from the molecule 3, or from the ZnO which reduces the light transmission through the substrate

In another hand, absorbance matrix M absorption threshold is reported at 350 nm, [35] which is the same as for ZnO würtzite nanoparticles. [34] Indeed, at 350 nm, the red curve representing M:ZnO is more intense than the matrix M (black) or the M:N (pink) ones. This may be attributed to the presence of aggregated ZnO nanoparticles which absorb more than theoretically well dispersed nanohybrid N, where ZnO should be stabilized by the emitter 3. Thus, the corresponding morphology and absorbance analyses confirm the presence of clusters of few hundreds nanometers in M:N.

Emissive property of the luminescent layers was studied by fluorescence spectrophotometry. Thanks to preliminary absorbance measurements, the main absorbance peak of the emitter 3, and even N was reported at 400 nm. Early emission tests (excitation at 400 nm) at the liquid state were performed on pure N and emitter 3 before their incorporation in the matrix (cf. chapter 1). Indeed, an emission range between 440 to 660 nm, representing a bluish green emission color was observed, and the pure N showed higher intensity than the emitter 3, which confirmed the AIE effect from the liquid to the solid states (cf. chapter 1). These observations should correspond to an efficient grafting between the organic and the inorganic structures. The following studies focus on the emissive property of the different luminescent layers excited at 400 nm, namely M ; M:N ; M:ZnO ; M:3 ; M:N:OA which are presented by the Figures 10b/c. As before, the same thicknesses and error 100 +/- 5 nm of the luminescent layers are measured. The noise was very consequent on the spectra, and some artefacts are listed at 480 and 540 nm, related to the spectrophotometer.

As shown by the Figure 10b, M and M:ZnO luminescent layers were not emissive when excited at 400 nm. This is correlated to the absorbance of these materials, being below their absorption threshold when excited at 400 nm. However, M:N and M:3 presented emission range from 440 to 650 nm, and this behavior was also illustrated by the fluorescence of pure nanohybrids N in the chapter 1. Even if these luminescent layers showed bluish-green light emission when

excited at 400 nm, no shift was observed between M:3 and M:N as it was noticed before for pure emitter 3 and N in the chapter 1. On the other hand, by adding OA (sample M:N:OA), a shift towards higher wavelengths was observed in emission, about 20 nm, as shown by the behavior of pure N OA, thus indicating a similar modification of the electronic structure of the nanohybrids N (Figure 10c).

### iii) Emission in thin films (excited at 350 nm):

Furthermore, when the luminescent samples were excited at 350 nm, namely on the absorbance peak attributed to ZnO nanoparticles and M, various behaviors were observed (Figure 11). Indeed, a blue emission was noted for M:ZnO and M as already proven in the literature, [35] between 330 to 550 nm.

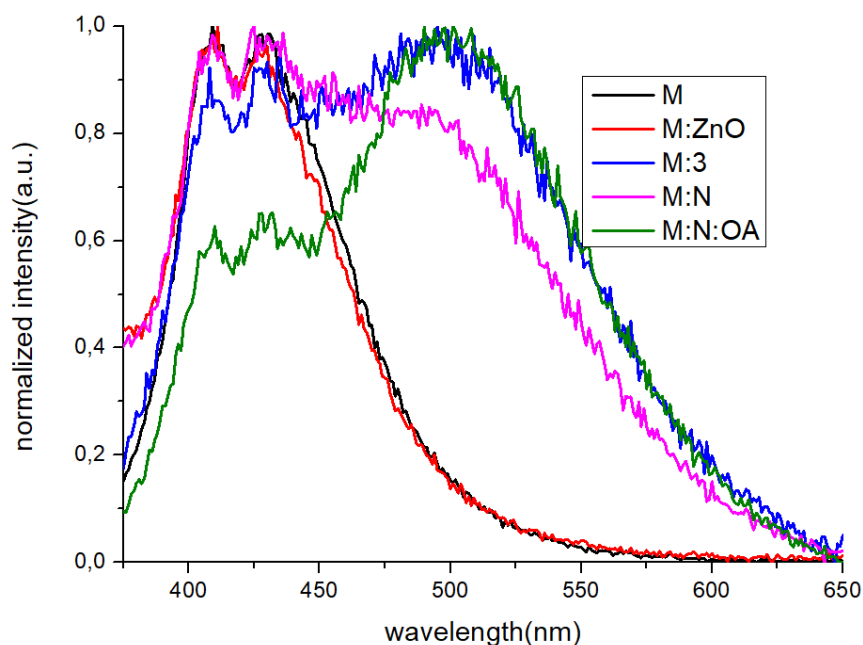


Figure 11 : Normalized intensity fluorescence spectra, thin films excited at 350 nm of M:3 ; M:ZnO ; M:N ; M:N OA ; M.

Interestingly, the matrix film containing the emitter 3 shows a broader emission band compared with M, i.e. from 330 to 650 nm, which means that an energy transfer occurs between the matrix M and the emitter 3 under excitation at 350 nm. In addition, different light intensities are observed between M:N and M:3 at 420 and 500 nm (figure 11). This may be explained either by aggregation of the nanohybrids N, or by the aggregation of ZnO nanoparticles, possibly not well bonded with the emitter 3. Thus, in this case, ZnO nanoparticles should contribute even more to blue emission with M and hide the bluish green emission of the emitter 3. We observed

that the energy transfer from M to N was even better while adding OA. Indeed, the emissions of the matrix and the ZnO decreased for a higher intensity in the bluish green area. It is important to mention again that the lowest amount of OA (0.2% v/v) in the luminescent layer cannot be decreased, otherwise aggregates would appear in the solution / substrate. Theoretically, the OA should be co-grafted together with the emitter 3, possibly in competition, on the surface of the ZnO nanoparticles. In addition it is reported that ZnO:OA NCs present strong blue emission, [34] while the N display a bluish-green color.

For the other amounts of N incorporated to the matrix M, same behaviors as N = 10% were observed, when the samples were excited at 400 nm (annexes 1/2). However, the energy transfer when excited at 350 nm from the matrix M to the nanohybrids N was weaker for N = 5%; while being more important for N = 15%, compared to N = 10%. It was found that 10% was a good compromise in terms of morphology and emissive properties.

#### iv) Photoluminescence Quantum Yield (PLQY):

The luminescence datas are completed by Table 2 showing the PLQY of the different materials used, excited at 400 nm. PLQY was deduced according to « John de Mello » method, [36] which do not depend on the thickness of the measured layer. The Table 2 is focused on the impact of the amounts of incorporated guests in the matrix M, namely X = 5%; 10% and 15%, comparing the luminescent materials: M:3<sub>x</sub>, M:N<sub>x</sub> and M:N<sub>x</sub>:OA.

Table 2 : Thin films PLQY of M:3<sub>x</sub> ; M:N<sub>x</sub> ; M:N<sub>x</sub>:OA with X = 5% ;10% ;15% of luminescent materials added to the matrix M

	Sample name	M:3 <sub>x</sub>	M:N <sub>x</sub>	M:N <sub>x</sub> :OA
PLQY(%)	X=5%	12 +/-1	11 +/-1	31 +/-3
	X=10%	10 +/-1	18 +/-2	37 +/-3
	X=15%	24 +/-2	22 +/-2	33 +/-3

From the Table 2, it is noted that the PLQY for X = 5% ;10% follow approximately the same increasing trend for each material namely M:3, M:N and M:N:OA. Indeed, for these amounts, M:3 and M:N films have very close PLQY about (10 to 18 +/-1%) which probably means that the bond between the organic emitter 3 and the inorganic ZnO nanoparticle is weakly efficient. As previous morphology images have confirmed, aggregated nanohybrids are on the surface of M:N films. In contrast, for X = 5% ;10%, the addition of OA (films referred as M:N<sub>x</sub>:OA)

induces a higher PLQY, which is about (31 to 37 +/- 3%), proving that well-dispersed nanohybrids N in the matrix M, and a better grafting help to enhance -approximately by factor 3- the PLQY compared to M:3 and M:N. In the Table 2, the amount X = 15% presents the same trend in the increasing of the PLQY as the other incorporated quantities. The difference remains in the PLQY of M:3 and M:N films, as they present twice higher PLQY compared with X = 5%, namely (22 to 24 +/- 2%). However, the maximum recorded PLQY for M:N<sub>15</sub>:OA is the same as the other amounts (33 +/- 3%). To sum up, for X = 15%, an enhancement of the PLQY by a factor 1.5 is observed with the OA treatment. In conclusion, OA in M:N helps to obtain smooth films and then to enhance the luminescence property of the layer, without changing the emission spectrum of M:3.

Furthermore, the impact of the OA quantity in M:N:OA is studied in Table 3, by comparing PLQY of three electroluminescent films, namely M:N:OA, M:N:OA<sub>2</sub> and M:N:OA<sub>3</sub>, containing respectively OA = 0.2% ;0.4% ;0.6% v/v.

Table 3. Thin films PLQY depending on three amounts (Y = OA ; Y = OA<sub>2</sub> ; Y = OA<sub>3</sub>) of OA in M:N<sub>10</sub>:OA<sub>Y</sub>.

	Sample name	M:N <sub>10</sub> :OA <sub>Y</sub>
PL Yield (%)	Y = OA (0,2% v/v)	35 +/-3
	Y = OA <sub>2</sub> (0,4% v/v)	33 +/-3
	Y = OA <sub>3</sub> (0,6% v/v)	35 +/-3

Firstly, fluorescence studies were done and revealed that the emission spectra do not change by adding more OA in M:N:OA, compared with M:3 luminescent films (annexe 3). Also, adding OA to the molecule 3 does not increase the PLQY (10 +/- 1 %). In Table 3, it is observed that the amount of OA added in M:N:OA also does not affect the PLQY of the luminescent layers and is about (35 +/- 3%), namely three times higher than that of M:3 or M:N films. In the same way, the increasing quantity of OA in M:N:OA does not change significantly the surface morphology (Figure 8). The study is completed in the following part by comparing the performances of several LED devices.

#### 4) LED devices using N incorporated in the matrix M as electroluminescent layers

LED performances are investigated in this part by electroluminescence spectra giving maximum radiance peak used to record intensity-voltage-luminance (JVL) curves. As proven before, M:N material cannot be used in LED device due to its high surface roughness. Preliminary devices were done with M:N electroluminescent layer but the devices presented high statistics of short-circuits and, when device was efficient, some non-homogeneous surface luminescence were observed. This is characteristic of bad performances and not associated to normal LED behavior. In contrast, the OA treatment in M:N solution leads to very reproducible and homogeneous emission of LEDs, as 100% of the devices were usually obtained and measurable. Devices were done using the following architecture: ITO / PEDOT:PSS (coated hole transport layer) / Electroluminescent layer / evaporated BCP (hole blocking layer) / evaporated Alq<sub>3</sub> (electron transport layer) / Lithium Fluoride / Aluminium. The stack is represented by the following figure 12a.

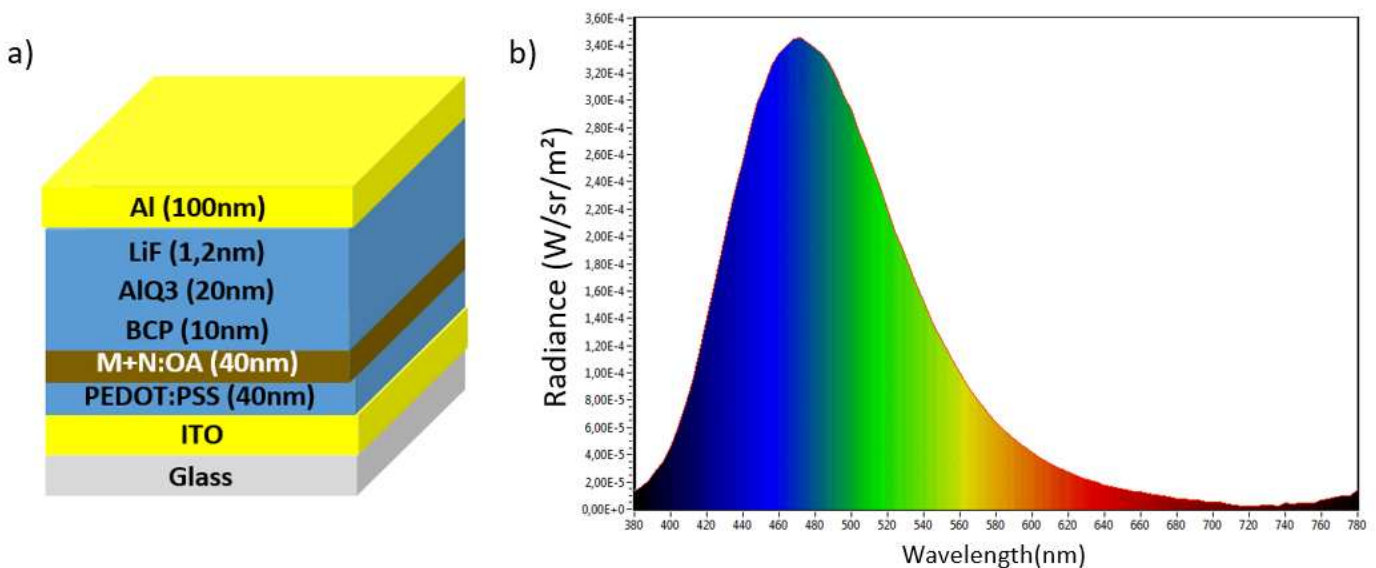


Figure 12 : a) Architecture of the studied LED devices, with yellow : electrodes, grey :substrate ;blue :interfacial transport / blocking layers ;brown :electroluminescent hybrid layer c) Radiance spectrum of LEDs containing M (PVK:OXD) as the active layer, recorded at 50 mA/cm<sup>2</sup>.

i) Impact of the OXD in M:

The first investigations were lead using pure PVK and PVK:OXD (M) as reference electroluminescent layers, at a concentration of 12:0 and 12:6 (mass ratio PVK:OXD = 2:1) mg/mL respectively, corresponding to a thickness of 50 +/- 5 nm. As described in literature and by the radiance spectrum of the figure 12b, M shows quite low performances and is reported as blue OLED. The PVK:OXD is an ambipolar electroluminescent film used for first generation OLED [37–40], and with the LED architecture of Figure 12a, it presented an EQE = 0.18%, a luminance efficiency of 0.28 cd/A and 0.12 lm/W for the power efficiency. These performances, which are quite low, are summarized by the following Table 4, annexe 4 and the figure 12b showing the radiance spectrum of M recorded at 50 mA/cm<sup>2</sup>.

Table 4 : reference LED performances, namely of the PVK and PVK:OXD (M)

PVK:OXD (mg/mL)	12:0	12:6
Threshold voltage (V)	4	4
EQE (%)	0,1	0,18
Power efficiency (lm/W)	0,05	0,12
Luminance efficiency (cd/A)	0,13	0,28

The performances of the host matrix confirm that the OXD is required to obtain efficient ambipolar film and to assure the transport properties of the luminescent layer. Indeed, without OXD in the PVK, the EQE (0.1%), the power efficiency (0.05 lm/W) and the luminance efficiency (0.13 cd/A) are approximately two times lower than with the presence of OXD (EQE = 0.18%).

ii) Effect of the electroluminescent layer thickness:

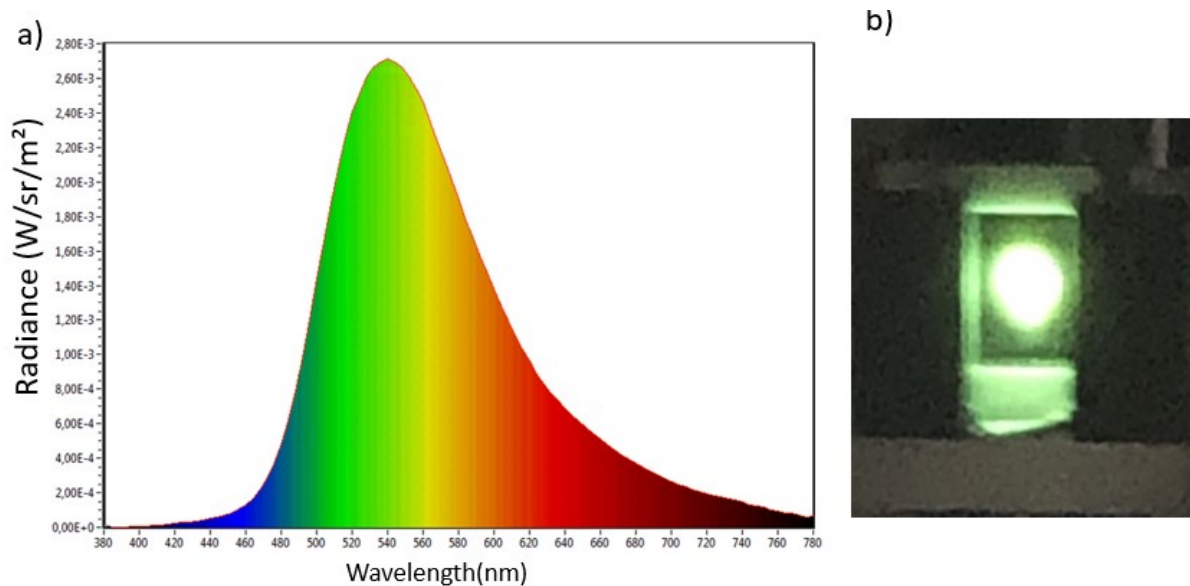


Figure 13: a) Radiance spectrum of LEDs containing molecule 3 in the active layer, recorded at 50 mA/cm<sup>2</sup>. b) Picture of LED device using M:N<sub>10</sub>:OA 50 nm thick as electroluminescent layer, recorded at 50 mA/cm<sup>2</sup>

All the LEDs done with molecule 3 in the matrix M present a main emission peak at 535 nm and a very similar radiance spectrum (figures 13 a/b). This is addressed to the emission of the 3 / ZnO:3 / ZnO:3:OA materials. In addition, it is well known in literature that the thickness of the organic electroluminescent layer has a big impact on the threshold voltage of the device. This parameter is studied for M:N<sub>10</sub>:OA with mass ratio of PVK:OXD = 2:1 in the Table 5.

Table 5 : Thickness of the electroluminescent layer M:N<sub>10</sub>:OA and associated device performances. Thicknesses measured via profilometry measurement with error +/- 5 nm

ACTIVE LAYER THICKNESS(+/-5nm)	100nm	65nm	<b>50nm</b>	40nm
Threshold voltage (V)	9	6	<b>4</b>	4,5
EQE (%)	0,38	0,34	<b>0,71</b>	0,72
Power efficiency (lm/W)	0,11	0,27	<b>0,82</b>	0,77
Luminance efficiency (cd/A)	0,67	1,32	<b>1,84</b>	2,05

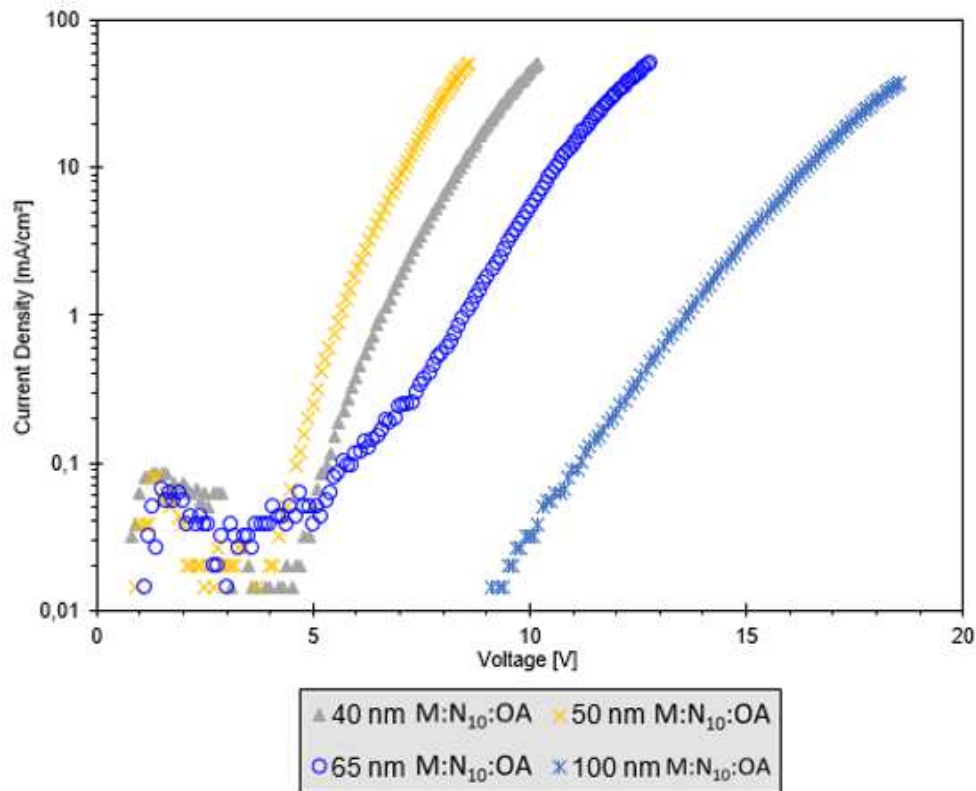


Figure 14 : JV curves of the devices presented in the table 5

The Table 5 and Figure 14 show that the thinner is the active layer is and the smaller is the threshold voltage of the device. For this electroluminescent system, the best performances are obtained for the 50 nm thick layer, with an EQE close to 0.7% with associated luminance efficiency of 1.84 cd/A and 0.82 lm/W for power efficiency. These performances are honorable regarding the literature of the 1<sup>st</sup> generation of LED which present EQE < 5% for the best 1<sup>st</sup> generation OLED materials [41]. As expected [42, 43], a big drop in performances is observed for the active layers above 50 nm thickness, with EQE going from 0.7% to 0.35%. Moreover, the LED performances recorded for 40 nm thickness are quite close to the ones at 50 nm, but the devices degraded faster under high voltage and the reproducibility was medium, which may be attributed to the active layer which was too thin. Therefore, it can be concluded that for these luminescent materials, the optimal electroluminescent layer thickness is 50 +/- 5 nm. This optimal thickness is used for the next study which is focused on the ratio of PVK:OXD in the Table 6 and Figure 15.

iii) Effect of the PVK:OXD ratio:

By keeping the electroluminescent layer at 50 nm thick, the impact of PVK:OXD ratio composing M as ambipolar polymer host matrix has been also studied on LED devices, as shown by the Figure 15 and the associated Table 6. Different ratio of PVK:OXD were tried namely 4:1 / 2:1 / 1.5:1, respectively 12:3 ; 12:6 ; 12:9 mg/mL, and reveal that the best ratio is PVK:OXD = 2:1. Indeed, as shown by Table 6, changing the ratio PVK:OXD can drastically decrease the performances, namely, the EQE dropped by half when adding twice more, or twice less (from 0.71 to 0.5%) OXD with the 12 mg/mL PVK. The threshold voltage is also higher (5,5 to 6V) when increasing or decreasing the optimal 2 :1 ratio (4V) of the matrix M.

Table 6 : PVK:OXD ratio of the electroluminescent layer M:N<sub>10</sub>:OA and associated device performances.

Ratio PVK:OXD (mg/mL)	12:9 (1,5:1)	<b>12:6 (2:1)</b>	12:3 (4:1)
Threshold voltage (V)	6	<b>4</b>	5,5
EQE (%)	0,5	<b>0,71</b>	0,5
Power efficiency (lm/W)	0,38	<b>0,82</b>	0,48
Luminance efficiency (cd/A)	1,42	<b>1,84</b>	1,62

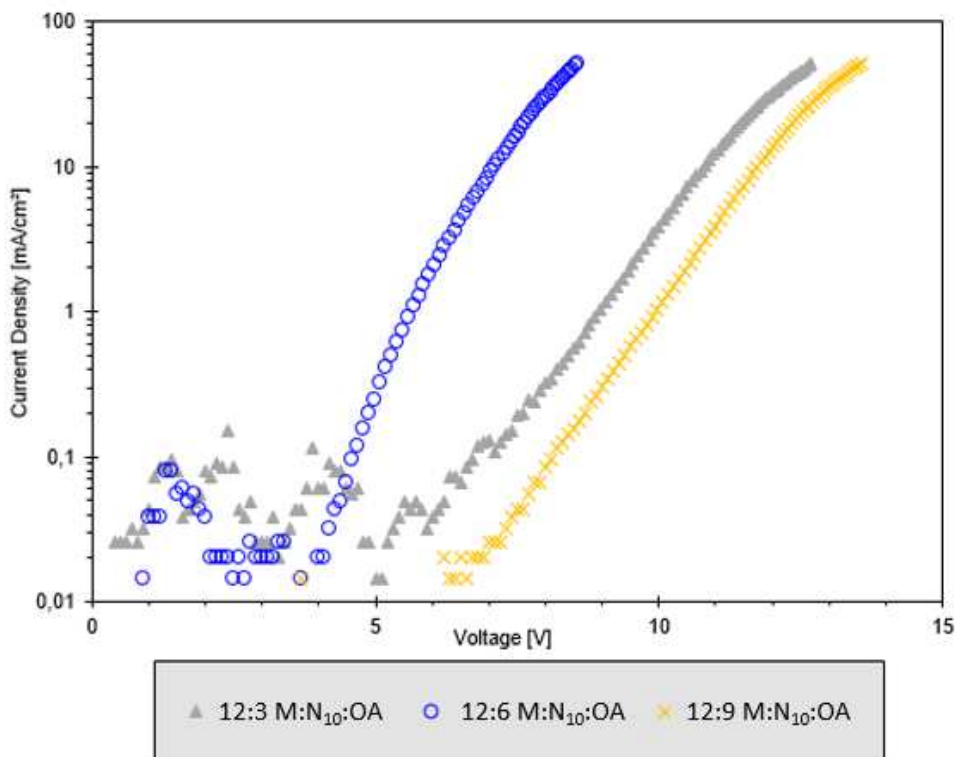


Figure 15 : JV curves of the devices presented in the table 6

iv) Effect of the amount (X%) of incorporated nano hybrids  $N_x$  in the matrix M:

Another important parameter is the amount of nano hybrids in the matrix M which has been investigated across the Table 7 showing the performances of the devices. These devices were realized according to the previous optimized parameters (50 nm thick electroluminescent layer and mass ratio 2:1 = PVK:OXD). Firstly, 0% is the reference M as neat electroluminescent layer. The obtained results are summarized by the figure 16 and table 7.

Table 7 : % N OA incorporated to M, with 50 nm thickness, associated device performances.

X% in M: $N_x$ :OA	20%	15%	<b>10%</b>	5%	0%(ref)
Threshold voltage (V)	9	8	<b>4</b>	6	4
EQE (%)	0,34	0,58	<b>0,71</b>	0,71	0,18
Power efficiency (lm/W)	0,24	0,36	<b>0,82</b>	0,66	0,12
Luminance efficiency (cd/A)	1,20	1,81	<b>1,84</b>	2,00	0,28

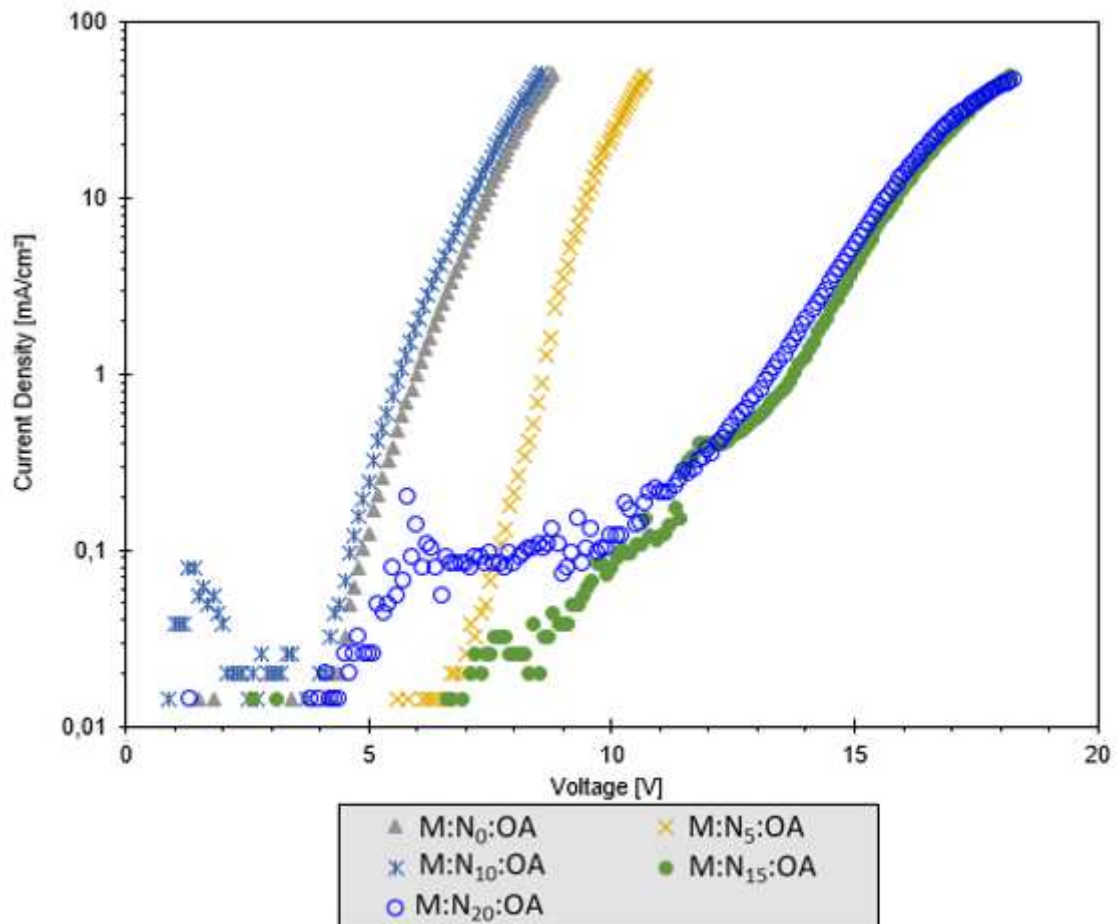


Figure 16 : JV curves of the devices presented in the table 7

By adding more than 10% nanohybrids N in the matrix M, the threshold voltage consequently increases from 4V ( $N_{10}$ ) to more than 9V ( $N_{20}$ ), but not necessarily the luminescence as shown in the Table 7. It was found that the optimal amount is 10% of nanohybrids N in M, while adding 15% or 20% lead to important drop in EQE, from 0.71% to 0.58% or 0.34%, respectively. Also, the luminance efficiency is affected, namely from 1.84 cd/A for  $N_{10}$  to 1.20 cd/A for  $N_{20}$ . The same decrease is observed regarding the power efficiency, which goes from 0.82 lm/W for  $N_{10}$  down to 0.24 lm/W for  $N_{20}$ . This is explained by the aggregation phenomenon of the nanohybrids which is more intense for  $N_{20}$  than  $N_{10}$ , as it was proved by TEM that adding more than 10% N in the matrix M leads to poor surface morphology. However, adding less than 10% of nanohybrids N induces also a detrimental shift in threshold voltage but not in power or luminance efficiencies. Indeed, the threshold voltage goes from 4V (M: $N_{10}$ :OA and M) to 6V (M: $N_5$ :OA), while the EQE of M: $N_5$ :OA remains the same than the LED done with M: $N_{10}$ :OA as electroluminescent layer. The next parameter studied is the concentration of OA in M:N:OA, by keeping N = 10%, and an electroluminescent film thickness about 50 nm, with a mass ratio of PVK:OXD = 2:1.

#### v) Effect of OA (Y) concentration in M: $N_{10}$ :OA<sub>Y</sub>:

In the previous parts, it was clearly established that the OA treatment is highly recommended in M:N electroluminescent material in order to obtain smooth and reproducible LED devices. The impact of the concentration of OA in M:N:OA is studied with Table 8 and Figure 17. This study reveals that increasing the OA concentration provokes small decreases in performances. Nevertheless, upon increasing OA amount, the threshold voltage is shifted from 4V to 7V, the EQE from 0.71% to 0.34% and the luminance efficiency from 1.84 cd/A to 1.32 cd/A. The biggest loss concerns power efficiency, dropping from 0.82 lm/W to 0.27 lm/W. These performance losses are understandable as far as OA is known to be a fatty acid, behaving as an insulating material. In another hand, reducing the OA concentration in the active layer does not affect much the EQE, luminance, neither the power efficiencies, but it induces a clear degradation of the electroluminescent layer morphology, lowering the possibilities to get homogeneous and reproducible performances.

Table 8 : OA concentration in M:N<sub>10</sub>:OA<sub>γ</sub> and the associated LED performances.

OA concentration (%) in M:N:OA <sub>γ</sub>	OA <sub>3</sub> (0,6% v/v)	OA <sub>2</sub> (0,4% v/v)	<b>OA (0,2% v/v)</b>	OA <sub>0,5</sub> (0,1% v/v)	OA <sub>0,25</sub> (0,05% v/v)
Threshold voltage (V)	7	6	<b>4</b>	6	6
EQE (%)	0,34	0,65	<b>0,71</b>	0,66	0,58
Power efficiency (lm/W)	0,27	0,61	<b>0,82</b>	0,56	0,36
Luminance efficiency (cd/A)	1,32	1,91	<b>1,84</b>	1,98	1,81

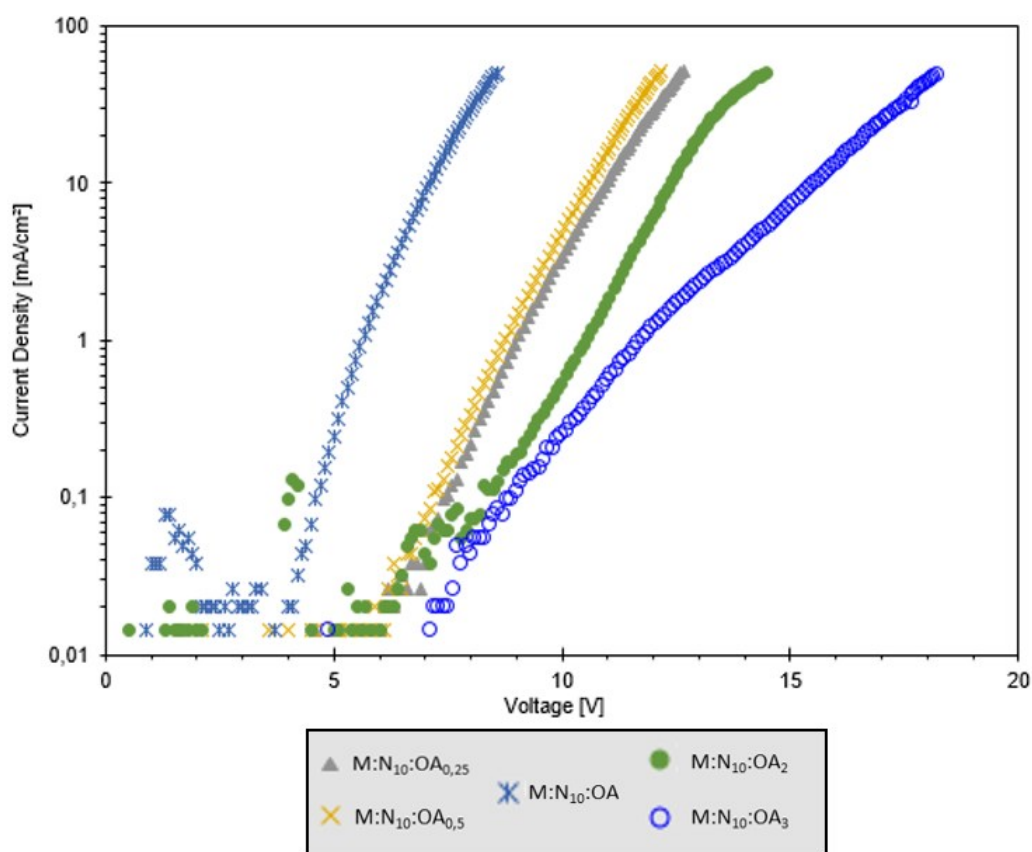


Figure 17 : JV curves of the devices presented in the table 8

In the end, for this device architecture presented in the figure 12a, the better optimized parameters are:

- Mass ratio PVK:OXD = 2:1
- Electroluminescent film thickness about 50 nm
- 10% N incorporated in the matrix M
- Concentration of OA in M:N:OA = 0.2% v/v

The JVL curve of this optimized system is presented by the figure 18, where the threshold voltage is noted at 4V, as demonstrated before, and the maximum luminance value is recorded at 10V, corresponding to 1000 cd/m<sup>2</sup>.

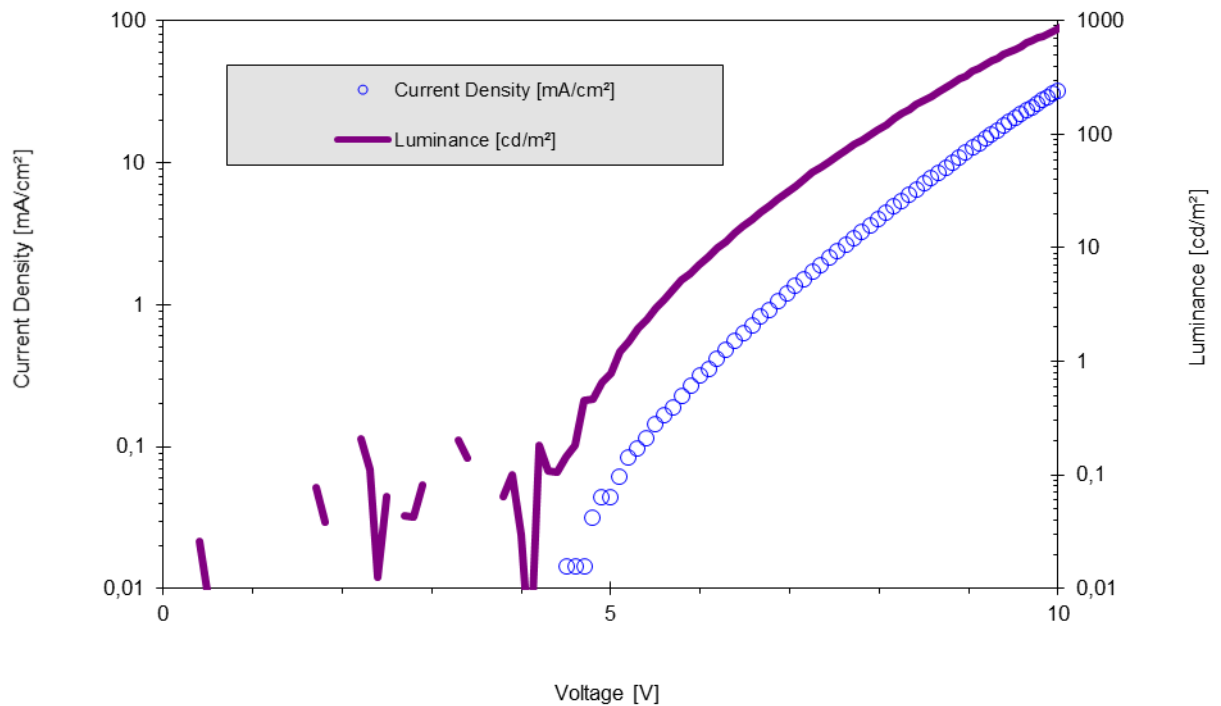


Figure 18: JVL curve of the LED containing M:N<sub>10</sub>:OA 50nm thick as electroluminescent layer

vi) Full solution approach to build LED:

Based on the previous optimizations done, full solution processed LED devices were tried in Marseille, and gave the same electrical behavior and characteristics than the ones done in Palaiseau with evaporated interfacial layers. All the investigations were done with ZnO nanoparticles grafted with EtNH (ethanolamine) ligand, such a material playing the role of electron transport layer instead of the evaporated BCP / Alq<sub>3</sub> / LiF [44]. The stacking is represented in the figure 19, with a working LED containing M:N<sub>10</sub>:OA 50 nm thick, as electroluminescent material.

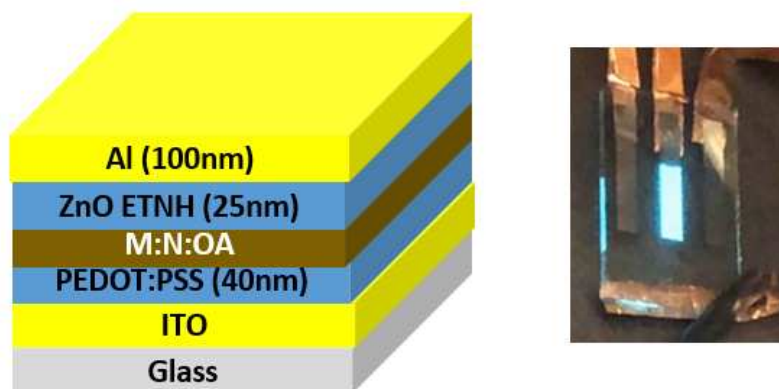


Figure 19: left: stacking of the full solution processed LED; right: full solution processed LED using M:N<sub>10</sub>:OA recorded at 50 mA/cm<sup>2</sup>.

Some other references such as M, M:ZnO and M:ZnO:OA with 100 nm active layer thickness are presented in annexe 5, which gave blue LEDs with relatively low intensity of luminance. As expected, the M:ZnO presents worst performances than M:ZnO:OA because of the high amount of aggregated ZnO in the layer based on M:ZnO, thus bringing bad surface morphology and electrical issues.

For the LED containing the compound 3 or the hybrids N, with the matrix M, a bluish-green emission is still noted, namely a maximum emission peak at 530 nm which corresponds to the maximum emission peak of the molecule 3, as well as a low threshold voltage below 5V for the optimal thickness (50 nm). The reproducibility of the full solution processed LEDs is very high (90%), thus proving that a large scale manufacturing is possible, for instance with ink jet printing. On the same way, the stability under air of non-encapsulated LEDs was investigated over a week, and the statistics were very similar (+/- 1V variation) (Figure 20). These last results show quite stable LEDs after 1 week under air with similar emission and electrical behaviors. Certainly, the stability has to be investigated further for longer durations.

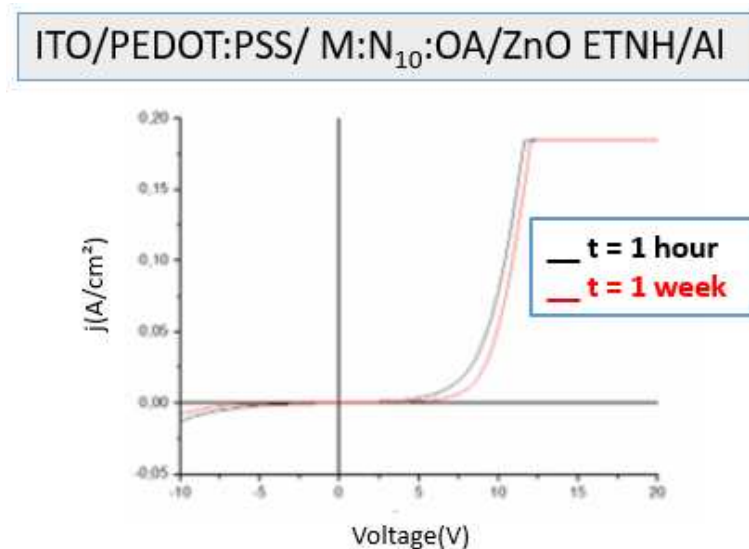


Figure 20: stability after 1 week under air of the non-encapsulated ITO/PEDOT:PSS/M:N<sub>10</sub>:OA/ZnO ETNH/Al LEDs.

## 5) Conclusions of PVK:OXD used as host embedding nanohybrids as guests

In conclusion, nanohybrids in solution were well combined with PVK:OXD host matrix allowing to obtain reproducible LED devices. Indeed, the use of the matrix M increases the transport properties of the emissive nanohybrids, without changing the PLQY, neither significantly altering the optical properties of the pure nanohybrids N. On another hand, the nanohybrids in the matrix still need the OA treatment, in order to increase the PLQY, to avoid cluster formations and electrical issues in the working devices. Many parameters were studied to optimize the LED performances, namely:

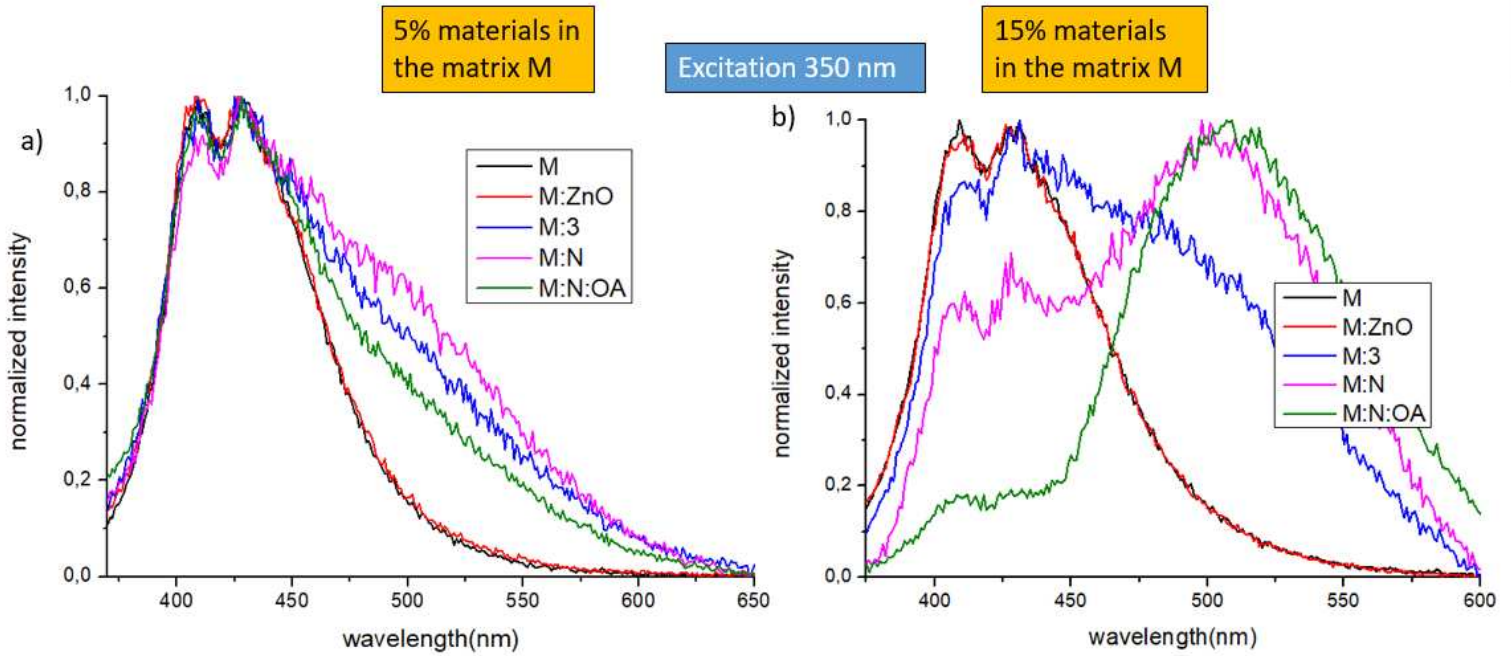
- The thickness of the electroluminescent layer, the best being close to 50 nm
- The ambipolar property of the matrix M, by changing the ratio of PVK to OXD, the best being 2 :1
- The concentration of the nanohybrids incorporated in the matrix, in optical performances and morphology the most convenient being 10%
- The quantity of OA with the nanohybrids, which helps to obtain smooth and reproducible layer, the best performances being obtained for OA = 0,2% v/v
- The devices with full solution approach were obtained and worked close to the devices done in LPICM with evaporated BCP / Alq<sub>3</sub> / LiF interfacial layers, thus, proving that a large scale manufacturing is conceivable.

To sum up, honorable reproducible performances were obtained with this device architecture, with an  $EQE_{\max}$  of 0.71%, but also with a working tension of 4V which is comparable with the literature value for other technologies as OLED or QLED.

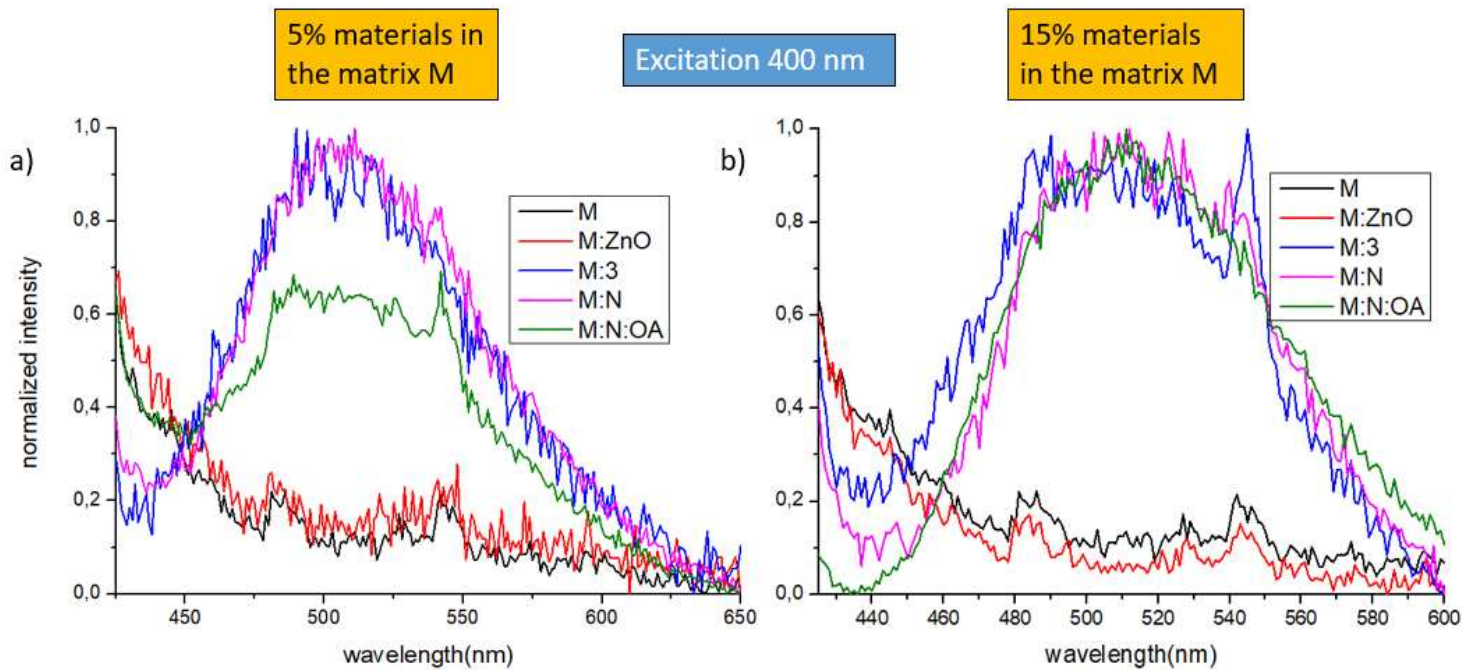
Now that a solid protocol to build reproducible LEDs has been developed, more performant graftable emitters will be investigated in the following chapter. Indeed, the objective of the ANR project was to obtain multi-colored LEDs, namely to achieve blue, green and red LEDs in the perspective to build a white LED by co-grafting of different graftable emitters on the nanoparticle surface. Therefore, the next part is focused on the building and the studies of the optical and morphological properties of new green, blue and red nanohybrids in solution and in thin films.

## ANNEXES:

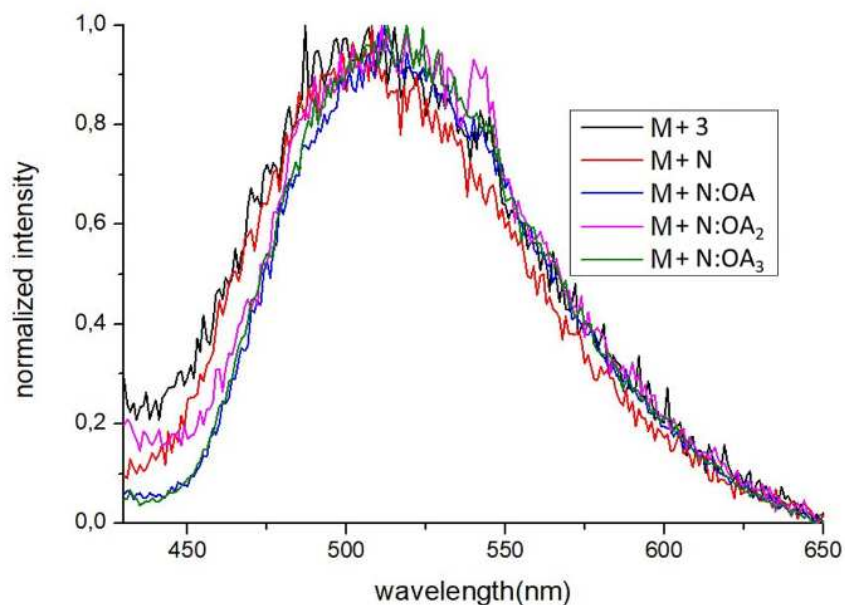
1 : Fluorescence spectra excited at 350 nm with N = 5% (a) ; 15% (b)



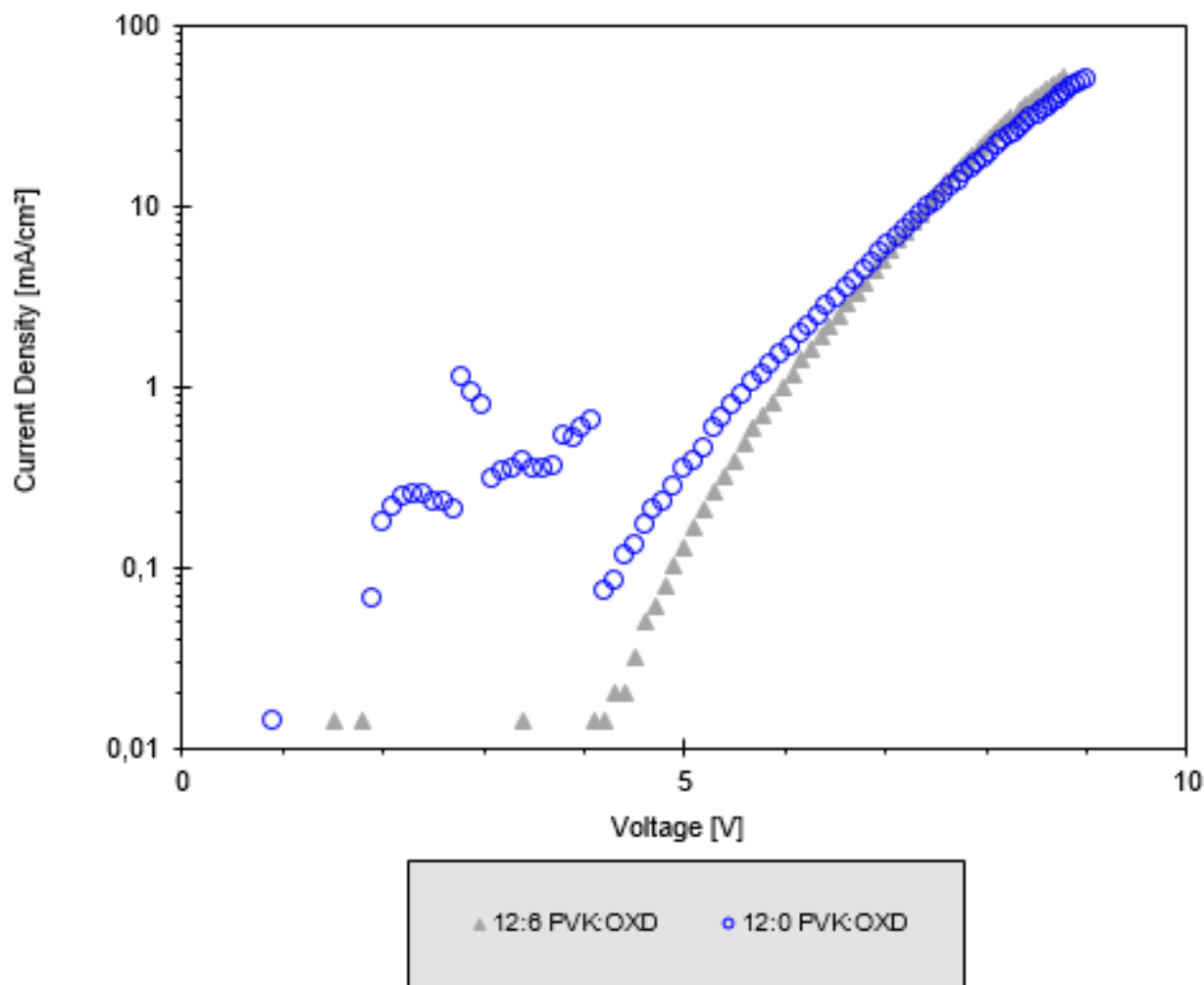
2 : Fluorescence spectra excited at 400 nm with N = 5% (a) ; 15% (b)



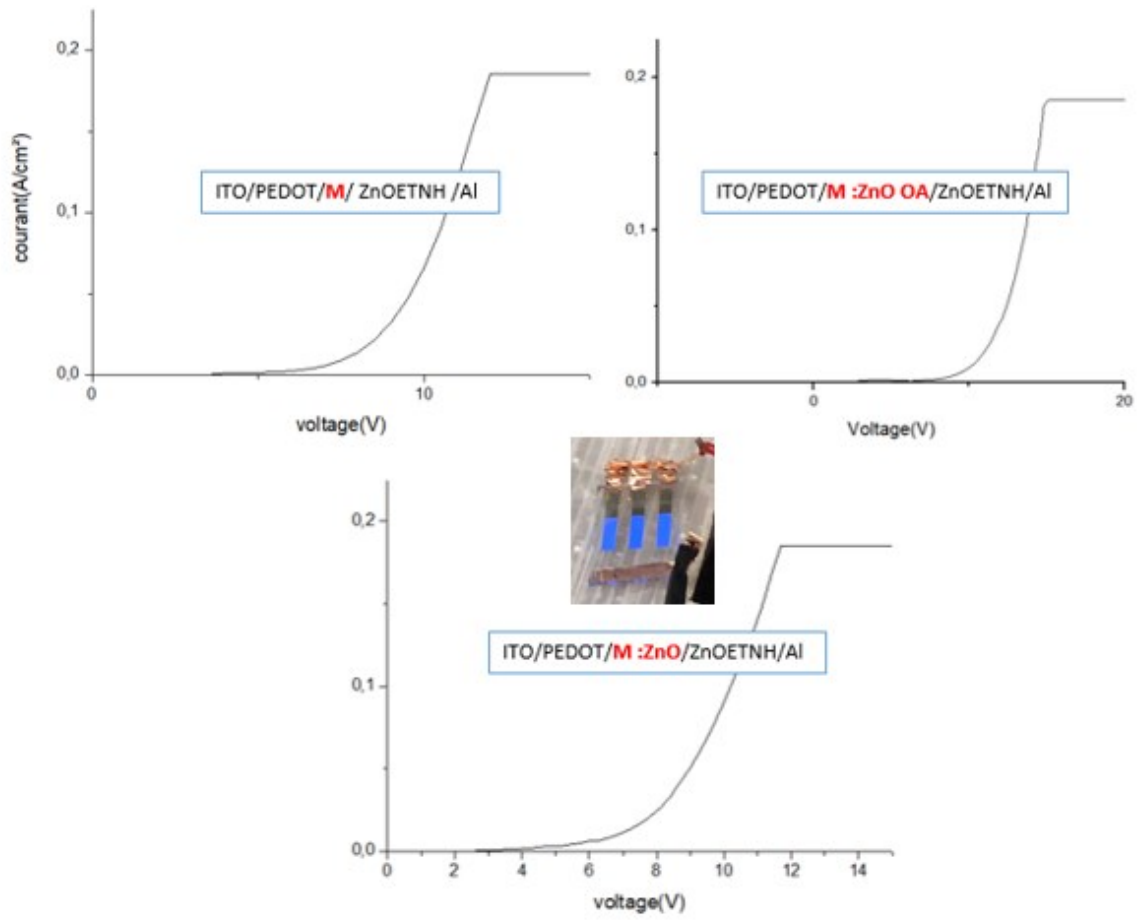
3 : Fluorescence spectra excited at 400 nm with 10% of luminescent materials in the matrix M



4 : JV curves of the reference LEDs associated to Table 4



5 : Reference solution processed LEDs represented by JV curves, compliance level at 0.18 A/cm<sup>2</sup>



## Bibliography:

- [1] Yang Zou & al. Design Strategy for Solution-Processable Thermally Activated Delayed Fluorescence Emitters and Their Applications in Organic Light-Emitting Diodes - 2018 - Advanced Optical Materials. [accessed 2022 Jan 14]. <https://onlinelibrary.wiley.com/doi/abs/10.1002/adom.201800568>
- [2] Sae Youn Lee. Thermally Activated Delayed Fluorescence Polymers for Efficient Solution-Processed Organic Light-Emitting Diodes - 2016 - Advanced Materials. [accessed 2022 Jan 14]. <https://onlinelibrary.wiley.com/doi/abs/10.1002/adma.201505026>
- [3] Kim HJ, Lee C, Godumala M, Choi S, Park SY, Cho MJ, Park S, Choi DH. Solution-processed thermally activated delayed fluorescence organic light-emitting diodes using a new polymeric emitter containing non-conjugated cyclohexane units. *Polymer Chemistry*. 2018;9(11):1318–1326. doi:10.1039/C7PY02113E
- [4] Bao W, Li M, Yang Y, Wan Y, Wang X, Bi N, Li C. Advancements and Frontiers in the High Performance of Natural Hydrogels for Cartilage Tissue Engineering. *Frontiers in Chemistry*. 2020 [accessed 2022 Jan 14];8. <https://www.frontiersin.org/article/10.3389/fchem.2020.00053>
- [5] Wang Y, Zhu Y, Xie G, Zhan H, Yang C, Cheng Y. Bright white electroluminescence from a single polymer containing a thermally activated delayed fluorescence unit and a solution-processed orange OLED approaching 20% external quantum efficiency. *Journal of Materials Chemistry C*. 2017;5(41):10715–10720. doi:10.1039/C7TC03769D
- [6] Wada Y, Kubo S, Kaji H. Adamantyl Substitution Strategy for Realizing Solution-Processable Thermally Stable Deep-Blue Thermally Activated Delayed Fluorescence Materials. *Advanced Materials*. 2018;30(8):1705641. doi:10.1002/adma.201705641
- [7] Guo J, Li X-L, Nie H, Luo W, Gan S, Hu S, Hu R, Qin A, Zhao Z, Su S-J, et al. Achieving High-Performance Nondoped OLEDs with Extremely Small Efficiency Roll-Off by Combining Aggregation-Induced Emission and Thermally Activated Delayed Fluorescence. *Advanced Functional Materials*. 2017;27(13):1606458. doi:10.1002/adfm.201606458
- [8] Yang Z, Mao Z, Xie Z, Zhang Y, Liu S, Zhao J, Xu J, Chi Z, Aldred MP. Recent advances in organic thermally activated delayed fluorescence materials. *Chemical Society Reviews*. 2017;46(3):915–1016. doi:10.1039/C6CS00368K
- [9] Chatterjee T, Wong K-T. Perspective on Host Materials for Thermally Activated Delayed Fluorescence Organic Light Emitting Diodes. *Advanced Optical Materials*. 2019;7(1):1800565. doi:10.1002/adom.201800565
- [10] Jian-Ru Gong & al. Direct Evidence of Molecular Aggregation and Degradation Mechanism of Organic Light-Emitting Diodes under Joule Heating: an STM and Photoluminescence Study | *The Journal of Physical Chemistry B* 2005, 109, 5, 1675–1682 <https://doi.org/10.1021/jp046509o>. [accessed 2022 Jan 14].
- [11] Ja Yeon Lee, Jaeseung Kim, Hyunjung Kim\*, and Min Chul Suh\*. Molecular Stacking Effect on Small-Molecular Organic Light-Emitting Diodes Prepared with Solution Process | *ACS Applied Materials & Interfaces* 2020, 12, 20, 23244–23251 <https://doi.org/10.1021/acsami.0c06597>. [accessed 2022 Jan 14]. <https://pubs.acs.org/doi/abs/10.1021/acsami.0c06597>

- [12] Liu D, Zhang M, Chen H, Ma D, Tian W, Sun K, Jiang W, Sun Y. Constructing host- $\sigma$ -guest structures to optimize the efficiency of non-doped solution-processed OLEDs. *Journal of Materials Chemistry C*. 2021;9(4):1221–1227. doi:10.1039/D0TC04959J
- [13] Paloma L. dos Santos & al. Using Guest–Host Interactions To Optimize the Efficiency of TADF OLEDs | *The Journal of Physical Chemistry Letters* 2016, 7, 17, 3341–3346 <https://doi.org/10.102/acs.jpcclett.6b01542>. [accessed 2022 Jan 14].
- [14] Takuji Hatakeyama & al. Ultrapure Blue Thermally Activated Delayed Fluorescence Molecules: Efficient HOMO–LUMO Separation by the Multiple Resonance Effect - 2016 - *Advanced Materials*. [accessed 2022 Jan 14]. <https://doi.org/10.1002/adma.201505491>
- [15] Yuan-Chieh Yeh & al. Nano-Based Drug Delivery or Targeting to Eradicate Bacteria for Infection Mitigation: A Review of Recent Advances | *Frontiers Chemistry*. [accessed 2022 Jan 14]. [doi.org/10.3389/fchem.2020.00286](https://doi.org/10.3389/fchem.2020.00286)
- [16] Xingdong Wang. Through-space charge transfer hexaarylbenzene dendrimers with thermally activated delayed fluorescence and aggregation-induced emission for efficient ... - *Chemical Science* (RSC Publishing) DOI:10.1039/C8SC04991B. [accessed 2022 Jan 14].
- [17] J.Phelipot & al. Highly Emissive Layers based on Organic/Inorganic Nanohybrids Using Aggregation Induced Emission Effect - 2022 - *Advanced Materials Technologies* -. [accessed 2022 Jan 14]. <https://onlinelibrary.wiley.com/doi/abs/10.1002/admt.202100876>
- [18] Ramos G, Belenguer T, Levy D. A Highly Photoconductive Poly(vinylcarbazole)/2,4,7-Trinitro-9-fluorenone Sol–Gel Material that Follows a Classical Charge-Generation Model. *The journal of physical chemistry. B*. 2007;110:24780–5. doi:10.1021/jp0629184
- [19] Shi Y-L, Liang F, Hu Y, Wang X-D, Wang Z-K, Liao L-S. High-efficiency quantum dot light-emitting diodes employing lithium salt doped poly(9-vinlycarbazole) as a hole-transporting layer. *Journal of Materials Chemistry C*. 2017;5(22):5372–5377. doi:10.1039/C7TC00449D
- [20] Geffroy C, Grana E, Mumtaz M, Cojocar L, Cloutet E, Olivier C, Uchida S, Toupance T, Segawa H, Hadziioannou G. Post-functionalization of polyvinylcarbazoles: An open route towards hole transporting materials for perovskite solar cells. *Solar Energy*. 2019;193:878–884. doi:10.1016/j.solener.2019.10.034
- [21] Paik KL, Baek NS, Kim HK, Lee J-H, Lee Y. White Light-Emitting Diodes from Novel Silicon-Based Copolymers Containing Both Electron-Transport Oxadiazole and Hole-Transport Carbazole Moieties in the Main Chain. *Macromolecules*. 2002;35(18):6782–6791. doi:10.1021/ma020406r
- [22] Bettenhausen J, Strohriegl P, Brütting W, Tokuhisa H, Tsutsui T. Electron transport in a starburst oxadiazole. *Journal of Applied Physics*. 1997;82(10):4957–4961. doi:10.1063/1.366396
- [23] Zacharias P, Gather MC, Rojahn M, Nuyken O, Meerholz K. New Crosslinkable Hole Conductors for Blue-Phosphorescent Organic Light-Emitting Diodes. *Angewandte Chemie International Edition*. 2007;46(23):4388–4392. doi:10.1002/anie.200605055
- [24] Jiang W, Ban X, Ye M, Sun Y, Duan L, Qiu Y. A high triplet energy small molecule based thermally cross-linkable hole-transporting material for solution-processed multilayer blue electrophosphorescent devices. *Journal of Materials Chemistry C*. 2014;3(2):243–246. doi:10.1039/C4TC02485K

- [25] Wu HB, Zou JH, Liu F, Wang L, Mikhailovsky A, Bazan GC, Yang W, Cao Y. Efficient Single Active Layer Electrophosphorescent White Polymer Light-Emitting Diodes. *Advanced Materials*. 2008;20(4):696–702. doi:10.1002/adma.200701329
- [26] Strassert CA, Chien C-H, Galvez Lopez MD, Kourkoulos D, Hertel D, Meerholz K, De Cola L. Switching On Luminescence by the Self-Assembly of a Platinum(II) Complex into Gelating Nanofibers and Electroluminescent Films. *Angewandte Chemie International Edition*. 2011;50(4):946–950. doi:10.1002/anie.201003818
- [27] Yang X, Müller DC, Neher D, Meerholz K. Highly Efficient Polymeric Electrophosphorescent Diodes. *Advanced Materials*. 2006;18(7):948–954. doi:10.1002/adma.200501867
- [28] Wu H, Zhou G, Zou J, Ho C-L, Wong W-Y, Yang W, Peng J, Cao Y. Efficient Polymer White-Light-Emitting Devices for Solid-State Lighting. *Advanced Materials*. 2009;21(41):4181–4184. doi:10.1002/adma.200900638
- [29] Michler GH. *Electron Microscopy of Polymers*. Springer Science & Business Media; 2008.
- [30] Dmitri V. Talapin\*†‡, Jong-Soo Lee†, Maksym V. Kovalenko†, and Elena V. Shevchenko‡. Prospects of Colloidal Nanocrystals for Electronic and Optoelectronic Applications | *Chemical Reviews* 2010, 110, 1, 389–458 <https://doi.org/10.1021/cr900137k>. [accessed 2022 Jan 14].
- [31] Aleshin AN, Sokolovskaya AD, Shcherbakov IP, Brunkov PN, Ulin VP. Organic light-emitting diodes based on polyvinylcarbazole films doped with polymer nanoparticles. *Physics of the Solid State*. 2013;55(3):675–680. doi:10.1134/S1063783413030037
- [32] Gupta BK, Kedawat G, Kumar P, Rafiee MA, Tyagi P, Srivastava R, Ajayan PM. An n-type, new emerging luminescent polybenzodioxane polymer for application in solution-processed green emitting OLEDs. *Journal of Materials Chemistry C*. 2015;3(11):2568–2574. doi:10.1039/C4TC02581D
- [33] Bhaskar R, Lakshmanan AR, Sundarrajan M, Ravishankar T, Jose MT, Lakshminarayan N. Mechanism of green luminescence in ZnO. *IJPAP Vol.47(11)* [November 2009]. 2009 Nov [accessed 2022 Jan 12]. <http://nopr.niscair.res.in/handle/123456789/6193>
- [34] Ying-Song Fu, Xi-Wen Du, Sergei A. Kulinich, Jian-Sheng Qiu, Wen-Jing Qin, Rui Li, Jing Sun, and Jim Liu. Stable Aqueous Dispersion of ZnO Quantum Dots with Strong Blue Emission via Simple Solution Route | *Journal of the American Chemical Society*. [accessed 2022 Jan 14]. <https://pubs.acs.org/doi/abs/10.1021/ja075604i>
- [35] Lessard BH, Beouch L, Goubard F, Wantz G, Marić M, Gigmes D, Dumur F. Poly(2-(N-carbazolyl)ethyl acrylate) as a host for high efficiency polymer light-emitting devices. *Organic Electronics*. 2015;17:377–385. doi:10.1016/j.orgel.2014.12.019
- [36] Dr. John C. de Mello, Dr. H. Felix Wittmann, Prof. Richard H. Friend. An improved experimental determination of external photoluminescence quantum efficiency 1997 - *Advanced Materials*. [accessed 2022 Jan 14]. <https://doi.org/10.1002/adma.19970090308>
- [37] Liu S-W, Yuan C-H, Yeh S-J, Wu M-F, Chen C-T, Lee C-C. Efficiency enhancement of solution-processed single-layer blue-phosphorescence organic light-emitting devices having co-host materials of polymer (PVK) and small-molecule (SimCP2). *Journal of the Society for Information Display*. 2011;19(4):346–352. doi:10.1889/JSID19.4.346

- [38] Lee C-C, Yuan C-H, Liu S-W, Liu L-A, Chen Y-S. Solution-Processed Electrophosphorescent Devices Based on Small-Molecule Mixed Hosts. *Journal of Display Technology*. 2011;7(12):636–639. doi:10.1109/JDT.2011.2160041
- [39] Liu J, Li L, Gong C, Yu Z, Pei Q. An ambipolar poly(meta-phenylene) copolymer with high triplet energy to host blue and green electrophosphorescence. *Journal of Materials Chemistry*. 2011;21(26):9772–9777. doi:10.1039/C1JM11212K
- [40] Fanghui Z, Dan Y, Xiufeng W. Luminescence mechanism of polymer light-emitting devices with MEH-PPV: PVK emitting layer. In: *Proceedings of the 2008 International Conference on Advanced Infocomm Technology*. New York, NY, USA: Association for Computing Machinery; 2008. p. 1–4. (ICAIT '08). <https://doi.org/10.1145/1509315.1509336>. doi:10.1145/1509315.1509336
- [41] Hong G, Gan X, Leonhardt C, Zhang Z, Seibert J, Busch JM, Bräse S. A Brief History of OLEDs—Emitter Development and Industry Milestones. *Advanced Materials*. 2021;33(9):2005630. doi:10.1002/adma.202005630
- [42] Méndez Pinzón H, Pardo-Pardo D, Cuéllar-Alvarado J, Salcedo J, Vera R, Paez-Sierra B. Analysis of the current-voltage characteristics of polymer-based organic light-emitting diodes (OLEDs) deposited by spin coating. *Universitas Scientiarum*. 2010;15:68–76.
- [43] Sharbati MT, Panahi F, Shourvarzi A, Khademi S, Emami F. Near-infrared electroluminescence from organic light emitting diode based on Imine oligomer with low turn on voltage. *Optik - International Journal for Light and Electron Optics*. 2013;124. doi:10.1016/j.ijleo.2012.01.002
- [44] Zhang Y-F, Xu Z, Zhang F-J, Wang Y, Zhao S-L. [White organic light emitting device with dyestuff DCJTB blended in polymer] PMID: 18619292. *Guang pu xue yu guang pu fen xi = Guang pu*. 2008;28(4):760–762.

# Chapter 3: Blue, green and red nano hybrids used as a tool to control the light emission in LED devices

## 1) Presentation of the new molecules (B, G, R, Y)

All the organic emitters presented in this part were synthesized by Nicolas Ledos, PhD student in the group of Pr. Muriel Hissler at Institut des Sciences Chimiques de Rennes. The choice of these molecules is related to their optical properties and to the fact that big amount (over a gram) of these materials can be synthesized. The synthesis of blue, green, and red (with harder protocol) emitters were achieved. To remind, the more we move towards red or infrared emission wavelengths, the lower the bandgap of the emitters. Therefore, it is also easier to pass the energy barrier by non-radiative relaxation (loss of energy by vibration of the molecule).

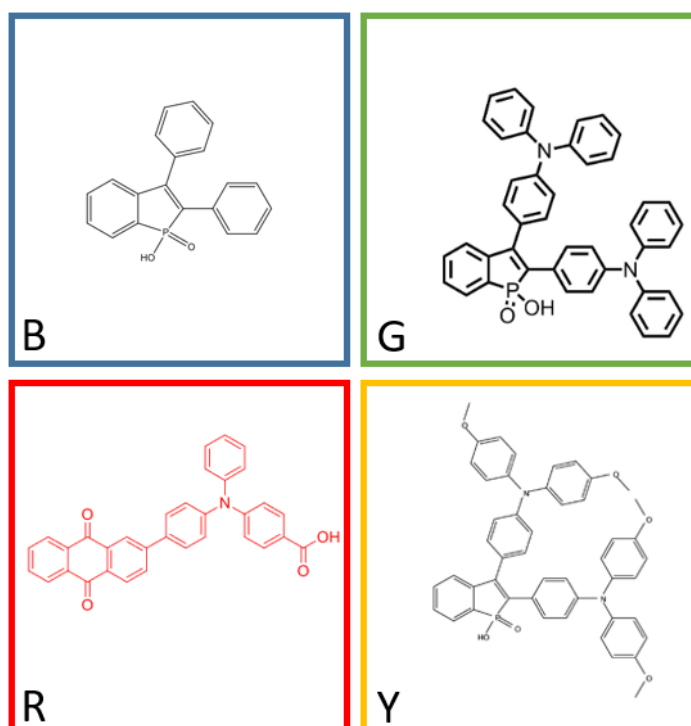


Figure 1: Structure of the new emitters, B=blue ;G=green ;R=red ;Y=yellow, in reference to their respective emission spectra.

According to the patent [1], by changing the structure of the emissive molecule, the emitted colour is also changed. The optical properties of these different emissive molecules are

presented in the figure 2. The main absorbance (in solution) and emission (in powder) peaks are listed, even though the maximum peaks can be shifted according to the used solvent:

- B: absorbance = 340 nm ; emission = 460 nm
- G: absorbance = 410 nm ; emission = 560 nm
- R: absorbance = 440 nm ; emission = 640 nm
- Y: absorbance = 425 nm ; emission = 610 nm

It is important to note that the emitter R is not really emitting in the red region, but more in the orange, however, a red-shift may be expected while grafting the COOH unit of R with ZnO surface (as discussed later in this chapter)

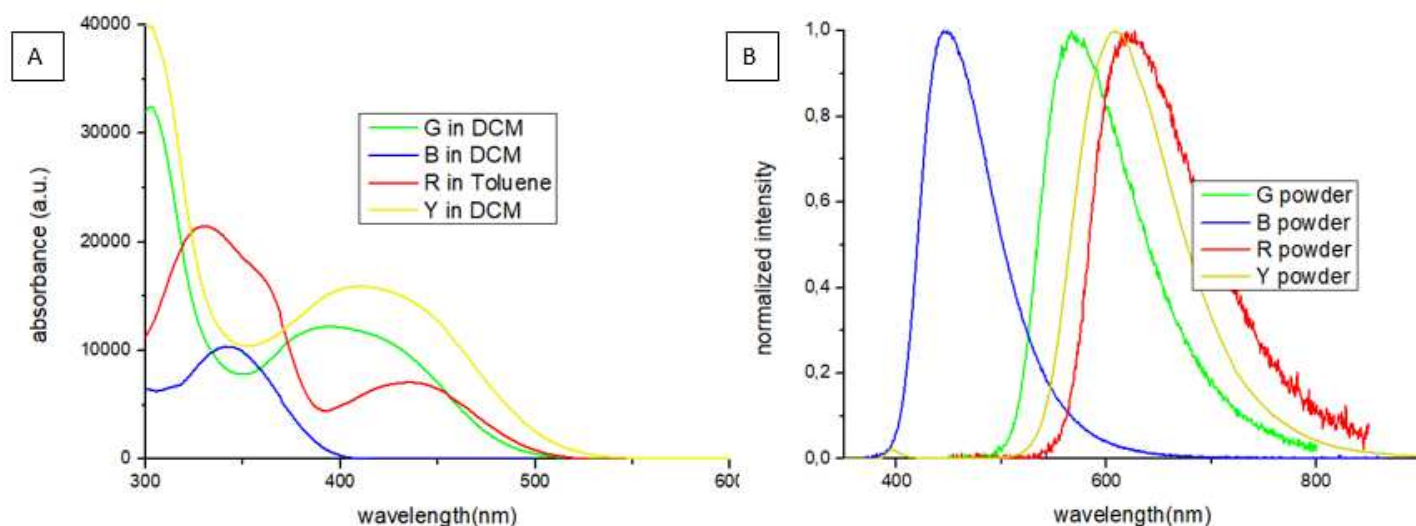


Figure 2: A) absorbance in solution (graph legend for solvents) B) emission in powder of the presented molecules from Figure 1,  $\lambda_{exB}=350\text{nm}$  ;  $\lambda_{exG}=410\text{nm}$  ;  $\lambda_{exR}=450\text{nm}$  ;  $\lambda_{exY}=420\text{nm}$ .

The same questions raised in the previous parts remain open for each new emitter, namely: is the grafting between NCs and the emissive molecule efficient? Is there an AIE effect? Are they usable as electroluminescent layer for LED device? Is OA still required to obtain reproducible surface morphology? Is the OA still increasing the PLQY of the nanohybrids? We will therefore deeply study the optical and morphological properties of the nanohybrids in the following sections.

## PLQY of the B; G ;R ;Y (graftable and non graftable) molecules :

Table 1: PLQY in powder and in solution of the B, G, R, Y, graftable and non graftable versions

PLQY (powder) %	B	G	R	Y
With Grafting Unit	82	34	3	17
W/o Grafting Unit	100	100	58	65
PLQY (solution) %	B	G	R	Y
With Grafting Unit	<1	17	44	3
W/o Grafting Unit	<1	34	* = [2]	9

The PLQY are investigated thanks to an integrative sphere and the recorded value is about 10% relative error. It is relevant to compare the behaviors between the liquid and the solid states (to know the presence of an AIE effect), and between the graftable and the non graftable versions of B, G, R and Y emitters (to know the effect of the OH vibrator). The PLQY of the non graftable version of the molecules are always higher than the graftable ones, because the stretching hydroxy grafting unit is a well-known non-radiative pathway, and it is important to quantify this effect. For the non-graftable emitters, the POOH (or COOH in the case of R) group, is replaced by deprotonated ( $\text{POO}^-$  or  $\text{COO}^-$ ), or by ester group.

First of all, the emitter B does not present PLQY at the liquid state, however, in powder, high PLQY are obtained, as the motion of the phenyl groups of the molecule is highly restricted, therefore this molecule presents a strong AIE effect. Also, the measured PLQY of the graftable B is about 82% while the non graftable one reaches 100%.

The emitter G, which is visually the shiniest molecule from the serie, has a medium PLQY in solution, over 17% for the graftable version, while the double was observed for the non graftable G, namely 34%. Nevertheless, in the solid state, these values are higher, namely, the graftable G is about 34% while the non graftable one about 100%, proving the strong AIE effect of this molecule

The emitter Y is in competition with the R, because the final objective is to combine, two or three emitters together to generate a white light, and these two emitters have close emission spectra. The Y presents very low PLQY at the liquid state, over 3% with OH grafting unit while 9% for the non graftable one. However, in solid state these values increase, namely it was recorded PLQY about 17% for graftable Y and 65% for the non graftable version, showing again, for this third hydroxyoxophosphole of the list, an AIE effect.

The emitter R is different from the other emissive molecules, because of the COOH grafting unit instead of the POOH. In solution, the PLQY value of the graftable R is about 44% which is very high (the PLQY of the non graftable version of R was not measured). However, in

powder form, the PLQY value of the graftable R is really low (3 %) in comparison with the liquid state PLQY (44 %), thus showing an ACQ effect. The non graftable R shows an interesting PLQY = 58 +/- 5 % at the solid state. More in details, it was expected that the R molecule presents TADF properties [2], and this will be discussed later in the part 4d.

In the end, it is observed that the candidates have different PLQY, and these values must be considered with precaution to build a quality white hybrid LED.

## 2) Preparation of the nanohybrids

Table 2: molar masses of the different used emitters, and corresponding masses at mol quantity constant

Emitter	3 (chapters 1&2)	B	G	R	Y
Molar mass g/mol	644,9	318,3	652,7	495,5	772,7
n (μmol)	1,55	1,55	1,55	1,55	1,55
Mass (mg)	1,0	0,5	1,0	0,8	1,2

The different structures of these new emissive molecules induce some changes in the initial preparation of the nanohybrids. The respective solutions of these emissive molecules are poorly soluble with the chlorobenzene / chloroform solvent mix, and therefore, a raise of temperature was needed to solubilize the molecules. The studied amount of emitter to graft with the ZnO NCs is calculated in coherence with the molar mass of compound 3 used in chapters 1 and 2, to be equimolar, namely a ratio (1:1) (1 mg ZnO : 1 mg 3 ; ~1 mg G ; ~0.5 mg B ; ~1.2 mg Y ; ~0.8 mg R). The pure nanohybrids (even with OA) are still unusable as electroluminescent layer for LED device because of cluster formations or weak transport properties, as it will be shown in the introduction of the section 6 in this chapter. The preparation still requires their incorporation in the host matrix M. Indeed, after the incorporation of ZnO and emissive molecule in the matrix M, the grafting quality can be increased by a stirring under 100 °C. The luminescent solution goes from turbid to clear under the influence of temperature, by breaking the cluster formations via self-assembly. However, it was generally observed that OA is still required to avoid the aggregation of the nanohybrids and further electrical problems. The OA is added once the solution is clear, and then, the luminescent M:N:OA solution can be spin-coated. The amount of OA with the nanohybrids incorporated in the matrix M was studied in the previous chapter, and the best quantity determined with the emitter 3 (i.e. OA = 0.2% v/v) will be kept constant in the following studies.

### 3) Optical properties in solution

In this part, the optical properties of the luminescent solutions containing either 10% of B ; G ; R or Y, with or without ZnO at ratio (1:1), incorporated in the host matrix M, are studied. The new nanohybrids are respectively named:  $N^B$ ;  $N^G$ ;  $N^R$ ;  $N^Y$  and, when incorporated in the matrix M, are named  $M:N^X$  with  $X = B; G; R; Y$ .

#### a) Emitter B

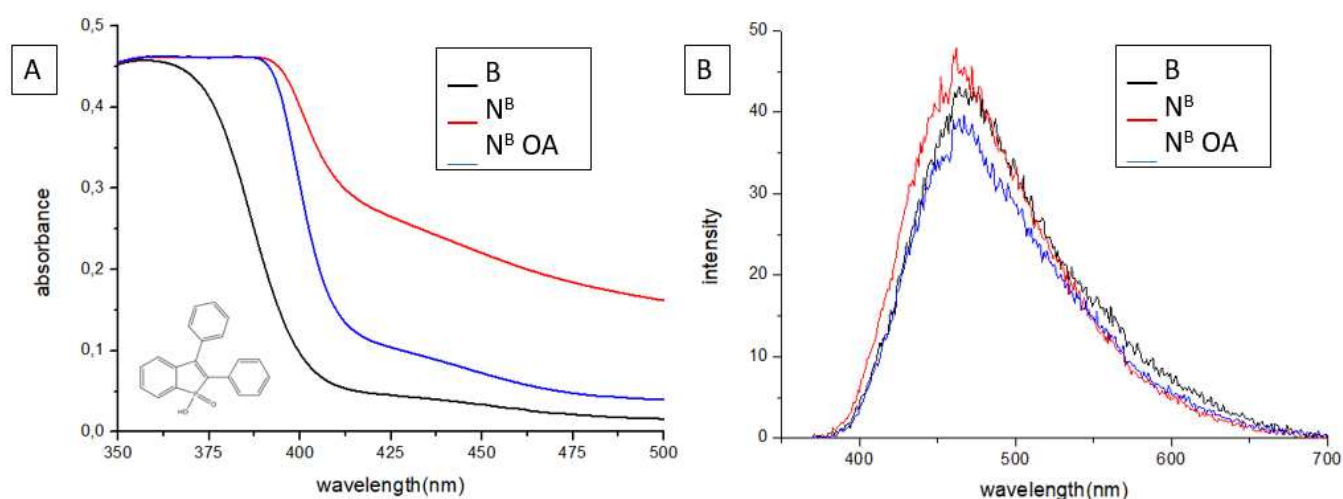


Figure 3: A) absorbance B)  $\lambda_{exc} = 350$  nm fluorescence in solution of B ;  $N^B$  ;  $N^B$  OA

The red curve ( $N^B$ ) presented in figure 3A shows a high rate of light scattering. Indeed, as mentioned, the B ; G ; R and Y are poorly soluble in solution, leading to turbid suspension at ambient temperature. However, the trend is analyzed with a maximum absorbance peak close to 350 nm, as displayed by Figure 2A. Also, a shift towards higher wavelengths is observed by grafting B with ZnO ( $N^B$ ). The OA treatment with  $N_B$  decreases drastically the scattering signal at 500 nm, meaning that OA helps to solubilize and break the nanohybrid clusters when excited at 350, the maximum emission peak is noted at 460 nm, in the blue region. In addition, no AIE neither OA caused luminescence enhancement effect was observed in the Figure 3B, as well as no shift in emission between B;  $N^B$  and  $N^B$  OA. Previous observations on emissive compound 3 brought the conclusion that the AIE effect is stronger while freezing the motion of

phenyl group by going through the solid state. The same effect stands with this emitter B in solution.

When the B materials are incorporated in the matrix M in solution, no scattering signal is observed anymore in Figure 4A, meaning that both the molecules / nanohybrids are now well dispersed and solubilized in the matrix M. The maximum absorbance peak is noted at 360 nm, almost the same as in Figure 3A.

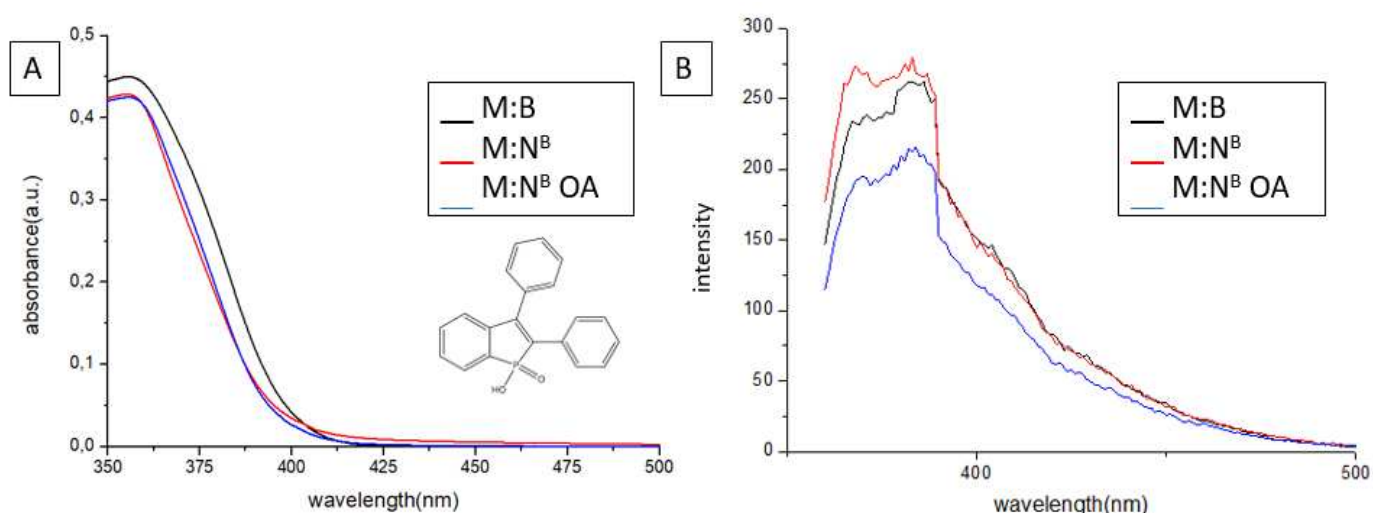


Figure 4: A) absorbance B)  $\lambda_{exc} = 350$  nm fluorescence in solution of M:B ; M:N<sup>B</sup> ; M:N<sup>B</sup>:OA

In emission, the M:N<sup>B</sup>:OA is slightly less intense. This is explained by the objects (nanohybrids) in solution which are smaller than without OA treatment. However, the emission spectrum is not the same anymore. The emission of pure B materials was from 400 to 650 nm, and once incorporated in matrix M from 300 to 500 nm. When excited at 350 nm, there is a strong energy transfer that occurs from the matrix M to the hybrids material, that is explained by the absorbance peak of PVK:OXD which is also at 350 nm. Thus, both material M and B are strongly emitting light when excited at 350 nm. However, even incorporated in matrix M, no enhancement of light intensity was recorded by adding ZnO or OA with B. Some investigations in solid state (thin films) are then presented in the next part to evaluate whether the lighting phenomenon occurs with B.

b) Emitter G

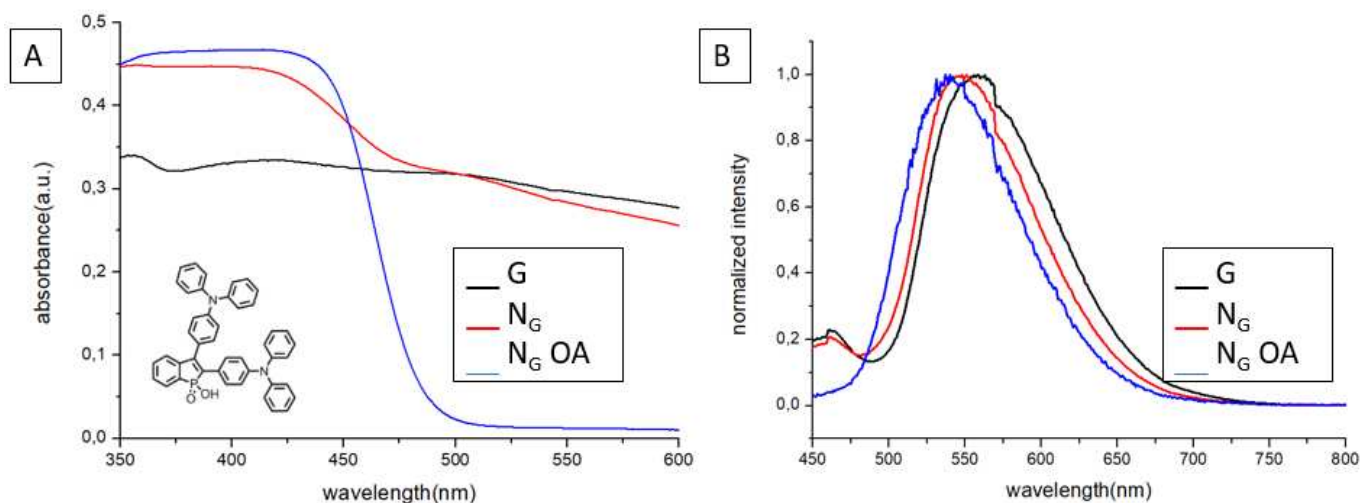


Figure 5: A) absorbance B)  $\lambda_{ex} = 410 \text{ nm}$  fluorescence in solution of G ; N<sup>G</sup> ; N<sup>G</sup> OA

The main absorbance and emission peaks are reported near 420 nm as maximum absorbance and 560 nm for the maximum emission (corresponding to a green emission). Because of the poor solubility of G, the light scattering signal is very important for G and N<sup>G</sup> materials. However, by adding OA with N<sup>G</sup>, the light scattering signal at 600 nm disappears (Figure 5A), thus well-dispersed nanohybrids are present instead of the aggregates for N<sup>G</sup>. This goes in line with the experimental observations, as the N<sup>G</sup> solution became clear after adding OA, and stirring at 100 °C with a solution that remains then stable with time. These observations are confirmed with the Figure 5B showing the normalized intensity of the emission. Indeed, a shift towards smaller wavelengths is noted while adding ZnO with G, and this shift is even stronger with the OA treatment. It means that the G molecules were not all grafted onto the ZnO surface before the OA treatment. The OA treatment helps the NCs dispersion and vies more accessible surface to the emitters for grafting. For this molecule, the emission shift is the witness of the electronic modification i.e., the grafting between the organic and inorganic parts. The optical properties of this new green emitter incorporated in the matrix M are investigated in the Figure 6.

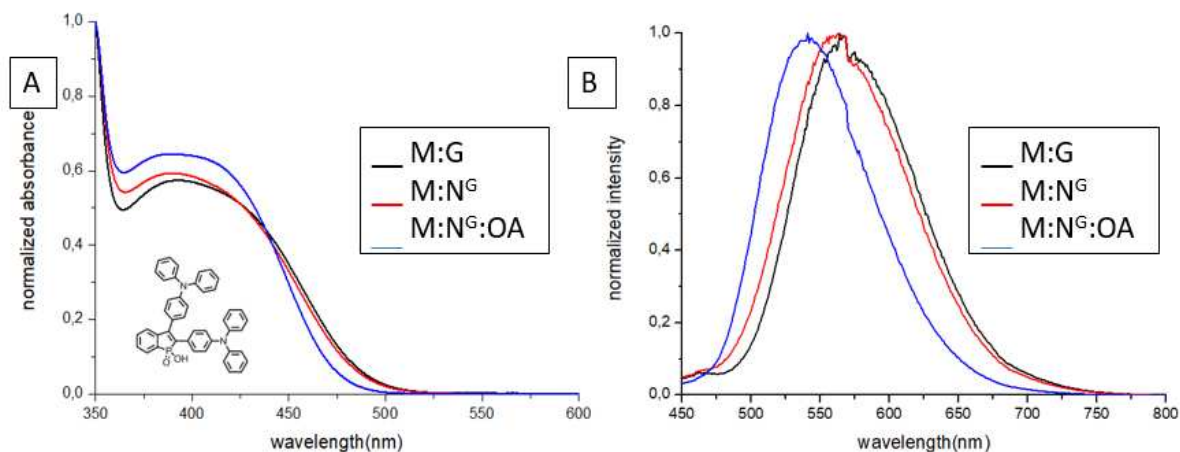


Figure 6: A) absorbance B)  $\lambda_{ex} = 410 \text{ nm}$  fluorescence in solution of M:G ; M:N<sup>G</sup> ; M:N<sup>G</sup>:OA

The absorbance of materials G incorporated in the matrix M shows no light scattering signal at all, as the solutions were clear and proving that the matrix helps in solubilizing the molecules. In absorbance, as for pure G materials, shifts are observed by adding ZnO nanocrystals with G, and are even stronger by adding OA in M:N<sup>G</sup>. The maximum absorbance wavelength recorded at 390 nm is smaller than the pure G (410 nm), because of the influence of the matrix M (Figure 6A). The same is observed for the emission, M:N<sup>G</sup>:OA maximum emission peak is noted at 540 nm instead of 560 nm for N<sup>G</sup> OA. The influence of the matrix M shifts the emission toward the blue region. In conclusion, as with the pure nanohybrids N<sup>B</sup>, the OA treatment in M:N<sup>B</sup> (giving M:N<sup>B</sup>:OA) leads to the same blue shift in emission, which suggests that the OA still helps to increase the quality of the grafting between ZnO NCs and B molecule.

### c) Emitter R

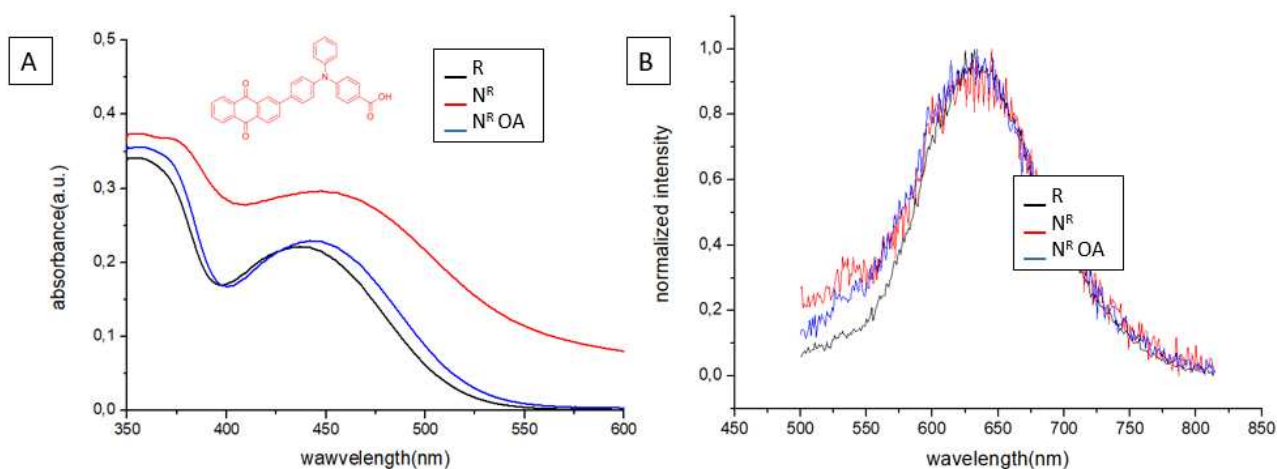


Figure 7: A) absorbance B)  $\lambda_{ex} = 440 \text{ nm}$  fluorescence in solution of R ; N<sup>R</sup> ; N<sup>R</sup> OA

The emitter R is different from the emitters B, G and Y because the grafting unit is a carboxylic acid COOH instead of POOH, and therefore different behavior may be suspected. The absorbance (Figure 7A) reveals a maximum absorbance peak at 440 nm, and is shifted toward higher wavelengths once grafted with ZnO or ZnO OA, proving that there is a modification of the electronic structure of the nano hybrids. Moreover, it was noted an important light scattering signal for N<sup>R</sup>. No shift is present in emission (Figure 7B), with a maximum emission noted at 640 nm for the three compounds. Thus, investigations in the matrix M must complete these observations.

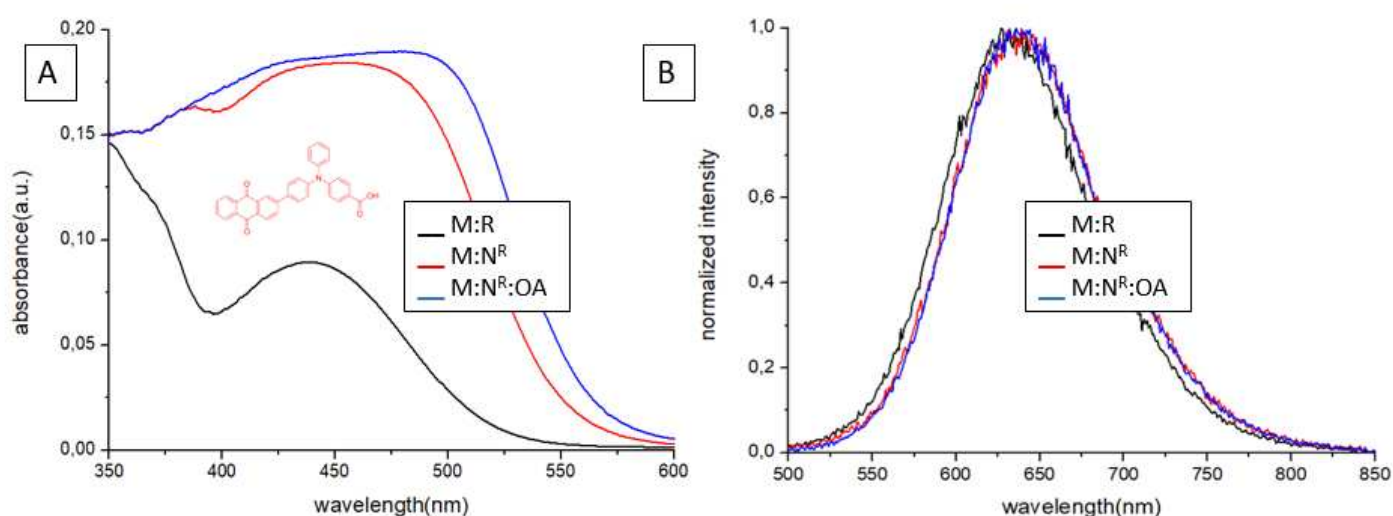


Figure 8: A) absorbance B)  $\lambda_{ex} = 440$  nm fluorescence in solution of M:R ; M:N<sup>R</sup> ; M:N<sup>R</sup>:OA

Figure 8A shows the absorbance behavior of the materials R incorporated in the matrix M. It is observed that the maximum absorbance peak is still at 440 nm after incorporation of the nano hybrids in the matrix M, but the absorbance of these solutions is shifted in the red region, indicating the modification of the structure and the energy levels of the molecule R. No light scattering signal was recorded for R compounds, the same was observed for M:G and M:B materials (Figures 8A / 6A / 4A). However, the absorbance peaks are broader than the pure materials with emitter R. Moreover, the materials containing molecule R require higher temperature (120 °C) of stirring for the self-assembly and the optimum grafting between organic and inorganic parts. On another hand, as the correlated emission of these materials in Figure 8B are weakly shifted (5 nm) towards the red region, we can ask ourselves if the grafting of R really occurs in the liquid state. The differences may be due to the grafting unit of R which is more in periphery compared to the other emitters (B, G and Y). Thus, the grafting of R with ZnO nanocrystals should have less influence on the electronic structure of the molecule.

#### d) Emitter Y

The emitter Y was optically investigated in solution, but at first, it was not the best candidate to generate later a white emission by co-grafting with blue, green and red emitters together on ZnO surface. Indeed, the emitter Y has been named as it emits a yellow light, but thanks to the grafting with the ZnO nanoparticle, a shift towards red region may be possible. The emitter Y could be then in competition with the emitter R for further experiments. As presented in Figure 9A, the emitter Y has a main absorbance peak at 420 nm which is blue-shifted once grafted with ZnO. However, the  $N^Y$  shows an important light scattering signal in absorbance, which suggests important cluster formations, whereas the light scattering signal disappeared thanks to the OA treatment in  $N^Y$  OA. The figure 9B confirms that the grafting between ZnO and Y is even more efficient with OA treatment. Indeed, there is a blue shift of the emission when Y is grafted on ZnO surface and the shift is more important with OA than without. This proves again that OA helps to avoid aggregate formation, and meantime promotes the molecular grafting of the emitters on the better accessible ZnO surface. On another hand, the maximum emission peak of Y is noted close to 610 nm, and once linked with ZnO and OA, it drastically shifts to the green region. Therefore, the maximum of emission of  $N^Y$  OA is 570 nm, in the yellow green area. The  $N^Y$  OA emission band does not cover the red region; which may be problematic to build later a white LED. The same emissions and shifts are observed by including the nanohybrids  $N^Y$  OA in the matrix M (Figure 9C). Compared with R, the molecule Y is not the best candidate for further investigations to generate white emission (annexe 1).

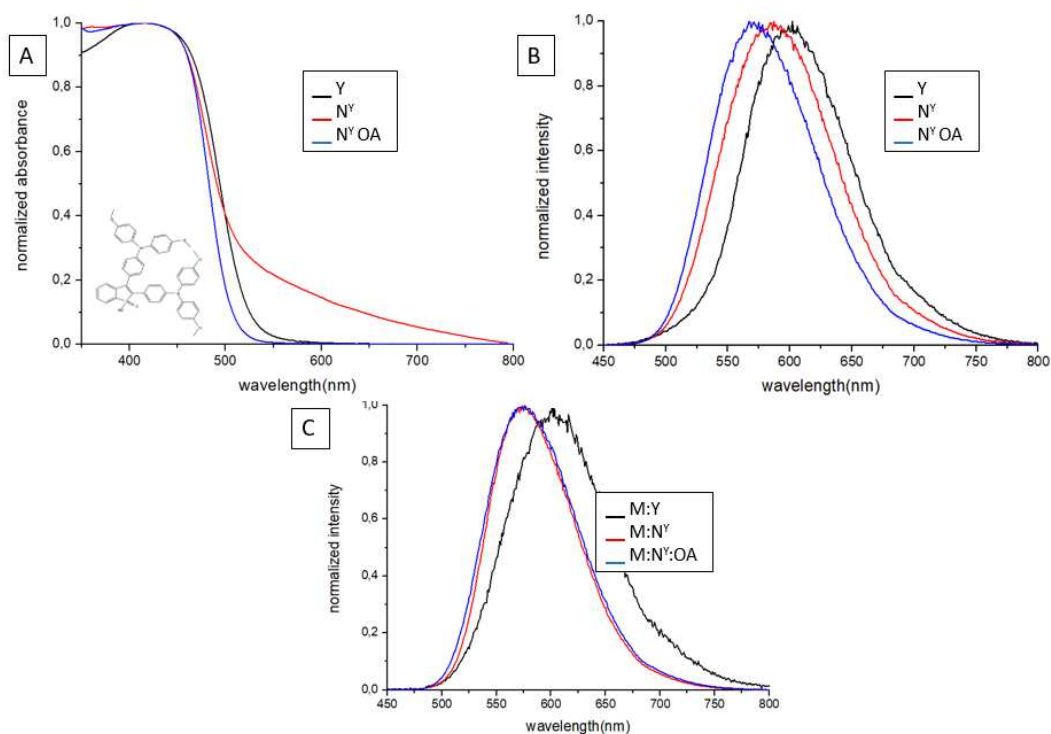


Figure 9: A) absorbance B) fluorescence  $\lambda_{exc} = 425$  nm C) fluorescence in matrix ; in solution of Y ;  $N^Y$  ;  $N^Y$  OA.

## 4) Optical properties in thin films

The luminescent solutions were spin-coated onto glass substrates with a corresponding thickness of approximately 50 nm, as presented before in the previous chapters.

The light emission in the solid state of the thin films was normalized because the angle from the incident beam to the sample and the detector was hard to reproduce with precision. Therefore, the emission intensities cannot be quantified between the samples, in addition to the point that the films do not have exactly the same thickness. Therefore, the shift in emission is observed with attention as a proof of grafting between the organic emitter and the inorganic nanoparticle, as it is a witness regarding the modification of the energy levels of the organic emitter. Quantitative studies of the respective emission of the thin films will then be analyzed in the part 4d, where PLQY measurements will be obtained in an integrative sphere thanks to a thickness-independent method. [3]

### a) Emitter B

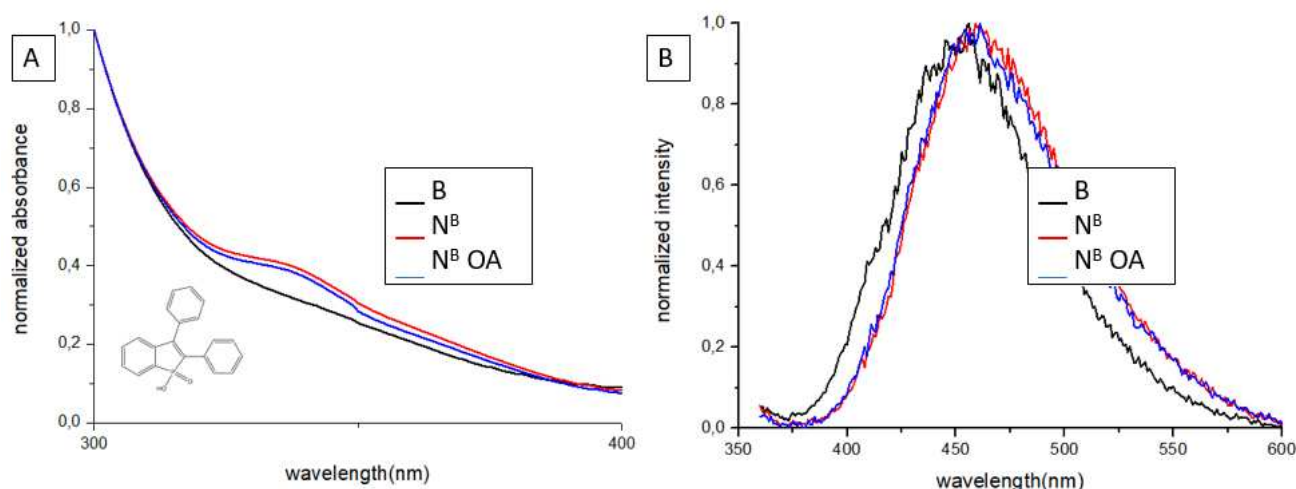


Figure 10: A) absorbance B)  $\lambda_{ex} = 350$  nm fluorescence in thin films of B ; N<sup>B</sup> ; N<sup>B</sup> OA

In the thin film state, the main absorbance peak of the B films is reported at 340 nm, which is slightly blue shifted compared to the solution one (~360 nm). This may be due to the nature and polarity of the used solvent in solution. In contrast with the liquid state (Figure 3B), by grafting ZnO or ZnO OA with B, a red shift in light emission about 20 nm is observed with a maximum emission peak for the nanohybrids at 460 nm. This suggests that there is a slight

modification of the energy levels, witness of the link between organic and inorganic parts in the film.

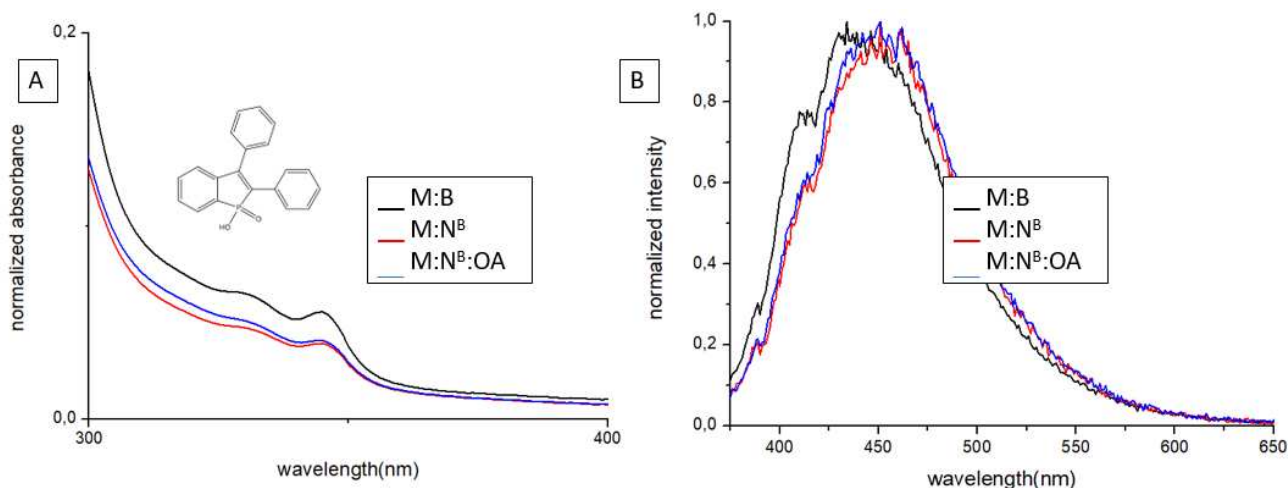


Figure 11: A) absorbance B)  $\lambda_{ex} = 350 \text{ nm}$  fluorescence in thin films of M:B ; M:N<sup>B</sup> ; M:N<sup>B</sup>:OA

According to the Figure 11A, adding the pure B; N<sup>B</sup> ; N<sup>B</sup> OA with the matrix M does not change the main absorbance peak at 340 nm, neither the emission. As remind, the matrix M has an important absorbance peak at 350 nm, the absorbance of B is then mingled with the M one. Indeed, there is a shift to the higher wavelengths by adding ZnO or ZnO OA with M:B for a maximum emission at 460 nm. It was assumed regarding the B emitter, that the AIE effect appears more obviously at the solid state because of the light emission shift, but this does not occur at the liquid state. In conclusion, when the B samples are excited at 350 nm, in figure 4B (solution) the emission is attributed to the matrix M, while in figure 11B (thin films) the emission is mostly attributed to the molecule B corresponding to an AIE effect signature (because in thin films, the motion of phenyls in B is more frozen which was not the case in solution).

## b) Emitter G

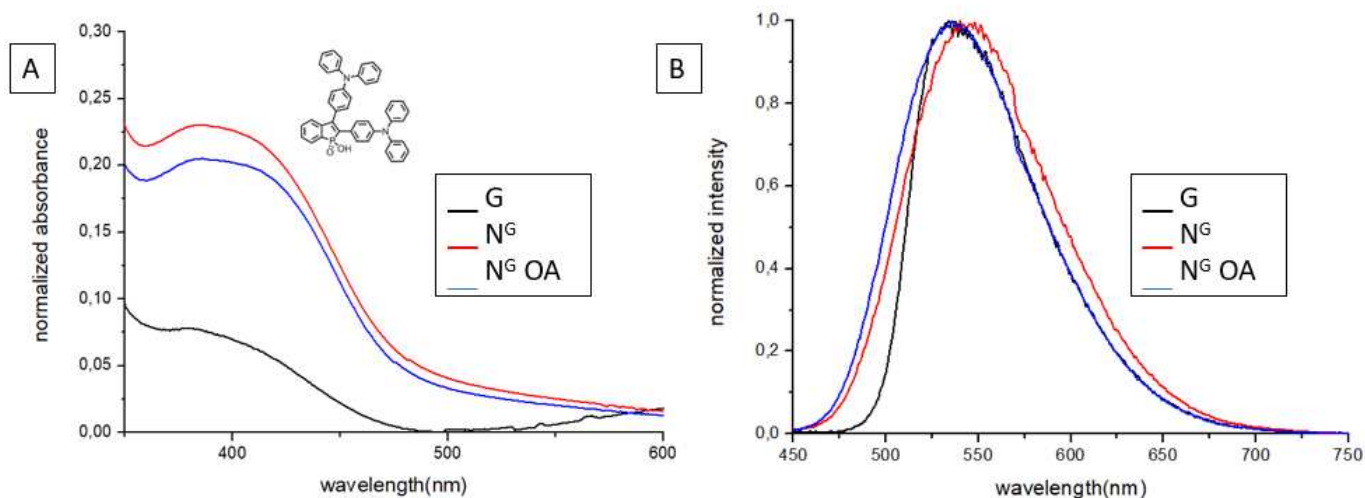


Figure 12: A) absorbance B)  $\lambda_{ex} = 410 \text{ nm}$  fluorescence in thin films of G ; N<sup>G</sup> ; N<sup>G</sup> OA

Pure materials containing G were investigated in thin films in the Figure 12. The absorbance behavior in thin films is close enough to the optical observations done in the liquid state. The maximum absorbance of G is reported at 400-410 nm. The coated layer of emitter G was opaque as the G needs temperature and stirring to be soluble in solution, and thus light scattering signal is observed at 600 nm and further. The N<sup>G</sup> OA layer globally absorbs less in the visible region than N<sup>G</sup>, meaning that the oleic acid treatment induces a better surface morphology, i.e., well-dispersed nanohybrids. Regarding the light emission, when excited at  $\lambda_{ex} = 410 \text{ nm}$ , the emitted color is green with a maximum at 540 nm. In addition, a shift is clearly identified between N<sup>G</sup> and N<sup>G</sup> OA toward smaller wavelengths. In another hand, the emission spectrum of G is narrower (from 475 to 700 nm) than N<sup>G</sup> or N<sup>G</sup> OA (from 450 to 700 nm), meaning that the energy levels of G are modified thanks to the bond with the inorganic NCs. The nanohybrids N<sup>G</sup> were then incorporated in the matrix M and optically investigated in the Figure 13.

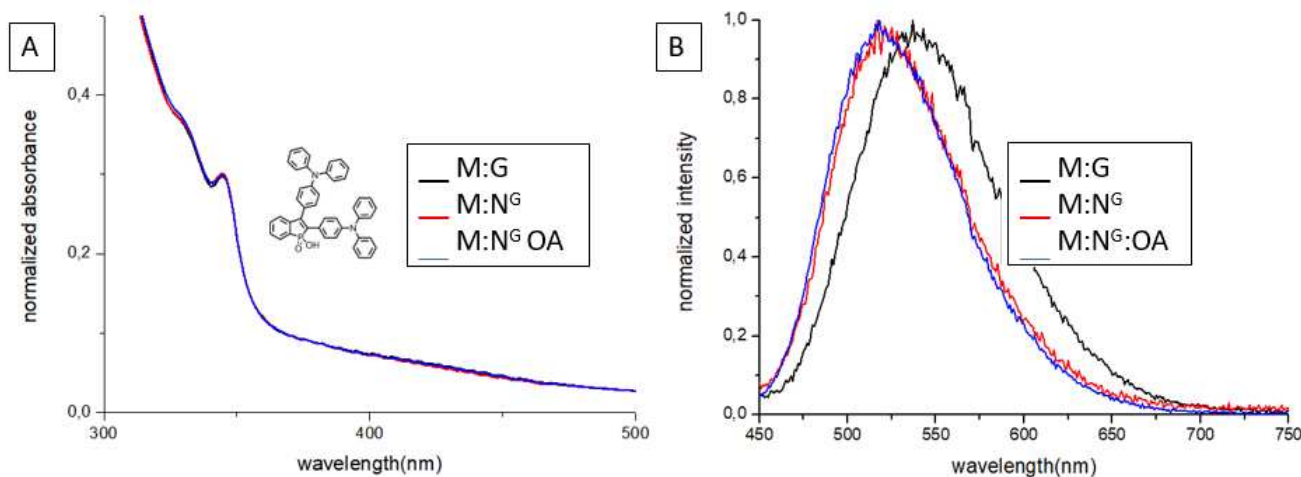


Figure 13: A) absorbance B)  $\lambda_{ex} = 410$  nm fluorescence in thin films of M:G ; M:N<sup>G</sup> ; M:N<sup>G</sup>:OA

All the coated materials of G in the matrix M gave transparent films thus having a smooth surface morphology. Indeed, in Figure 13A, no light scattering signal was observed. The absorption threshold of G at 410 nm, was not seen neither and it may be due to the thickness of the analyzed layers which is probably too low, together with the concentration of G which is much lower than M. However, in Figure 13B, a shift in light emission is noted between M:G (max at 550 nm) on one side, and M:N<sup>G</sup> and M:N<sup>G</sup>:OA (max at 520 nm) on the other side, which is a proof of an efficient grafting between the organic and inorganic parts inside the matrix M. In the end, it has been concluded that adding N<sup>G</sup> in the matrix M helps to increase the link between the organic and inorganic parts and thus to obtain smooth and homogeneous surfaces.

### c) Emitter R

In the liquid state, the R materials did not present any shift in emission upon grafting (Figure 7B), that we could attribute to a grafting unit located at the periphery of the molecule (thus having limited impact on the electronic structure). Contrarily to the other emissive molecules presented in this manuscript, we observed that an ACQ effect was present using this emitter. The nanohybrids containing emitter R are now investigated at the solid state in thin films in Figure 14.

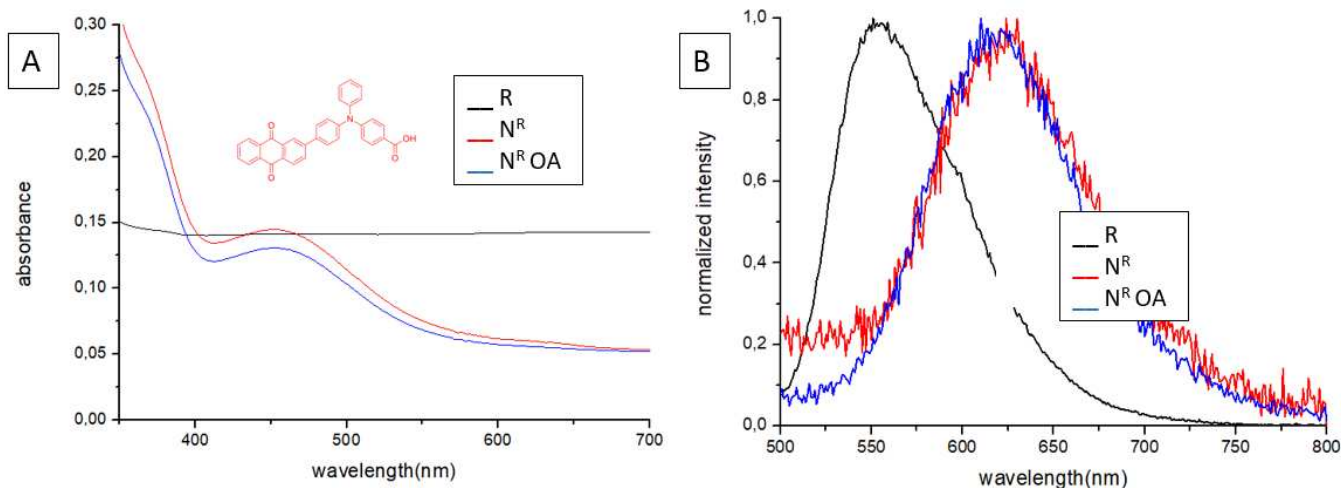


Figure 14: A) absorbance B)  $\lambda_{ex} = 440$  nm fluorescence in thin films of R ;  $N^R$  ;  $N^R$  OA

The layer of pure R was very opaque, as the emissive molecule is not stabilized with ZnO in order to obtain smooth and homogeneous surface morphology. Thus, in Figure 14A, the absorbance light scattering signal of emitter R is huge, and the absorption threshold of the molecule at 440 nm is not visible. However, by bonding the molecule R with ZnO surface, the absorption threshold of the nanohybrids is visible and reported at 450 nm. The OA treatment in  $N^R$  OA helps to decrease the absorbance signal in the visible, compared with  $N^R$ . In addition, the emission spectra of molecule R is in the yellow / orange region from 500 to 700 nm, but the grafting with the ZnO NCs brings an important red-shift about 80 nm. The emission spectra of  $N^R$  and  $N^R$  OA are the same, namely from 525 to almost 750 nm, with a maximum at 640 nm, exactly the same as the ones obtained in solution for these three materials. We can therefore conclude that the thin film composed by emitter R alone presents strong intermolecular coupling (possibly partial  $\pi$ - $\pi$  stacking) that modifies strongly the emission spectra (maximum at 560 nm). On the contrary, thin films of  $N^R$  and  $N^R$  OA still present the same emission spectra as in solution, as no intermolecular interactions may occur.

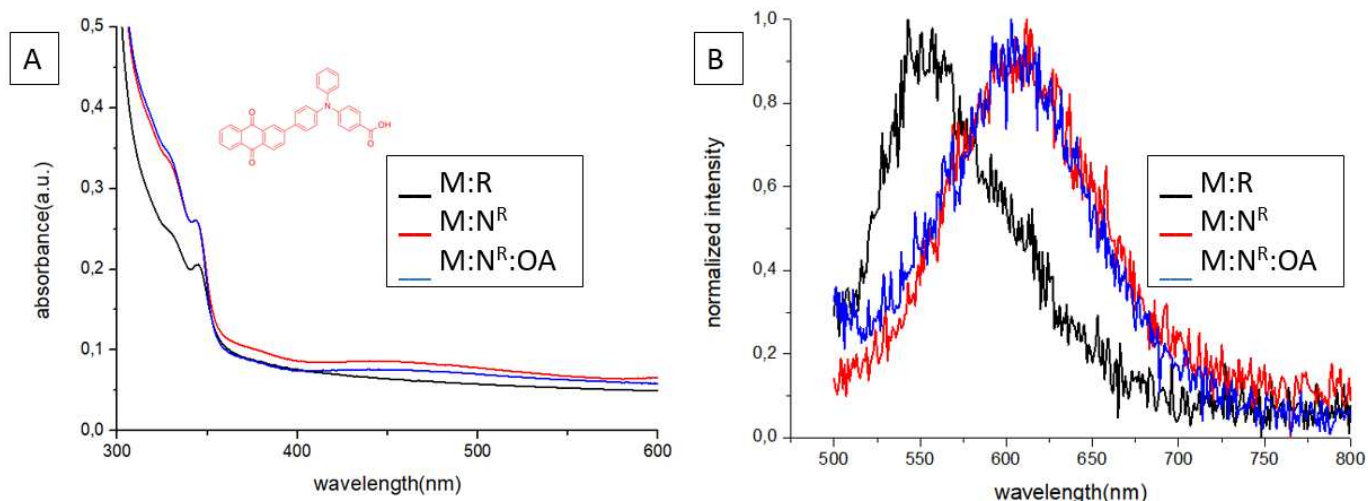


Figure 15: A) absorbance B)  $\lambda_{ex} = 440 \text{ nm}$  fluorescence in thin films of M:R ; M:N<sup>R</sup> ; M:N<sup>R</sup>:OA

As presented by the Figures 15A/B, the incorporation of the R materials in the matrix M does not change significantly the optical behaviors compared to pure materials. Indeed, the absorption threshold of the hybrids is still observed at 450 nm, and the important emission shift is still occurring between M:R on one side, and M:N<sup>R</sup> / M:N<sup>R</sup>:OA on the other side, presenting finally an orange / red emitted color for the nanohybrid structures.

Optically, in order to build solution-processed white nanohybrids for further applications, it was deduced that the emitters B, G and R can be used as organic emitters when combined with ZnO NCs and incorporated to the matrix M.

#### d) Photoluminescence Quantum Yield (PLQY)

The PLQY of the new nanohybrids at the solid state were investigated, sometimes in and out of the matrix M at different incorporated hybrid percentages (10% ;15% ;20%), and at different mass ratios of ZnO:emissive molecule. Quantitative studies of the respective emission of the thin films will then be analyzed in this part, where PLQY measurements are obtained in an integrative sphere thanks to a thickness-independent method. [3] This allows for a direct comparison of the photoluminescent properties of the different materials.

## Emitter B

Table 3: PLQY(%) in thin films of the pure B materials, with ratio (1:1) ZnO:B deposited on glass substrate. (Measured by Nicolas Ledos, PhD student from Pr. Muriel Hissler group at Institut Sciences Chimiques de Rennes).

Sample name	B	(1:1) N <sup>B</sup>	(1:1) N <sup>B</sup> OA
PLQY solid (%)	39 +/- 4	19 +/- 2	22 +/- 2

The PLQY presented in the Table 3 of the pure molecule B in thin film does not follow the the same behavior as observed in the powder form (Table 1). Indeed, the pure B reaches only PLQY = 39 +/- 4% instead of 82% in powder displayed by Table 1. However, the morphology of pure B coated on glass substrate was bad, with inhomogeneous parts and globally opaque. By adding ZnO NCs to emitter B, the PLQY decreases drastically by a factor two (PLQY = 19 +/- 2 %), and the same result was obtained with OA treatment in N<sup>B</sup> (PLQY = 22 +/- 2%), even though the layers were homogeneous and transparent. However, we know that emitter B in solution does not present any noticeable emission (PLQY < 1% from Table 1), and therefore we note an AIE effect in thin films based on the nanohybrids. Even if the PLQY are rather limited and far from the PLQY (39 +/- 4%) of the pure molecule films, the PLQY values at 19% (N<sup>B</sup>) and 22% (N<sup>B</sup> OA) attest of this emission enhancement.

## Emitter G

The PLQY of the G materials were investigated first as pure materials, and then when 10% mass were incorporated to the matrix M (Table 4).

Table 4: PLQY(%) in thin films of the G materials in and outside the matrix M (materials incorporated at 10%), with ratio (1:1) to (1:4) N<sup>G</sup> OA, measured on glass substrate coated with luminescent thin films.

Sample	G	(1:1) N <sup>G</sup>	(1:1) N <sup>G</sup> OA	(1:2) N <sup>G</sup> OA	(1:3) N <sup>G</sup> OA	(1:4) N <sup>G</sup> OA
PLQY solid (%)	32 +/- 3	43 +/- 4	60 +/- 6	65 +/- 6	<b>71 +/- 7</b>	67 +/- 6
Sample	M:G	M:(1:1) N <sup>G</sup>	M:(1:1) N <sup>G</sup> :OA	M:(1:2) N <sup>G</sup> :OA	M:(1:3) N <sup>G</sup> :OA	M:(1:4) N <sup>G</sup> :OA
PLQY solid (%)	43 +/- 4	43 +/- 4	62 +/- 6	69 +/- 7	<b>85 +/- 8</b>	77 +/- 8

The PLQY in thin films of the G molecule is about 32 +/- 3 % which is coherent with the value obtained in power in the Table 1. After self-assembly, by mixing emitter G with ZnO NCs, the PLQY increases to 43 +/- 4 %, in a similar phenomenon observed with molecule 3 in chapter

1. The quality of  $N^G$  solution contains nanohybrid clusters, thus the grafting between organic and inorganic materials is not optimal. However, adding OA with  $N^G$  increases the PLQY to 60 +/- 6 %, and it was established that the nanohybrids were well dispersed, and the corresponding surface morphology of the film was homogeneous in roughness. Additionally, by changing the ratio of  $N^G$ , the PLQY value increases to more than 70 % for the ratio (1:3). Therefore, the PLQY values reflect that the motions of the phenyl groups of the emitter G are even better blocked when a higher amount of molecules is present on ZnO NCs surface.

Once incorporated at 10% mass regarding PVK in the matrix M, the G materials follow the same trend as without the matrix. However, in the matrix M, some PLQY values, such as the best ratio (1:3)  $N^G$  or the G emitter, are a bit higher than without the matrix, with PLQY = 85 +/- 8 % and PLQY = 43 +/- 4 % respectively. This may be due to an effect of the matrix M which constrains the motion of the molecules. To complete the PLQY (thin films) study with G materials, different amounts of nanohybrids (1:3)  $N^G$  were incorporated in the matrix M and are presented by the Table 5.

*Table 5: PLQY(%) in thin films of the G materials with various amounts (X%=10% ;15% ;20%) in the matrix M, with ratio (1:3)  $N^G$  OA measured on glass substrate coated with luminescent thin films.*

M:(1:3) $N_x^G$ :OA	X=10%	X=15%	X=20%
PLQY solid (%)	85 +/- 4	94 +/- 9	98 +/- 10

The PLQY values presented in the Table 5 are very high, and reach the values from the non graftable G in powder form, that was about 100 % PLQY (Table 1). Indeed, with 15% or 20% incorporated (1:3)  $N^G$  OA in the matrix M, the maximum PLQY reaches 98 +/- 10%. Therefore, it may be assumed that the G emitter is fully grafted on ZnO surface for 20% hybrids in the matrix M at the ratio (1:3)  $N^G$ . In literature, it is shown that with optimized surface chemistry, core shell quantum dots can present near 100% PLQY and therefore represent the best choices as emissive materials for QDLEDs. [4] However, in our case, too much hybrid materials in the matrix M can lead to easier cluster formations and electrical issues such as: short cuts due to aggregates or increase of threshold voltage in the LED device. The electroluminescent properties of the G materials will be evaluated in a serie of LED devices comparing their performances in the section 6.

## Emitter R:

In contrast with the other emitters, the PLQY of the R materials were not well reproducible. The PLQY of the R materials in and out of the matrix M (at 10% hybrids incorporated), at different (ZnO:R) ratios were investigated, and are presented by the Table 6 :

Table 6: PLQY(%) in thin films of the R materials in and outside the matrix M, with ratio (1:1) to (1:3) of ZnO:R, (materials incorporated at 10% in M), measured on glass substrate coated with luminescent thin films.

Sample	R	(1:1) N <sup>R</sup>	(1:1) N <sup>R</sup> OA	(1:2) N <sup>R</sup> OA	(1:3) N <sup>R</sup> OA	(2:1) N <sup>R</sup> OA
PLQY solid (%)	1 +/- 1	4 +/- 1	4 +/- 1	13 +/- 1	1 +/- 1	4 +/- 1
Sample	M:R	M:(1:1)N <sup>R</sup>	M:(1:1)N <sup>R</sup> :OA	M:(1:2)N <sup>R</sup> :OA	M:(1:3)N <sup>R</sup> :OA	M:(2:1)N <sup>R</sup> :OA
PLQY solid (%)	2 +/- 1	12 +/- 1	7 +/- 1	17 +/- 2	5 +/- 1	16 +/- 2

Without the matrix M, the PLQY of R is at the lowest 1%, as measured in powder form from the Table 1. Furthermore, by linking the ZnO surface with the emitter R, a very small increase of PLQY is noted (4 +/- 1 %) and it remains the same and still very low with OA treatment. However, by changing from the initial (1:1) = ZnO:R mass ratio to (1:2), the PLQY increases to 13 +/- 1%.

Once incorporated in the matrix M at 10% mass (with respect to PVK), the same trend is observed, with the best PLQY = 17 +/- 2 % which is noted for M:(1:2)N<sub>10</sub><sup>R</sup>:OA. On another hand, the ratio (2:1) of ZnO:R has a PLQY value about 16 +/- 2 %, but this one presents cluster formations, as there are more unstabilized ZnO than graftable emitter R. From the Table 7 presenting PLQY in thin films, different amounts of nanohybrids were incorporated at a ratio (1:2) of ZnO:R in the matrix, and it shows clearly that adding more than 10% hybrids in the matrix leads to a decrease in the PLQY values, 10% being thus the optimized load. The PLQY values displayed by the R materials are low, but it is observed that the ACQ effect can be reduced by mixing the emissive molecule R with ZnO NCs.

Table 7: PLQY(%) in thin films of the R materials in various amounts (X%=10% ;15% ;20%) in the matrix M, with ratio (1:3) of ZnO:R, measured on glass substrate coated with luminescent thin films.

M:(1:2)N <sub>x</sub> <sup>R</sup> :OA	X=10%	X=15%	X=20%
PLQY film (%)	17 +/- 2	5 +/- 1	7 +/- 1

Importantly, the TADF property of the R materials was investigated on thin films in collaboration with Nicolas Ledos working with the group of Pr. Muriel Hissler in Institut Sciences Chimiques de Rennes, and is presented by the following Table 8 and Figure 16. Measurements were done at 298 K and 77 K to determine if the process is dependent of the temperature, to distinguish the TTA (triplet triplet annihilation) from the TADF behavior. Moreover, the lifetime values  $\tau_D$  and  $\tau_P$  are extracted using a decreasing exponential fit thanks to the software of the machine [5].

Table 8: TADF measurements on luminescent films, with measured  $\tau_P$  (ns) lifetime direct (prompt) fluorescence,  $\tau_D$  ( $\mu$ s) delayed lifetime fluorescence,  $i_D/i_P$  ratio of the delayed fluorescence over the direct fluorescence.

Film	$i_D / i_P$	$\tau_P$ (ns)	$\tau_D$ ( $\mu$ s)
R	Signal too low to be recorded		
(1:3) N <sup>R</sup>	6,6	2,3	0,94
PMMA:(1:3)N <sub>10</sub> <sup>R</sup>	1,7	8,4	1,24
M:(1:3)N <sub>10</sub> <sup>R</sup>	0,85	15,9	1,60
M:(1:3)N <sub>10</sub> <sup>R</sup> :OA	0,11	10,4	0,72

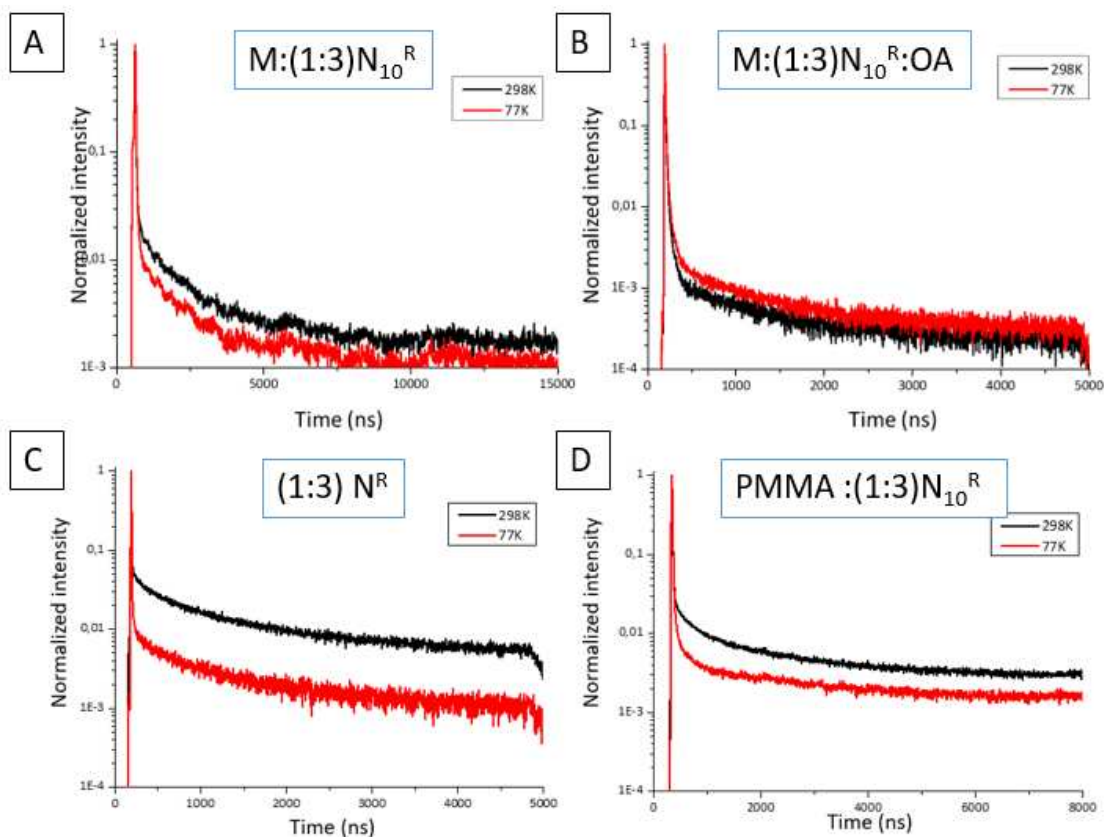


Figure 16: Associated TADF investigations lifetime-normalized intensity curves

Firstly, the R molecule was suspected to present TADF property thanks to the anthraquinone derivative group. [2] Indeed, in the literature, this groupment together with the spirobifluorene group are known to exhibit TADF property [6]. On the table 8, the signal of the R compound was too low to be considered therefore meaning that no TADF behavior is present with emitter R. Indeed, a compound is considered as TADF efficient if the ratio of the fluorescent intensities  $i_d/i_p > 1$ . However, by grafting the ZnO NCs with R at a ratio (1:3), interesting TADF property was recorded. Indeed, the ratio of the fluorescent intensities is recorded at 6.6. The removal of the OH group from the R molecule by grafting the R with ZnO NCs together with constraints from ZnO surface induce an increase of the TADF property.

This effect is extremely interesting and important as it opens the way to create TADF films from materials that do not present TADF effect in the pure form. On another hand, the incorporation of the red TADF nanohybrids in a matrix, for instance PMMA ( $i_d/i_p = 1.70$ ) or M ( $i_d/i_p = 0.85$ ) leads to a decrease of the fluorescent intensity ratio. Thus, it is concluded that the choice of the matrix has an influence on the TADF property of the red nanohybrids. Also, OA treatment was applied in the M:(1:3)N<sub>10</sub><sup>R</sup> luminescent material and it was observed that the intensity ratio was close of 0 ( $i_d/i_p = 0.11$  may be attributed to an artefact), meaning that the use of OA with the red TADF nanohybrid decreased strongly his TADF property.

To conclude, the nanohybrids approach may be powerful to design TADF materials, however a careful choice of host matrix and required co-ligands are extremely important. The electroluminescence properties of the films need to be investigated by comparing device performances in section 6.

## 5) Morphological properties of the nanohybrids

Optical observations have shown that the B, G and R emissive molecules are good candidates once linked with ZnO NCs to generate light, but the morphology of the thin films must be analyzed to go toward efficient and reproducible LED devices. Therefore, TEM and AFM analyses were done with layers containing nanohybrids at 10% mass regarding PVK in the matrix M. The study is focused on the presence of nanohybrid clusters with and without OA treatment. For sample preparation, a modification of the floating-layer technique was applied. [7] Firstly, a sacrificial PEDOT:PSS material was coated on a substrate before the M:N<sup>x</sup> emissive layer was spin-coated on top of it. After a brief annealing to dry the layers, the PEDOT:PSS film was dissolved in deionized water. Floating thin films of the emissive layer

were then recovered and deposited on a holey carbon coated TEM grid as shown in Chapter 2 (Figure 3a).

a)  $M:N_{10}^B$

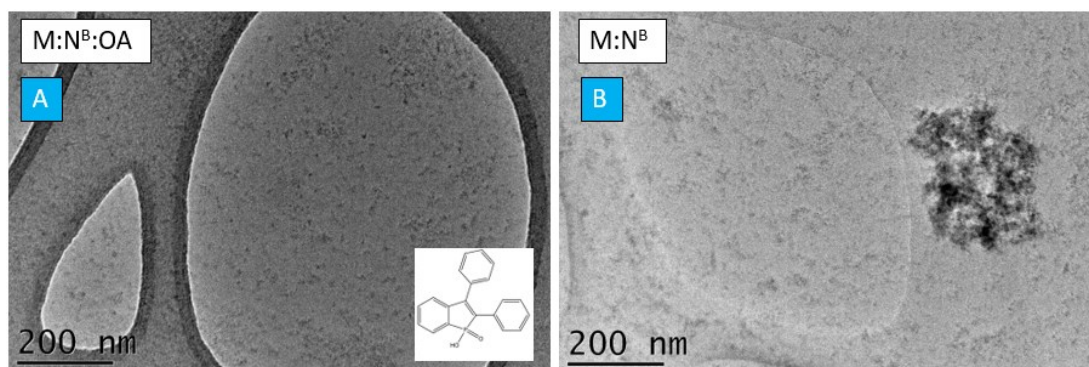


Figure 17: TEM images on holey grid A)  $M:N^B:OA$  B)  $M:N^B$

The TEM images presented by Figure 17 show the films of  $M:N^B$  (OA), and the TEM image is a projection of the 50 nm thick film. It is clearly noted that the OA treatment is required even when the  $N^B$  are dispersed in the matrix M. Indeed, the morphology of  $M:N^B$  is illustrated by cluster formation such as the ones observed over 200 x 200 nm scale on figure 17B. On another hand, the TEM image of  $M:N^B:OA$  presents some very small particle stacks (about 1 to 3 nanohybrids) which is suitable to be processed as electroluminescent material.

The AFM images at wider scale (10 x 10  $\mu\text{m}$ ) are displayed by Figure 18 to confirm these observations. Figure 18B confirms the presence of aggregates over 100 nm height and 200 x 200 nm wide, with a RMS roughness above 5,0 nm which is high for  $M:N^B$  film. Therefore, this will not be suitable to have a further efficient working LED device, as the optimal thickness of active layer determined in the previous chapter was below 100 nm (50 nm was the optimal for  $M:N^3:OA$ ). As usual, the OA treatment helps to obtain smooth and homogeneous morphology at 10 x 10  $\mu\text{m}$  scale. Indeed, no aggregate was found, and the RMS roughness is about 1,2 nm. To sum up, the observations done by TEM are confirmed by the AFM measurements.

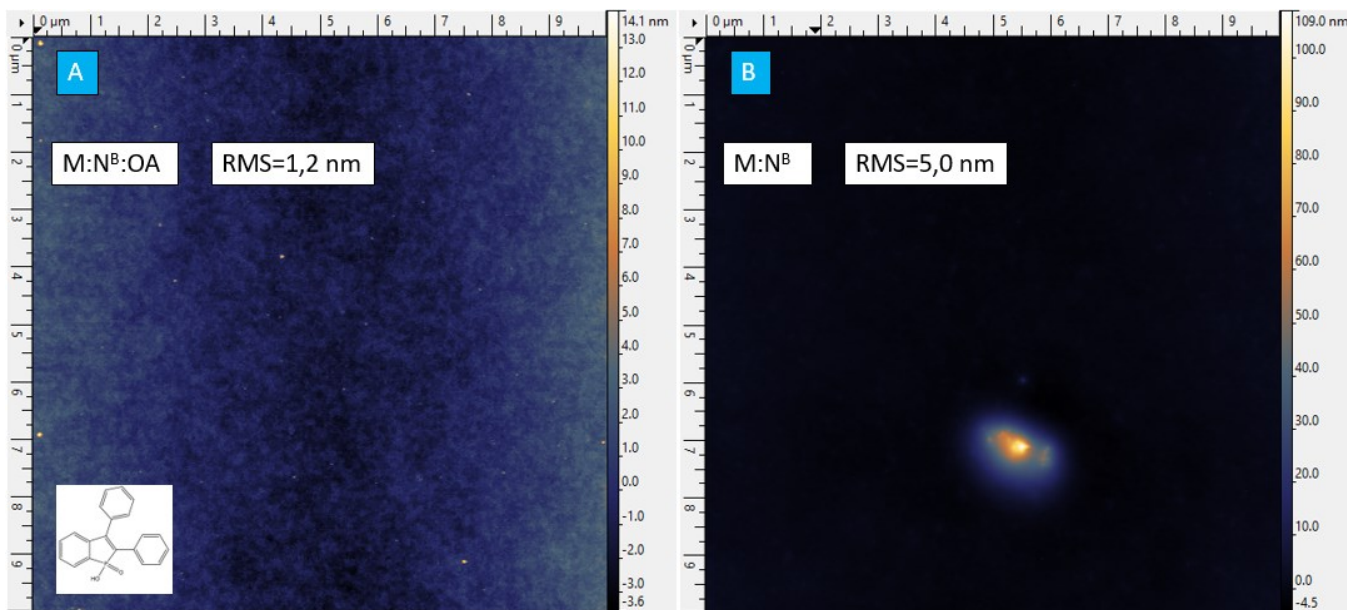


Figure 18: AFM images at 10 x 10  $\mu\text{m}$  A)  $M:N^B:OA$  B)  $M:N^B$

b)  $M:N_{10}^G$

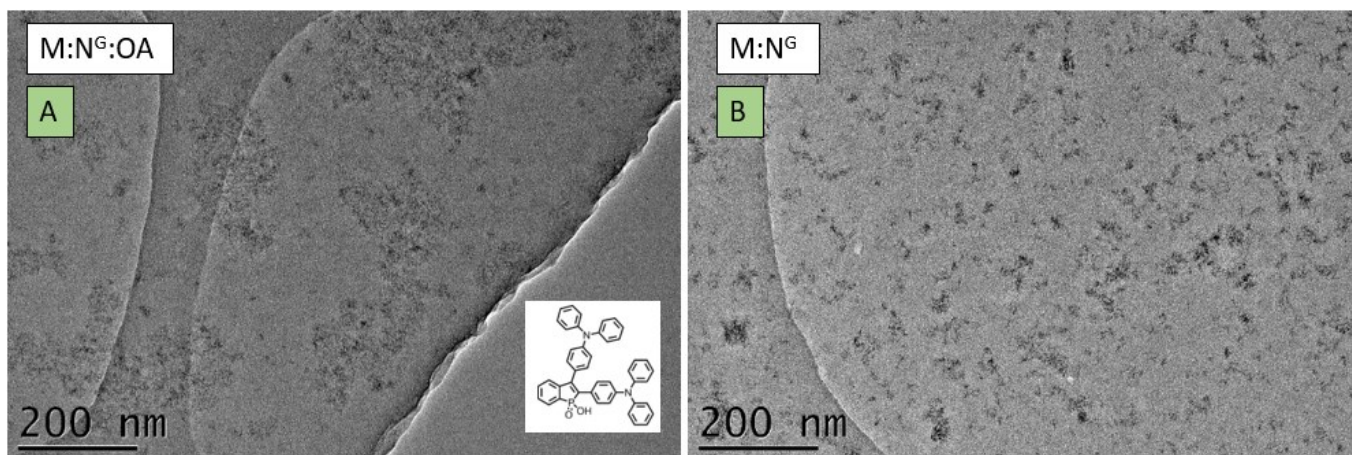


Figure 19: TEM images on holey grid A)  $M:N^G:OA$  B)  $M:N^G$

The morphology of  $M:N^G$  and  $M:N^G:OA$  films is first investigated by TEM (Figures 19A/B). The  $M:N^G$  film is characterized by several small / medium stacks of nanohybrids of different ranges. Indeed, very small stacks of few nanohybrids (10-20 nm) are observed, but also bigger ones about 40 nm. However, these stacks are much smaller than the previous ones observed with emitter B, and they do not appear problematic to build a working LED device, as far as the

analyzed surface looks quite homogeneous. Nevertheless, the OA treatment of  $M:N^G$  brings a better homogeneity, and the Figure 19A shows very small stacks of nanohybrids (less than 20 nm).

Furthermore, AFM images of these films at a wider scale ( $20 \times 20 \mu\text{m}$ ) are presented by the following figure. The  $M:N^G$  roughness is analyzed via Figure 20B, where nanohybrid clusters are observed with a height over 100 nm, and  $1 \times 1 \mu\text{m}$  wide, even though this was not observed in the TEM images (Figure 19B). The corresponding RMS roughness is then high, namely  $\text{RMS} = 4,9 \text{ nm}$ . In opposite, the OA treatment in  $M:N^G$  improves the roughness, as the RMS drastically decreases at  $1,7 \text{ nm}$ , with only very small aggregate visible on the image (a perfect surface morphology is very hard to obtain at a large scale with nanoparticles). Therefore, it was deduced that  $M:N^G:OA$  solution is suitable to be used as electroluminescent material for reproducible LED device.

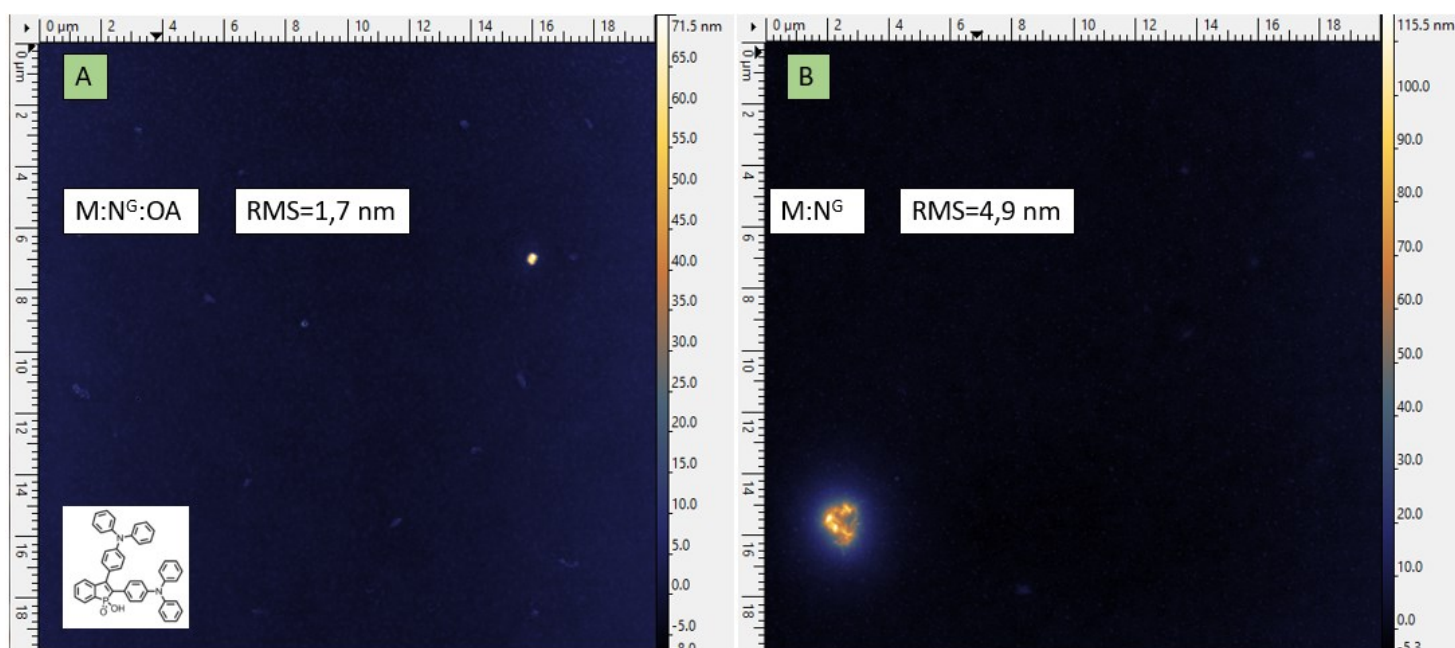


Figure 20: AFM images at  $20 \times 20 \mu\text{m}$  A)  $M:N^G:OA$  B)  $M:N^G$

c)  $M:N_{10}^R$

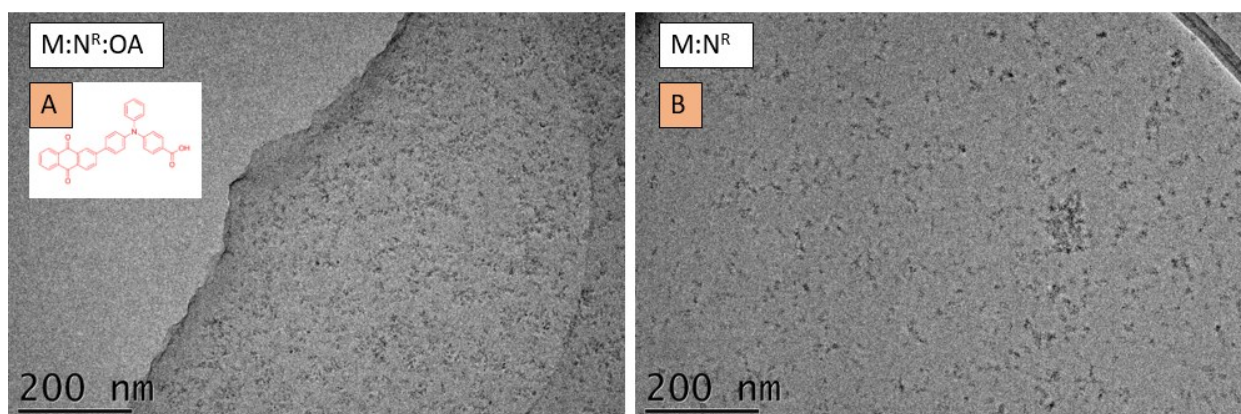


Figure 21: TEM images on holey grid A)  $M:N^R:OA$  B)  $M:N^R$

The morphology of  $M:N^R$  and  $M:N^R:OA$  films is analyzed by TEM in the Figure 21. First observations of  $M:N^R$  and  $M:N^R:OA$  led us to conclude that with or without the OA treatment, the homogeneity of the surface was excellent, without any considerable, visible nanohybrid aggregates contrarily to the both previous cases with emitters B and G. The AFM images are presented in the following figure 22 to confirm these observations at a wider scale, namely  $5 \times 5 \mu\text{m}$ .

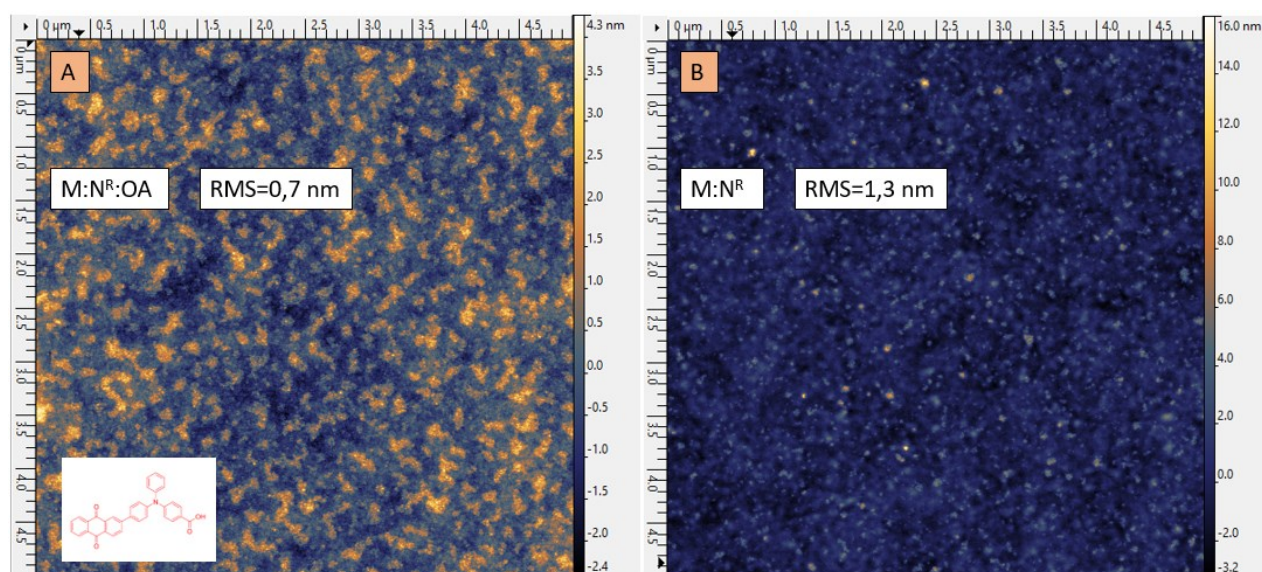


Figure 22: AFM images at  $5 \times 5 \mu\text{m}$  A)  $M:N^R:OA$  B)  $M:N^R$

The roughness was investigated in AFM over the figure 22, and it confirms the observations done with TEM images in figure 21. Indeed, the M:N<sup>R</sup> layer presents a very low surface roughness with a RMS = 1,3 nm. The layer is very smooth and homogeneous, as displayed by Figure 22B. However, the OA treatment with M:N<sup>R</sup> still helps to obtain a lower surface roughness namely RMS = 0,7 nm. Finally, it is concluded that the OA is maybe not required to obtain efficient reproducible red LED devices. Both with and without OA were then tried as electroluminescent films in further devices (section 6).

To sum up, all the new nanohybrids N<sup>B</sup>, N<sup>G</sup> and N<sup>R</sup> with OA treatment give lower RMS roughness values and thus are in the range of those obtained by other spin-coated guest-host films used in electroluminescent OLED devices [8–10].

## 6) Hybrid RGB LED devices as proof of concept and optimization

Most of the commercial OLEDs are made by evaporation process, but some are done in liquid approach [11, 12] as it presents many advantages such as the large scale production or the low cost manufacturing compared with evaporated OLEDs. The architectures of the LED devices used in this part are presented by the Figure 23. Full solution processed LED devices were done in CINaM Marseille and gave the same electrical behavior than the ones done in LPICM Palaiseau with evaporated interfacial layers. All the investigations were first done with ZnO EtNH (ethanolamine) as electron transport layer instead of evaporated BCP/Alq<sub>3</sub>/LiF. The figure 23A represents the fully characterized (JVL) devices done in Palaiseau LPICM, while the figure 23B shows the full solution processed LED characterized only by JV curves. Chronologically, the liquid approach LEDs were first done in CINaM Marseille and were optimized thanks to their visual aspect and their electrical behavior (morphology, homogeneity of the shining, intensity of the emitted light). Afterwards, the optimized devices were made by myself in LPICM Palaiseau by changing the solution processed ZnO EtNH ETL by the more convenient evaporated interfacial layers, such as BCP, Alq<sub>3</sub> and LiF, with expected better performances. [13–16] In the previous chapter, the optimal electroluminescent layer thickness was studied and deduced for 50 nm, and therefore it remains the same for the three new luminescent materials. The same stands for the mass ratio PVK:OXD = 2:1 composing M, that will also be kept constant in this chapter.

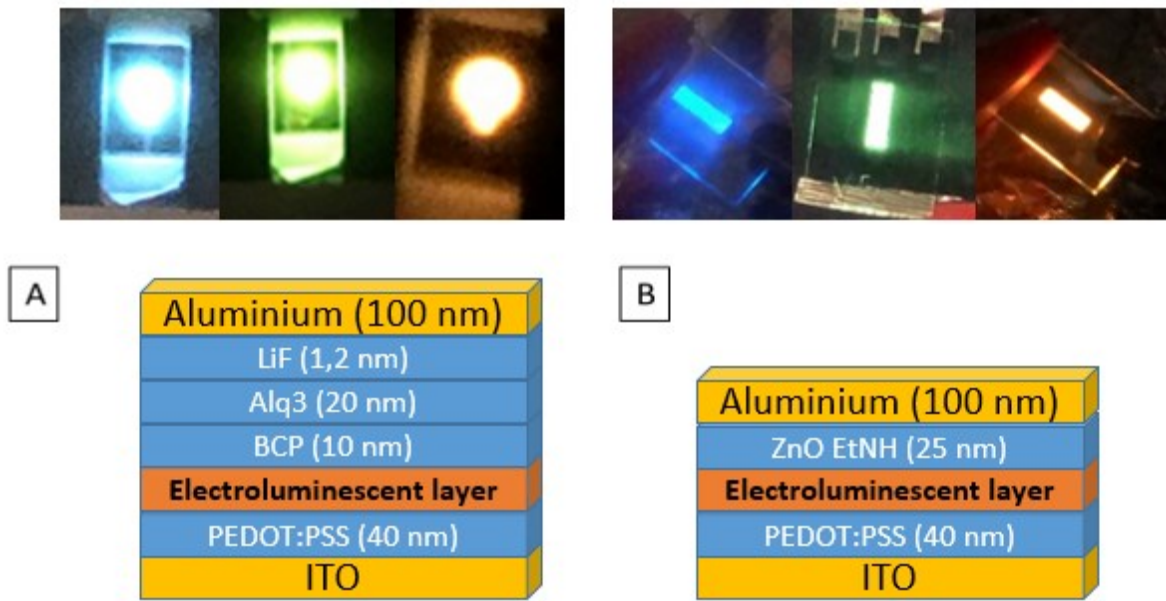


Figure 23: architecture of LED devices A) with evaporated interfacial layers B) in full solution process

As in chapter 1, pure nanohybrids without the matrix were employed as electroluminescent layer in LED device. The concentration of the coated luminescent solutions was about 15 mg/mL with a ratio (ZnO:R, G) = (1:3). The device architecture was the one presented by the figure 23B. In order to avoid short cut and electrical problems linked to the nanohybrid cluster formations, the size of the active area was decreased from 27 mm<sup>2</sup> to 15 mm<sup>2</sup>.

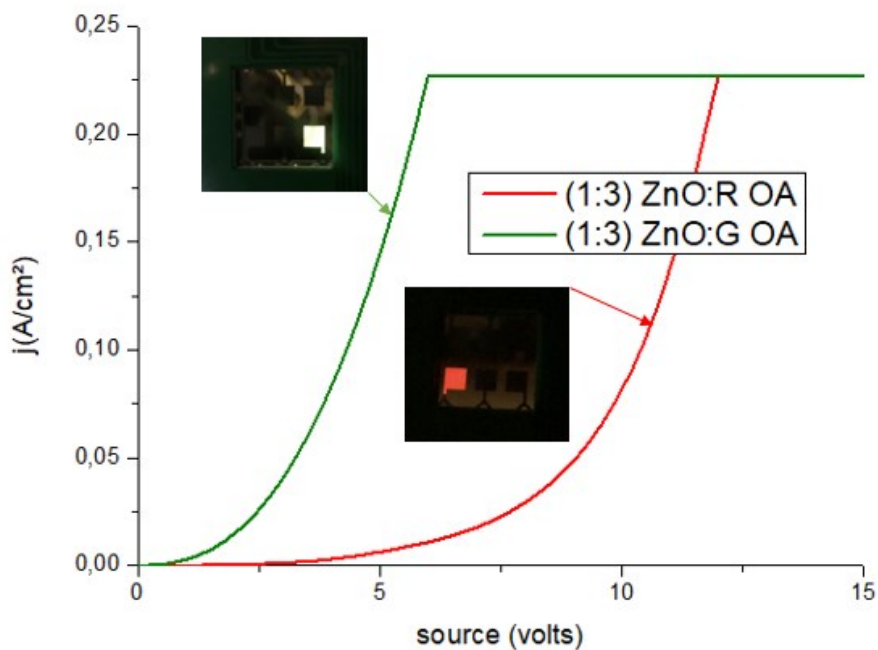


Figure 24: JV curves of hybrid LEDs containing pure nanohybrids (1:3) ZnO:G OA and (1:3) ZnO:R OA

Firstly, the blue nanohybrids were unusable in their pure forms without the matrix as electroluminescent layer (presence of too many aggregates). Several concentrations and ratios were tried of N<sup>B</sup> OA and the corresponding LEDs were not shining. On another hand, the green and red nanohybrids worked as electroluminescent layer. The green LED presented nice performances such as very low threshold voltage (1 volt) and has nice luminescence intensity. The reproducibility of the green LEDs was about 8 out of 10 samples but this was attributed to a lower active area, in order to avoid aggregates presence (as widely studied) and to increase the performances. Same observations were done on the pure red nanohybrids without the matrix, as electroluminescent layer, namely a threshold voltage of 3V and homogeneous surface lightning were noted. In addition, the reproducibility of the red LEDs was perfect, about 10 out 10 samples, and this may be explained by the better surface interaction between R and ZnO NCs, as TEM and AFM pictures showed. In the end, it was globally concluded that the incorporation of the nanohybrids in a matrix should lead to better LED performances, as for the nanohybrid using the molecule 3 (chapters 1 and 2) thanks to better transport properties of the materials.

## a) Emitter B

### i) Electroluminescent properties

A serie of blue LEDs (ITO/PEDOT:PSS/M:N<sup>B</sup>:OA/BCP/Alq<sub>3</sub>/LiF) was done to investigate the electrical and luminous performances between the molecule B, and the nanohybrids at different ratio (ZnO:B) incorporated in the matrix M. These performances are presented by the Table 9 and the corresponding figure 25.

*Table 9: LED performances with B materials incorporated at 10% in the matrix M, variation of the ratio ZnO:B from (1:1) to (1:3)*

LED name	M:B <sub>10</sub>	M:(1:1)N <sub>10</sub> <sup>B</sup> :OA	M:(1:2)N <sub>10</sub> <sup>B</sup> :OA	M:(1:3)N <sub>10</sub> <sup>B</sup> :OA
Voltage (V)	5	5	5	5
Power efficiency (lm/W)	0,11-0,26	0,26	0,21	<b>0,31-0,24</b>
Luminance efficiency (cd/A)	0,32-0,76	0,78	0,70	<b>0,92-0,84</b>
EQE (%)	0,17-0,31	0,42	0,37	<b>0,44-0,40</b>

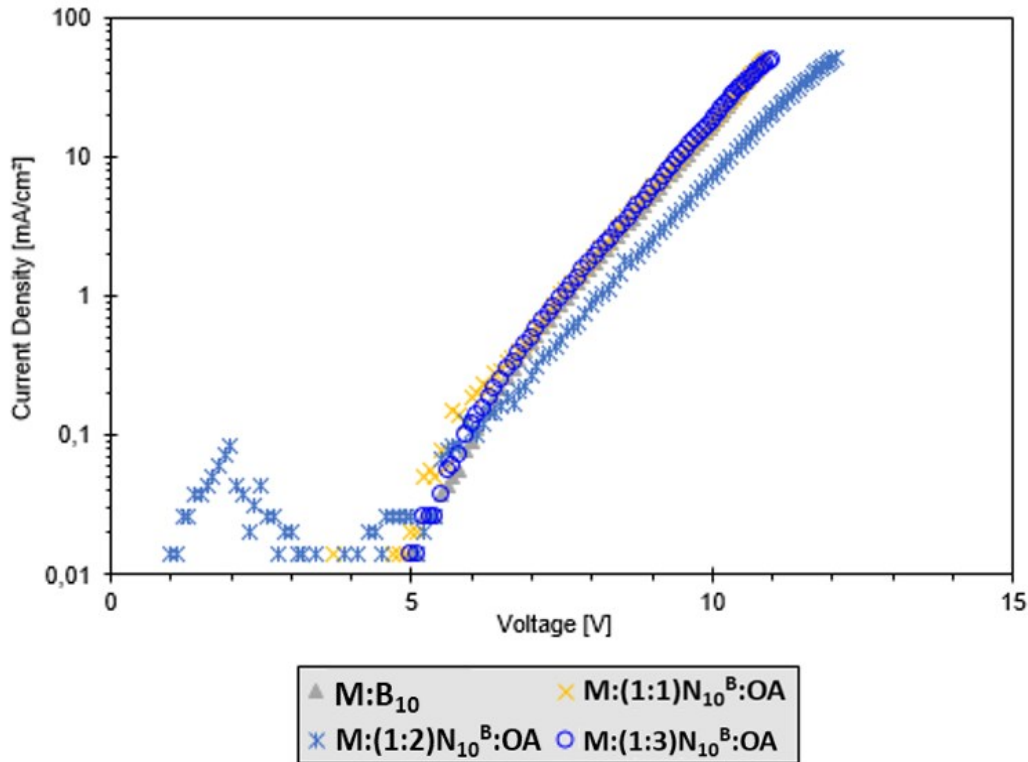


Figure 25: JV curves of the blue LED devices presented in the Table 9.

Firstly, it is observed that the  $M:B_{10}$  reference and all the ratios  $ZnO:B$  in  $M$  present the same threshold voltage, namely 5V, which is in the range of OLED literature as honorable working tension [17]. In terms of reproducibility, the  $M:B$  electroluminescent layer is low. The power efficiency varies from 0.11 to 0.26 lm/W on a same LED serie, while the EQE gives broad distributions from 0.17% to 0.31%. These discrepancies can be explained by the morphology of the electroluminescent film of  $M:B$  which was not optimal, due to the low solubility of emitter B when non-grafted. However, by adding  $ZnO$  NCs and OA with  $M:B$ , the performances of the LEDs are reproducible as the electroluminescent layer morphology is now homogeneous (statistics show success rate for 9 out of 10 samples). Indeed, for the ratio  $ZnO:B = (1:3)$ , the power efficiency reaches 0.24 to 0.31 lm/W (similar to the  $M:B$ ), and a maximum EQE about 0.44% which is 1.5 times higher than the  $M:B$  reference. Even if the measured EQE are quite low, it is in the range of the literature for fluorescent OLED blue emitters, which are generally considered as the first generation of OLED emitters with an EQE < 5 % [18]. On another hand, from the ratio  $ZnO:B = (1:1)$  to  $(1:3)$ , the electrical and luminous performances are very close, even if the  $M:(1:3)N_{10}^B:OA$  appears to be the best. In the end, it can be concluded that adding blue hybrid structures ( $ZnO:OA$  combined with B molecule) in the matrix  $M$  helps to obtain reproducible LED devices with higher performances and homogeneity compared to the  $M:B$  reference.

The next study is based on the amount of incorporated nanohybrids  $N^B$  in the matrix  $M$ , namely 10%, 15% or 20% with a ratio  $ZnO:B = (1:1)$ . The corresponding performances are presented by the Table 10 and the associated figure 26.

Table 10: LED performances with B materials incorporated at different amounts in the matrix M (10% ;15% ;20%) at a ratio (1:1) = ZnO:B.

LED name	M:B <sub>10</sub>	M:(1:1)N <sub>10</sub> <sup>B</sup> :OA	M:(1:1)N <sub>15</sub> <sup>B</sup> :OA	M:(1:1)N <sub>20</sub> <sup>B</sup> :OA
Voltage (V)	5	<b>5</b>	5-6	6
Power efficiency (lm/W)	0,11-0,26	<b>0,26</b>	0,12-0,15	0,14-0,18
Luminance efficiency (cd/A)	0,32-0,76	<b>0,78</b>	0,41-0,46	0,51-0,40
EQE (%)	0,17-0,31	<b>0,42</b>	0,23-0,27	0,20-0,18

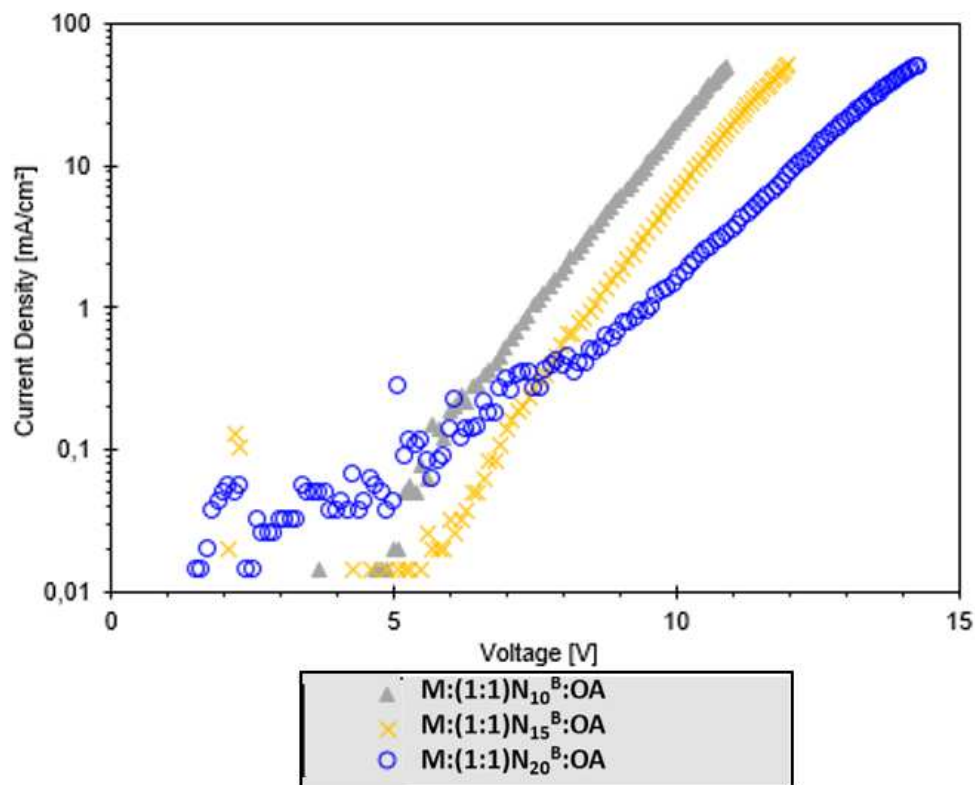


Figure 26: JV curves of the blue LED devices presented in the Table 10.

As it could be expected, the threshold voltage increases by adding more nanohybrid materials  $N^B$  OA in the matrix M [19]. Indeed, in the Figure 26, the working tension goes from 5 to 6V between 10% and 20% hybrid materials added in matrix M. The  $M:(1:1)N_{20}^B:OA$  presents a small leakage current between 1 and 5 volts because of the high amounts of nanohybrids in the matrix M, thus probably inducing higher cluster formations than in the lower amounts (as it was already proven in the chapter 2 with the molecule 3). Also, the luminous performances decrease drastically by adding more  $N^B$  OA in M. Indeed, for  $M:(1:1)N_{10}^B:OA$  a power efficiency of 0.26 lm/W and EQE = 0.42 % is noted while only 0.14 - 0.18 lm/W and EQE = 0.20 % is obtained for  $M:(1:1)N_{20}^B:OA$ . Even if the performances drop by adding more emissive compounds in the matrix M, the reproducibility of such electroluminescent hybrid layers remains very good, as 9 samples out of 10 were homogeneous (which was not the case using the reference M:B). Therefore, the use of ZnO NCs and OA with the emitter B in the matrix is relevant as it opens the way to reproducible and smooth electroluminescent layers for further LED elaboration.

ii) Shift in emitted color from M:B reference to  $M:N^B:OA$  :

Because the electroluminescence process is different than the fluorescence one, the radiance spectra of the devices M:B and  $M:(1:3)N_{10}^B:OA$  are displayed to investigate the emission spectra of these LEDs by the following figure 27. Fluorescence spectra previously showed that M:B presents a slightly broader emission band, more pronounced on the blue region, compared to  $M:(1:3)N_{10}^B:OA$ .

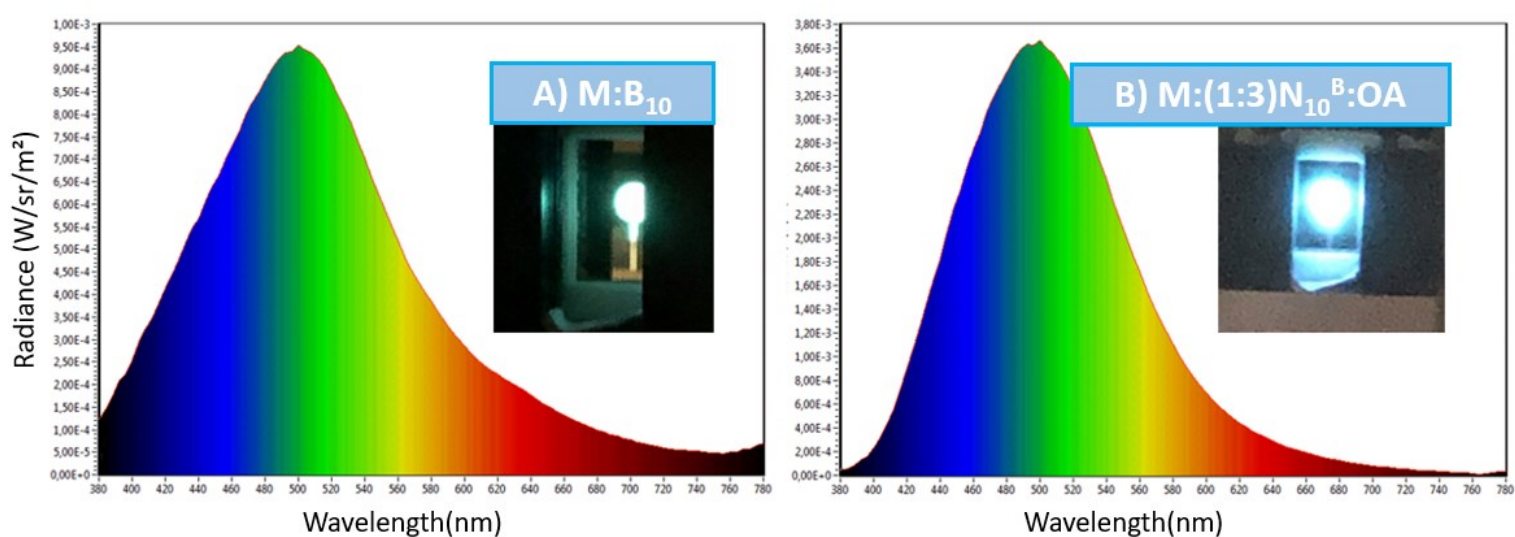


Figure 27: Radiance spectra recorded at 50 mA/cm<sup>2</sup> A) M:B<sub>10</sub> ; B) M:(1:3)N<sub>10</sub><sup>B</sup>:OA

It is clearly observable that there is a difference in the emitted color between LED based on M:B<sub>10</sub> and LED based on M:(1:3)N<sub>10</sub><sup>B</sup>:OA. Indeed, in Figure 27A, the emission spectrum is noted from 360 to 750 nm with a maximum at 500 nm, thus giving a bluish green color to the LED based on M:B<sub>10</sub>. On another hand, the LED based on M:(1:3)N<sub>10</sub><sup>B</sup>:OA emits light from 380 to 700 nm with a maximum at 490 nm, with a narrower emission band than the reference LED. The color seems therefore purer in the blue color.

## b) Emitter G

### i) Electroluminescent properties

A serie of green LEDs (ITO/PEDOT:PSS/M:N<sup>G</sup>:OA/BCP/Alq<sub>3</sub>/LiF) was done to investigate the electrical and luminous performances between the molecule G and the nanohybrids at different ratio (ZnO:G) incorporated in the matrix M. These performances are presented by the Table 11 and the corresponding figure 28.

*Table 11: LED performances with G materials incorporated at 10% in the matrix M, variation of the ratio ZnO:G from (1:1) to (1:3)*

LED name	M:G <sub>10</sub>	M:(1:1)N <sub>10</sub> <sup>G</sup> :OA	M:(1:2)N <sub>10</sub> <sup>G</sup> :OA	M:(1:3)N <sub>10</sub> <sup>G</sup> :OA
Voltage (V)	6-5	5	5	<b>4+</b>
Power efficiency (lm/W)	0,36-0,41	1,10-1,14	1,25-1,09	<b>1,42-1,36</b>
Luminance efficiency (cd/A)	1,41-1,50	3,47	3,76-3,45	<b>3,85-3,78</b>
EQE (%)	0,50-0,52	1,18	1,27-1,15	<b>1,35</b>

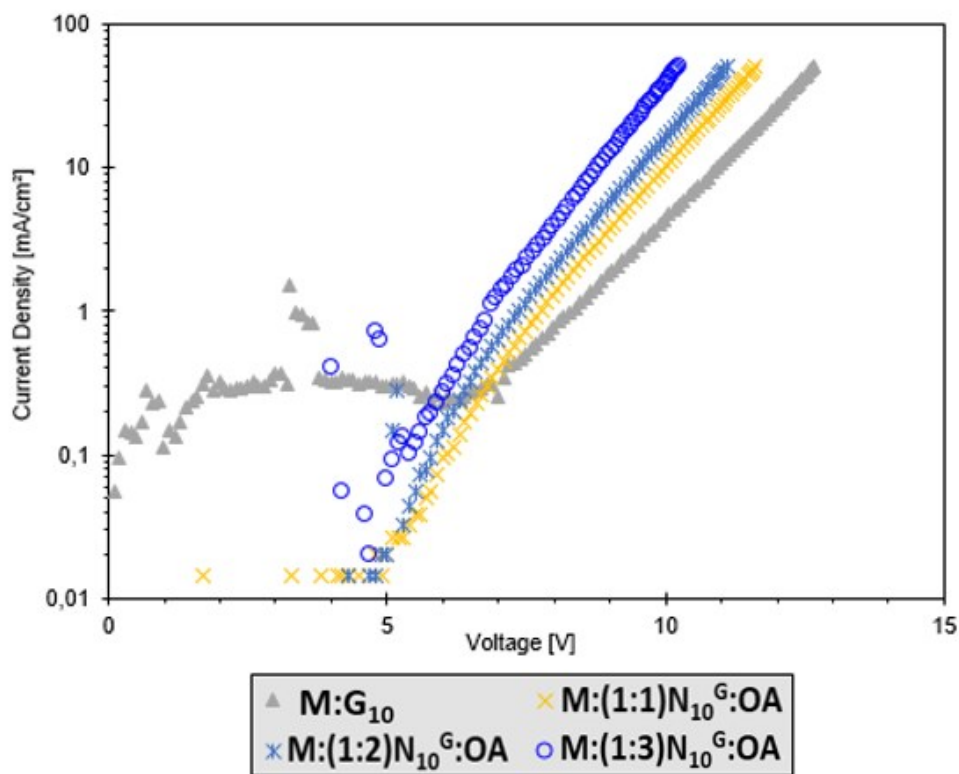


Figure 28: JV curves of the green LED devices presented in the Table 11

From Figure 28 and Table 11, it is observed that the threshold voltages are not the same for all the LEDs. Indeed, M:G working tension is about 6V, while it is progressively getting improved by increasing the ZnO:G ratio from (1:1) to (1:3), respectively from 5 to 4V. These values are in the range of OLED literature. Furthermore, the M:G LED presents important leakage current about 0.5 mA/cm<sup>2</sup> from 1 to 5 volts (Figure 28), which is probably related to the surface morphology that is quite rough. Even if the performances are reproducible, the molecule G, when non grafted, offers poor solubility and is subject to aggregate formation, thus leading to considerable leakage current. It is well known that the solution processing of host guest doped OLEDs faces phase separation problems, inducing important aggregation of the luminescent molecules (for instance B, G and R in our case) and resulting in emission quenching effects [20, 21]. As for the performances, it was recorded a power efficiency of 0.36 – 0.41 lm/W with corresponding EQE = 0.50 - 0.52 %.

On another hand, adding ZnO:OA with G molecule in the matrix leads to better morphology of electroluminescent films and therefore to better electrical and luminescent performances of the LEDs. Indeed, M:(1:1)N<sub>10</sub><sup>c</sup>:OA presents a power efficiency of 1.10 to 1.14 lm/W and an associated EQE = 1.18 %, which is 2.5 times higher than the reference M:G<sub>10</sub>. In addition, the increase of the ratio ZnO:G from (1:1) to (1:3) leads also to improvements in electrical and

luminous performances. For the ratio (1:3), a threshold voltage of 4V is noted while the power efficiency increases to 1.42 lm/W with EQE as high as 1.35 %. The maximum recorded EQE of 1.35 % is fully in the range of the first generation green fluorescent OLED emitters (the green Alq<sub>3</sub> is an example with an EQE about 1 % [22]). However, a ratio (1:4) = ZnO:G was also tried, but it gives rough surface morphology, as far as the G molecule starts to be less and less soluble, thus less reproducible. It was determined that the best ratio of ZnO:G to incorporate in the matrix M is (1:3) in terms of performances, morphology and reproducibility. For the ratios (1:1), (1:2) and (1:3), statistics showed that 9 coated layers out of 10 were optically and physically the same.

The next parameter studied is the variation of incorporated nanohybrids N<sup>G</sup> OA in the matrix M, namely 10%,15% or 20% with ratio ZnO:G = (1:1) and are presented by the figure 29 and the associated LED performances Table 12.

Table 12: LED performances with G materials incorporated at different amounts in the matrix M (10% ;15% ;20%) at a ratio (1:1) = ZnO:G.

LED name	M:G <sub>10</sub>	M:(1:1)N <sub>10</sub> <sup>G</sup> :OA	M:(1:1)N <sub>15</sub> <sup>G</sup> :OA	M:(1:1)N <sub>20</sub> <sup>G</sup> :OA
Voltage (V)	6-5	<b>5</b>	5	5
Power efficiency (lm/W)	0,36-0,41	<b>1,10-1,14</b>	1,05-1,03	0,72-0,80
Luminance efficiency (cd/A)	1,41-1,50	<b>3,47</b>	3,11-2,96	2,24-2,34
EQE (%)	0,50-0,52	<b>1,18</b>	1,07-1,01	0,81

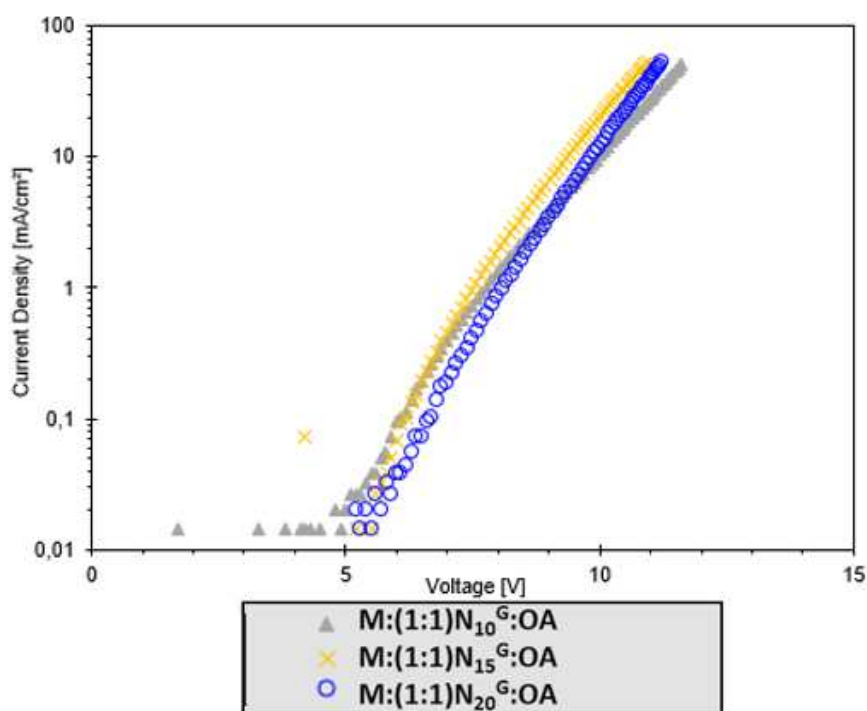


Figure 29: JV curves of the green LED devices presented in the Table 12

As for the nanohybrids  $N^3$  OA (chapter 2) or  $N^B$  OA, by increasing the amounts of incorporated nanohybrids in the matrix M, the threshold voltage should also increase. Nevertheless, it is not the case for the G materials: by increasing the percentage of  $N^G$  OA in M, the working tension remains the same, i.e. 5V. However, the performances drastically decrease by comparing the  $N_{10}^G$  OA sample with  $N_{20}^G$  OA. Respectively, the power efficiency goes from 1.10 to 0.80 lm/W and EQE from 1.18 to 0.81 %. Therefore, it was concluded that the best amount of  $N^G$  OA in M for efficient LED device is 10% with a ratio ZnO:G = (1:3). It is clear that ZnO and OA treatment are required to obtain smooth reproducible and efficient electroluminescent films with the molecule G.

ii) Shift in emitted color from M:G reference to M: $N^G$ :OA :

Fluorescence spectra previously showed that a shift in emission is observed between M:G and M: $N^G$ :OA toward the smaller wavelengths. Because the electroluminescence process is different than the fluorescence one, the radiance spectra of the devices M:G and M:(1:3) $N_{10}^G$ :OA are displayed to investigate the change of emission of these LEDs, as shown by the following figure 30.

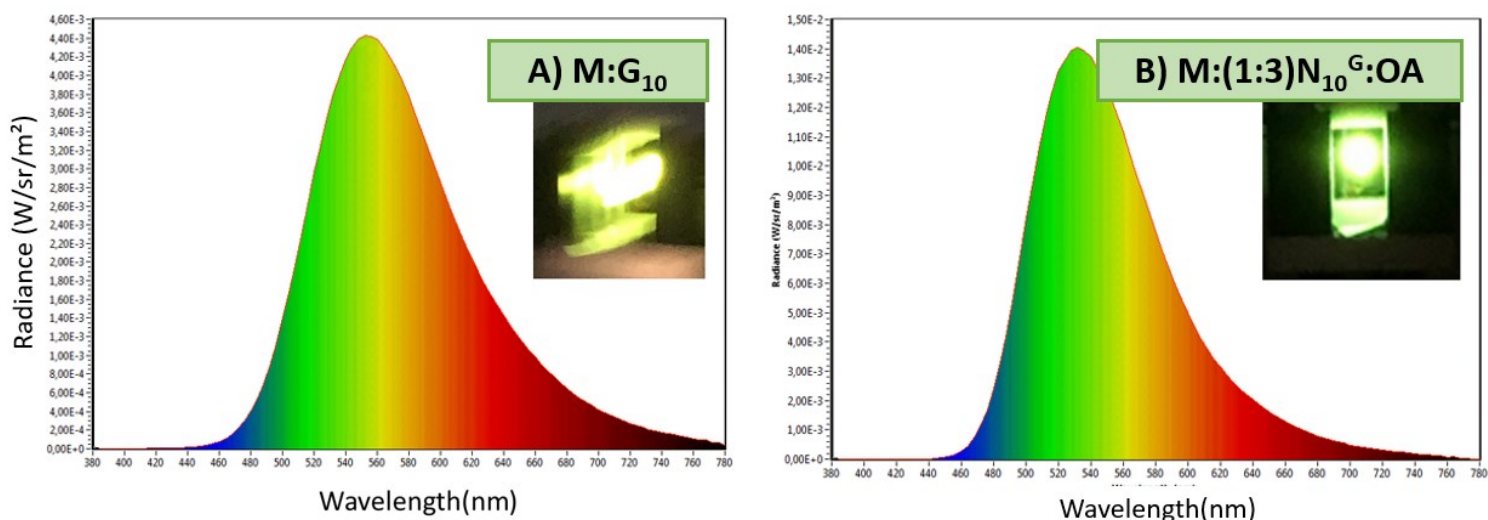


Figure 30: Radiance spectra recorded at 50 mA/cm<sup>2</sup> A) M:G<sub>10</sub> ; B) M:(1:3)N<sub>10</sub><sup>G</sup>:OA

The emission spectra recorded at 50 mA/cm<sup>2</sup> for the reference M:G<sub>10</sub> is slightly different from the electroluminescent layers containing green nano hybrids, for instance M:(1:3)N<sub>10</sub><sup>G</sup>:OA. Indeed, the reference emission spectra ranges from 460 to 760 nm, with a maximum radiance peak at 555 nm (yellowish green color), while the LED composed of M:(1:3)N<sub>10</sub><sup>G</sup>:OA electroluminescent layer has a narrower emission spectra with a maximum radiance peak recorded at 530 nm (green color).

### c) Emitter R

#### i) Electroluminescent properties

A serie of red LEDs (ITO/PEDOT:PSS/M:N<sup>R</sup>:OA/BCP/Alq<sub>3</sub>/LiF) was done to investigate the electrical and luminous performances between the molecule R, and the nano hybrids at different ratio (ZnO:R) incorporated in the matrix M. These performances are presented by the Table 13 and the corresponding figure 31.

Table 13: LED performances with R materials incorporated at 10% in the matrix M, variation of the ratio ZnO:R from (1:1) to (1:3)

LED name	M:R <sub>10</sub>	M:(1:1)N <sub>10</sub> <sup>R</sup> :OA	M:(1:2)N <sub>10</sub> <sup>R</sup> :OA	M:(1:3)N <sub>10</sub> <sup>R</sup> :OA
Voltage (V)	7-6	6	6	<b>6-5</b>
Power efficiency (lm/W)	0,45	0,2-0,18	0,28	<b>0,28-0,36</b>
Luminance efficiency (cd/A)	1,73-1,86	0,87-0,72	1,11	<b>0,95-1,32</b>
EQE (%)	0,61-0,65	0,34-0,30	0,48	<b>0,50-0,58</b>

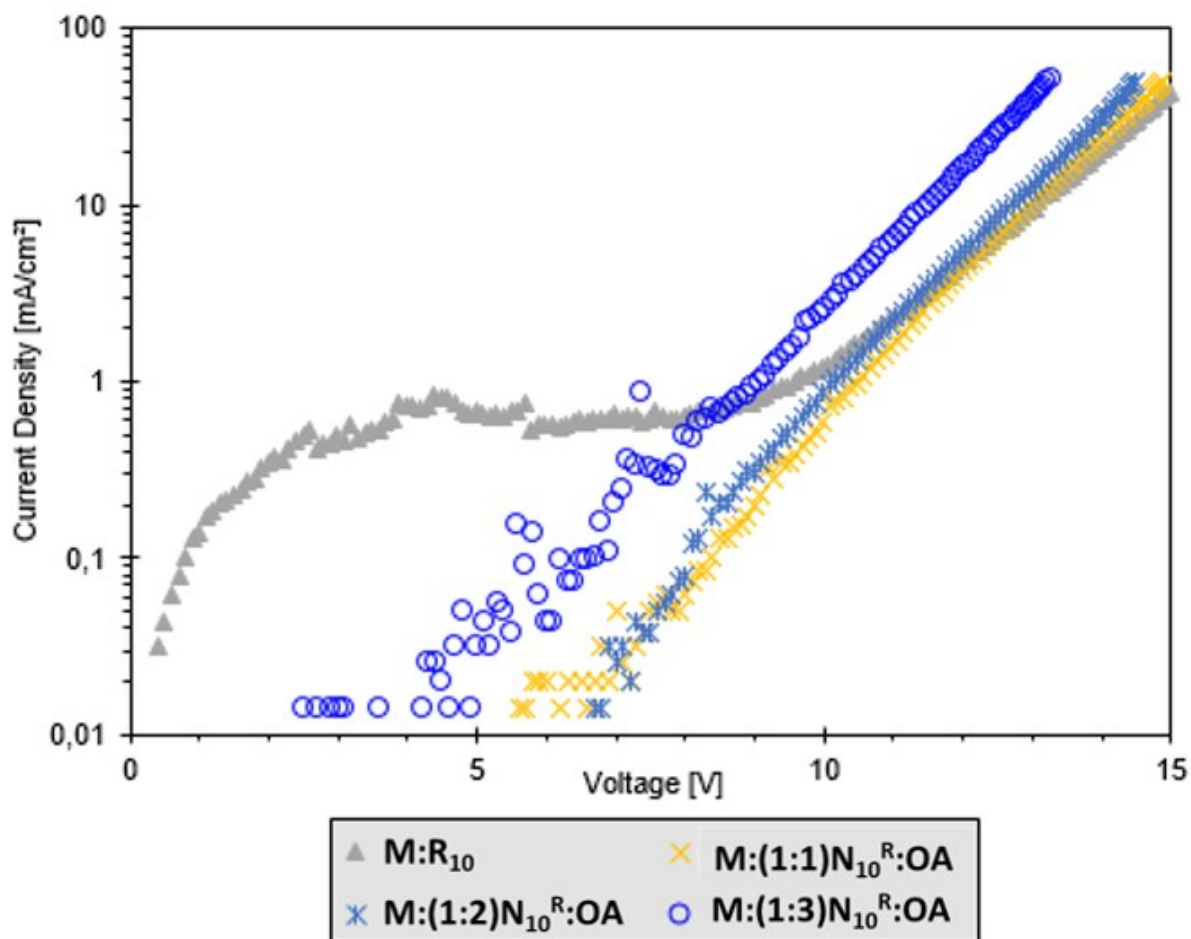


Figure 31: JV curves of the red LED devices presented in the Table 13

As for the G emitters used in LED devices, it is observed that the threshold voltages decrease by increasing the ratio ZnO:R from (1:1) to (1:3), with the working tension shifting from 6 to 5V. The reference LED with M:R<sub>10</sub> active layer presents a higher threshold voltage about 7V, and,

as for the M:G LED, an important leakage current is recorded from 1 to 6 volts which is the consequence of a non-homogeneous surface roughness. Again, it suffers from medium reproducibility and poor solubility. However, by mixing N<sup>R</sup> OA with the matrix M, almost no leakage current and surface defects have been detected, and the reproducibility of the electroluminescent layers was excellent (10 out of 10 samples). In addition, by increasing the ratio ZnO:R, the performances were also improved. For a ratio (1:1) = ZnO:R, the power efficiency is about 0.2 lm/W and EQE = 0.34 %, while the ratio (1:3) is almost twice better with a power efficiency of 0.36 lm/W and EQE = 0.58 %. Nevertheless, the phenomenon is different from the other emitters (B and G). Indeed, the reference M:R<sub>10</sub> presents the best luminous performances of the serie presented in the table 13; with a power efficiency of 0.45 lm/W and EQE = 0.65 %, which is close to the best red hybrid LED done with M:(1:3)N<sub>10</sub><sup>R</sup>:OA electroluminescent film. Even if the measured EQE are below 1 %, it is in the range of the literature for fluorescent red emitters used in OLED, which are generally hard to synthesized due to their small bandgap [23] and considered as the first generation of OLED emitters with an EQE < 5 %. For instance, in 1989, two orange / red emitters were used and presented EQE about 2,3 %. [24]

The next parameter studied is the variation of incorporated nanohybrids N<sup>R</sup> OA in the matrix M, namely 10% ;15% ;20% with ratio ZnO:R = (1:1) and are presented by the figure 32 with the associated LED performances in Table 14.

Table 14: LED performances with R materials incorporated at different amounts in the matrix M (10% ;15% ;20%) at a ratio (1:1) = ZnO:R.

LED name	M:R <sub>10</sub>	M:(1:1)N <sub>10</sub> <sup>R</sup> :OA	M:(1:1)N <sub>15</sub> <sup>R</sup> :OA	M:(1:1)N <sub>20</sub> <sup>R</sup> :OA
Voltage (V)	<b>7-6</b>	6	6	6
Power efficiency (lm/W)	<b>0,45</b>	0,2-0,18	0,23-0,31	0,35-0,21
Luminance efficiency (cd/A)	<b>1,73-1,86</b>	0,87-0,72	0,82-1,17	1,32-0,80
EQE (%)	<b>0,61-0,65</b>	0,34-0,30	0,35-0,46	0,49-0,29

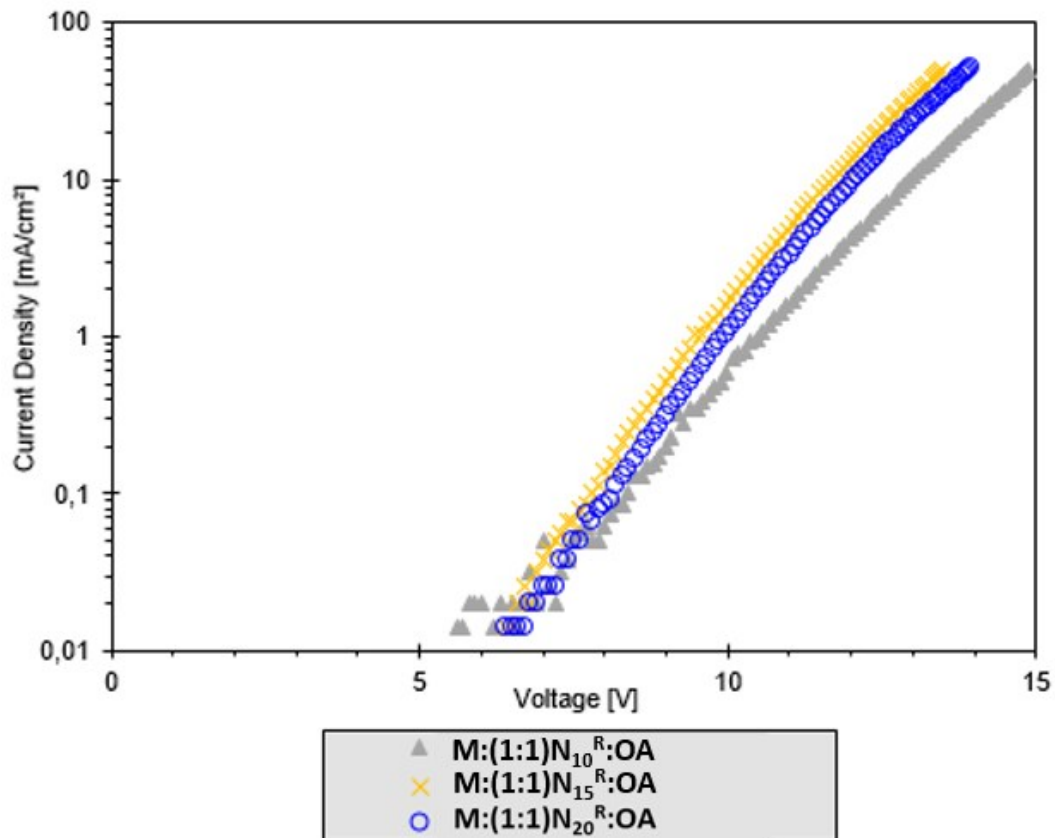


Figure 32: JV curves of the red LED devices presented in the Table 14

In contrast with B luminescent materials, and similarly to the G ones, increasing the amount of  $N^R$  OA in M do not rise the threshold voltage, which is noted about 6 volts for all the incorporated quantities. On another hand, increasing the amount of  $N^R$  OA in M leads to better electrical and luminous performances. For example,  $M:N_{10}^R:OA$  gives a power efficiency about 0.2 lm/W and EQE = 0.34 % with a good reproducibility. However, for 20% of red nanohybrid materials incorporated in M, it presents higher performances, namely power efficiency of 0.35 lm/W and EQE = 0.49 %. However, the reproducibility is medium in this case (5 out of 10 samples were working). This is probably due to the easier hybrid cluster formations, leading to defects in the active layer and thus further short cuts / electrical problems [25].

Finally, it is concluded that the use of  $N^R$  OA instead of R in the matrix M leads to better reproducibility (10 out of 10 samples for  $M:N^R:OA$  while only 5 out of 10 samples for  $M:R$ ). Also, it was assumed that the best ratio ZnO:R is (1:3) but its performances are not as high as the reference  $M:R$ . It has to be kept in mind that, for this emitter R, both OA addition and the matrix M itself were proven to have detrimental effects on the TADF properties. Careful choice of the additive and matrix would allow for improving these performances using “red” nanohybrids.

ii) Shift in emitted color from M:R reference to M:N<sup>R</sup>:OA :

In the perspective to build a white LED by combining the different colored nanohybrids, it is important to look at the emission in radiance spectra of M:N<sup>R</sup>:OA samples, in comparison with M:R. Fluorescence spectra previously showed that an important red-shift about 80 nm in light emission is observed between M:R and M:N<sup>R</sup> OA. The radiance spectrum of M:R and M:(1:3)N<sub>10</sub><sup>R</sup>:OA are shown in the following figure 33.

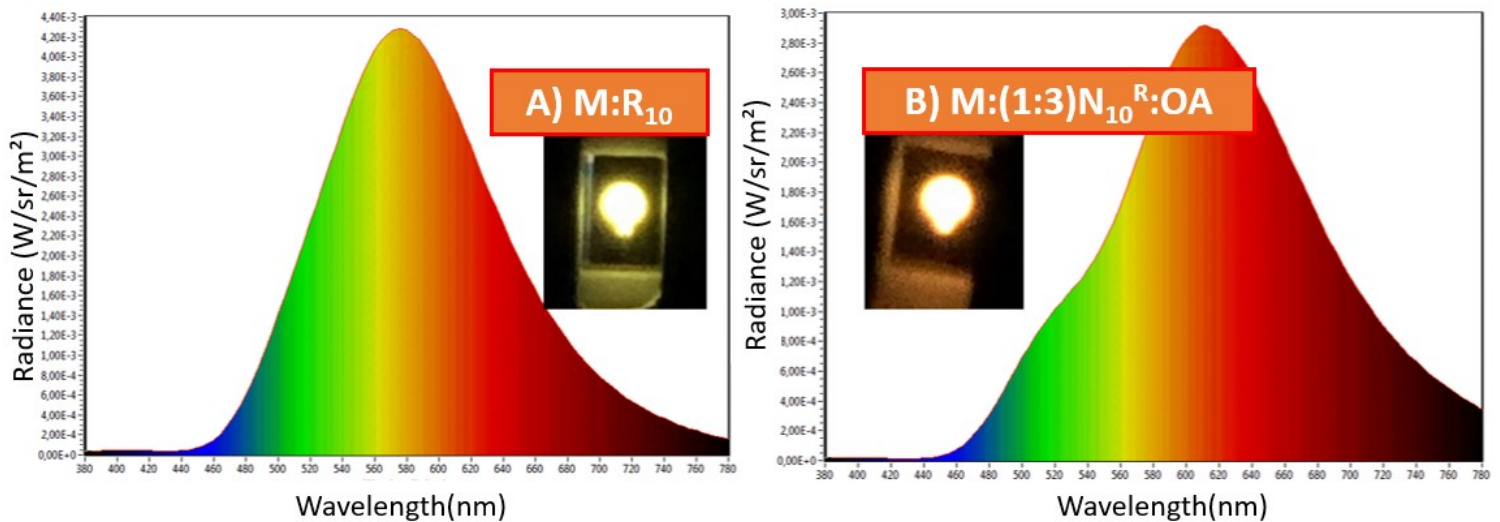


Figure 33: Radiance spectra recorded at 50 mA/cm<sup>2</sup> A) M:R<sub>10</sub>; B) M:(1:3)N<sub>10</sub><sup>R</sup>:OA

The radiance spectra recorded at 50 mA/cm<sup>2</sup> for the reference M:R<sub>10</sub> is again different from the electroluminescent nanohybrids layers M:(1:3)N<sub>10</sub><sup>R</sup>:OA. Indeed, the reference M:R<sub>10</sub> emission spectrum ranges from 440 to approximately 800 nm with a maximum radiance peak at 580 nm (yellow orange color), while the LED composed of M:(1:3)N<sub>10</sub><sup>R</sup>:OA electroluminescent layer presents a broader emission range in the red region, with a maximum radiance peak recorded at 630 nm (reddish orange color). However, the radiance spectra of the LEDs containing N<sup>R</sup> OA show a shoulder at low wavelengths in the green region. Several hypotheses can be done to explain this phenomenon, as it may be due to the green emission of residual ZnO NCs, or more probably due to a small rate of charge recombination in the green Alq<sub>3</sub> interfacial layer. Moreover, the emission of M:N<sup>R</sup>:OA is not really red, but it might be enough to generate a further white emission in LED device. In conclusion, the LEDs based M:N<sup>R</sup>:OA layer emit more in the red area than the ones based with M:R, thus M:N<sup>R</sup>:OA is more suitable for white light emission when it will be combined to blue and green emitters, compared with LEDs based on M:N<sup>Y</sup>:OA emitting in the yellow area (annexe 1).

## 7) Additional characterizations of the emissive nanohybrid layers

### a) Space Charge Limited Current (SCLC) mobility measurements

The SCLC is a method to determine the vertical mobilities of electrons and holes in thin films. The SCLC devices were done by myself at CINaM, and the extraction of mobility from the measured JV curves was done in collaboration with Pr. B. Geffroy and Dr. Payal Manzi, and is presented in the following Table 15. The fabrication process and the associated device architectures are explained in the experimental section. The measurement was realized on several active layers, for each emitters (with and without OA treatment), for the optimized electroluminescent layers, meaning 10% incorporated in the matrix M at a ratio (1:3) = ZnO:emitter.

Table 15: SCLC, Extracted hole and electron mobilities in  $\text{cm}^2/\text{Vs}$  for each optimized (RGB) electroluminescent layer.

Electrolum. material	Hole mobility ( $\text{cm}^2/\text{Vs}$ )	Electron mobility ( $\text{cm}^2/\text{Vs}$ )
M	$2 * 10^{-7} \pm 5$	$5 * 10^{-5} \pm 5$
M:(1:3) $\text{N}_{10}^{\text{B}}$	$2 * 10^{-8} \pm 2$	$5 * 10^{-6} \pm 2$
M:(1:3) $\text{N}_{10}^{\text{B}}$ :OA	$2 * 10^{-7} \pm 8$	$2 * 10^{-5} \pm 1$
M:(1:3) $\text{N}_{10}^{\text{G}}$	$2 * 10^{-8} \pm 8$	$1 * 10^{-5} \pm 8$
M:(1:3) $\text{N}_{10}^{\text{G}}$ :OA	$4 * 10^{-7} \pm 8$	$2 * 10^{-5} \pm 8$
M:(1:3) $\text{N}_{10}^{\text{R}}$	$1 * 10^{-8} \pm 3$	$1 * 10^{-6} \pm 1$
M:(1:3) $\text{N}_{10}^{\text{R}}$ :OA	$1 * 10^{-5} \pm 2$	$1 * 10^{-6} \pm 1$

As literature already shown, the hole mobility of M is quite low, around  $10^{-8}$  to  $10^{-9}$   $\text{cm}^2/\text{Vs}$  [26], and according to table 15, the hole mobility of M is here a little bit higher than in literature, close to  $2 * 10^{-7}$   $\text{cm}^2/\text{Vs}$  and about  $5 * 10^{-5}$   $\text{cm}^2/\text{Vs}$  for the electron. The incorporation at 10% of (1:3)  $\text{N}^{\text{B}}$  ;  $\text{N}^{\text{G}}$  or  $\text{N}^{\text{R}}$  in the matrix M leads to a slight decrease of the hole mobility value by a factor 10, while even smaller variations of the electron mobility were noted, i.e.  $5 * 10^{-6}$   $\text{cm}^2/\text{Vs}$  for  $\text{N}^{\text{B}}$ ,  $1 * 10^{-5}$   $\text{cm}^2/\text{Vs}$  for  $\text{N}^{\text{G}}$  and  $1 * 10^{-6}$   $\text{cm}^2/\text{Vs}$  for  $\text{N}^{\text{R}}$ . On another hand, when OA treatment was applied in the matrix M containing the blue and green nanohybrids, the hole mobility came back close to the reference value of pure M, namely  $2 * 10^{-8}$   $\text{cm}^2/\text{Vs}$ . In addition, the electron mobility value for green and blue nanohybrids with OA treatment remains the same as the pure

matrix M, i.e.  $2 \cdot 10^{-5} \text{ cm}^2/\text{Vs}$ . However, while OA treatment was applied to the red nanohybrids, the hole mobility surprisingly increased by a factor 100 ( $1 \cdot 10^{-5} \text{ cm}^2/\text{Vs}$ ), while the electron mobility did not change much ( $1 \cdot 10^{-6} \text{ cm}^2/\text{Vs}$ ) in comparison with the pure matrix M. In the end, it may be assumed that the incorporation of blue and green nanohybrids in the matrix M had no considerable impact on the hole and electron mobilities, except for the red nanohybrids which increased the hole mobility.

### b) Post annealing of the LEDs:

With devices done by solution process, it is relevant to try to post annealing of the LED once the last layer –aluminium electrode- is deposited. Indeed, it can induce a better solvent evaporation, as solvent may be trapped in the different coated layers: water for PEDOT:PSS, chlorobenzene / chloroform regarding the electroluminescent layer or isopropanol and ethanolamine (EtNH) for the ZnO EtNH electron transport layer. The post annealing was tried at several temperatures, on the luminescent systems:  $M:(1:3)N_{10}^X:OA$  with  $X = B;G;R$ , from 140 to 200 °C. The case of LEDs based on  $M:(1:3)N_{10}^G:OA$  is summarized by the following JV curves in Figure 34.

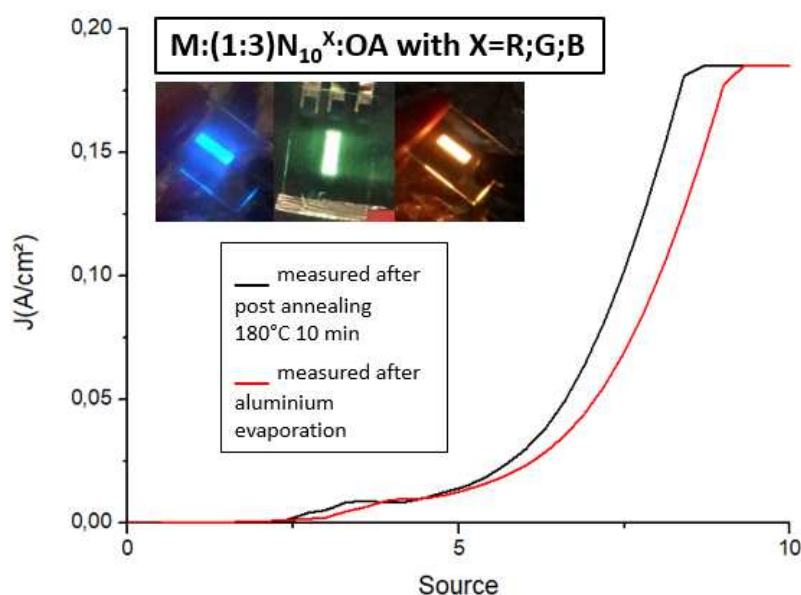


Figure 34: JV curves of  $M:(1:3)N_{10}^G:OA$ , black curve : measured after post annealing at 180 °C for 10 minutes, red curve : measured after aluminium evaporation

It was observed that the biggest gain in threshold voltage correspond to 10 minutes post annealing at 180 °C, and this for the three emitters. In the Figure 34, the compliance level set at 0.2 mA/cm<sup>2</sup> is reached 1 volt before for the post annealing LED at 180 °C (10 minutes).

However, the luminescence intensity of the LED is never improved whatever the temperature ranges from 140 to 180 °C. Lower annealing temperatures induce a very low decrease in the threshold voltage. However, to post anneal more than 10 minutes or at more than 180 °C involves changes in morphology and considerable losses in luminance.

### c) Encapsulation of LEDs based on $M:(1:3)N_{10}^G:OA$ as electroluminescent layer

Atomic Layer Deposition (ALD) was used in a collaboration at CINaM with Dr. Lionel Santinacci and Dr. Clémence Badie, in order to encapsulate the LED devices. LED device was encapsulated with a first layer of alumina 10 +/- 1 nm followed by titania 10 +/- 1 nm processed at 90°C and the device was then stored in air under atmospheric conditions for 2 months.

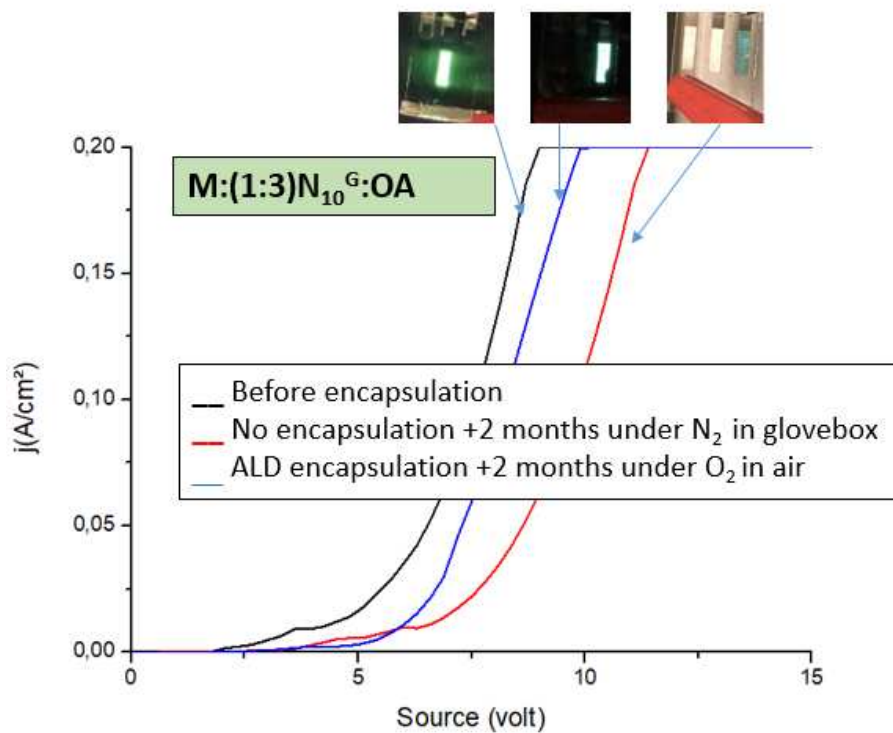


Figure 35: JV curves of LED with  $M:(1:3)N_{10}^G:OA$  as electroluminescent layer, black : measured before encapsulation, red : No encapsulation measured after 2 months storage under  $N_2$  in glovebox, blue : ALD encapsulation measured after 2 months storage under  $O_2$  in air.

For this study, LED devices were done with  $M:(1:3)N_{10}^G:OA$  used as electroluminescent layer. In the figure 35, before encapsulation, the LED presents a nice electrical behavior, with a very low threshold voltage about 2 volts (compliance level reached at 8 volts), and a homogeneous and intense shining. However, without encapsulation, when the device was stored under  $N_2$  atmosphere (in glovebox) and was then measured after 2 months, it shows important drops in

performances. Even if the threshold voltage increases to 4 volts and the compliance level is reached at 11 volts, a big loss in luminance was observed. On another hand the ALD encapsulated device presents still nice electrical answer, with a low threshold voltage of 4 volts and a compliance level reached at 9 volts, but more importantly, the intensity of luminance is close to the freshly prepared devices before encapsulation.

## 8) Conclusions & Perspectives for hybrid white LED

In conclusion, we could demonstrate that the nanohybrids could serve as a tool to manufacture homogeneously dispersed various organic emitters in a matrix-based layer by solution deposition. This approach is very convenient especially when the emitters are non-soluble (or may have a tendency to aggregate), in order to avoid costly evaporation processes.

The beneficial effect of OA with the nanohybrids has been generalized to other emitters. For all of them, the morphology of the thin films was improved, thanks to an efficient size reduction of the aggregates. For all of them, the OA also helped for a better grafting of the emitters and thus gave higher PLQY for thin films than the references without OA. Importantly, we could also show that nanohybrid formation could create TADF effect that was not initially present on the emitter before grafting. In this case, OA did quench the TADF effect and therefore future developments should improve this aspect.

These new nanohybrids were also incorporated in a matrix, and thus processed as electroluminescent layer in different LED architectures. A new panel of colored LED was obtained, from the deep blue to the orange-red area. Three new nanohybrids were selected in order to create a further white emission, and white LED: these nanohybrids are  $N^B$ ,  $N^G$  and  $N^R$  with OA treatment incorporated in the matrix M. The building of the white emission can be imagined by the co-grafting of two or three emitters (B ;G ;R), together on the same ZnO nanoparticle surface. These possibilities will be explored in the last chapter.

The different structures used and their emitted color in LED are presented briefly in the following figure 36.

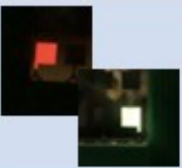
Electrolum. Material	M:B	M:N <sup>B</sup> :OA	M:G	M:N <sup>G</sup> :OA	M:Y	M:N <sup>Y</sup> :OA
LED						
Electrolum. Material	M:R	M:N <sup>R</sup> :OA	M	M:3	M:N <sup>3</sup> :OA	Pure N <sup>G</sup> OA and N <sup>R</sup> OA
LED						

Figure 36: Electroluminescent materials used as active layer with corresponding powered LED device

## ANNEXES:

### 1) Yellow LED with M:N<sup>Y</sup>:OA :

Characterized optically at the liquid state in the previous part, the M:(1:1)N<sub>10</sub><sup>Y</sup>:OA solution emits a greenish yellow color while M:Y<sub>10</sub> a yellow one. This material has been tried as electroluminescent layer in LED device, their JV curves are presented in the Figure 36.

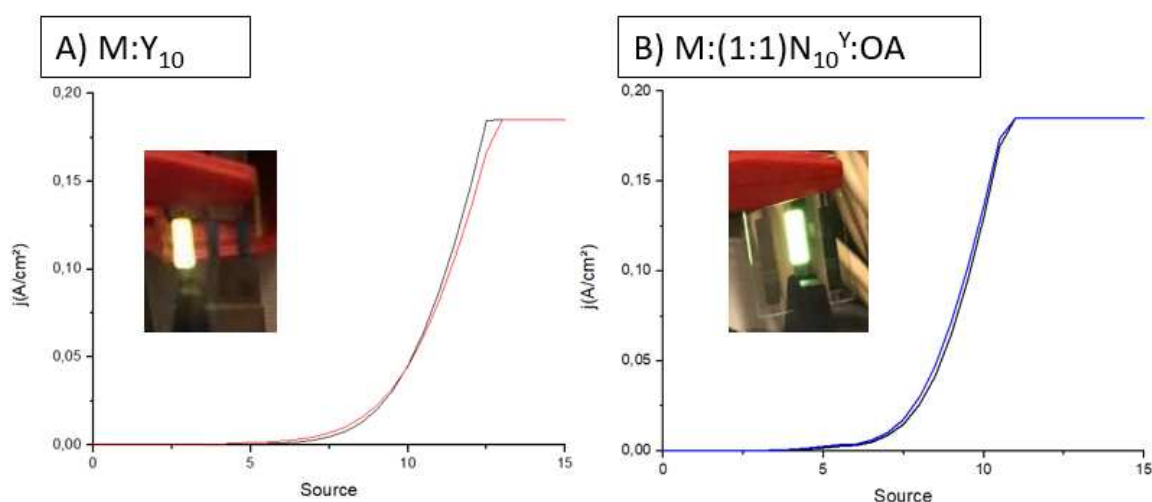


Figure 37: JV curves of the LED with A) M:Y<sub>10</sub> ; B) M:(1:1)N<sub>10</sub><sup>Y</sup>:OA as electroluminescent layer.

In the Figure 37, the threshold voltage of the reference M:Y<sub>10</sub> is noted at 7V, that is higher than the 5V recorded for M:(1:1)N<sub>10</sub><sup>Y</sup>:OA. Electrically the electroluminescent nanohybrid layer is more suitable for LED than the pure organic M:Y<sub>10</sub>. Indeed, the morphology of M:N<sub>10</sub><sup>Y</sup>:OA was smoother than the reference. It is assumed that the bonding between Y and ZnO OA is efficient because of the shift regarding the emitted color – yellow for M:Y<sub>10</sub> and greenish yellow for M:(1:1)N<sub>10</sub><sup>Y</sup>:OA-, which may be translated by the modification of the energy levels of the Y molecule. By eyes, the intensity of both devices was close enough.

## Bibliography:

- [1] Ackermann J, Margeat O, Hissler M, Bouit PA. Nanomatériaux Hybrides Luminescents À Émission Induite Par Agrégation. 2015 Aug 27 [accessed 2021 Dec 20]. <https://patentscope.wipo.int/search/fr/detail.jsf?docId=WO2015124802>
- [2] Bin Huang, Ji Y, Li Z, Zhou N, Jiang W, Feng Y, Lin B, Sun Y. Simple aggregation–induced delayed fluorescence materials based on anthraquinone derivatives for highly efficient solution–processed red OLEDs. *Journal of Luminescence*. 2017;187:414–420. doi:10.1016/j.jlumin.2017.03.038
- [3] Dr. John C. de Mello, Dr. H. Felix Wittmann, Prof. Richard H. Friend. An improved experimental determination of external photoluminescence quantum efficiency 1997 - *Advanced Materials*. [accessed 2022 Jan 14]. <https://doi.org/10.1002/adma.19970090308>
- [4] Prachi Patel \* Quantum dots are behind new displays | *IEEE Journals & Magazine | IEEE Xplore* pages 14 - 17 ( Volume: 49, Issue: 8, August 2012). [accessed 2022 Jan 4]. DOI: 10.1109/MSPEC.2012.6247547
- [5] Nakagawa T, Ku S-Y, Wong K-T, Adachi C. Electroluminescence based on thermally activated delayed fluorescence generated by a spirobifluorene donor–acceptor structure. *Chemical Communications*. 2012;48(77):9580–9582. doi:10.1039/C2CC31468A
- [6] Nakagawa T, Ku S-Y, Wong K-T, Adachi C. Electroluminescence based on thermally activated delayed fluorescence generated by a spirobifluorene donor–acceptor structure. *Chemical Communications*. 2012;48(77):9580–9582. doi:10.1039/C2CC31468A
- [7] Michler GH. *Electron Microscopy of Polymers*. Springer Science & Business Media; 2008.
- [8] Phelipot J, Ledos N, Dombrey T, Duffy MP, Denis M, Wang T, Didane Y, Gaceur M, Bao Q, Liu X, et al. Highly Emissive Layers based on Organic/Inorganic Nanohybrids Using Aggregation Induced Emission Effect. *Advanced Materials Technologies*.:2100876. doi:10.1002/admt.202100876
- [9] P. Brunkov Organic light-emitting diodes based on polyvinylcarbazole films doped with polymer nanoparticles | *Physics of the Solid State*, 2013 Vol. 55, No. 3, pp. 675–680. © Pleiades Publishing, Ltd., [accessed 2022 Jan 3]. DOI: 10.1134/S1063783413030037
- [10] Gupta BK, Kedawat G, Kumar P, Rafiee MA, Tyagi P, Srivastava R, Ajayan PM. An n-type, new emerging luminescent polybenzodioxane polymer for application in solution-processed green emitting OLEDs. *Journal of Materials Chemistry C*. 2015;3(11):2568–2574. doi:10.1039/C4TC02581D
- [11] Deepak KumarDubey. Solution Process Feasible Highly Efficient Organic Light Emitting Diode with Hybrid Metal Oxide Based Hole Injection/Transport Layer | *Organic Electronics* Volume 69, June 2019, Pages 232-240. [accessed 2022 Jan 3]. <https://doi.org/10.1016/j.orgel.2019.03.001>
- [12] Duan L, Hou L, Lee T, Qiao J, Zhang D, Dong G, Wang L, Qiu Y. Solution processable small molecules for organic light-emitting diodes. *J. Mater. Chem*. 2010;20. doi:10.1039/B926348A
- [13] Wang Y-M, Teng F, Zhou Q-C, Wang Y-S. Multiple roles of bathocuproine employed as a buffer-layer in organic light-emitting diodes. *Applied Surface Science - APPL SURF SCI*. 2006;252:2355–2359. doi:10.1016/j.apsusc.2005.04.006

- [14] Liu J. Deep-blue efficient OLED based on NPB with little efficiency roll-off under high current density. *Applied Physics A* volume 123, Article number: 191 (2017). 2017. doi:10.1007/S00339-017-0840-6
- [15] Lian J, Liu Y, Niu F, Zeng P. Improved electron injection of OLEDs with a thin PBD layer at Alq3/Cs2CO3 interface *Applied Surface Science* Volume 257, Issue 10, 1 March 2011, Pages 4608-4611. 2011. doi:10.1016/J.APSUSC.2010.12.092
- [16] Duan L, Wang G, Duan Y, Lei D, Qian F, Yang Q. Design Simulation and Preparation of White OLED Microdisplay Based on Microcavity Structure Optimization. *Journal of Spectroscopy*. 2021;2021:e5529644. doi:10.1155/2021/5529644
- [17] Chatterjee T, Wong K-T. Perspective on Host Materials for Thermally Activated Delayed Fluorescence Organic Light Emitting Diodes. *Advanced Optical Materials*. 2019;7(1):1800565. doi:10.1002/adom.201800565
- [18] Zheng C-J, Zhao W-M, Wang Z-Q, Huang D, Ye J, Ou X-M, Zhang X-H, Lee C-S, Lee S-T. Highly efficient non-doped deep-blue organic light-emitting diodes based on anthracene derivatives. *Journal of Materials Chemistry*. 2010;20(8):1560–1566. doi:10.1039/B918739A
- [19] Aleshin AN, Sokolovskaya AD, Shcherbakov IP, Brunkov PN, Ulin VP. Organic light-emitting diodes based on polyvinylcarbazole films doped with polymer nanoparticles. *Physics of the Solid State*. 2013;55(3):675–680.
- [20] Gong J-R, Wan L-J, Lei S-B, Bai C-L, Zhang X-H, Lee S-T. Direct Evidence of Molecular Aggregation and Degradation Mechanism of Organic Light-Emitting Diodes under Joule Heating: an STM and Photoluminescence Study. *The Journal of Physical Chemistry B*. 2005;109(5):1675–1682. doi:10.1021/jp046509o
- [21] Lee JY, Kim J, Kim H, Suh MC. Molecular Stacking Effect on Small-Molecular Organic Light-Emitting Diodes Prepared with Solution Process. *ACS Applied Materials & Interfaces*. 2020;12(20):23244–23251. doi:10.1021/acsmi.0c06597
- [22] Tang CW, VanSlyke SA. Organic electroluminescent diodes. *Applied Physics Letters*. 1987;51(12):913–915. doi:10.1063/1.98799
- [23] Gloria Hong & al. A Brief History of OLEDs—Emitter Development and Industry Milestones - - 2021 - *Advanced Materials* - 33, 2005630. [accessed 2022 Jan 3]. <https://doi.org/10.1002/adma.202005630>.
- [24] Tang CW, VanSlyke SA, Chen CH. Electroluminescence of doped organic thin films. *Journal of Applied Physics*. 1989;65(9):3610–3616. doi:10.1063/1.343409
- [25] Sujith Sudheendran Swayamprabha, & al. Approaches for Long Lifetime Organic Light Emitting Diodes - *Advanced Science* - Volume8, Issue1 January 6, 2021 2002254. [accessed 2022 Jan 3]. doi.org/10.1002/advs.202002254
- [26] D'Angelo P, Barra M, Cassinese A, Maglione MG, Vacca P, Minarini C, Rubino A. Electrical transport properties characterization of PVK (poly N-vinylcarbazole) for electroluminescent devices applications. *Solid-State Electronics*. 2007;51(1):123–129. doi:10.1016/j.sse.2006.11.008

# Chapter 4: Co-grafting of several emitters on nanocrystals, towards white emission

## 1) Elaboration of white emissive nanohybrids in solution

In the previous chapter, different organic emitters were widely studied and selected as candidates in order to generate a white emission in further LED device. Thus, the molecules B, G and R were chosen. Principally, it exists two kinds of white light, a warm white which is illustrated by a yellow-white emission (night mode screen in smartphone) [1, 2], or a cold white illustrated by a blue-white color (TV, car flares, computer screens...) [2, 3]. The color coordinates are often described in literature by CIE diagram and Kelvin unit. There are many methods which can be applied to obtain white light emission. The state of the art chapter mentioned the different approaches to achieve a white LED device. For instance, in literature, it is often reported that a consecutive stacking of single blue, single green and single red electroluminescent layers may be built [4, 5]. Another regular and widely used method is the simultaneous co-evaporation of different organic emitters, in OLED for example, but these approaches remain complicated, costly and hard to process [6, 7]. Indeed, the co-evaporation of small molecules at the same time gives high quality of layers, but it requires high energy and technology for a deep vacuum level. The solution approach is much easier and suitable, but with a drop of quality compare to the evaporated process. Indeed, for QDLED technology, white electroluminescent devices are built by the mixing of single red, green and blue QDs in a same solution [8], however this technology is used so far as photoluminescent layer and not electroluminescent one. The creation of white light requires deep study of the amount of blue, green and red emitters. Usually, the blue emitter are predominant in front of the green and the red one, but it depends also on their respective PLQY and electroluminescence properties. In this chapter is presented a solution processable white electroluminescent material, which opens the way for further and easier large scale production. Therefore, we focused on two methods to obtain white LED devices :

- combination of nanohybrids  $N^B$  and  $N^R$  with OA treatment in the matrix M
- combination of nanohybrids  $N^B$ ,  $N^G$  and  $N^R$  with OA treatment in the matrix M

The new nanohybrids formed are then named such as  $N^{B^X/G^Y/R^Z}$  with X = a.u. of incorporated B; Y = a.u. of G ; Z = a.u. of R emitters. This notation will help to clearly see the volume ratios of the different emitters in the nanohybrids sample. The experimental section gives a Table

with the corresponding mass of the different quantities used for the building of the new nanohybrids. Experimentally, the host matrix M solution is still prepared using a mass ratio 2:1 = PVK:OXD, and the ZnO is added at 10% w / w (related to PVK) to the luminescent solution. Separately, the organic emitters are combined together and, after a while, added to the M:ZnO solution. Thus, the self assembly takes place under stirring and heating the solution at 80 °C. Once the luminescent solution becomes more clear, the OA is added at 0.2% v/v, and the solution is then ready to be processed as thin film. The thickness of the electroluminescent layer remains the same as in chapter 3, namely 50 nm. The different architectures presented in this chapter are illustrated in the figure 1.

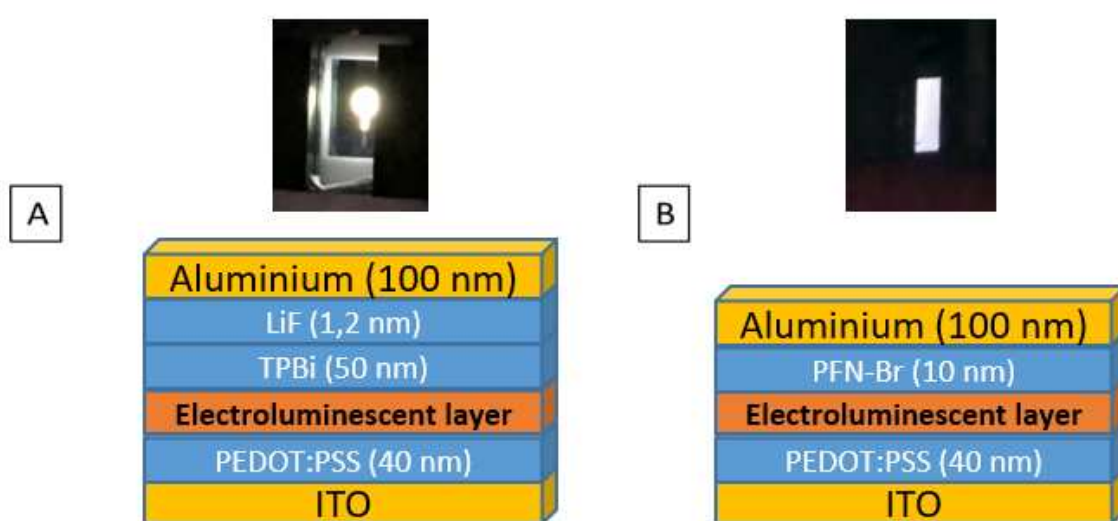


Figure 1: Architecture of the white LED A) with evaporated electron injection layers B) with solution processable electron injection layers.

As figure 1 shows, in this part, different electron injection layers are tried, namely evaporated TPBi and LiF [9, 10], and one solution processed Poly(9,9-bis(3'-(N,N-dimethyl)-N-ethylammonium-propyl-2,7-fluorene)-alt-2,7-(9,9-dioctylfluorene))dibromide referred as PFN-Br [11, 12] which are both widely used in literature for OLED device fabrication. Thus, the influence of the interfacial layers will be studied.

## 2) Matrix M combined with two or three emissive nanohybrids

### i) White LED devices using TPBi and LiF as electron transport material

#### ZnO Co-grafting with 2 emitters in the matrix M:

A serie of white LEDs was done with 10% w / w of ZnO in the matrix, with various quantities of B and R molecules, thus giving two different nanohybrids in M, namely N<sup>B</sup> OA and N<sup>R</sup> OA. The main goal was to obtain a white LED and to investigate the electrical and the luminous performances according to the different nanohybrid compositions incorporated in the matrix M. In this serie, two B quantities were fixed, namely 40 or 50, and variations of R were done from 3 to 25, thus giving the volume ratio of these emitters. These performances are presented by the Table 1 and the corresponding figure 3. The precise measure of the emitted color was recorded with working LED device at 50 mA/cm<sup>2</sup> thanks to the CIE Diagram and the associated coordinates.

Table 1: performances of white LEDs done with two nanohybrids N<sup>B</sup> OA and N<sup>R</sup> OA in the matrix M, with their CIE coordinates recorded at 50 mA/cm<sup>2</sup>.

LED name	M:N <sup>B40/R3</sup> :OA	M:N <sup>B40/R7</sup> :OA	M:N <sup>B50/R8</sup> :OA	M:N <sup>B50/R25</sup> :OA
EQE (%)	0,8	0,64	0,81	0,82
Lum. eff. (Cd/A)	2,01	1,56	2,00	1,97
Voltage (V)	5,0	7,0	5,5	5,5
CIE (x,y)	0,395 0,434 ✖	0,408 4,35 ✖	0,416 0,443 ✖	0,43 0,45 ✖

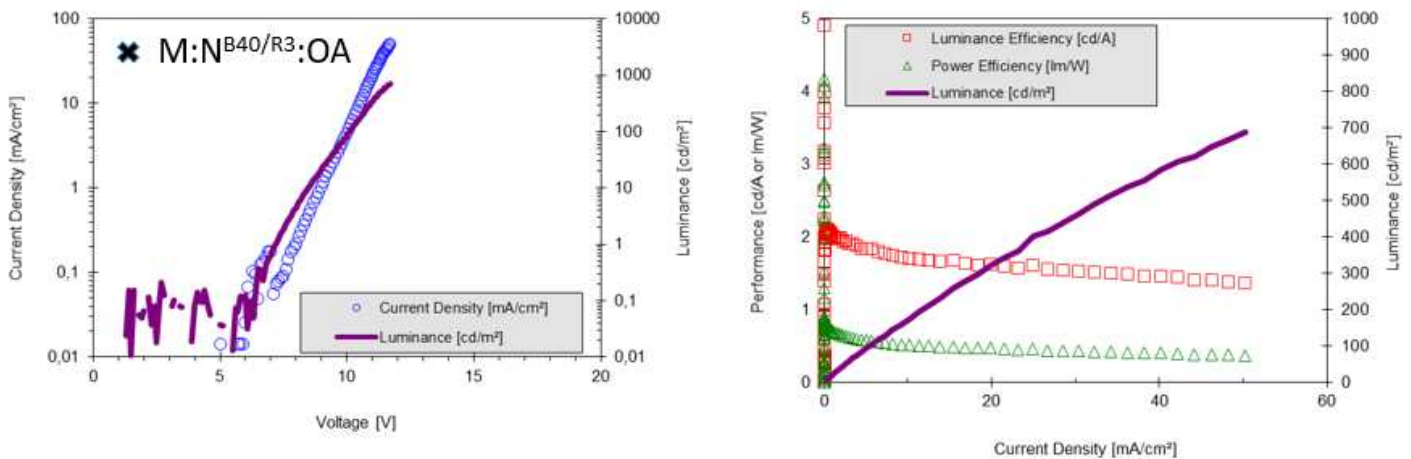


Figure 3: A) JVL curve B) Performances cd/A and lm/W with current density mA/cm<sup>2</sup> and luminance in cd/m<sup>2</sup> of M:N<sup>B40</sup>/R3:OA

First of all, it is observed that the serie of white LED with 2 nanohybrid emitters in matrix M are very reproducible and the different tried compositions gave close emission spectra and performances. Indeed, the EQE is at 0.8 % for all the LEDs. Only the M:N<sup>B40</sup>/R7:OA presents a slightly lower EQE = 0.64 % but it can be explained by the presence of inhomogeneities in its active area. Indeed, the threshold voltage is noted at 7.0 volts, while for the other electroluminescent layer compositions, only 5.0 volts threshold voltage is noted. On another hand, the luminance efficiency measured is close to 2.00 cd/A for all the compositions. The maximum luminance value recorded was 700 cd/m<sup>2</sup> at 50 mA/cm<sup>2</sup>, even though in the literature, it is often found values that can reached 100,000 of cd/m<sup>2</sup> in OLED devices [13, 14]. The obtained performances in Table 1 are then not the best of the literature but it is in the range of the 1<sup>st</sup> generation OLED devices. [13, 15]

On another hand, as the main goal was to obtain white LED, the CIE coordinates were investigated. Comparing from M:N<sup>B40</sup>/R3:OA to M:N<sup>B40</sup>/R7:OA, the coordinates shift a little bit from (x = 0.395 y = 0.434) to (x = 0.408 y = 0.435), which are both in the warm white area, close to the border with the greenish yellow area (figure 6 CIE diagram). For B = 50, bigger R variation was done, from R = 8 to R = 25. Therefore, the noted CIE coordinates for M:N<sup>B50</sup>/R8:OA were (x = 0.416 y = 0.443) while for M:N<sup>B50</sup>/R25:OA were measured (x = 0.43 y = 0.45), the corresponding color for both being even closer of the borderline with the greenish yellow area. As expected, adding more R emitter in the hybrid composition leads to a shift in the device emission, toward the warm colors. Therefore, in order to obtain a purer white color (ideally CIE x = 0.35 y = 0.35), the emitter R was kept constant at R = 3 while the emitter B was decreased from 40 to 20. Their performances are displayed over the Table 2 and the Figure 4.

Table 2: performances of white LEDs done with two nano hybrids  $N^B$  OA and  $N^R$  OA in the matrix M, with their CIE coordinates recorded at 50 mA/cm<sup>2</sup>.

LED name	M:N <sup>B20</sup> /R <sup>3</sup> :OA	M:N <sup>B40</sup> /R <sup>3</sup> :OA
EQE (%)	0,69	0,8
Lum. eff. (Cd/A)	1,75	2,01
Voltage (V)	5,0+	5,0
CIE (x,y)	0,376 0,426 ✘	0,395 0,434 ✘

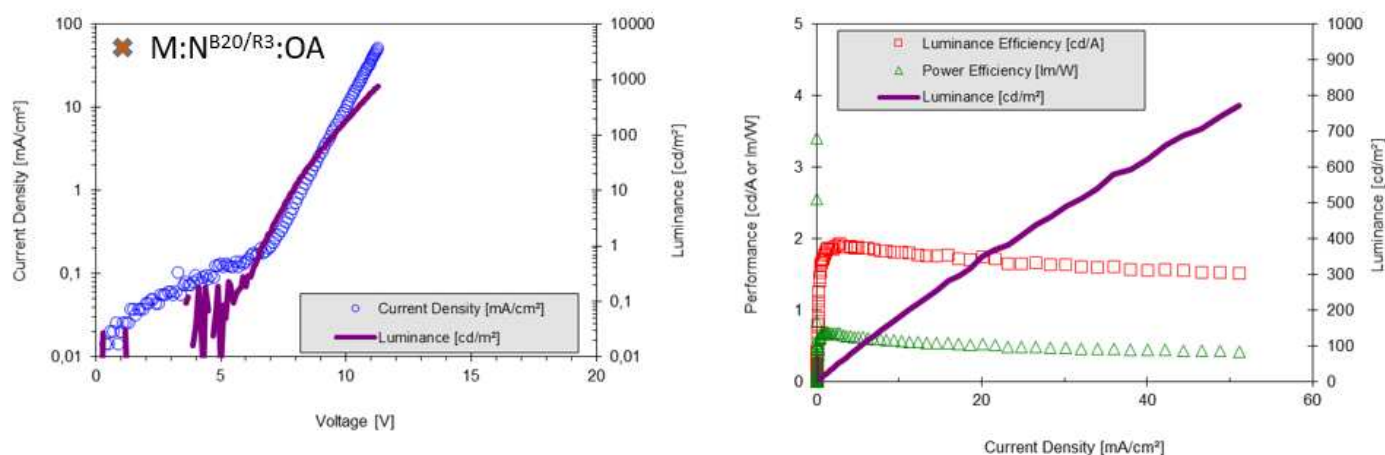


Figure 4: A) JVL curve B) Performances cd/A and lm/W with current density mA/cm<sup>2</sup> and luminance in cd/m<sup>2</sup> of M:N<sup>B20</sup>/R<sup>3</sup>:OA

As previously mentioned, the M:N<sup>B40</sup>/R<sup>3</sup>:OA electroluminescent layer used in LED presents a quite low threshold voltage of 5.0 volts. By decreasing the amount of B molecule from 40 to 20 it leads to slightly lower performances as the ones observed in the Table 1, namely an EQE = 0.69 %, luminance efficiency of 1.75 cd/A and a threshold voltage of 5.0 volts. Nevertheless, the Figure 4A show in the JVL curve that before the working tension, there are some small leakage current about 0.05 to 0.1 mA/cm<sup>2</sup> indicating the presence of possible rough active surface, and explaining the small drop of performances in comparison with the other LEDs shown in the table 1.

As comparison, the datas presented in the chapter 3 regarding the blue and red (as single) emitters in devices, gave similar threshold voltage values, around 5 volts. Moreover, the maximum EQE value recorded for blue and green hybrid LEDs were respectively EQE<sub>maxB</sub> = 0.44 %; EQE<sub>maxR</sub>=0.60 %. Therefore, it is concluded that the combination of both nano hybrid emitters in the matrix M leads to more efficient LED devices, in addition to shine white (without exceeding the ratio 1:3, to 1:4 for instance).

Concerning the emitted color, the decrease of the B amount in the luminescent solution leads to a small shift toward the center of the white area. Indeed, the CIE coordinates goes from  $x = 0.395$   $y = 0.434$  (M:N<sup>B40/R3</sup>:OA) to  $x = 0.376$   $y = 0.426$  (M:N<sup>B20/R3</sup>:OA), which is in between the center white and the yellow green area. By adding less nanohybrids (N<sup>R</sup> OA or N<sup>B</sup> OA) in matrix M, it cannot be excluded that the matrix M participates more intensely to the electroluminescence emission, leading to a shift toward the smaller wavelengths / CIE coordinates.

### ZnO Co-grafting with 3 emitters in the matrix M:

Even if the previous LEDs with 2 nanohybrids emitters in the matrix M over table 1 and 2 are in the same CIE diagram area, the proof of concept for (warm) white LED using nanohybrids was realized. The following figure 5 and table 3 present performances of LED with 3 nanohybrids emitters incorporated to the matrix M, namely N<sup>B</sup> OA, N<sup>G</sup> OA and N<sup>R</sup> OA. The goal is to prove that it is possible to achieve white LED by, in theory, the co-grafting of 3 emitters (BGR) on the surface of ZnO nanoparticle. The first tried luminescent solution used to build a LED device was chosen arbitrarily as M:N<sup>B30/G6/R14</sup>:OA, and then, according to the emitted color, the quantities of the 3 emitters were adjusted. Indeed, because the previous LEDs without the emitter G were close to the yellow green area, and because the N<sup>G</sup> material is much more electroluminescent than N<sup>B</sup> and N<sup>R</sup> (cf. chapter 3), the quantity of G was then fixed at 1. Thus, the other compositions are M:N<sup>B50/G1/R6</sup>:OA, M:N<sup>B60/G1/R8</sup>:OA and M:N<sup>B40/G1/R5</sup>:OA. First of all, it is observed that the performances in Table 3 are lower than the combination of matrix M with two emitters. The quality of the layers was good but maybe containing more aggregates or bigger objects, or probably because of the grafting competition between all the molecules (BGR) on the ZnO surface. Even for the best composition M:N<sup>B40/G1/R5</sup>:OA in figure 5A, it is observed a considerable leakage current below 1 mA/cm<sup>2</sup>, probably due to aggregates presence in the active area of the device. Consequently, higher threshold voltages were generally observed between 6.0 and 7.0 volts, with EQEs from 0.6 to 0.73 % (while it was previously 5.0 volts as working tensions and 0.8 % EQEs for the combination of matrix M with two nanohybrid emitters). As comparison, the most optimized LED using single nanohybrid green emitter in the matrix M, presented threshold voltage about 4.0 volts for EQE = 1.35 %, while 5.0 volts for blue and red emitters with respectively EQE = 0.44 % and 0.60 % (cf. chapter 3).

Table 3: performances of white LEDs done with three nanohybrids  $N^B$  OA;  $N^G$  OA;  $N^R$  OA in the matrix M, with their CIE coordinates recorded at 50 mA/cm<sup>2</sup>.

LED name	M:N <sup>B30/G6/R14</sup> :OA	M:N <sup>B50/G1/R6</sup> :OA	M:N <sup>B60/G1/R8</sup> :OA	M:N <sup>B40/G1/R5</sup> :OA
EQE (%)	0,62	0,63	0,60	0,73
Lum. eff. (Cd/A)	1,67	1,68	1,61	1,86
Voltage (V)	7,0	6,5	7,0	6,0
CIE (x,y)	0,456 0,479 <span style="color:blue">●</span>	0,415 0,467 <span style="color:yellow">●</span>	0,440 0,466 <span style="color:green">●</span>	0,383 0,445 <span style="color:white">●</span>

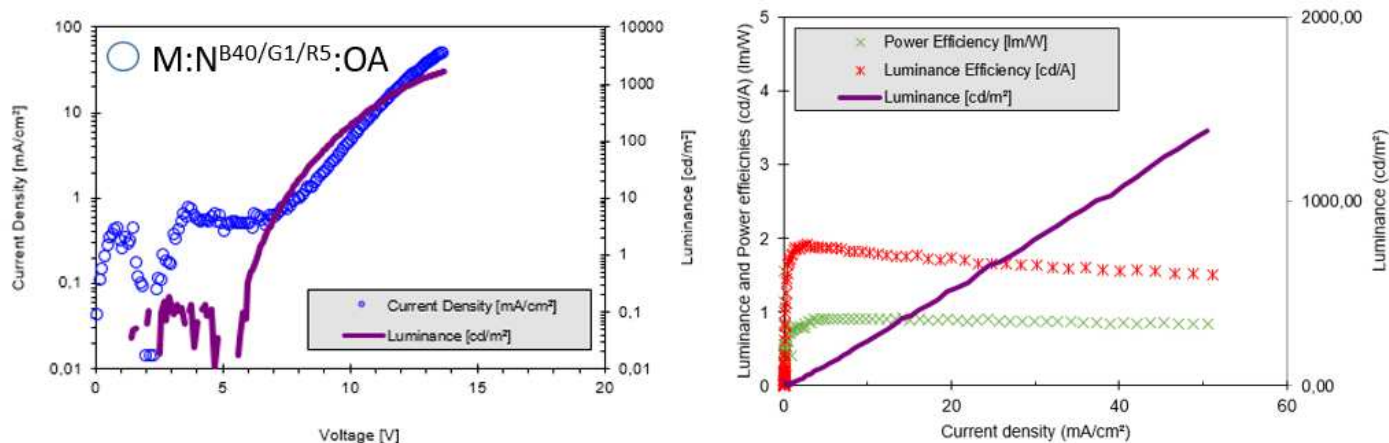


Figure 5: A) JVL curve B) Performances cd/A and lm/W with current density mA/cm<sup>2</sup> and luminance in cd/m<sup>2</sup> of M:N<sup>B40/G1/R5</sup>:OA

Thanks to CIE coordinates, it was shown that the first composition M:N<sup>B30/G6/R14</sup>:OA was emitting too much in the yellow area ( $x = 0.456$   $y = 0.479$ ), as expected. The same was observed for M:N<sup>B60/G1/R8</sup>:OA, with associated CIE ( $x = 0.440$   $y = 0.466$ ). The other compositions containing less G and R emitters are closer to the white color but still too much present in the yellow-green area. For instance, the best composition with 3 nanohybrid emitters is M:N<sup>B40/G1/R5</sup> with associated CIE ( $x = 0.383$   $y = 0.445$ ). As figure 6 shows, it is just at the border between white and yellow green colors. In the end, it is assumed that the control of the light may be harder with three nanohybrid emitters than two, as far as molecule G is far too emissive in the green region, even at very low concentration.

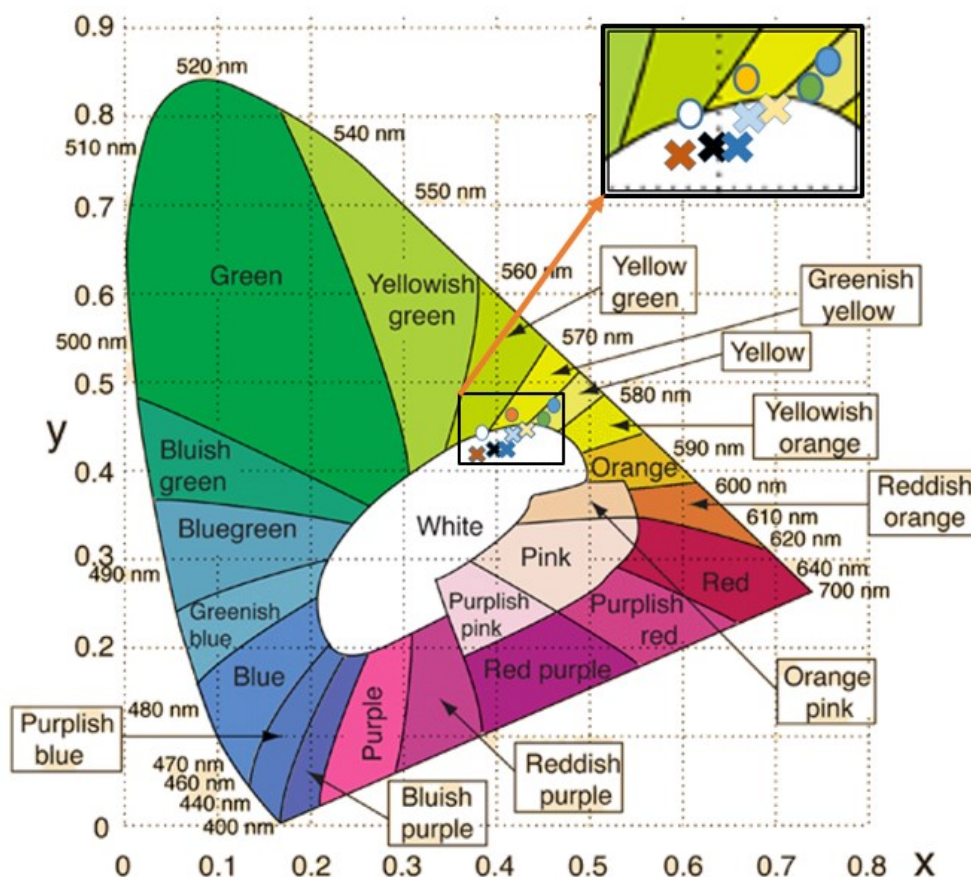


Figure 6: CIE diagram associated to Table 1, 2 and 3, cross =  $M + 2$  nano hybrids emitters; circle =  $M + 3$  nano hybrids emitters.

To sum up, it is concluded that solution processable warm white LEDs were achieved by co-grafting two or three emissive organic molecules on ZnO surface added together in the matrix M. The reproducibility was good enough and homogeneous light was obtained over the whole active area of the device. However, only the warm white was achieved with this device architecture (figure 1A). Further advanced experiments are required in order to generate a very pure white LED, or a colder white LED. The influence of the electron interfacial layer and the choice of the matrix are investigated in the following parts.

## ii) Optical analyzes of $M:N^{B40/R3}:OA$ films:

An electroluminescent film of  $M:N^{B40/R3}:OA$  was coated on glass substrate in order to analyze its photoluminescence property when excited at 350 nm (thus on the matrix M and  $N^B$  main absorbance peak) to create an absorption / emission cascade. The same film was used and presented as warm white LED device in the upper part, when its electroluminescence spectrum

was recorded at 50 mA/cm<sup>2</sup>. The comparison between photoluminescence and electroluminescence spectra is presented by the Figure 7.

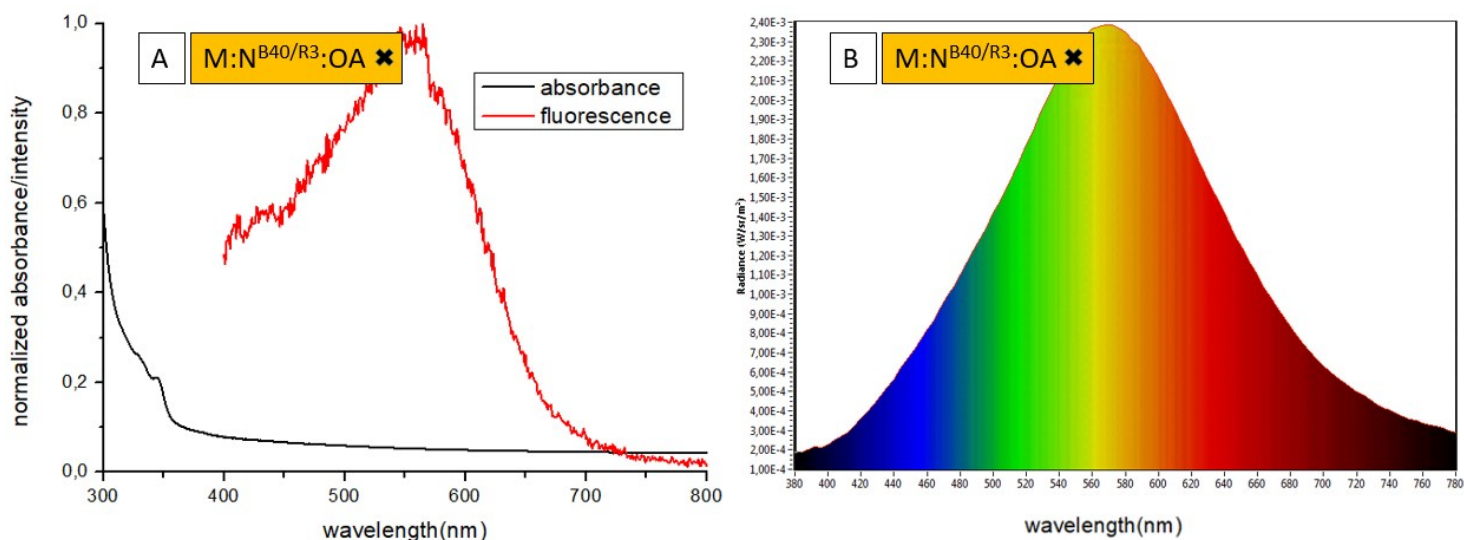


Figure 7: A) absorbance and fluorescence (excited at 350 nm) of M:N<sup>B40/R3</sup>:OA film, B) associated electroluminescence radiance spectrum of LED containing M:N<sup>B40/R3</sup>:OA as electroluminescent layer recorded at 50 mA/cm<sup>2</sup>.

The figure 7A shows a photoluminescence spectrum from 400 to 750 nm with a high dominant part in the warm colors. The electroluminescence spectrum shows a broad emission area from 400 to 780 nm, with also a dominant part in the warm colors. This confirms the recorded CIE coordinates of the warm white M:N<sup>B40/R3</sup>:OA film used in LED.

### iii) Morphology of M:N<sup>B40/R3</sup> films:

The morphology of the same electroluminescent films composed of M:N<sup>B40/R3</sup> was investigated by TEM images on holey grid in figure 8. The comparison is done with and without OA treatment of the solution.

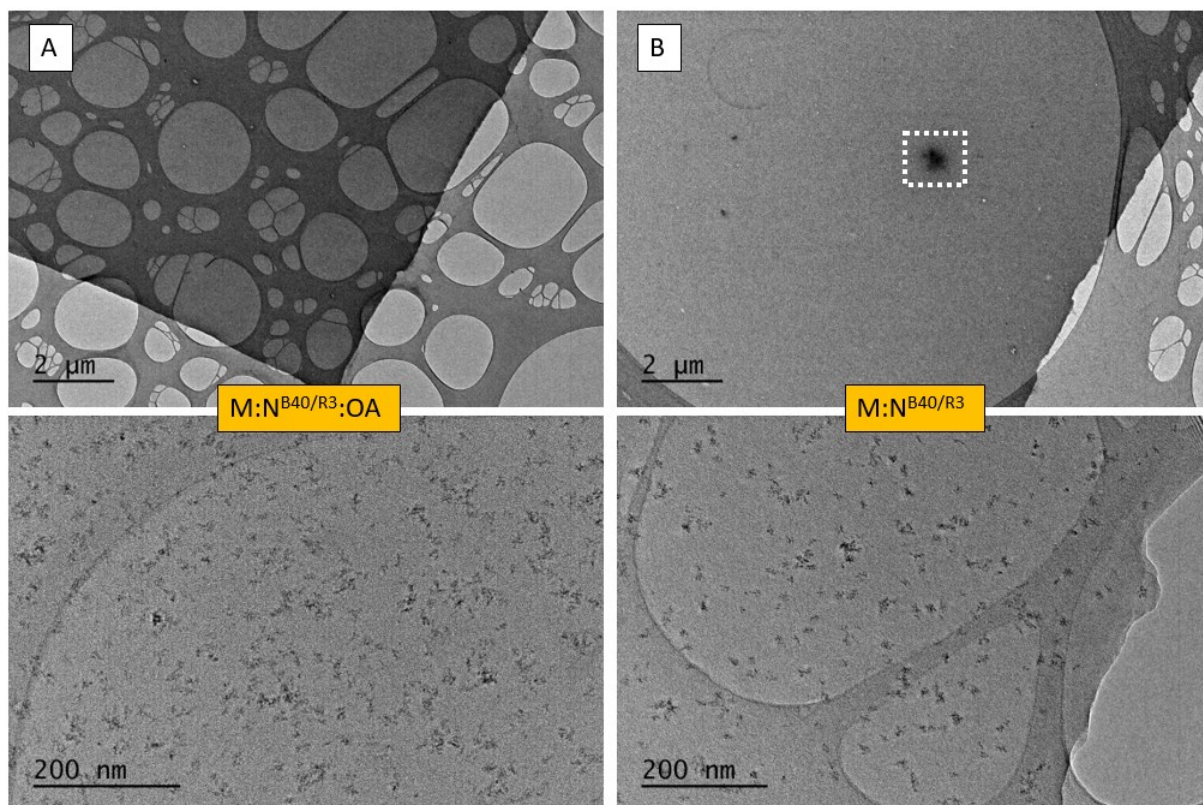


Figure 8: TEM images on holey grid of the thin films composed of A)  $M:N^{B40/R3}:OA$  B)  $M:N^{B40/R3}$  (films obtained by floating layer technic).

On the film without OA treatment, the image at 2  $\mu\text{m}$  scale on the figure 8B shows the presence of aggregate over 500 nm (white dotted squares). At 200 nm scale, no aggregate was found and the spreading of the nanohybrids in the matrix M seems quite homogeneous. This may be attributed to the good surface affinity between emitter R and ZnO nanoparticle, which was demonstrated in chapter 3 as smooth and homogeneous, even without OA treatment. On another hand, with OA treatment in the luminescent solution, the corresponding film did not present any cluster formation at 2  $\mu\text{m}$  scale (Figure 8A). Moreover, the magnification shows better spread nanohybrids in the matrix M in comparison with  $M:N^{B40/R3}$ . It is concluded that the OA treatment is still required to obtain better surface morphology and is more suitable for further efficient LED devices.

iv) Morphology of  $M:N^{B120/G1/R5}$  films:

The morphology of electroluminescent films composed of  $M:N^{B120/G1/R5}$  was investigated by TEM images on holey grid in figure 9. Again, the comparison is done with and without OA treatment.

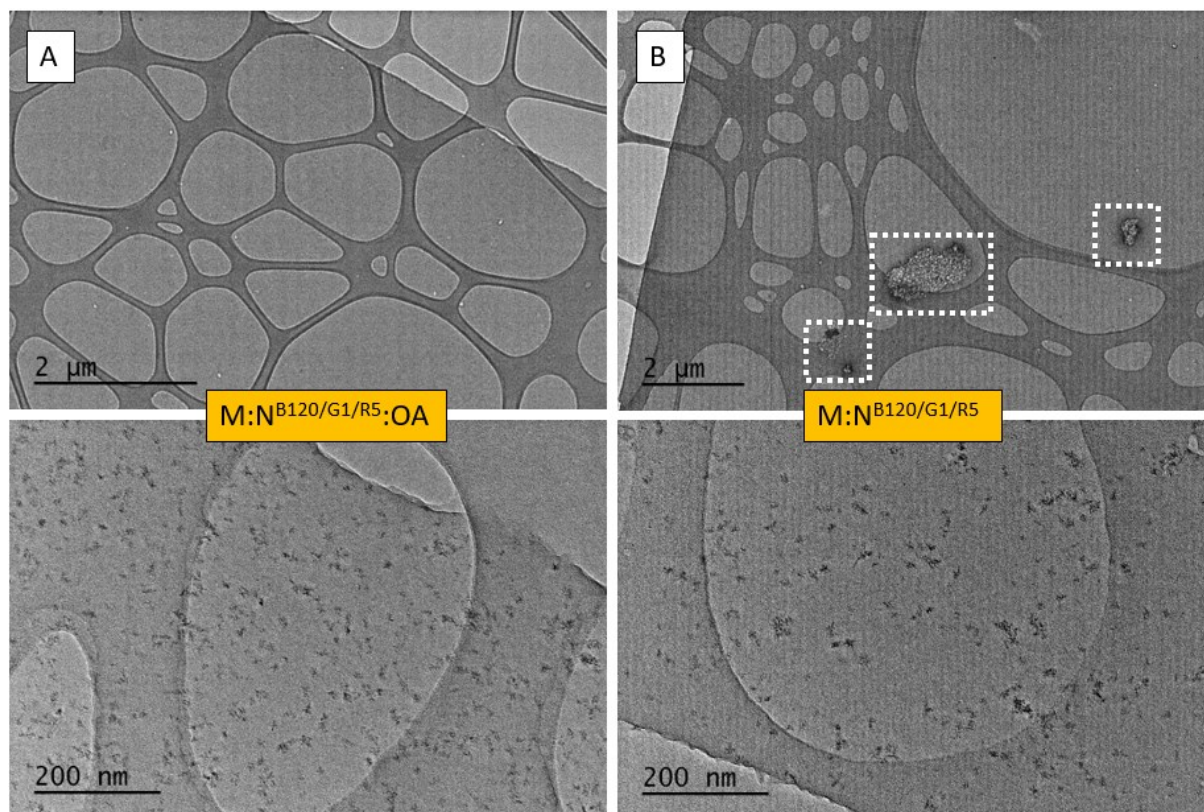


Figure 9: TEM images on holey grid of the thin films composed of A)  $M:N^{B120/G1/R5}·OA$  B)  $M:N^{B120/G1/R5}$

On the film without OA treatment, in opposite with the electroluminescent layer composed of 2 nanohybrid emitters incorporated at 10% in the matrix M, it seems that with 3 emitters in the matrix M the cluster formation is more important. Indeed, as presented by the figure 9B at 2  $\mu\text{m}$  scale, the presence of aggregates over 2  $\mu\text{m}$  is detected (white dotted squares), and when the scale was decreased to 200 nm, the nanohybrids form also small clusters of 10 to 30 nm. Nevertheless, the OA treatment presented in Figure 9A shows a very smooth morphology without any aggregate detected at 2  $\mu\text{m}$  scale. In addition, at 200 nm scale, the small nanohybrid clusters seem to be better dispersed in the matrix M. In conclusion, with three nanohybrid emitters in the matrix M, it is again highly recommended to use OA treatment in order to have more suitable electroluminescent layer for LED device.

### 3) Matrix F (F8:F8BT) combined with two emissive nanohybrids

Previously, all the characterizations were done with M (PVK:OXD) host matrix, but the (F8:F8BT) matrix referred as F, is also briefly studied in this chapter using the figure 1A architecture. The mass ratio of F8:F8BT is 19:1 for a total of 10 mg / mL luminescent solution [16]. The matrix F is a green emitter, also widely used in OLED literature, and is a combination of two polymers from 1<sup>st</sup> generation OLED (fluorescent polymers) when both materials (F8 and F8BT) are associated [16–20]. The green F matrix is therefore much more efficient in electrical and luminance properties in comparison with blue M matrix. However, because the F matrix strongly emits in the green area, the 10% incorporated nanohybrids were N<sup>B</sup> OA and N<sup>R</sup> OA, as far as N<sup>G</sup> OA emission is replaced by F matrix, thus hiding the nanohybrids emission (which was not the case of the M matrix). Indeed, the M matrix is more transparent regarding the nanohybrid emission as far as it emits in the deep blue region and the transport properties are weaker than F matrix. The chemical structures of F8 and F8BT are illustrated in the figure 2.

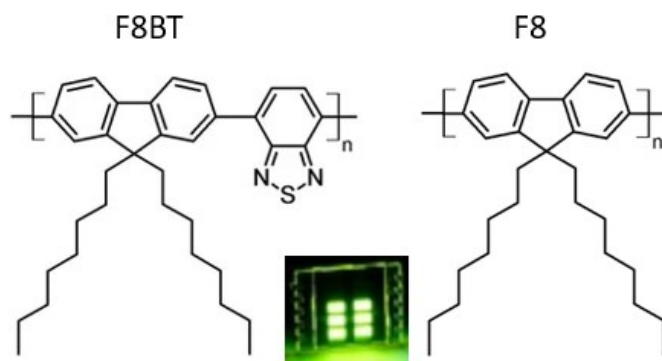


Figure 2: F8BT and F8 chemical structures leading to F matrix, shining in green light emitting diode with ITO/PEDOT:PSS/TFB/F8BT/F8imBT-Br\*/Ca/Al [16, 20]

#### i) ZnO Co-grafting with 2 emitters in the matrix F:

As for matrix M, a serie of theoritical white LEDs was done with 10% w / w of ZnO with various quantities of B and R molecules, thus giving two different nanohybrids in F, namely F:N<sup>B</sup>:OA and F:N<sup>R</sup>:OA. The main goal was to obtain a white LED and to investigate the electrical and the luminous performances according to the different nanohybrid compositions incorporated in the matrix F. In this serie, two B quantities were tried, namely 100 or 50, with two amounts of R from 80 to 25, together with ZnO, OA and the matrix F. The last device on the right of the

Table 4 (F:N<sup>B50/R25</sup>:OA), contains an electroluminescent layer which is twice thicker than the regular F:N<sup>B50/R25</sup>:OA, in order to see the influence on the electroluminescence properties. These performances are presented by the Table 4 and the corresponding figure 10.

Table 4: performances of white LEDs done with three nanohybrids N<sup>B</sup> OA; N<sup>R</sup> OA in the matrix F, with their CIE coordinates recorded at 50 mA/cm<sup>2</sup>.

LED name	F:N <sup>B100/R80</sup> :OA	F:N <sup>B50/R25</sup> :OA	F:N <sup>B50/R25</sup> :OA*
EQE (%)	0,04	1,71	0,86
Lum. eff. (Cd/A)	0,96	5,10	3,48
Voltage (V)	8+	6,0	14+
CIE (x,y)	0,41 0,544 ▲	0,324 0,447 ▲	0,305 0,370 ▲

\* = twice thicker

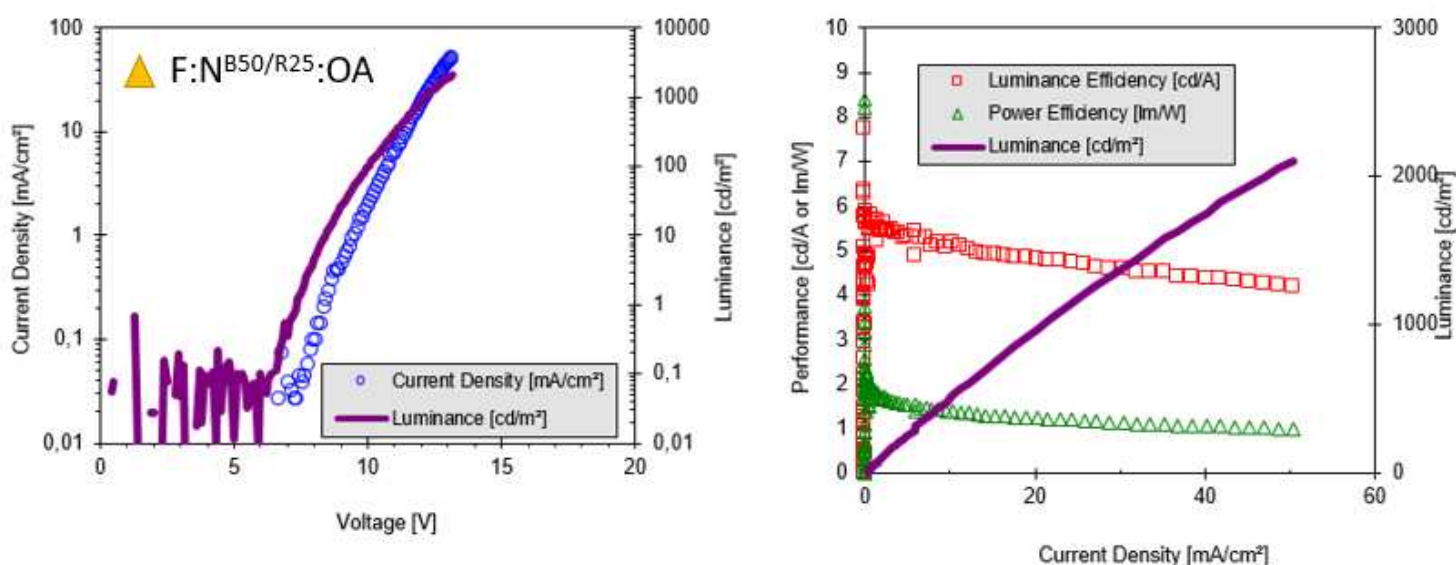


Figure 10: A) JVL curve B) Performances cd/A and lm/W with current density mA/cm<sup>2</sup> and luminance in cd/m<sup>2</sup> of F:N<sup>B50/R25</sup>:OA

According to the table 4, the device performances varied a lot from F:N<sup>B100/R80</sup>:OA to F:N<sup>B50/R25</sup>:OA. Indeed, the first cause which explains the difference is the surface morphology which was not as good as with the matrix M. Indeed, the device done with F:N<sup>B100/R80</sup>:OA electroluminescent layer contains large aggregates leading to leakage current and electrical problem. The recorded performances are then very low, EQE = 0.04 %; threshold voltage of 8 volts and luminous efficiency of 0.96 cd/A. The device using F:N<sup>B50/R25</sup>:OA contains less

emitters and more homogeneous layers could be obtained. However, by comparing the devices done with  $F:N^{B50/R25}:OA$  and  $F:N^{B50/R25}:OA$  (twice thicker), logically the threshold voltages increased from 6 to 14 volts, with a significant drop in performances as predicted by literature [21, 22]. Indeed, the EQE for the thinner electroluminescent layer was 1.71 % and dropped to 0.86 % when the thickness was twice higher. In addition, the F matrix gives higher EQE performances as predicted in comparison with M matrix, where the maximum EQE was measured for optimized  $M:(1:3)N_{10}^G:OA$ , close to  $EQE = 1.35 \%$ .

The translated CIE coordinates displayed in the Table 4 are illustrated by the figure 11, representing the  $F:N^{Bx/Rz}:OA$  devices at  $50 \text{ mA/cm}^2$  in CIE Diagram. It is observed that the composition  $F:N^{B100/R80}:OA$  electroluminescent layer used in device was very far from the white color, CIE ( $x = 0.41 \text{ } y = 0.544$ ), thus in the yellow green area. In addition, the active layer composition  $F:N^{B50/R25}:OA$  was still far from the center white, with CIE ( $x = 0.324 \text{ } y = 0.447$ ) in the yellowish green color. However, by getting twice thicker electroluminescent  $F:N^{B50/R25}:OA$  layer, the emitted color at  $50 \text{ mA/cm}^2$  is very close to the center white area, with CIE ( $x = 0.305 \text{ } y = 0.370$ ), and except the high threshold voltage noted at 14 volts, the performances are not so bad regarding the 1<sup>st</sup> generation OLEDs.

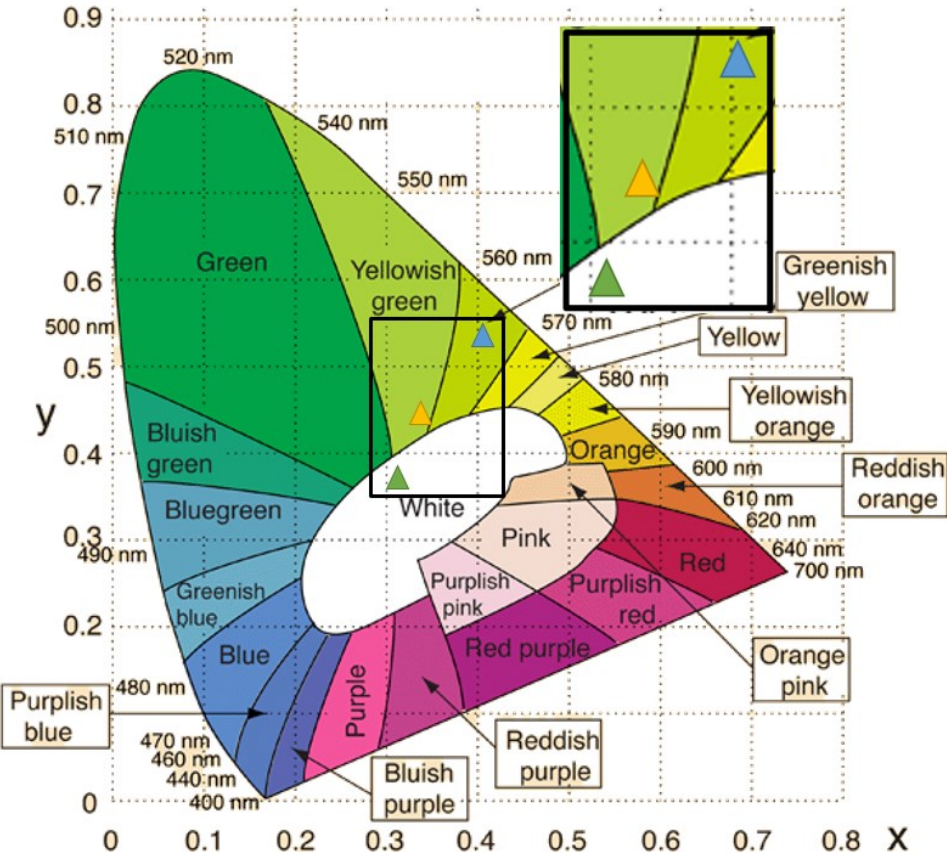


Figure 11: CIE diagram associated to Table 4, triangle = F + 2 nanohybrids emitters.

To sum up, it is concluded that solution processable white LEDs was achieved by co grafting two emissive organic molecules on ZnO surface together added in a more efficient matrix F. This time the reproducibility was medium (6 out of 10 samples) and highly depends on the quantity of mixed organic emitters with ZnO. It was also confirmed that the matrix F (green emitter) is much more efficient than matrix M (blue emitter), but consequently, the nanohybrids emission is hidden by the matrix F. On this serie of LEDs based on F:N:OA electroluminescent layer, it was concluded that the matrix F was the main emitter of the device, presenting a green emission. Even by adding important quantities of emitters B and R (respectively 100 and 80) within the matrix F, the emitted light is not further shifted to the white, but to the green area, in opposite with the LEDs based on M:N:OA. This may be assumed by the morphology of the layers based on F:N:OA, which contained large aggregates despite the OA treatment (see bellow). The charges are thus ineffectively injected from the matrix F to the nanohybrids, and the emission of the nanohybrids may be very low compared to the matrix F. To avoid this aggregation problem, it may be supposed that the twice thicker electroluminescent layer minimizes the loss of charges in N, but it induces a higher threshold voltage. Further advanced experiments are required in order to have a better control of the emitted light of the nanohybrids and the matrix F with lower threshold voltage values.

## ii) Morphology of F:N<sup>B50/R25</sup> films:

The morphology of electroluminescent films composed of F:N<sup>B50/R25</sup> was investigated by TEM images on holey grid in figure 12. The comparison is done with and without OA treatment.

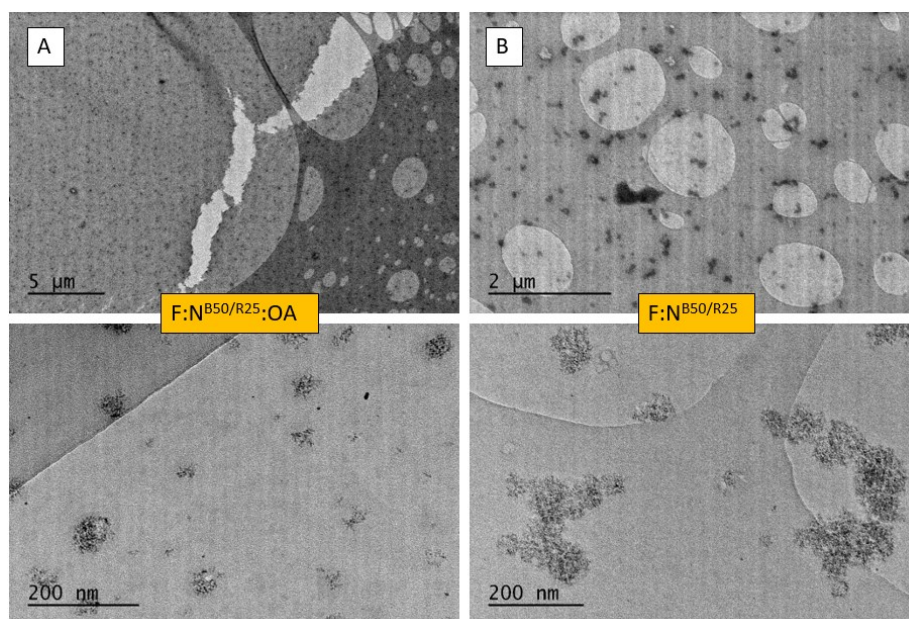


Figure 12: TEM images on holey grid of the thin films composed of A) F:N<sup>B50/R25</sup>:OA B) F:N<sup>B50/R25</sup>.

First of all, the performances displayed by LED using F:N<sup>B50/R25</sup>:OA as electroluminescent layer show medium reproducibility. In cause, the aggregates are present over the whole active area of the devices. The figures 12A/B at 5 and 2  $\mu\text{m}$  scales present high concentration of nanohybrid clusters in the film. The same observations were done at 200 nm scale. It is observed that the electroluminescent film which did not contain OA presented even bigger aggregates, namely 200 x 200 nm for F:N<sup>B50/R25</sup> and 40 x 40 nm for F:N<sup>B50/R25</sup>:OA. Interestingly, this is the first time that the OA treatment is only weakly efficient to disperse the nanohybrids. This treatment is therefore dependent from the host matrix used.

#### 4) SCLC mobility measurements

The SCLC devices were done at CINaM in collaboration with Dr. Payal Manzhi and Dr. Bernard Geffroy from LPICM, and the extraction of mobility from the measured JV curves (recorded from 0 to 10 volts) was done by Payal Manzhi and is presented in the following Table 5. The fabrication process and the associated device architectures are detailed in the experimental section. The measurement was based on the composition of the white electroluminescent layer, including either two or three nanohybrid emitters, with and without OA treatment included in the matrix M.

*Table 5: SCLC, Extracted hole and electron mobilities in  $\text{cm}^2/\text{Vs}$  for white electroluminescent layer, including either two or three nanohybrid emitters, JV curves recorded from 0 to 10 volts (R/G/B).*

Electrolum. material	Hole mobility ( $\text{cm}^2/\text{Vs}$ )	Electron mobility ( $\text{cm}^2/\text{Vs}$ )
M	$2 * 10^{-7} \text{ +/- } 5$	$5 * 10^{-5} \text{ +/- } 5$
M:N <sup>B40/R3</sup>	$9 * 10^{-9} \text{ +/- } 2$	$5 * 10^{-6} \text{ +/- } 2$
M:N <sup>B40/R3</sup> :OA	$3 * 10^{-8} \text{ +/- } 100$	$2 * 10^{-5} \text{ +/- } 1$
M:N <sup>B120/G1/R5</sup>	$3 * 10^{-9} \text{ +/- } 10$	$6 * 10^{-6} \text{ +/- } 3$
M:N <sup>B120/G1/R5</sup> :OA	$4 * 10^{-8} \text{ +/- } 100$	$1 * 10^{-5} \text{ +/- } 4$

In comparison with the pure matrix M, the M:N<sup>B40/R3</sup> and M:N<sup>B120/G1/R5</sup> electroluminescent materials have their hole mobilities which decreased by almost a factor 100, respectively  $9 * 10^{-9} \text{ cm}^2/\text{Vs}$  and  $3 * 10^{-9} \text{ cm}^2/\text{Vs}$ . Their electron mobilities also decreased by a factor 10 in comparison with the pure matrix M. In addition, the OA treatment was applied in these electroluminescent layers and led to various hole mobility values from  $10^{-6}$  to  $10^{-9} \text{ cm}^2/\text{Vs}$ ,

which could be attributed to the presence of aggregates in the active area. However, the electron mobilities of the electroluminescent layers which contained OA are close enough to the pure matrix M, in the range of  $10^{-5}$  cm<sup>2</sup>/Vs. According to the mobility results presented in the chapter 3 and in table 5, it may be assumed that adding more than one nanohybrid emitter in the matrix M leads to a drastic decrease of the hole mobility, while the electron mobility remained the same in comparison with the single matrix M. This behavior may explain the difficulties to obtain better performing devices when using several emitters at the same time, compared to the use of single emitter within the matrix M.

## 5) Effect of the interfacial layers

### i) ZnO Co-grafting with 2 emitters in the matrix M:

Chronologically, the first white LED devices were done with ZnO EtNH electron injection layer. The obtained results / colors from such devices are very close to the ones with evaporated TPBi / LiF electron injection materials: namely a warm white emission. In order to reach a cold white LED, the influence of this interfacial layer was investigated. Indeed, these two injection layers were replaced by solution processed PFN-Br. Therefore, a serie of white LED was done with two nanohybrids emitters (N<sup>B</sup> OA and N<sup>R</sup> OA) incorporated to the matrix M. The LEDs were made in CINaM Marseille then sent for characterization in LPICM Palaiseau. The luminescence of the devices was visible but their performances remained very low. Even if the recorded threshold voltages were about 4 to 5 volts with high reproducibility, the corresponding luminance values were below 5 cd/m<sup>2</sup>. Because the JV curves of the LEDs are electrically good, namely such as exponential diode behavior, it was assumed that the loss of luminance may come from charge recombinations in the injection layer. Indeed, the PFN-Br is known to be a blue emissive material [23] and may process to this phenomenon. Table 6 and the figure 13 illustrate the different active layer compositions with their related CIE coordinates, for 10% w / w of ZnO co-grafted with B and R emitters, and OA incorporated in the matrix M.

Table 6: CIE coordinates recorded at 50 mA/cm<sup>2</sup> of cold white LEDs done with two nano hybrids N<sup>B</sup> OA and N<sup>R</sup> OA in the matrix M.

LED name	M:N <sup>B80/R40</sup> :OA	M:N <sup>B80/R20</sup> :OA	M:N <sup>B80/R8</sup> :OA	M:N <sup>B100/R8</sup> :OA	M:N <sup>B40/R8</sup> :OA	M:N <sup>B60/R3</sup> :OA
CIE (x,y)	0,357 0,303	0,308 0,296	0,269 0,260	0,243 0,234	0,303 0,285	0,270 0,271
Symbol on CIE						

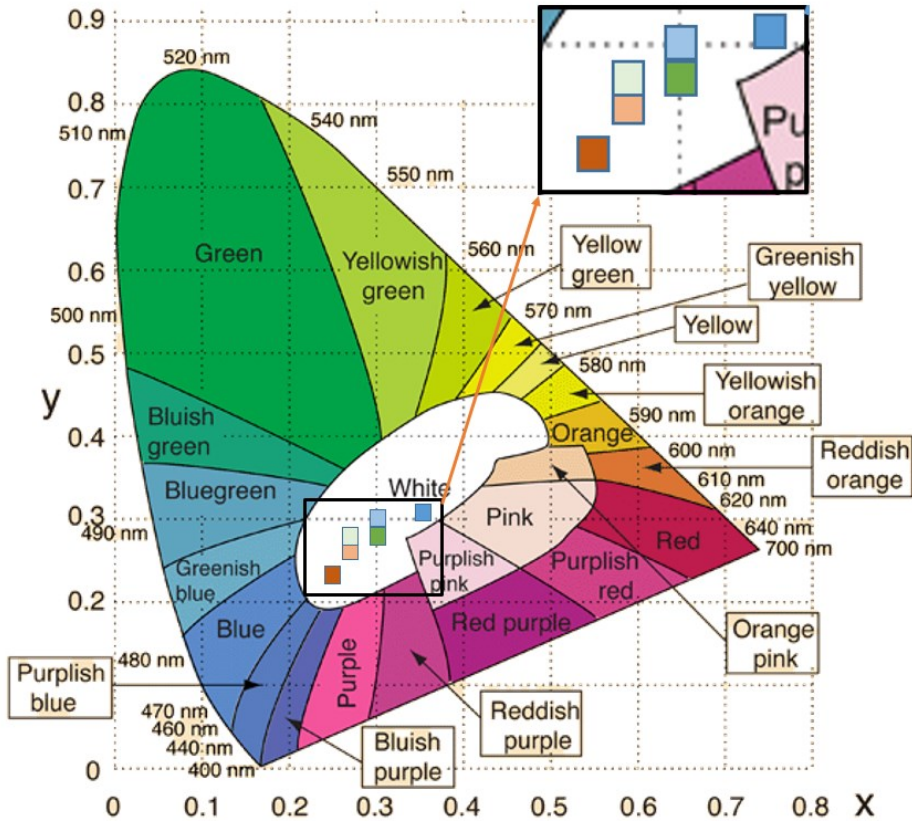


Figure 13: CIE diagram associated to Table 6, square = M + 2 nano hybrids emitters.

The first analyze was done by keeping R = 8 and decreasing the quantity of B from 100 to 80 then 40 in M:N<sup>Bx/R8</sup>:OA. The higher amount of B = 100 gave CIE coordinates (x = 0.243 y = 0.234) which is in the cold white area close to the blue border, as seen in the figure 13. When B = 80, the CIE coordinates shifted at x = 0.269 y = 0.260, in between the purple and blue white. And for B = 40, the value of CIE (x = 0.303 y = 0.285) corresponds to a reddish purple white. Therefore, by decreasing the amount of B in M:N<sup>Bx/R8</sup>:OA, it shifts the emission color from cold white to a reddish purple white color, closer to the pure white (namely CIE coordinates x = 0.35 y = 0.35). The second comparison was established by changing the active layer composition, namely keeping B = 80, and varying the amount of R from 20 to 40. Indeed, the M:N<sup>B80/R20</sup>:OA presents CIE coordinates (x = 0.308 y = 0.296), which corresponds almost

to a pure white color, while for  $R = 40$ , the emitted color is more in the purplish pink white area CIE ( $x = 0.357$   $y = 0.303$ ), as seen in the figure 8.

To sum up, low performances and reproducible cold white LEDs were achieved using full solution process LED devices, using PFN-Br as electron injection layer and two nanohybrids emitters in the matrix M as electroluminescent material. The shift of the emission to a colder white region (together with drop of performances) may be attributed to the blueish participation of the emission from the PFN-Br injection layer.

## ii) ZnO Co-grafting with 3 emitters in the matrix M:

The same study was reproduced but with 3 emitters B, G and R grafted on the surface of ZnO, and added to the matrix M. Finally, it was expected with the 3 emitters to reach a central white LED, namely CIE ( $x = 0.35$   $y = 0.35$ ). Therefore, different compositions of active layer were tried in LED devices, and their emission were recorded at  $50 \text{ mA/cm}^2$  (Figure 14, Table 7). The previous observations on the electrical performances of the LEDs containing two nanohybrid emitters are the same with three nanohybrid emitters in the matrix M, namely high reproducibility, low threshold voltages and low luminance performances, again attributed to the PFN-Br injection layer which may be not suitable for such system.

Table 7: CIE coordinates recorded at  $50 \text{ mA/cm}^2$  of white LEDs done with three nanohybrids  $N^B$  OA;  $N^G$  OA;  $N^R$  OA in the matrix M.

LED name	M:N <sup>B120/G1/R3</sup> :OA	M:N <sup>B120/G1/R6</sup> :OA	M:N <sup>B120/G1/R10</sup> :OA	M:N <sup>B80/G1/R3</sup> :OA	M:N <sup>B80/G1/R8</sup> :OA	M:N <sup>B60/G1/R3</sup> :OA
CIE (x,y)	0,270 0,271	0,292 0,303	0,352 0,344	0,399 0,416	0,417 0,410	0,311 0,317
Symbol on CIE						

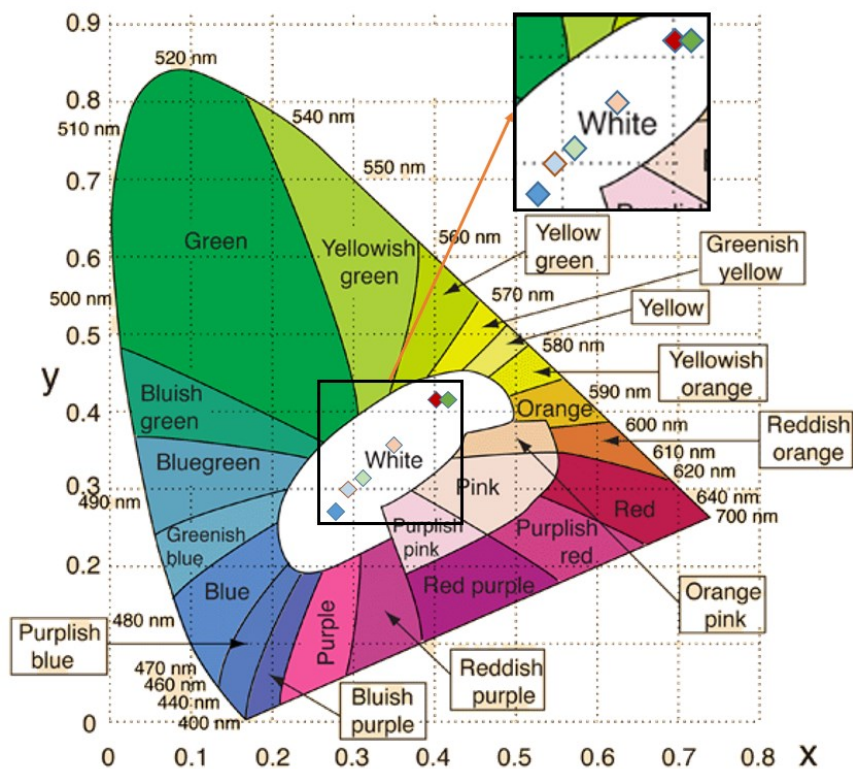


Figure 14: CIE diagram associated to Table 7, diamond = M + 3 nanohybrids emitters.

The first comparison was done by keeping B = 80 and G = 1 constant, and by varying R = 3 to 8. Indeed, as presented in the figure 14, for R = 8, the CIE ( $x = 0.417$   $y = 0.410$ ) corresponds to a warm white emission close to the greenish yellow area. When R was decreased to 3, the CIE coordinates shifted a little bit to ( $x = 0.399$   $y = 0.416$ ), but the observed color was the same (warm white). The second comparison was done by keeping B = 120 and G = 1 and varying the quantity of R from 3 to 6, then 10 in the luminescent solution. The observed color for M:N<sup>B120/G1/R3</sup>:OA was a cold white (CIE  $x = 0.270$   $y = 0.271$ ), while, when R = 6, the previous observed cold white shifted to blue-purple white emission (CIE  $x = 0.292$   $y = 0.303$ ). Finally, the last composition M:N<sup>B120/G1/R10</sup>:OA gave a perfect central white LED emission, with associated CIE coordinates of ( $x = 0.352$   $y = 0.344$ ).

To sum up, low performances and reproducible cold white, warm white and pure white LEDs were achieved using full solution process LED devices, using PFN-Br as electron injection layer and three nanohybrids emitters in the matrix M as electroluminescent material. Even though the emitter G was used, the blueish contribution from PFN-Br injection layer allows emission in the white region and limits the participation to the emission of the electroluminescent layer (which was not the case when using other interfaces such as ZnO EtNH or TPBi / LiF). However, this good color rendering has a huge cost as the performances are very low.

## 6) Conclusions

Finally, it is concluded that white LEDs were obtained with two or three nanohybrid emitters incorporated to the matrix M, or to the matrix F. The solution of the matrix M containing two or three nanohybrids was used as electroluminescent layer in LED device and gave honorable performances compared with 1<sup>st</sup> generation material for OLED, for a corresponding warm white color with evaporated injection layers.

The matrix F shows better electrical and luminous performances than matrix M, but the morphological analyzes of the films F:N:OA show high amount of aggregates above 200 x 200 nm size. The OA treatment on F:N was weakly efficient compared with the OA treatment in M:N. The presence of large aggregates in F:N:OA induced a very weak emission of the nanohybrids N, as far as the charges were inefficiently injected in the nanohybrids. Therefore, a peculiar attention must be given to the nanohybrids morphology within the matrix, as only a good morphology guarantees an emission from the nanohybrids.

The other shades of white were obtained by changing the composition of the electroluminescent layer, but also by changing the electron injection layer by solution processed PFN-Br. Even if the performances of the full solution process white LEDs were quite low, the total control of the emitted color was proved and could be improved in the future, by choosing suitable interfacial layers allowing a better charge injection in the electroluminescent layer and avoiding undesirable charge recombination.

## Bibliography:

- [1] Song E, Zhou Y, Yang X-B, Liao Z, Zhao W, Deng T, Wang L, Ma Y, Ye S, Zhang Q. Highly Efficient and Stable Narrow-Band Red Phosphor Cs<sub>2</sub>SiF<sub>6</sub>:Mn<sup>4+</sup> for High-Power Warm White LED Applications. *ACS Photonics*. 2017;4(10):2556–2565. doi:10.1021/acsp Photonics.7b00852
- [2] Burattini C, Piccardi L, Curcio G, Ferlazzo F, Giannini A maria, Bisegna F. Cold LED lighting affects visual but not acoustic vigilance. *Building and Environment*. 2019;151. doi:10.1016/j.buildenv.2019.01.022
- [3] Pimputkar S, Speck JS, DenBaars SP, Nakamura S. Prospects for LED lighting. *Nature Photonics*. 2009;3(4):180–182. doi:10.1038/nphoton.2009.32
- [4] Kang C-Y, Lin C-H, Lin C-H, Li T-Y, Huang Chen S-W, Tsai C-L, Sher C-W, Wu T-Z, Lee P-T, Xu X, et al. Highly Efficient and Stable White Light-Emitting Diodes Using Perovskite Quantum Dot Paper. *Advanced Science*. 2019;6(24):1902230. doi:10.1002/advs.201902230
- [5] Jung S-M, Lee TH, Bang SY, Han SD, Shin D-W, Lee S, Choi HW, Suh Y-H, Fan X-B, Jo J-W, et al. Modelling charge transport and electro-optical characteristics of quantum dot light-emitting diodes. *npj Computational Materials*. 2021;7(1):1–11. doi:10.1038/s41524-021-00591-9
- [6] Juang F-S, Huang KC, Chen JY, Kuo L, Hong LA. Lifetime study of white organic light emitting diodes fabricated by both solution and vacuum evaporation processes. *IOP Conference Series: Materials Science and Engineering*. 2021;1045(1):012035. doi:10.1088/1757-899X/1045/1/012035
- [7] Ma D, Duan L, Qiu Y. Orange-red- and white-emitting diodes fabricated by vacuum evaporation deposition of sublimable cationic iridium complexes. *Journal of Materials Chemistry C*. 2016;4(22):5051–5058. doi:10.1039/C6TC00738D
- [8] Wepfer S, Frohleiks J, Hong A-R, Jang HS, Bacher G, Nannen E. Solution-Processed CuInS<sub>2</sub>-Based White QD-LEDs with Mixed Active Layer Architecture. *ACS Applied Materials & Interfaces*. 2017;9(12):11224–11230. doi:10.1021/acsa mi.6b15660
- [9] Yang Q, Hao Y, Wang Z, Li Y, Wang H, Xu B. Double-emission-layer green phosphorescent OLED based on LiF-doped TPBi as electron transport layer for improving efficiency and operational lifetime. *Synthetic Metals*. 2012;3–4(162):398–401. doi:10.1016/j.synthmet.2011.12.027
- [10] Wang Y, Li B, Jiang C, Fang Y, Bai P, Wang Y. Study on Electron Transport Characterization in TPBi Thin Films and OLED Application. *The Journal of Physical Chemistry C*. 2021;125(30):16753–16758. doi:10.1021/acsj pcc.1c04138
- [11] Lozano-Hernández LA, Maldonado JL, Hernández-Cruz O, Nicasio-Collazo J, Rodríguez M, Barbosa-García O, Ramos-Ortiz G, Zolotukhin MG, Scherf U. Structurally simple OLEDs based on a new fluorinated poly(oxindolylidenearylene). *Dyes and Pigments*. 2020;173:107989. doi:10.1016/j.dyepig.2019.107989
- [12] Ohisa S, Kato T, Takahashi T, Suzuki M, Hayashi Y, Koganezawa T, McNeill CR, Chiba T, Pu Y-J, Kido J. Conjugated Polyelectrolyte Blend with Polyethyleneimine Ethoxylated for Thickness-Insensitive Electron Injection Layers in Organic Light-Emitting Devices. *ACS Applied Materials & Interfaces*. 2018;10(20):17318–17326. doi:10.1021/acsa mi.8b00752

- [13] Hong G, Gan X, Leonhardt C, Zhang Z, Seibert J, Busch JM, Bräse S. A Brief History of OLEDs—Emitter Development and Industry Milestones. *Advanced Materials*. 2021;33(9):2005630. doi:10.1002/adma.202005630
- [14] Chatterjee & al. Perspective on Host Materials for Thermally Activated Delayed Fluorescence Organic Light Emitting Diodes - 2019 - *Advanced Optical Materials*. [accessed 2022 Jan 18]. <https://onlinelibrary.wiley.com/doi/abs/10.1002/adom.201800565>
- [15] Bruno A, Mauro ADGD, Nenna G, Haque S a., Minarini C. Insights on photophysical properties of DCM dye in PVK host matrix. *Polymer Composites*. 2013;34(9):1500–1505. doi:10.1002/pc.22441
- [16] F8BT | >99.9% Purity, CAS 210347-52-7. Ossila. [accessed 2022 Jan 18]. <https://www.ossila.com/products/f8bt>
- [17] McNeill C, Greenham N. Conjugated-polymer blends for optoelectronics. *Advanced Materials* Volume21, Issue38-39 October 19, 2009 Pages 3840-3850. 2009. doi:10.1002/ADMA.200900783
- [18] Zhang Y, Blom PWM. Electron and hole transport in poly(fluorene-benzothiadiazole). *Applied Physics Letters*. 2011;98(14):143504. doi:10.1063/1.3574907
- [19] Cicoira F, Santato C. Organic Light Emitting Field Effect Transistors: Advances and Perspectives. *Advanced Functional Materials*. 2007;17:3421–3434. doi:10.1002/adfm.200700174
- [20] Suh M, Bailey J, Kim SW, Kim K, Yun D-J, Jung Y, Hamilton I, Chander N, Wang X, Bradley DDC, et al. High-Efficiency Polymer LEDs with Fast Response Times Fabricated via Selection of Electron-Injecting Conjugated Polyelectrolyte Backbone Structure. *ACS Applied Materials & Interfaces*. 2015;7(48):26566–26571. doi:10.1021/acsami.5b07862
- [21] Meng G, Chen Z, Tang H, Liu Y, Wei L, Wang Z. Application of a novel cationic iridium(III) complex as a red phosphor in warm white light-emitting diodes. *New Journal of Chemistry*. 2015;39(12):9535–9542. doi:10.1039/C5NJ02032H
- [22] Zhang G, Chou H-H, Jiang X, Sun P, Cheng C-H. Highly efficient white organic light-emitting diodes based on broad excimer emission of iridium complex. *Organic Electronics*. 2010;11. doi:10.1016/j.orgel.2010.04.016
- [23] Qian X-Y, Tang Y-Y, Zhou W, Shen Y, Guo M-L, Li Y-Q, Tang J-X. Strategies to Improve Luminescence Efficiency and Stability of Blue Perovskite Light-Emitting Devices. *Small Science*. 2021;1(8):2000048. doi:10.1002/sssc.202000048

## General conclusion:

In the chapter 1, nanohybrids using ZnO nanocrystals combined with a fluorescent compound were synthesized and used as electroluminescent layer in LED devices. However, due to the presence of undesirable aggregates, the reproducibility of such layers was poor. The co-grafting of ZnO with this emissive molecule together with oleic acid led to very homogeneous and smooth electroluminescent layers. The use of oleic acid has been shown to be very important as far as it helped to obtain very smooth layers and also to improve strongly the PLQY of the emissive materials, thanks to a better grafting of the emitters on the more accessible surface. The new hybrid material, with the help of oleic acid, was used as electroluminescent layer, and the performances were very reproducible but remained very low as the charge transport properties of such material were inadequate. This problem of transport was solved in the chapter 2, as far as the nanohybrids were dispersed as guests in a polymer host matrix of PVK:OXD. Thus, the performances of the LED using such an electroluminescent layer were improved compared to the ones without matrix assistance.

The third chapter focused on generalizing this approach to other emitters and to tune the light with different nanohybrids, using ZnO and different new graftable fluorescent organic emitters incorporated in the matrix M. The study showed that the oleic acid treatment is still required to obtain smooth, homogeneous electroluminescent layer and also to improve systematically the PLQY of the emissive organic material. Therefore, blue, green, yellow and red LEDs were built, optimized and characterized. Their performances were modest, but were comparable to the 1<sup>st</sup> generation of organic emitter used in OLED. The study revealed also that the red organic emitter could spontaneously obtain TADF property in the nanohybrid form, which was negatively affected by both the oleic acid treatment and the matrix assistance.

In the last chapter, different kind of white (cold, warm, pure) LEDs were successfully built thanks to the combination of different graftable organic emitters on ZnO nanocrystal, after been incorporated to different matrices. Even if the performances were not always recordable, warm white LEDs were achieved with almost 1% EQE and low threshold voltage, using ZnO co-grafted with two or three organic emitters using oleic acid and dispersed in a matrix. The effect of the nature of the matrix and interfacial materials were also studied and showed various consequences on performances and emitted color.

In a future work, this new approach using solution-processed nanohybrids could be improved in many ways, such as:

- To use better appropriate, and more efficient polymer host matrix.

- To use more efficient graftable organic emitter, using for example the TADF light phenomenon, which is for the moment the most promising one, compared to fluorescent and phosphorescent phenomenon, having in mind that the nanohybrids combination could improve the TADF response.
- To use more convenient interfacial layers related to the LED architecture itself, as presented in the state of the art chapter, to enhance the EQE of LED devices with better out-coupling properties thanks to oriented interfacial layers, in the way to not lose the emitted light on the sides of the device.
- To build better adapted architectures, in the way to reduce the energy barriers of the energy diagram of the LED structure.
- To use more efficient inorganic nanoparticle, for instance the CsPbX<sub>3</sub> perovskites, which present high and pure light intensity, with a narrow emission width of 20-30 nm.

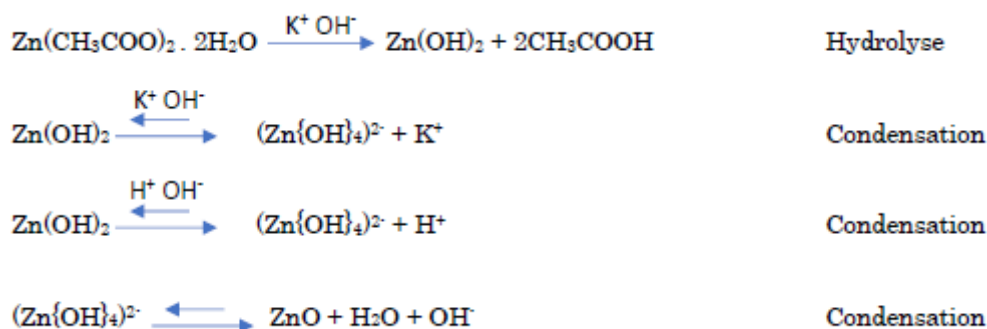
# Experiment section

## Synthesis of nanomaterials:

### 1) Synthesis of ZnO

The ZnO nanoparticles were prepared as published elsewhere [1, 2]. Briefly, the hydrothermal synthesis is carried out by taking 2 flasks, the first of 500 mL containing the precursor (SigmaAldrich Zinc Acetate 99.99% trace metals basis) with corresponding mass  $m_{\text{ZnOacetate}} = 4.101$  g in a volume of methanol (Alfa Aesar Methanol Anhydrous 99.9%)  $V_{\text{MeOH}} = 210$  mL. The second 250 mL flask contains KOH (SigmaAldrich Potassium hydroxide 99.99% trace metals basis) playing the role of the base with correlated mass  $m_{\text{KOH}} = 2.2075$  g in a volume of methanol  $V_{\text{MeOH}} = 115$  mL.

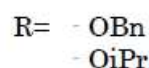
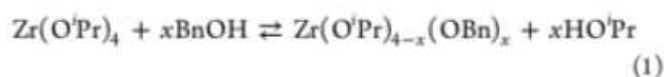
The first flask is warmed up to 60 °C in an oil bath, while the distilled water is added in it with a corresponding volume of  $V_{\text{H}_2\text{O}} = 1.25$  mL, in order to initiate hydrolysis reaction thus forming  $\text{Zn}(\text{OH})_2$ . The KOH is added drop by drop via a column under a flow of argon or  $\text{N}_2$  for 20 minutes. The second step consists in stirring for 3 hours at 60 °C. Phase changes are observed during the condensation steps, as the solution will become alternately transparent then opaque. At the end of the synthesis, a white “milky” precipitate is recovered. Centrifugation at 7800rpm for 12min is carried out in order to recover only the ZnO nanoparticles which will be dispersed in methanol and then stored in a glove box. The centrifugation step also helps to remove any residual compounds from the synthesis. To be applied in optoelectronic applications, the ZnO solution is centrifuged again to transfer from methanol to the desired solvent, and is then ready for grafting with specific surface ligand in order to have monodisperse particles.



## 2) Synthesis of ZrO<sub>2</sub>

The protocol followed is in accordance with the literature [3], it used a precursor of zirconium Zirconium (IV) isopropoxide isopropanol complex (SigmaAldrich) in an amount of 0.2268 g mixed with 4.5 mL of solvent Benzyl Alcohol 99% (Alfa Aesar). This solution is prepared in a glove box under an inert atmosphere in a 10mL glass vial, closed with a PTFE / Teflon cap. The sealed tube is then taken out of the glove box and is inserted inside the microwave SP Discover CEM  $\mu$ WAVES.

The advantage of using the microwave rather than an autoclave in an oven is important here. Indeed, the reaction time goes from 2 days to 4 hours [3–6]. This is explained by the way the microwave heats the vial, which is more homogeneous than oven. The reaction is started by raising the temperature in the microwave. A first step of stirring at temperature 60 °C is carried out for 30 minutes, and is continued with a second step of stirring at 250 °C for 4 hours. Benzylalcohol (BnOH) is the reducing species, it will reduce the Zr(O'Pr)<sub>4</sub> complex in the first step. In the second step, there is an elimination of ether thus forming ZrR<sub>3</sub>-O-ZrR<sub>3</sub> and the residual product Bn-O-Bn. This allows the surface stabilization of the ZrO<sub>2</sub> crystal thus optimizing the synthesis and more particularly the purity of the ZrO<sub>2</sub> nanocrystals [19] [22]. At the end of these steps, the ZrO<sub>2</sub> nanoparticles should exhibit cubic crystallization, due to the choice of parameters and reaction species [3].



Once the reaction is complete, a white milky precipitate is recovered which is washed 3 times with 2 mL of (Sigma Aldrich > 99.5%) diethyl ether by ultrasonic baths, vortexing and centrifuging at 2500 rpm for 2 minutes. The final solution is thus dispersed in a chloroform type solvent (Sigma Aldrich CHROMASOLV® for HPLC > 99.8%) or chlorobenzene (Sigma Aldrich anhydrous 99.8%). As for the ZnO nanoparticles, ZrO<sub>2</sub> solution needs to be stabilized by grafting with surface ligand in order to have monodisperse particles and to go toward applications.

### 3) Synthesis of CsPbX<sub>3</sub>

In the glove box, under a Nitrogen inert atmosphere, the precursor PbI<sub>2</sub> (0.087 g, 18.87 mmol) is introduced into a 150 mL three-necked flask. A magnetic bar and 5 mL of octadecene are introduced in the balloon which is then taken out of the glove box. The flask is placed in a 120°C oil bath under vacuum for 1 hour. Then, the flask is placed under an argon atmosphere for 10 minutes, in order to remove all traces of oxygen inside the balloon. A solution of organic ligand is previously heated up to 85°C containing oleic acid (0.5 mL) and oleylamine (0.5 mL) and is injected into the flask, in order to stabilize and form homogeneous CsPbX<sub>3</sub> nanocrystals [7]. The balloon is then placed under vacuum for 30 minutes until the PbI<sub>2</sub> is completely dissolved in the octadecene. The temperature is modified according to the desired size for the quantum dots (60°C for 3.4 nm, 130°C for 5 nm or 185°C for 12.5 nm). The cesium oleate precursor (0.4 mL) previously heated at 85°C is then injected. The solution changes color depending on the size of the quantum dots (from deep red for 12.5 nm to light orange for 3.4 nm). The reaction is stopped with an ice bath 5 seconds after addition of the cesium oleate precursor, as the reaction is then frozen and complete. All the washing steps are carried out in the glove box, avoiding any oxygen contamination. The methyl acetate (20 mL) is introduced into the flask. The reaction crude is transferred to a Falcon tube and then centrifuged at 7800 rpm for 5 minutes. The supernatant is removed and the quantum dots are dispersed in hexane (0.3 mL) and methyl acetate (0.3 mL) is added. The solution is centrifuged at 7800 rpm for 2 minutes. The supernatant is again removed, the hexane (2 mL) added and then the tube is centrifuged at 4000 rpm for 5 minutes. The solution is transferred into a tube and placed in the dark at 4°C for 48 hours, to remove the last undesirable species. Finally, the solution is centrifuged at 4000 rpm for 5 minutes, and the as synthesized quantum dots solution is stored into a tube in the dark.

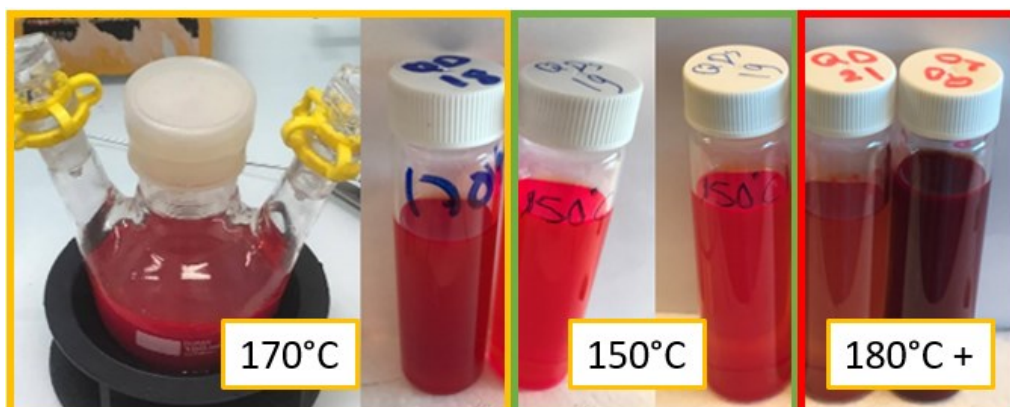


Figure 1: different synthesis of CsPbI<sub>3</sub> done at different temperatures, according to [7]

## Optical characterization:

### 1) Absorption

The UV-visible absorption spectroscopy measurements presented in this manuscript were carried out using a Cary 5000 UV-vis-NIR type spectrophotometer. They were done for both diluted solutions and films deposited on glass substrates.

UV-Visible spectroscopy is the study of the interaction of the visible and part of the UV radiations with chemical species. Visible light consists of wavelengths ranging from 380 nm (blue violet) to 720 nm (red). Light travels in packets of energy called photons. Each photon has a specific energy related to a certain frequency or wavelength ( $E = h\nu = hc/\lambda$ ). If only a portion of the light is absorbed and the rest is transmitted, the color of the sample is determined by the transmitted light. The colorless substances have an absorption spectrum which takes place in the infrared or the ultraviolet region and not in the visible region. The following figure illustrates the relationship between the light absorbed by a sample and its corresponding color.

Table 1: The relation between the color of the substance with respect to the absorbed light [8].

Colour of light absorbed	Approx. $\lambda$ ranges / nm	Colour of light transmitted
Red	700-620	Green
Orange	620-580	Blue
Yellow	580-560	Violet
Green	560-490	Red
Blue	490-430	Orange
Violet	430-380	Yellow

The light energy absorbed by a compound must match exactly the energy required to cause the movement of an electron from the ground state to the excited state, a phenomena known as electronic transition. The more easily excited the electrons (i.e. lower energy gap between

the occupied and the non-occupied levels), the longer the wavelength of light it can absorb. Transmittance of the surface of a material is another property that can be deduced from the UV-vis spectrophotometer. It is the fraction of the incident electromagnetic power that is transmitted through a sample. And it is defined as below:

$$T = \frac{I}{I_0} = \frac{\text{intensity of transmitted light}}{\text{intensity of incident light}}$$

Thus, the absorbance (A) is defined as the negative logarithm of the transmittance.

$$A = -\log T = -\log \frac{I}{I_0}$$

## 2) Fluorescence

Fluorescence investigations were carried out on solutions and layers using a CARY Eclipse Spectrometer. Photoluminescence is a type of luminescence that corresponds to the light emitted from a material after the absorption of photons. The photoexcitation causes an electron to move from the ground state to the excited state. Various relaxation processes typically occur after the excitation and may include either radiative processes like the emission of light or non-radiative processes. The emitted light is usually of a lower energy compared to the absorbed light ( $E_{exc} > E_{PL}$ ) (Stokes shift), thus it is of higher wavelength [9]. However, anti-stokes exists too.

## 3) FTIR

The IR spectra of the solid samples were recorded at room temperature using a Perkin-Elmer FT-IR Paragon 1000 PC spectrometer in a range between 4000-400  $\text{cm}^{-1}$ .

IR spectroscopy deals with the infrared light of the electromagnetic spectrum that has a longer wavelength than the visible light. This spectroscopy involves the interaction of the infrared

radiation with the matter under study. This technique is mainly used to identify the composition of a substance by providing information on the nature of the chemical bonds and the functional groups present in both organic and inorganic (metal complexes) species. Samples of several physical states (solid, liquid, and gas) can be analyzed by Infrared Spectroscopy. This method is conducted using an infrared spectrometer capable of producing an infrared spectrum. This IR spectrum can be obtained by simply plotting the intensity of the infrared light absorbed or transmitted vs. wavenumbers in ( $\text{cm}^{-1}$ ) or wavelength ( $\mu\text{m}$ ). The energy required to excite and vibrate the bonds of a molecule occurs in the Infrared region, where the sample is subjected to a frequency range between 400 and  $4000\text{ cm}^{-1}$ . When the frequency of the IR is the same as the vibrational frequency of a bond, the energy of the incident wave is absorbed with respect to the selection rules. Different functional groups absorb specific frequencies of IR radiation, hence give the characteristic peak value; thus the IR spectrum is the fingerprint of the molecule. There are 2 types of molecular vibrations. The first type is the stretching vibration that occurs at high energy ( $4000\text{-}1250\text{ cm}^{-1}$ ) along the line of a bond. They consist of symmetrical and asymmetrical stretchings. The symmetrical stretching is when two bonds increase or decrease in length simultaneously while the asymmetrical stretching occurs when one bond length is increased and the other is decreased. The second type is the bending vibration, also called deformations. These vibrations occur at low energy ( $1400\text{-}666\text{ cm}^{-1}$ ) but not along the line of the bond, only the bond angle is altered. They are of 2 types: the in-plane bending (scissoring and rocking) and the out of plane bending (wagging and twisting) [9].

#### 4) PLQY integrative sphere (Palaiseau LPICM)

The integrating sphere is an instrument used to perform various optical measurements (Figure 2). It is an object with spherical geometry which allows the integration of light over its entire internal surface. The sphere used has a diameter of 6 inches. It has 7 openings: an opening for placing the supports (located on the top of the sphere), an opening of 0.5 inch (1.27 cm) in diameter allowing the placement of the sensors (located under the sphere) and 5 openings 1 (2.54 cm) or 1.25 inch (3.175 cm) in diameter for various purposes depending on handling. The inside coating of the sphere is a white Teflon-based paint called "spectralon" very diffusing, usable from 250 nm to 2500 nm, robust and stable over time. This coating thus causes multiple reflections of the incident flux in the sphere which, by virtue of its geometry, will somehow average this flux on the internal surface. For some manipulation, we need to open the sphere through one of the holes (this is the case with photoluminescence measurements). It is said in the documentation of this sphere that the measurements therefore the integration remain

correct as long as less than 5% of the internal surface is not covered with spectralon [10]. Thus the sensor located below the sphere will only receive part of the light but we can deduce the total light from it. This makes possible to know the total luminous flux of a sample diffusing in all directions of space. Also, if the sample diffuses light directly on the sensor, the measurement will be false since these rays will not have time to integrate; this is why there are panels near the photodiode (Figure 2C) to prevent this phenomenon.

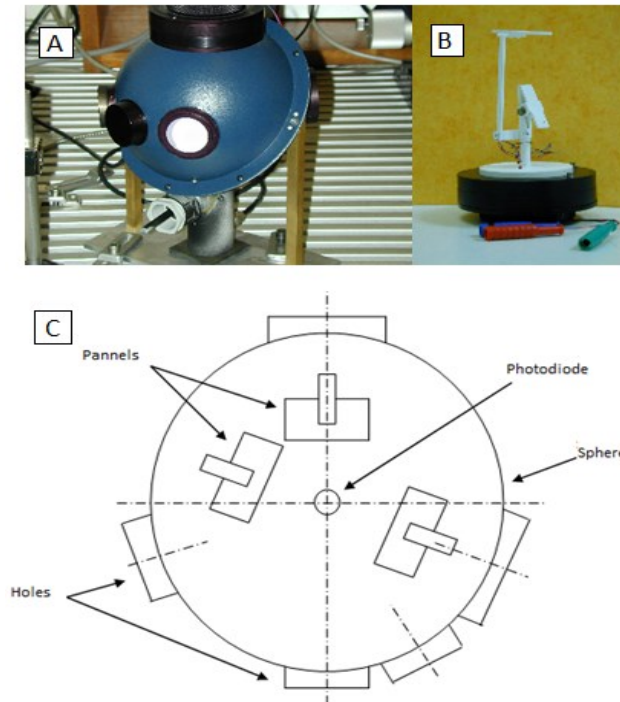


Figure 2: A) picture of the integrative sphere B) sample holder C) scheme of integrative sphere from above

### Principle of measurement:

One of the qualitative evaluation methods for OLED materials is photoluminescence quantum Yield (PLQY), which can be easily obtained in solution since they have an isotropic angular distribution. However, it is not like this for thin film measurement (anisotropy in the angular distribution, wave-guiding effects, etc.).

The Photoluminescence Quantum Yield,  $\eta$ , is expressed in the following equation.

$$\eta = \frac{\text{number of emitted photons}}{\text{number of absorbed photons}}$$

For this measurement, we use the Integrating Sphere. In the ideal case, we can suppose that the light is redistributed isotropically over the inner sphere surface regardless of the angular dependence of the emission. So,  $N_{\Omega}$  is total photons detected over a solid angle  $\Omega$ , we can express detected a number of photons like this.

$$N_{detector} = N_{\Omega} \frac{4\pi}{\Omega}, \quad \Omega : \text{solid angle of the detector.}$$

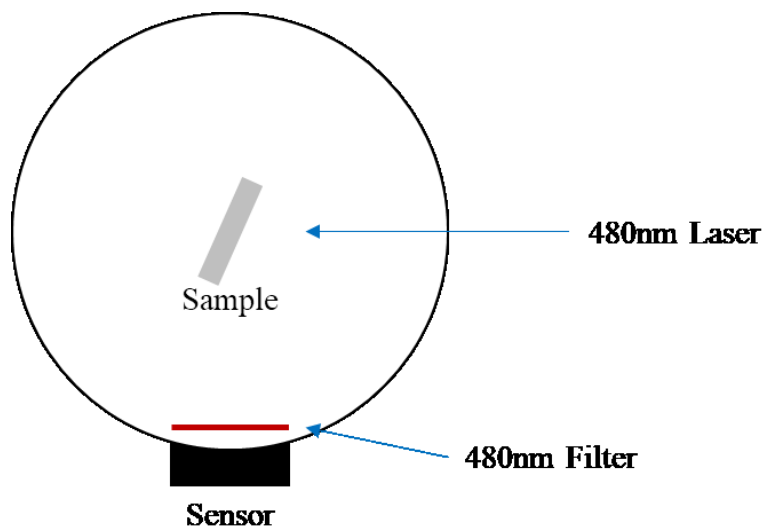


Figure 3: Schematics of integrated sphere.

We have to do six measurements for obtaining PLQY. (a) No sample & filter (a') No sample & no filter (b) placed sample to strike laser directly & filter (b') placed sample to strike laser directly & no filter (c) placed sample to avoid laser directly & filter (c') placed sample to avoid laser directly & no filter. If  $A$  is a fraction that is a part of the incident light absorbed by the sample. Then,  $(1-A)$  will be transmitted or reflected by the sample. Moreover,  $B$  is a fraction that scattered light is absorbed by the sample.  $I_a, I_b$  and  $I_c$  are then the value of output laser light intensity  $I'_a, I'_b$  and  $I'_c$  are the value of emitted light intensity.

$$I_c = I_a(1 - B)$$

$$I_b = I_c(1 - A)$$

$$I_b = I_a(1 - A)(1 - B)$$

Then, the absorption coefficient is:

$$A = 1 - \frac{I_b}{I_c}$$

Also, the total amount of photon that strikes to the detector with absorption fraction is represented by the scattered laser light, and the following equation:

$$(1 - A)(I_c + I'_c)$$
$$I_b + I'_b = (1 - A)(I_c + I'_c) + \eta I_a A$$

Finally, we can calculate  $\eta$  with:

$$\eta = \frac{I'_b - (1 - A)I'_c}{I_a A}$$

In this measurement, we used glass with coated electroluminescent thin film as sample.

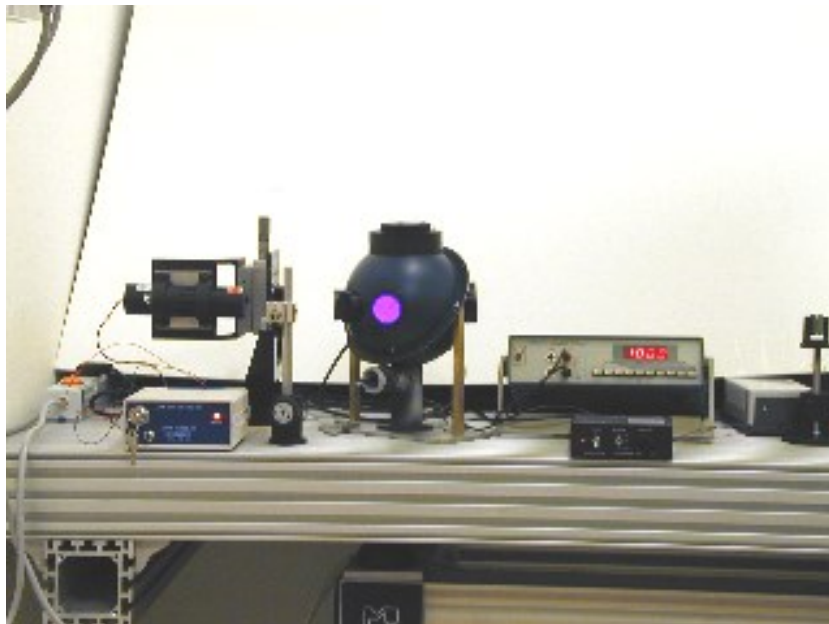


Figure 4: Measurement machines (excitation source : laser diode 405 nm).

## Morphological characterizations:

### 1) Dynamic Light Scattering (DLS)

The size distribution and the charge surface of the nanoparticles within the solution were determined using a Nano ZetaSizer DLS from Malvern Instruments. DLS is a non-destructive technique that determines the size distribution profile and the zeta potential of small dispersed particles in a diluted suspension. The basic principle is illuminating the small particles within the solution with a monochromatic light source, usually a laser through a polarizer. This causes the light to scatter in all directions (Rayleigh scattering) in case the particles are small compared to the wavelength (below 250 nm). The scattered light then passes through a second polarizer where it is collected by a photomultiplier and the resulting image is projected onto a screen. This technique measures the intensity of the light scattered by the particles over time. Although the light source is monochromatic and coherent, the scattering intensity fluctuates over time leading to a change in the distance between the scatterers in the solution. These fluctuations are due to the Brownian motion of the small molecules in solution (which is the random motion of particles in a fluid resulting from their collision with the fast moving molecules). These movements depend on the viscosity of the surrounding medium, its temperature and the size of particles. Thus, analyzing the variations of the intensity of the diffused light will provide an information about certain characteristics of these particles, such as their sizes. The coefficient of diffusion  $D$  is often used to calculate the hydrodynamic radius  $R_h$  of a spherical particle using the Stokes-Einstein equation:

$$R_h = \frac{KT}{6\pi\eta D}$$

In which  $K$  is the Boltzmann's constant,  $T$  the temperature and  $\eta$  is the dynamic viscosity. It is important to mention that the size of the particles determined by DLS includes any other molecules or solvent molecules moving with the particles. The results are given according to three different displays, the size distribution of the studied compounds in number, in volume and in intensity. [9]

## 2) Transmission Electron Microscopy (TEM)

TEM is a microscopic technique based on visualizing a specimen with a high energy beam of electrons. These electrons are emitted upon heating a tungsten filament and they can be accelerated by a voltage between 200 and 1000 kV. An image is formed due to the interaction of the electrons with the sample when the beam is transmitted through the specimen. This image is then magnified and focused onto an imaging device. The difference in the electron density causes contrast difference on the image, thus the darker areas of the image correspond to those areas of the sample where few electrons are transmitted through, while the lighter areas represent the inverse. Indeed, the high energy electrons (300kV) deflected by the crystal lattice of the nanoparticles will give a black image, while the transmitted electrons will give a white image (organic ligand). Furthermore, only the inorganic part is visible in the image, even if organic films can also be observed with specific sample preparation (holey grid).

The basic principles of the TEM are close to those of the optical microscope but uses electrons instead of light. Thus, they are capable of imaging at higher resolution than the light microscopes, this is due to the smaller de Broglie wavelength of electrons compared to the wavelength of light. This enables the instrument to capture fine details of internal structure even thousands of times smaller than a resolvable object seen in a light microscope (TEM can reveal the crystal structure). By adjusting the magnetic lenses, an electron diffraction patterns can be generated. The diffraction patterns give an information about the crystallinity of the material, thus a pattern of dots is an indication of a single crystal while a series of rings reveals a polycrystalline material. Chemical analysis can also be performed [9]. The TEM images were captured with a JEOL JEM-3010 microscope operating at 300 kV and a JEOL JEM-2010 operating at 200 kV. The samples were prepared by drop-casting a diluted solution onto the grid. The grids used were carbon-coated copper S160-3s from Oxford Instruments. In another way, the electroluminescent active layers were studied, by coating of PEDOT:PSS on ITO or glass substrate, then the luminescent layer was spin-coated on top of this polymer injection hole layer. After annealing of the different coated layers, PEDOT:PSS film was dissolved in deionized water bath, to collect only the electroluminescent film via the Holey grid “s147-3 holey carbon film mesh copper” according to the following figure.

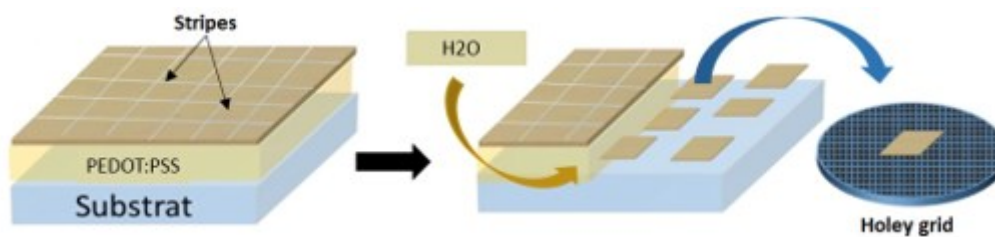


Figure 5: TEM sample preparation on Holey grid, known as "floating layer technic"

### 3) Scanning Electron Microscopy (SEM)

The SEM images were detected using a Jeol JSM 7900F microscope. SEM is a type of electron microscopy that produces images of a sample after scanning the surface with a focused beam of electrons. After the interaction of the electrons with the atoms in the sample, various signals will be produced. This process will provide information about the surface topography of the sample. The SEM can provide three dimensional images and it offers two million as a maximum level of magnification.

### 4) Atomic Force Microscopy (AFM)

AFM is a scanning technique which demonstrate the resolution on the order of a nanometer and is commonly used to study the surface morphology of the organic semiconductor films. Its principle is based on a probe which constitutes a cantilever accompanied with a sharp tip that interacts with the sample to scan its surface. The cantilever could be either silicon or silicon nitride with a tip of nanometric radius. When the tip is in contact with the sample surface, the forces between the tip and the sample deflect the cantilever according to Hooke's law. Thus, AFM measures the mechanical contact forces, van der Waals forces, chemical bonding, electrostatic forces, magnetic forces, and others. The reaction of the probe to the forces imposed by the sample can be used to form a three-dimensional image (topography) of the sample surface at a high resolution. The AFM is also essential for measuring the surface roughness ( $R_a$ , or average absolute deviation) over a wide range: from  $R_a = 0.03$  nm to 500 nm. Also, the root mean square roughness (RMS) can be detected. In general, AFM can be operated using different modes depending on the application. Possible imaging modes are divided into static (also called contact) modes and other dynamic (non-contact or "tapping") modes [9]. AFM images were recorded with a NTEGRA Prima of the brand NT-MDT in tapping

mode. The tips used were MicroMasch HQ:NSC15 / AL BS. The layers were deposited by spin coating the solutions on ITO substrates or photoactive blends.

### 5) Profilometry

Profilometry is an instrument used to identify the thickness of the layers. It consists of a diamond stylus with a radius ranging from 20 nm up to 50  $\mu\text{m}$ . To scan the surface of the sample, this stylus moves laterally across the sample with a specified distance and speed by applying a specific contact force. By the vertical stylus displacement as function of the position, a profilometer can measure small surface variations. The height position of the diamond stylus generates an analog signal which is converted into a digital signal that is stored, analyzed, and displayed <sup>7</sup>. The profilometer used in our studies was of type Dektak XTS (Bruker, Germany) equipped with a stylus of 2  $\mu\text{m}$  radius. A scratch was done on the film using a wooden tip, thus creating a channel corresponding to the thickness of the layer.

### 6) X-Ray Photoelectron Spectroscopy (XPS) (collaboration with Mats Fahlman – University of Linköping)

The measurements were calibrated by referencing to Fermi level and Au 4f 7/2 peak position of the Ar<sup>+</sup> ion sputter-clean gold foil. The samples were prepared by spin coating the solution on ITO substrates with the resulting film thickness  $\approx 100$  nm.

It is a surface-sensitive quantitative spectroscopic technique that is used to measure the elemental composition, the empirical formula (which is the integer ratio of the atoms found in a chemical compound), the chemical state (known as the oxidation state when referred to metal cations) and the density of the electronic states of the elements that exist within a material. It is mainly used to analyze inorganic compounds, metal alloys, semiconductors, polymers and many others. In principle, XPS detects all elements with an atomic number (Z) above or equal to 3, thus hydrogen (Z = 1) or helium (Z = 2) cannot be easily detected. XPS is used to analyze the surface chemistry of a material as it is or after some treatments and exposures to heat or UV. The principle is based on the simultaneous measurement of the kinetic energy and the number of electrons escaping from the sample surface after being irradiated with a beam of X-rays. Thus, the XPS spectrum is a plot of the number of electrons detected as function of the binding energy of the electrons. XPS requires

high vacuum ( $P \sim 10^{-8}$  millibar) or ultra-high vacuum (UHV;  $P < 10^{-9}$  millibar) conditions. Each element produces a characteristic set of XPS peaks at characteristic binding energy values that directly identify each element existing in or on the surface of the material under study. These characteristic spectral peaks correspond to the electron configuration of the electrons within the atoms, e.g., 1s, 2s, 2p, 3s, etc. XPS can detect only the electrons that escape from the sample surface into the vacuum of the instrument, and reach the detector. However, the photo-emitted electrons can undergo recombination or can be trapped in various excited states within the material, all of which can reduce the number of escaping photoelectrons. Thus, the results depend on the thickness of the layers [13]. XPS measurements were performed in an ultrahigh vacuum (UHV) surface analysis system with a Scienta-200 hemispherical analyzer and a monochromatized Al K $\alpha$  source ( $h\nu = 1486.6$  eV).

## 7) X-Ray Diffraction (XRD)

XRD is one of the nondestructive analytical techniques which is considered rapid. It is principally used for identifying the phase of an unknown crystalline material (e.g. minerals, inorganic compounds). It can provide information about the unit cell dimensions, average grain size, crystallinity and sample purity.

The X-rays of the diffractometer are generated in an X-ray tube and filtrated to produce monochromatic radiations, which are concentrated and directed toward the sample. These diffracted X-rays are then detected, processed and counted. When conditions satisfy Bragg's law ( $n\lambda=2d\sin(\theta)$ ), the interaction of the incident rays with the sample will produce constructive interference. This law relates the wavelength of electromagnetic radiation  $\lambda$  to the diffraction angle  $\theta$  (which is the angle between the incident and the diffracted rays) and the lattice spacing in a crystalline sample  $d$ . By scanning the sample through a range of  $2\theta$  angles, all possible diffraction directions of the lattice should be attained due to the random orientation of the powdered material. The obtained diffraction peaks are converted into  $d$ -spacing to identify the unknown material as each has its own characteristic set of  $d$ -spacing. Typically, this is achieved by comparing the obtained  $d$ -spacing to the standard reference patterns [9]. The crystallinity of the nanoparticles was measured by using an X-Ray diffraction device mounted on Cu rotating anode, Rigaku RU 200BH.

## Devices elaboration:

### 1) Cleaning of ITO substrate ultrasonic baths and UV ozone:

The ITO substrates purchased from LUMTEC company were cleaned before use. This process is highly recommended to remove organic compounds, impurities or any dust particles from the ITO surface. The handling of the substrates was done using metal tweezers to avoid any further contamination. The cleaning process of the ITO substrates consists of many steps.

The substrates were first placed in a specific sample holder as shown by the figure 6a below. To ensure that the spin coating was done on the ITO surface and not on the glass surface, a digital multimeter was used to check the conductivity of the surface before the substrates were placed into the holder. The holder was immersed into a glass container with enough deionized water to cover the glass ITO substrates. The container was then placed in an ultrasonic bath at room temperature for 15 minutes. The ultrasonication cleaning process helps in removing any traces of contaminants that can be adhered on the ITO surface. For further cleaning and removal of organic residues, the holder was submerged in another container filled with acetone. This container is placed in an ultrasonic bath at room temperature for 30 minutes. The holder was taken out of the acetone and submerged in ethanol for 10 minutes with ultrasonication. Finally, the substrates were placed in isopropanol for the last 15 minutes in ultrasonic treatment. The purpose of this step is to remove any traces of acetone and ethanol that would leave marks on the ITO surface when dried. The last step of the cleaning process is to place the substrates inside a UV ozone cleaner for 15 minutes at 80 °C, in order to clean the surface but also to activate hydroxy groups on the surface for the well coating of the deposited solutions. The UV ozone machine presented in the figure 6b was purchased from NOVASCAN and is referenced PSD Pro Series Digital UV Ozone System.

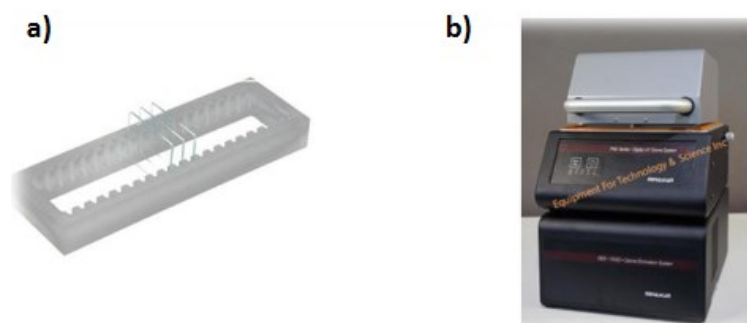


Figure 6: (a) ITO sample holder (b) UV ozone cleaner with his ozone pumping system below

## 2) Glovebox

The glovebox is referenced MB 200B and is used in particular to prepare materials for synthesis, to deposit solutions on layer with spin-coater or to measure optoelectronic devices, thus providing a minimal contamination rate ( $O_2 < 100\text{ppm}$ ;  $H_2O < 0.1\text{ppm}$ ) since the atmosphere is inert and under Nitrogen.



*Figure 7: Glovebox room*

## 3) Centrifuge machine

This apparatus is referenced SigmaAldrich 2-16P. The machine is used for the step of purification in the end of a synthesis. This can be done at different rotational speeds 0 to 7800 rpm and variable duration. The centrifugation is useful to recover the nanoparticles aggregated at the bottom of a sample holder, and/or to change the initial solvent.

#### 4) Preparation of LED device

##### Spin coater

The spin coating process was used for the deposition of the solution-processed layers. In general, this process consists of several steps as shown by the figure 8 below. Starting from the deposition of a solution on top of a glass, silicon, or ITO substrate, followed by spinning at a specific speed for a period of time, resulting in a precise controlled thickness. The thickness of the layer can be optimized by the speed of rotation and the viscosity of the solution. The last step is the evaporation of the solvent either by thermal annealing or under vacuum. The laboratory has one spin coater which is exposed to atmospheric condition, and another inside the glovebox.

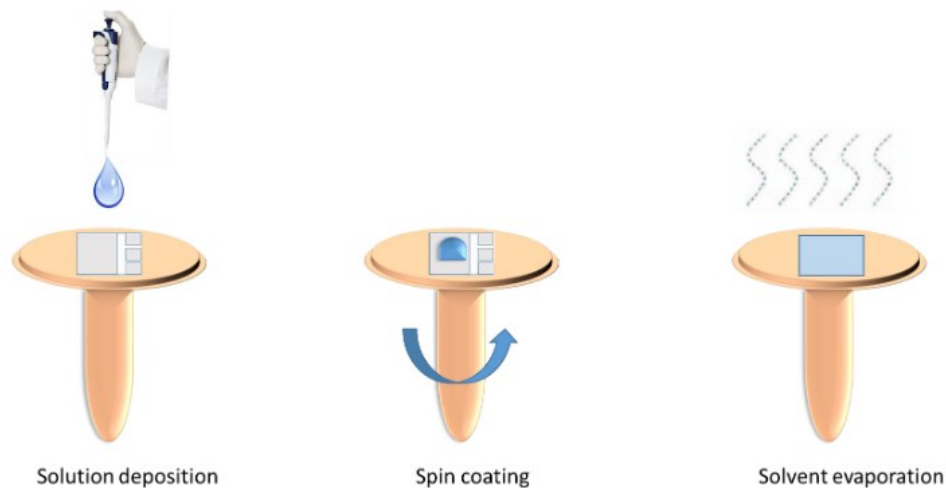


Figure 8 : How to spin coat a solution on a solid substrate

##### Evaporator, masks and current density voltage measurements (Marseille CINaM)

The mask was used to define the active area to  $0.27 \text{ cm}^2$ . The current density voltage (JV) characteristics of the devices were measured using a Keithley 238 Source Measure Unit with. The shadow mask and the MBRAUN evaporator used for the deposition of the electrodes are shown by the figure 9c. The different evaporations were done at a pressure of  $10^{-6}$  mbar. The active area  $0.27 \text{ cm}^2$  will generate the light phenomenon of the LEDs and is represented by the shining part of the figure 9b.

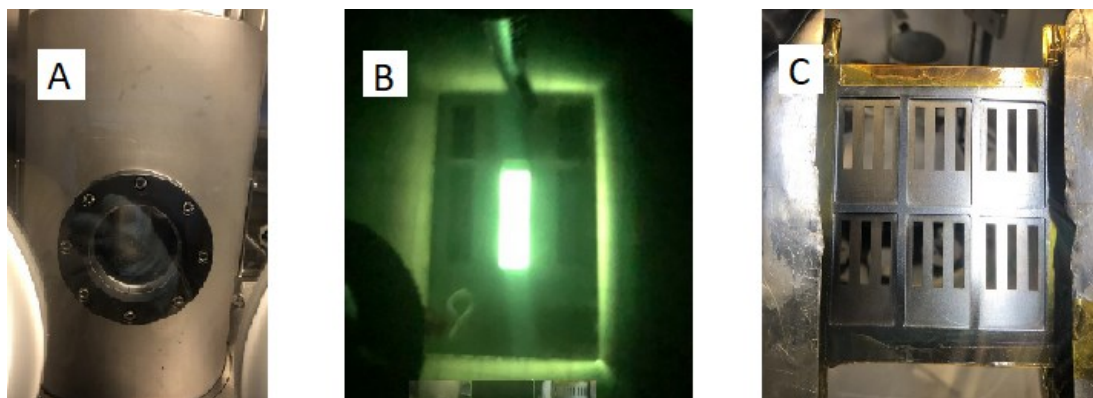


Figure 9: A) Evaporator B) LED shining (active area 27 mm<sup>2</sup>) C) Evaporator mask

### Evaporator, masks (Palaiseau LPICM)

The evaporations done in Palaiseau LPICM are done with MECA-2000 evaporator and concern the following materials: CuPc, TPBi, AlQ<sub>3</sub>, BCP, LiF and Aluminium, the process is done at pressure of 10<sup>-8</sup> mbar. The design of the cathode is circular, in order to be measured by the camera SpectraScan, and then to deduce the important values describing LED performances.

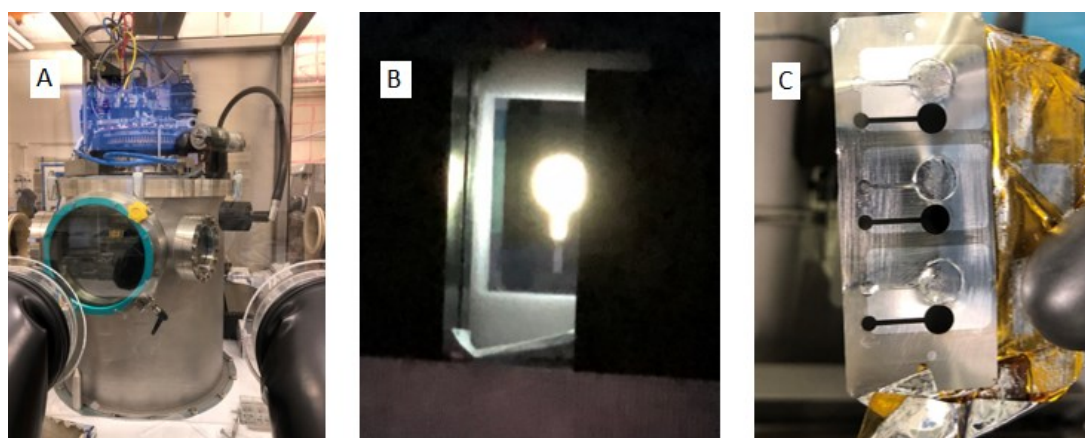


Figure 10: A) Evaporator B) LED shining (active area 25 mm<sup>2</sup>) C) Evaporator mask

### 5) Preparation of a regular architecture LED

Hybrid LEDs having the regular device structures were processed as follow: the PEDOT:PSS HTLs were spin coated inside the glovebox on the pre-cleaned ITO glass substrates at a speed of 4000 RPM for 1 minute followed by heating on a hot plate at 130 °C for 15 minutes. The PEDOT:PSS can also be deposited in the spin coater outside, giving the same film quality.

Polyvinylcarbazole (PVK) + oxadiazole (OXD) composing M (or F8 + F8BT composing F) electroluminescent blends were spin coated at a speed of 4000 to 5000 RPM for 45 seconds, respectively. The layers were annealed with a hot plate at 150°C for 5 minutes on average. Interlayers of ZnO nanoparticles and ethanolamine were processed by spin coating ZnO (synthesized) solutions with a concentration of 5 mg/mL on top of the active layers at 2000 RPM for 1 minute followed by annealing at 100 °C for 2 minutes. Other solutions of electron injection layers were used as 0.5 mg/mL PFN-BR (or 5 mg/mL ZrO<sub>2</sub> with methoxy-ethoxy-acetic acid). Finally, the samples were put into MBRAUN evaporator inside the glovebox, in which Al metal was thermally evaporated at  $2 \times 10^{-6}$  mbar pressure through a shadow mask up to 100 nm thickness.

## 6) Preparation of hybrid active layers

The matrixes M or F were prepared at different concentration one day before the deposition of the different layers composing the LED. Indeed, the matrixes were dissolved in a solution of chlorobenzene:chloroform = 4:1 volume, at 50°C over one night. The next day, half an hour before the deposition of the electroluminescent layer, ZnO nanoparticles, emissive molecules are added to the matrix, creating a solution of matrix containing nanohybrids N. The solution of M:N or F:N is then stirred and heated at 100°C in order to increase the grafting rate between ZnO and the emissive molecules. Once the luminescent solution is transparent (aggregate-free assumed), the OA is added to the solution of M:N or F:N, thus giving the M:N:OA or F:N:OA. Finally, 1 more minute of stirring is useful to homogenize the luminescent solution which can be afterward coated.

## 7) Preparation of SCLC devices

The SCLC devices were done by Payal Manzhi and Jonathan Phelipot. The architectures of the SCLC devices are presented by the figure bellow (the electroluminescent layer is about 100 nm thick)

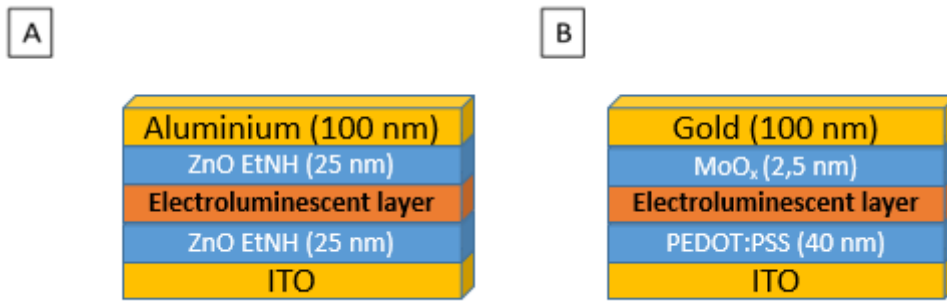


Figure 11: SCLC device architecture of a) electron only devices b) hole only devices

Once the SCLC devices done, we applied voltage from 0 to 5V or 10V, two values of compliance voltage were used in order to check the reproducibility of the measurement. The extraction of mobility from the measured JV curves was done following the method presented in literature [11] (see supporting information S15).

## Bibliography:

- [1] Dkhil SB, Duché D, Gaceur M, Thakur AK, Aboura FB, Escoubas L, Simon J-J, Guerrero A, Bisquert J, Garcia-Belmonte G, et al. Interplay of Optical, Morphological, and Electronic Effects of ZnO Optical Spacers in Highly Efficient Polymer Solar Cells. *Advanced Energy Materials*. 2014;4(18):1400805. doi:10.1002/aenm.201400805
- [2] Mattioli G, Dkhil SB, Saba MI, Mallocci G, Melis C, Alippi P, Filippone F, Giannozzi P, Thakur AK, Gaceur M, et al. Interfacial Engineering of P3HT/ZnO Hybrid Solar Cells Using Phthalocyanines: A Joint Theoretical and Experimental Investigation. *Advanced Energy Materials*. 2014;4(12):1301694. doi:10.1002/aenm.201301694
- [3] Katrien De Keukeleere†, Jonathan De Roo†‡∇, Petra Lommen†, José C. Martins∇, Pascal Van Der Voort§, and Isabel Van Driessche\*†. Fast and Tunable Synthesis of ZrO<sub>2</sub> Nanocrystals: Mechanistic Insights into Precursor Dependence | *Inorganic Chemistry* 2015 , 54, 7, 3469–3476. [accessed 2022 Jan 21]. doi.org/10.1021/acs.inorgchem.5b00046
- [4] Garnweitner G, Goldenberg LM, Sakhno OV, Antonietti M, Niederberger M, Stumpe J. Large-Scale Synthesis of Organophilic Zirconia Nanoparticles and their Application in Organic–Inorganic Nanocomposites for Efficient Volume Holography. *Small*. 2007;3(9):1626–1632. doi:10.1002/sml.200700075
- [5] Luo K, Zhou S, Wu L, Gu G. Dispersion and functionalization of nonaqueous synthesized zirconia nanocrystals via attachment of silane coupling agents. *Langmuir: the ACS journal of surfaces and colloids*. 2008;24(20):11497–11505. doi:10.1021/la801943n
- [6] Zhou S, Garnweitner G, Niederberger M, Antonietti M. Dispersion behavior of zirconia nanocrystals and their surface functionalization with vinyl group-containing ligands. *Langmuir: the ACS journal of surfaces and colloids*. 2007;23(18):9178–9187. doi:10.1021/la700837u
- [7] Loredana Protesescu†‡, Sergii Yakunin†‡, Maryna I. Bodnarchuk†‡, Franziska Krieg†‡, Riccarda Caputo†, Christopher H. Hendon§, Ruo Xi Yang§, Aron Walsh§, and Maksym V. Kovalenko\*. Nanocrystals of Cesium Lead Halide Perovskites (CsPbX<sub>3</sub>, X = Cl, Br, and I): Novel Optoelectronic Materials Showing Bright Emission with Wide Color Gamut | *Nano Letters* 2015, 15, 6, 3692–3696. [accessed 2021 Dec 20]. <https://doi.org/10.1021/nl5048779>
- [8] These Riva Al’Karsifi Synthesis and Characterization of Composite Nanomaterials as Interfacial Layers in Organic Solar Cells December 2019. [accessed 2022 Jan 21]. [https://theses-univ-amu-fr.lama.univ-amu.fr/191219\\_ALKARSIFI\\_723flun7mlh969exnxou750podva\\_TH.pdf](https://theses-univ-amu-fr.lama.univ-amu.fr/191219_ALKARSIFI_723flun7mlh969exnxou750podva_TH.pdf)
- [9] Mourdikoudis S, Pallares RM, Thanh NTK. Characterization techniques for nanoparticles: comparison and complementarity upon studying nanoparticle properties. *Nanoscale*. 2018;10(27):12871–12934. doi:10.1039/C8NR02278J
- [10] Catalogue Labsphère, Sphere systems and instrumentation, 1997. [accessed 2022 Jan 21].
- [11] Baert F, Cabanetos C, Leliège A, Kirchner E, Segut O, Alévêque O, Allain M, Seo G, Jung S, Tondelier D, et al. A bridged low band gap A–D–A quaterthiophene as efficient donor for organic solar cells. *Journal of Materials Chemistry C*. 2014;3(2):390–398. doi:10.1039/C4TC02212B